Ach was, alles Unsinn:
Lava und Magma und Fumarolen und Eruptionen -
im Berg sitzt ein scheußlich schwarzer Teufelskerl,
der mit glühenden Steinen schmeißt.

(Max Kruse. "Urmel im Vulkan", München, 1982)

MULTI-COMPONENT EVOLUTION, AGE AND PLATE-TECTONIC SETTING OF HIGH-MG LAMPROPHYRIC DIKES AND SMALL GABBROIC INTRUSIONS ON ISLA MARGARITA (VENEZUELA)

Dissertation

zur Erlangung des Grades eines
Doktors der Naturwissenschaften
der Fakultät für Geowissenschaften
an der Ruhr-Universität Bochum

CLAUDIA KAISER
INSTITUT FÜR GEOLOGIE
RUHR-UNIVERSITÄT BOCHUM
1997

TABLE OF CONTENTS

1.

ABSTRACT

1.1 ABSTRACT

Isla Margarita (Venezuela) is located at the southern boundary of the Caribbean plate and represents a compositionally heterogeneous piece of crust composed of peridotites, metamorphic units, various types of magmatic rocks and sedimentary cover. Late magmatic rocks intrusive into the metamorphic complex of the island provide a geochronological reference system for the younger tectonic history of Margaritan crust. The origin of the magmas and timing of emplacement are important clues for unravelling the tectonic history at the southern margin of the Caribbean plate and testing of plate tectonic scenarios.

The late igneous rock suite on Margarita is a series of Eocene lamprophyric dikes and small gabbroic intrusions. Geochemically the Margarita igneous rock suite is basaltic to andesitic in composition, although overall high compatible element concentrations (Mg, Cr, Co, Ni) are striking and together with intermediate compositions (48-59 wt% SiO_2) suggest fractionated magmas from principally large percentage mantle melts. Variable enrichment in trace and light REE elements, as well as high radiogenic strontium and lead isotopic ratios, imply an additional subduction zone component. A multi-component model is favored to contribute to the observed element patterns:

(1) metasomatism of the mantle wedge by LILE-enriched fluids from dehydration of the subducted slab in the Aves/Proto-Lesser Antillean island arc regime; (2) melting of depleted mantle peridotite, which was inhomogeneously metasomatized by LILE-enriched fluids; (3) polybaric differentiation with fractionation of olivine, clinopyroxene and chromite; (4) equilibration at crustal level under low pressure and hydrous conditions, with amphibole taking over as the fractionating ferromagnesian phase, concomittant with assimilation of variable portions of crustal material.

Subsequent high-temperature hydrothermal action, leading to pervasively altered rocks, is diagnostic of the lamprophyre dike suite and is marked by leaching of K_2O and slight enrichment of H_2O, CO_2 and MgO.

The $^{40}Ar/^{39}Ar$ age spectra on hornblende from dikes and small gabbroic intrusions indicate disturbed K-Ar systems and are diagnostic of excess ^{40}Ar, but roughly establish isotopic ages of the gabbro and dike intrusions of 64 and 56-43 Ma respectively. The emplacement of the late gabbros and dikes, together with volumetrically minor basalts and andesites from other Venezuelan offshore islands, is constrained into the hiatus between the Aves and Proto-Lesser Antillean island arc magmatism.

The ages of the gabbro and dike intrusions as such provide a keystone for the reconstruction of the younger tectonic history of the southern Caribbean region, in particular for Isla Margarita, for which a detailed model of pressure-temperature-time-deformation evolution exists. Accordingly, at 50 Ma b.p. Isla Margarita was located at the northwestern corner of the South American continent, at the southern tip of the Aves ridge. The emplacement of the lamprophyre dikes along preexisting conjugate shear fractures indicates that the

corresponding country rocks resided in a shallow crustal level after major tectonic reorganization, hence above the brittle ductile transition zone. The crustal slice exposed on Margarita remained in a shallow position close to the southern Caribbean plate boundary from 50 Ma to present. The history of Margarita is in perfect accordance with plate tectonic reconstructions which favor a Pacific origin and eastward migration of the Caribbean plate since the Cretaceous.

1.2 ZUSAMMENFASSUNG

Die Isla Margarita (Venezuela) befindet sich am Südrand der Karibischen Platte und besteht aus einem heterogenen Krustenkomplex aus Peridotiten, Metamorphiten, diversen Magmatiten und sedimentärem Deckgebirge. Die in den metamorphen Komplex der Insel eingedrungenen Magmatite stellen ein geochronologisches Bezugssystem für die jüngere tektonische Entwicklung der Insel dar. Die Entstehung der Magmen und die zeitliche Einordnung der Platznahme sind wichtige Anhaltspunkte für die Aufschlüsselung der tektonischen Entwicklung des Südrandes der Karibischen Platte und erlauben eine Korrelation mit plattentektonischen Modellen.

Die jüngste magmatische Gesteinsserie der Isla Margarita wird von eozänen Lamprophyrgängen und geringvolumigen gabbroiden Intrusionen gebildet. Die Intrusivgesteine sind basaltisch-andesitischer Zusammensetzung, wobei ein generell hoher Anteil an den kompatiblen Elementen Mg, Cr, Co und Ni besonders auffallend ist und, in Verbindung mit intermediärer Zusammensetzung (48-59 Gew.% SiO_2), auf starke Fraktionierung bei relativ hohen partiellen Aufschmelzgraden deutet. Variable Anreicherung an leichten Seltenen Erden und LILE (Large Ion Lithophile Elements) sowie erhöhte Strontium- und Blei-Isotopenverhältnisse lassen auf eine zusätzliche Subduktionskomponente schließen. Die Elementverteilungen der Intrusivserie werden durch ein multikomponenten Modell erklärt:

(1) Metasomatose des Mantelkeils durch LILE-angereicherte Fluide infolge der Dehydratation der subduzierten Platte in der Region des Aves-/Proto-Antillenbogens; (2) Aufschmelzung von verarmtem Mantelperidotit mit ungleichmäßiger Anreicherung an LILE; (3) polybare Differentiation der Magmen mit Fraktionierung von Olivin, Klinopyroxen und Chrom-Spinell; (4) Equilibrierung im krustalen Stockwerk bei geringem Druck und wasserreichen Bedingungen, unter denen Amphibol als eisen- und magnesiumhaltige Phase fraktioniert wurde. Zusätzlich fand eine Assimilation des Nebengesteins statt. Die lamprophyrische Ganggesteinsserie wurde nachfolgend durch hydrothermale Prozesse alteriert, wobei diese insbesondere an K_2O abgereichert und an H_2O, CO_2 und MgO angereichert wurde.

Die $^{40}Ar/^{39}Ar$ Altersdatierungen an Hornblenden der Ganggesteine und Gabbros zeigen unsystematische K-Ar Verhältnisse und deuten auf das Vorhandensein von Überschuß-Argon hin. Die ungefähren Alter können jedoch auf 64 Ma (Gabbro) bzw. 56-43 Ma (Gänge) festgelegt werden. Die Platznahme der Intrusivgesteine auf der Isla Margarita kann zeitlich mit geringvolumigen Basalten und Andesiten der benachbarten Venezuela vorgelagerten Inseln korrelliert werden. Die Gesteinsalter überlappen bzw. schließen an den letzten magmatischen Zyklus des Aves-Rückens an, sind aber deutlich älter als die Gesteine des Antillenbogens.

Die Altersbestimmungen an Hornblenden der Gabbro- und Gangintrusionen leisten einen wichtigen Beitrag zur Entwicklungsgeschichte der südlichen Karibik, insbesondere der Isla Margarita, für die ein detailliertes Modell der Druck-, Temperatur-, Alters- und

Verformungsgeschichte bereits existiert. Demzufolge befand sich die Isla Margarita vor ca. 50 Ma an der Nordwestspitze Südamerikas und bildete die südliche Verlängerung des Aves-Rückens. Die Platznahme der lamprophyrischen Gänge auf Margarita in bereits existierende konjugierte Scherbrüche signalisiert, daß sich das Nebengestein zum damaligen Zeitpunkt in einem seichten Krustenstockwerk oberhalb des spröd-duktilen Übergangs befand. Die Gabbros und Gänge wurden nur noch spröde in mehreren Stadien verformt. Der Margarita Komplex befindet sich bis heute in diesem seichten Krustenstockwerk und driftet mit der Karibischen Platte relativ zu Südamerika nach Osten. Dies ergibt eine perfekte Übereinstimmung mit plattentektonischen Modellen, denen ein pazifischer Ursprung der karibischen Platte zugrunde liegt.

2.

INTRODUCTION

2. INTRODUCTION

The Caribbean area, as defined here, including Central America, the Greater and Lesser Antilles and the northern boundary of South America, had a rich and varied igneous and tectonic history since the Mesozoic to the present time, related to the separation of North and South America. Igneous rock associations allow suggestions how they are related to contemporary tectonics and may also characterize certain time intervals.

The major associations of Caribbean igneous rocks are Jurassic to Late Cretaceous oceanic basalts and minor mafic and siliceous plutons (e.g. Netherland Antilles, Santamaria, 1972), Cretaceous to Tertiary calc-alkaline suites (e.g. Aves Ridge, Venezuelan offshore islands, Fox et al., 1971; Santamaria, 1972) and Tertiary to Holocene calc-alkaline and alkalic basaltic suites (e.g. Lesser Antilles; Donnelly et al., 1990).

Magmatic events, including granitic, trondhjemitic and basaltic to andesitic intrusions, occurred since Late Cretaceous time on Isla Margarita which is located on the northern margin of an active seismic zone, parallel to the Caribbean Mountain system of Venezuela. This zone is generally considered as the Southern Caribbean plate boundary. In northern Venezuela and Trinidad the plate boundary has been defined by many workers as being parallel to subparallel to the northern margin of South America (Speed, 1985, Ross & Scotese, 1988; Robertson & Burke, 1989; Pindell & Barrett, 1990). Their data indicate that this mountain system is the site of present right-lateral movement of the Caribbean plate. A consideration of the present-day right lateral strike-slip nature of this boundary and Mesozoic high-pressure metamorphic assemblages found there mark a fundamental difference between the present and Mesozoic tectonic regime.

The study of the geochemistry and geochronology of post-tectonic intrusive rocks, occurring as dikes and small gabbroic intrusions on Isla Margarita will provide a possibility to test the present plate tectonic models for the evolution of the southern Caribbean region (Burke et al., 1984, Ross & Scotese, 1988; Erlich & Barrett, 1990; Avé Lallemant, 1991). In particular, data can be provided on the origin of igneous rock suites generated during the period of transform plate interaction. While subduction produces a characteristic geochemical variation in rock types across an island arc, so that the polarity of the subduction can be determined, transform plate boundaries as yet are not characterized by any particular igneous rock suites; the study of intrusive magmatic rocks on Isla Margarita, situated close to a subduction zone and a transform fault may thus be able to contribute valuable information to the solution of this problem.

2.1 TECTONIC EVOLUTION OF THE CARIBBEAN

The origin of the Caribbean plate (Fig. 2.1) has been discussed with intense controversy on the question of *in situ* origin vs. genesis in the Pacific realm, followed by eastward movement relative to the American plate. Amongst numerous summaries and syntheses of the evolution of the Caribbean region, treating the Caribbean sea as a foundered landmass or a relict ocean basin, surrounded by island arcs, are those of Schuchert (1935) and Woodring (1954). The evolution of the Caribbean region, however, can apparently be better related to former plate boundaries between North and South America and to strike-slip, extensional and compressional motions.

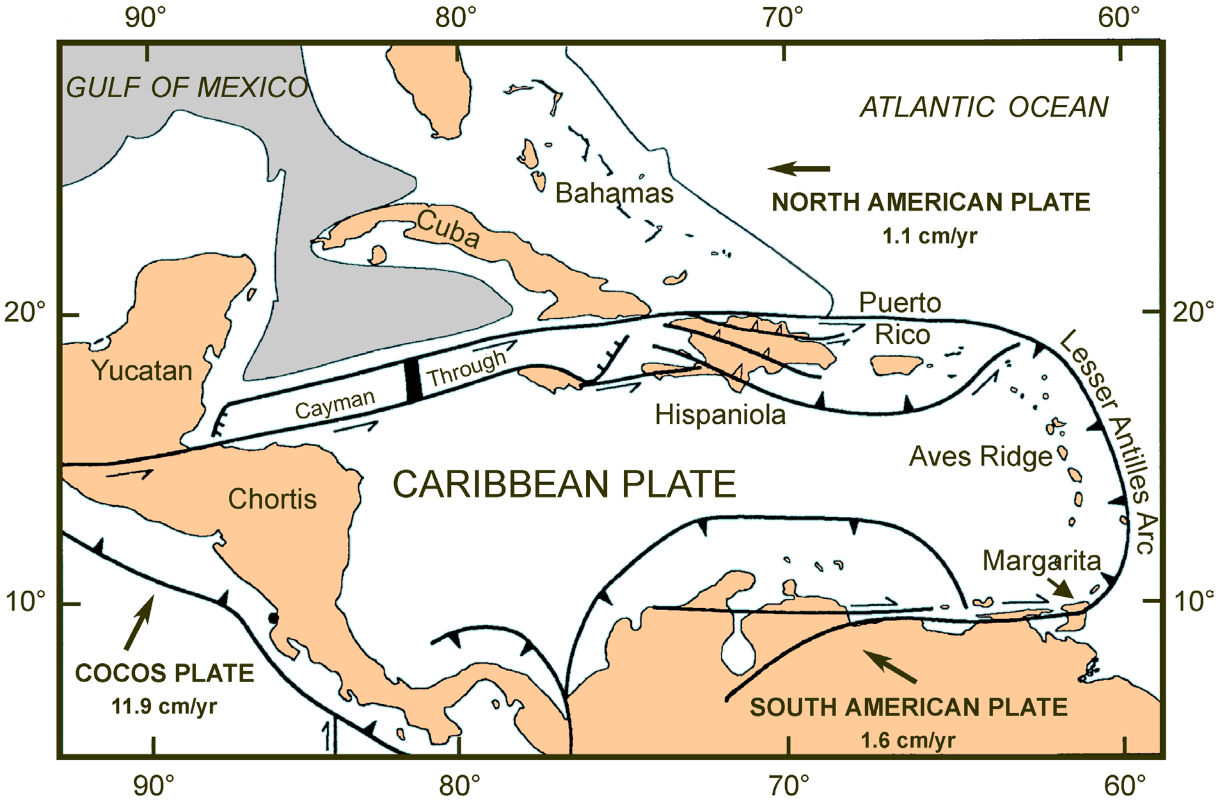

Figure 2.1:

Index map showing the position of Isla Margarita with respect to Caribbean geographic localities, geologic provinces and major structures after MacDonald (1990).

The presence of a Caribbean island arc terrane located on the northeastern corner of the Caribbean plate, the Bermeja Complex of Puerto Rico, which is significantly older than the Caribbean Sea, assures that *in situ* models are incorrect (Montgomery et al., 1994). Additional strati-graphic data and plate tectonic models suggesting Pacific origin were presented by Burke et al. (1984), Schellekens et al. (1990) and Montgomery et al. (1992).

Molnar & Sykes (1969), Pindell & Dewey (1982), Sykes et al. (1982) and Burke et al. (1984) suggested that the Caribbean crust is a fragment of the original Pacific plate which has been shaped by the interaction of the Farallon, North American and South American plate. The Caribbean plate was wedged eastwards between North and South America, as the two continents drifted apart. The major characteristics, shaping the present margins of the Caribbean plate, are the magnitudes and directions of relative motion of the plates bordering the Caribbean plate, and the crustal characteristics of the plates themselves. Estimates of present-day eastward movement of the Caribbean plate relative to the American plates are given with 2-4 cm/y (Burke et al., 1984). DeMets et al. (1990), however, postulated eastward movement with a rate of 1-1.5 cm/y.

The Caribbean - South American plate boundary in northeastern Venezuela is characterized by a series of strike-slip faults (Molnar & Sykes, 1969). Additional diffuse seismicity may be related to underthrusting of the Caribbean plate beneath South America, or microplates such as the Andean or Maracaibo blocks, or to details of deformation within the plate-boundary zone (McCann & Pennington, 1990). One of the remaining disagreements in southern Caribbean tectonics is the significance of earthquakes at intermediate depths beneath South America. Pennington (1981) showed that these earthquakes lie along an apparent Benioff zone continuous with oceanic crust of the Caribbean Sea north of Colombia, and presumed that they represented active subduction of the Caribbean plate beneath the overriding Andean block. Pérez & Aggarwal (1981), on the other hand, considered the seismicity to be a remanent feature, and concluded that current subduction, if there is any, is insignificant.

Reconstructions of the Cenozoic plate history of the southern corner of the Caribbean, in particular the northern Venezuela-Trinidad area, (Erlich & Barrett, 1990), indicate another terrane represented by the "Margarita Block", including Isla Margarita, the Araya/Paria Peninsula, Tobago and N-Trinidad (Figure 2.2). This block is considered to have moved approximately 550 km towards the east since Middle Eocene time (Erlich & Barrett, 1990). Lithologic, biostratigraphic and geochemical data suggest that the metamorphic rocks of Isla Margarita, the Araya/Paria Peninsula, Tobago and the Northern Range of Trinidad were once part of the Cordillera de la Costa of Venezuela (Erlich & Barrett, 1990). The present tectonic position is immediately north of what is generally considered as the southern Caribbean plate boundary.

Isla Margarita is situated along the southern continuation of the N-S trending, extinct Aves volcanic arc and southwest of the active Lesser Antilles arc. Accordingly, it represents a unique location considering this zone as a plate junction and allows testing of current plate tectonic models for the evolution of the Caribbean. The study of post-metamorphic igneous rocks occurring as dikes and small gabbroic intrusions on Margarita island will thus be profitable in the discussion of the younger tectonic history of the island.

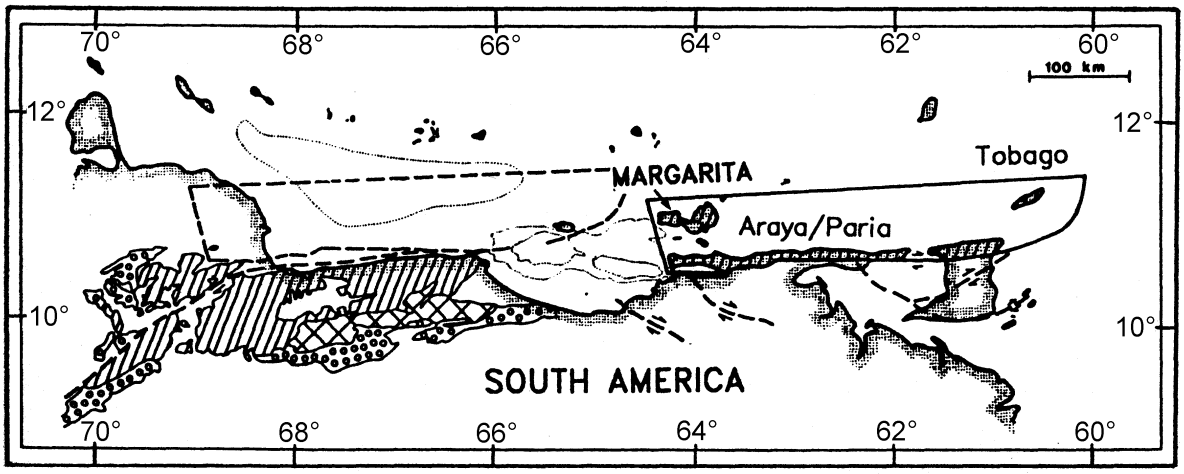

Figure 2.2:

The Margarita Block with Isla Margarita, the Araya/Paria Peninsula and N-Tobago in its present (solid line) and mid-Eocene (dashed line) position as defined by Erlich & Barrett (1990). Signatures indicate corresponding basement rocks. (Oblique hatching: Cordillera de la Costa; cross hatching: Villa de Cura Group; circles: Paleocene to Eocene flysch deposits).

2.2 GEOLOGY OF ISLA MARGARITA

The Island of Margarita is located approximately 30 km off the northeastern coast of Venezuela and covers an area of 1150 km^2. The E-W extension of the island is about 65 km, the N-S extension about 35 km. Margarita Island can be divided physiographically into two parts connected by lagoons and beach deposits (Figure 2.3). The western peninsula is generally known as Macanao, the larger eastern part as Paraguachoa. Elevations reach about 700 m a.s.l. on Macanao and 1000 m a.s.l. on Paraguachoa.

Figure 2.3:

Overall view of Isla Margarita with Paraguachoa (foreground) and Macanao (background).

Among the first geologically oriented investigations Sievers (1898) studied the geology of the islands located north of Venezuela, from Aruba to Margarita. Geological studies of the Peninsula de Paria and Isla Margarita have been published by Kugler (1957), Metz (1968) and Gonzalez de Juana (1974). The geological setting of Margarita has been described in detail by Hess & Maxwell (1949), Taylor (1960), Schubert (1971), Gonzalez de Juana & Vignali (1971), Maresch (1971, 1972, 1975), Maresch & Abraham (1981), Beets et al. (1984), Chevalier (1987), Avé Lallemant (1991), Guth & Avé Lallemant (1991) and Stöckhert et al. (1993, 1995).

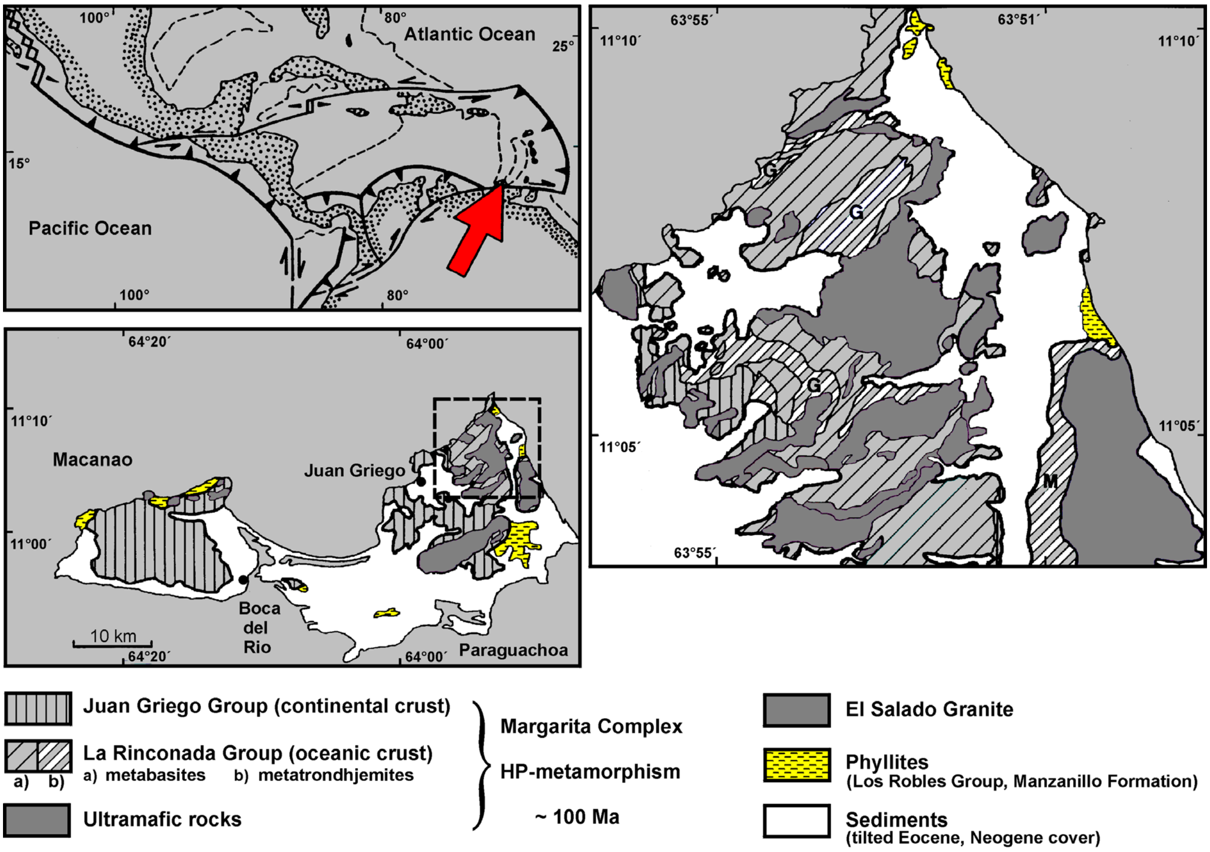

Figure 2.4:

Plate tectonic setting and geological map of Isla Margarita (after Stöckhert et al., 1995).

Accordingly, the basement rocks of Margarita (Figure 2.4) consist of four major, strongly deformed lithological units:

1) mantle peridotites (largely serpentinized)
2) "La Rinconada Group" (eclogite to epidote-amphibolite -facies metabasites, representing former oceanic crust)
3) "Juan Griego Group" (greenschist-facies acid gneisses and metasediments containing relics of earlier high-pressure assemblages, representing earlier continental crust)
4) "Los Robles Group" (greenschist-facies metasediments and acid metavolcanics lacking older metamorphic remnants)

Magmatic intrusions into the metamorphic units provide a reference system for the tectonic events. Among these are Metatrondhjemites of type Guayacán orthogneis (114-105 Ma, Kluge et al, 1992) which intruded into the "La Rinconada Group". High-pressure barroisitic amphibole occurring in these metatrondhjemites give evidence that the high-pressure event is younger than the intrusions. Another intrusive complex in the "La Rinconada Group" is the "El Salado granite" (86 Ma, Kluge et al., 1992) which is strongly sheared but shows no sign of high-pressure metamorphism and consequently defines the age of the high-pressure metamorphic event as older than 86 Ma. Further intrusive rock suites include metagabbros, concentrated along shear zones, undeformed small gabbroic intrusions and lamprophyric dikes which intruded into various rock units. Younger rock units on Isla Margarita include faulted and tilted Eocene sediments and horizontal terrigenous clastic deposits which have been described by Hunter (1978) to be of Late Miocene age.

The structural and petrological evolution of Isla Margarita might be best represented by a detailed model established by Stöckhert et al. (1993, 1995), which can be correlated to plate tectonic reconstructions by Ross & Scotese (1988) (Figure 2.5).

The evolutionary history of Margarita, presented by Stöckhert et al. (1993, 1995), assumes four major steps through different tectonic environments such as (1) deep level of an accretionary complex, where continental and oceanic crust and mantle material were welded together and suffered high pressure metamorphism with temperatures of 500 to 600°C, (2) intermediate level of a newly developing magmatic arc, possibly related to changing subduction polarity, with trondhjemitic and granitic intrusions emplaced into mantle peridotite, dated with 112 and 86 Ma respectively, (3) intermediate crustal level with strong deformation under upper greenschist-facies conditions less than 86 Ma b.p.. The development of a horizontal, NE to ENE stretching lineation indicates that the Margarita Complex was situated close to a conservative plate boundary and deformed in a strike-slip regime, (4) shallow level within a strike-slip regime, close to a conservative plate boundary, with gabbroic intrusions concentrated in shear zones. Transition into the brittle field is associated with repeated changes of the regional stress field and opening of conjugate shear fractures. Basaltic to andesitic magmas rise again and result in small gabbroic complexes and in dikes concentrated in the preexisting conjugate shear fractures.

The tectonic record of Isla Margarita as such provides valuable constraints on the evolution of the southern Caribbean region, particularly during the late Mesozoic.

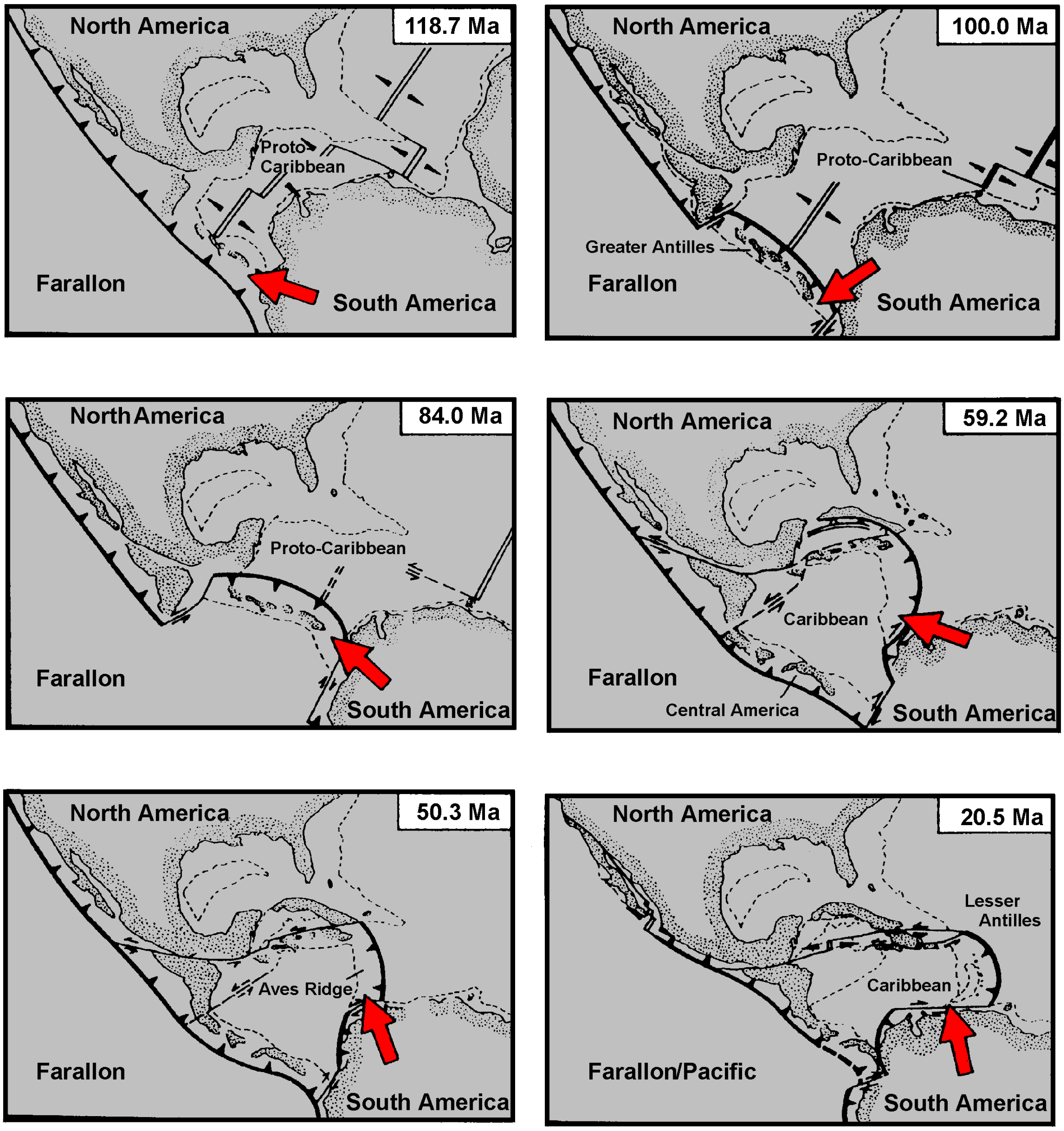

Figure 2.5:

Position of Isla Margarita from 118.7 to 20.5 Ma (arrow, after Stöckhert et al., 1993, 1995) in relation to plate-tectonic reconstructions of the Caribbean region after Ross & Scotese (1988).

2.3 OBJECTIVES OF THIS STUDY

This study was initiated as an attempt to interpret the pre-Neogene geochemical and tectonic evolution of the late igneous rock suite, occurring as small gabbroic intrusions and lamprophyric dikes on Isla Margarita. This work also includes some petrographic and geochemical investigations on earlier metagabbros.

Petrographic and mineral chemistry studies, as well as whole rock analyses, including major-, trace-, rare earth element, isotopic and geochronological investigations, should reveal geologically relevant data on the problem of magma genesis along the southern Caribbean plate boundary. The distribution of major and trace elements is used to interpret the origin and evolutionary history of the igneous rocks.

Isotopic composition of the rock suite studied allows constraints on magma sources and/or contamination processes. Age dating of dike and gabbro samples by $^{40}Ar/^{39}Ar$ analyses permits correlation of this late intrusive period with plate tectonic scenarios. Consequently, the magmatic rocks provide an important reference system for the late tectonic history of the Margarita crust. The objectives in detail are to determine:

(1) the source composition and role of partial melting

(2) the role of crystal fractionation

(3) the possible role of crustal contamination

(4) spatial and temporal variations of distinct
magmatic suites

(5) temporal correlation of dike and gabbro intrusions
with plate tectonic reconstructions

3.

THE MARGARITA IGNEOUS ROCK SUITE

3. THE MARGARITA IGNEOUS ROCK SUITE

3.1 LAMPROPHYRIC DIKES

The youngest igneous rocks on Isla Margarita represent unmetamorphosed, calc-alkaline lamprophyric dikes, occurring within the metamorphic complex of the island. The dikes are mainly exposed in coastal areas and road cuts, in the northern parts of the eastern peninsula (Paraguachoa), between Juan Griego and El Agua and on the western peninsula (Macanao) between Robledal and La Auyama. Four different dike suites have been sampled and named after their local occurrence as the Manzanillo suite, Cabo Negro suite, Playa Caribe suite and the Macanao suite. Sample localities are shown in Figure 12.1 (Appendix).

Figure 3.1:

Near-vertical dike swarm at Playa Caribe. See human for scale.

Figure 3.2:

Manzanillo dikes following country-rock fractures. Long side of photograph ca. 15 m.

The dikes appear as grey to slightly greenish, fine to medium grained rocks, with amphibole and/or clinopyroxene phenocrysts no larger than 0.5 mm. They occur as swarms (Figure 3.1) or isolated dikes, frequently showing chilled margins ranging between a few millimeters to one centimeter. Magmatic flow orientation could not be recognized macroscopically. Country rock xenoliths occur sparsely near dike margins. The dikes are generally simple, near-vertical tabular intrusions, their widths vary between 0.15 to 1.50 m, the majority clustering about 0.20-0.30 m. The dikes cut across folds and schistosity of the Margarita country rocks. They frequently follow preexisting conjugate shear fractures (Figure 3.2) and crosscut earlier quartz veins. The dikes themselves are cut by various faults, including a set of reverse faults (Figure 3.3).

Figure 3.3:

Faulted Manzanillo dike showing dextral displacement of ca. 25 cm. Long side of photograph ca. 3 m.

Dike orientation

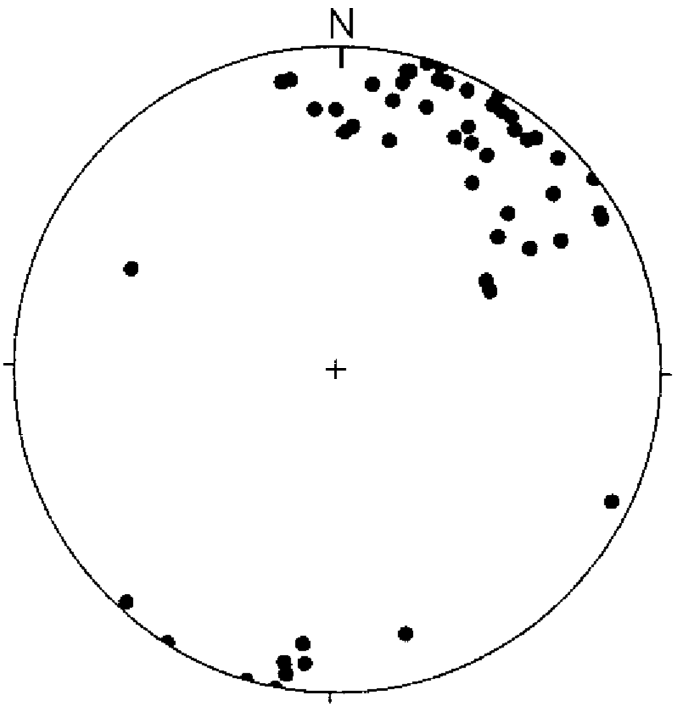

Figure 3.4:

Lower hemisphere equal area pro-jection of poles of dikes from Isla Margarita.

The great majority of dikes strikes NW-SE, roughly normal to the NE trending stretching lineation of the metamorphic basement of Margarita (Stöckhert et al., 1993). A small number of dikes has no particular relationship. Dipping of the dikes varies from 53 to 90 degrees, averaging around 82 degrees (Figure 3.4).

3.2 SMALL GABBROIC INTRUSIONS

Two macroscopically different, nonmetamorphic gabbroic units can be distinguished within the metamorphic Manzanillo Formation, along the northeastern coast of Isla Margarita, at Punta Cazonero between Cabo Negro and Playa El Agua. The widths of the intrusions exposed along the coastal outcrop does not exceed 5-6 m; the continuation inland exceeds 25 m, but can not be recognized exactly. Both gabbros are relatively homogeneous and undeformed, but they are crosscut by a younger dike (Figure 3.5) and offset about 2.5 m by a minor fault.

Figure 3.5

Faulted Cabo Negro Gabbro (6055) crosscut by dike (6056). Long side of photograph 3m.

The two gabbros differ mainly in color with one light- and one dark grey, medium to coarse grained type. Plagioclase and hornblende are the major constituents. Crystal size averages around 3-4 mm. Limited mixing between the two gabbroic varieties can be recognized macroscopically. Igneous lamination is absent and the Margarita gabbros differ from larger, layered intrusions in this respect.

3.3 METAGABBROS

Several metamorphic and foliated gabbros are concentrated along the shear zone south of Playa El Agua at Punta Cabo Blanco (Figure 3.6), showing strong deformation and metamorphism under greenschist-facies conditions. The distinct metagabbroic units display elongate shapes ranging in widths from 0.4 to 1.8 m and lengths up to several meters. Orientation of the shear zone is generally NE-SW. The color of metagabbros ranges from dark grey to green and grain size ranges from medium to coarse. Plagioclase, hornblende and actinolite could be macroscopically observed as the major mineral phases.

Figure 3.6:

Foliated metagabbro at Punta Cabo Blanco. Long side of photograph ca. 25 cm.

4.

PETROGRAPHY

4.1 LAMPROPHYRIC DIKES

4.1.1 TEXTURES

The lamprophyric dike suites of Isla Margarita display heterogeneous textures, however, two major textural types can be distinguished, intersertal to porphyric with occasional occurrence of flow orientation (Figure 4.1). Clinopyroxene and amphibole are the dominant phenocrysts and occur locally as glomerophyric aggregates (Figure 4.2). Plagioclase is a minor phenocryst, but occurs frequently in the groundmass. Potassium feldspar is absent.

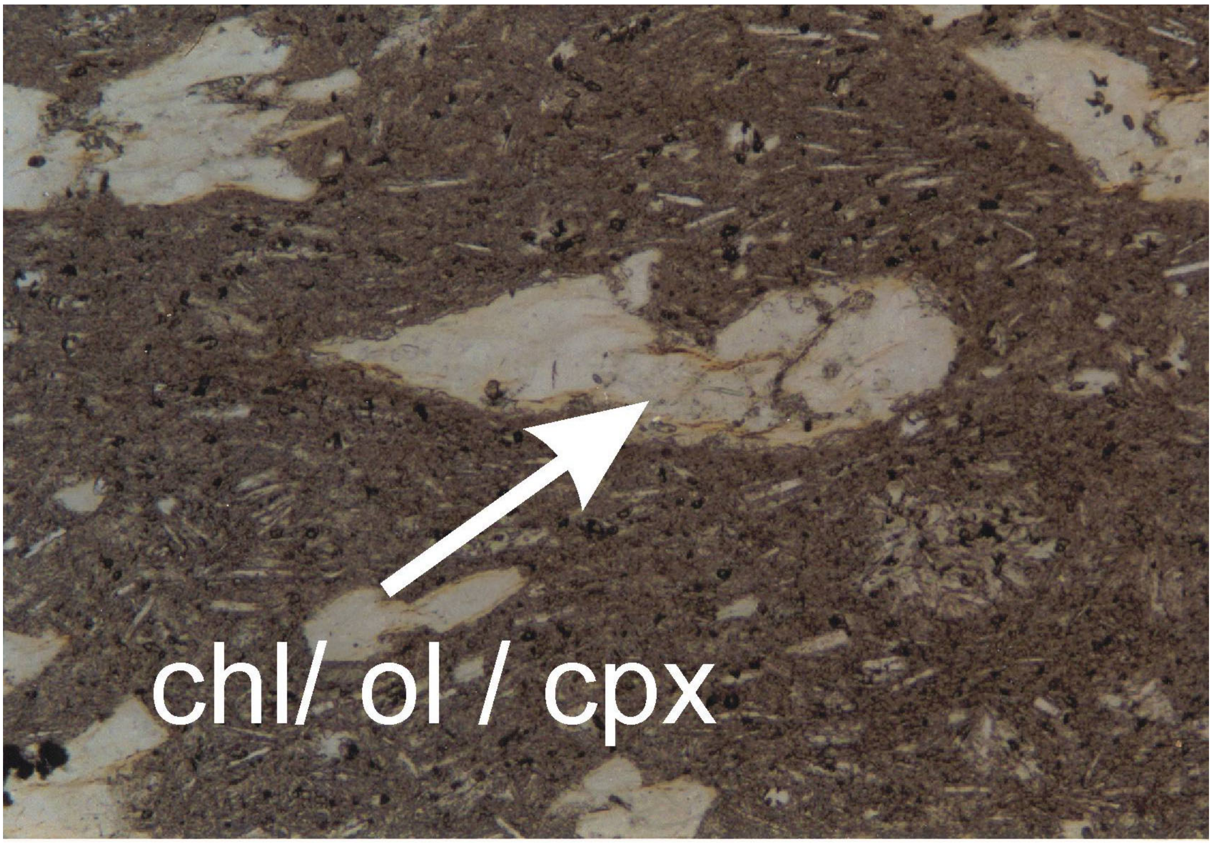

Figure 4.1:

Flow orientation in Manzanillo dike (6007) with chlorite replacing olivine?/clinopyroxene phenocrysts. Long side of photomicrograph 1.75 mm.

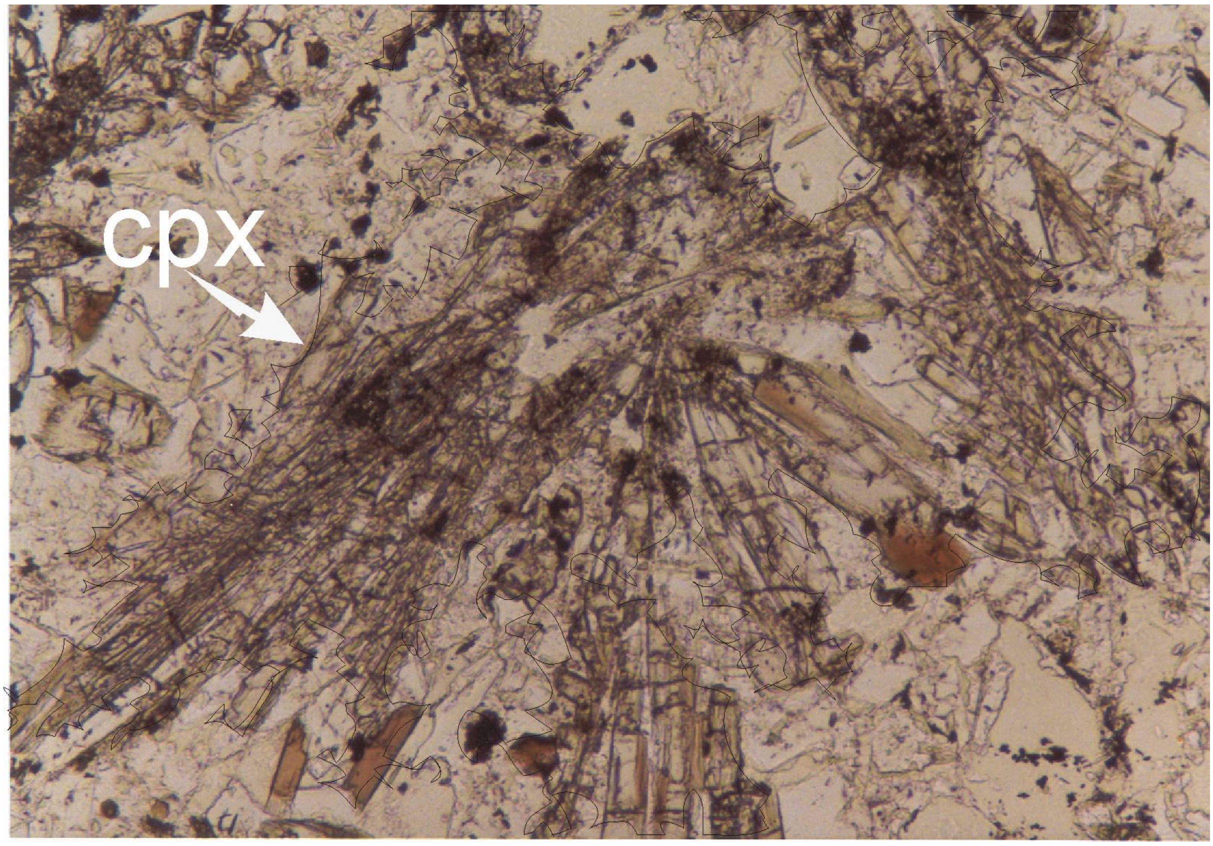

Figure 4.2:

Clinopyroxene as glomerophyric aggregate in dike (6107) from Playa Caribe. Long side of photomicrograph 3.5 mm.

Given these mineralogical criteria, the lamprophyres can be further classified as spessartites with plagioclase > alkalifeldspar in the groundmass and clinopyroxene and hornblende as the dominant phenocryst phases (Rock, 1984; Wimmenauer, 1985). They share the same (clinopyroxene-, hornblende-, plagioclase-) mineralogy as basalts and basaltic andesites, however, some criteria distinguish the Margarita lamprophyres from common basaltic - andesitic suites, as they lack orthopyroxene, but contain primary (in the sense of late magmatic) carbonate and sulphate (galena).

The principal diagnostic feature of the Margarita lamprophyres and lamprophyres in general are the two generations of euhedral mafic minerals, clinopyroxene and amphibole. Pseudomorphs after olivine phenocrysts occur in the most basic dike samples; magnetite may have been present but is now replaced by hematite. Plagioclase is the dominant groundmass phase, but rare phenocrysts or microphenocrysts also occur. Even in the "freshest" rocks phenocrysts and groundmass display variable degrees of hydrothermal alteration with chlorite, actinolite, epidote and sericite as the dominant alteration products.

A characteristic feature of the lamprophyre suite is the presence of spherical or ellipsoidal patches, termed ocelli, which reach 1 to 2 mm in diameter (Figure 4.3). They are concentrated in samples taken from the center of the dikes and absent in samples from dike margins.

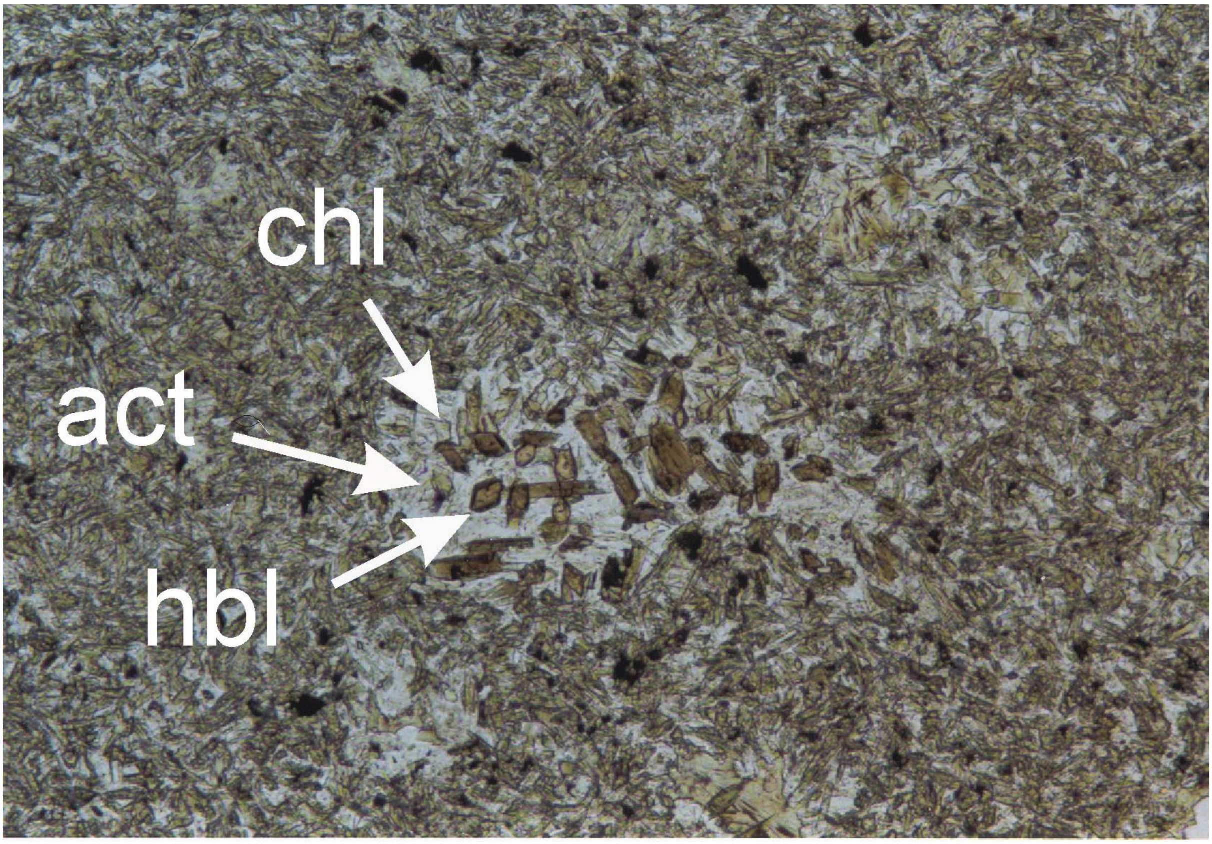

Figure 4.3:

Photomicrograph of ocellus with hornblende (hbl), actinolite (act), chlorite (chl) and carbonate (cc) filling in dike (6041) from Cabo Negro. Long side of photomicrograph 3.5 mm.

Most ocelli are composed of tangentially arranged minerals such as hornblende, actinolite, plagioclase, opaque phases and calcite. Ocelli frequently coalesce to give irregular segregations and veins (Figure 4.4). Segregation veins and locally irregular matrix concentrations display the same mineralogical character as the spheroidal bodies described above.

Formation of the spheroidal and segregation structures in the Margarita rocks is characteristic for the abundance of H_2O, CO_2 and other volatile components in lamprophyres. It can be attributed to vesiculation when crystallization is advanced and the melt phase is drawn into the remaining space of the vesicle (Cooper, 1979).

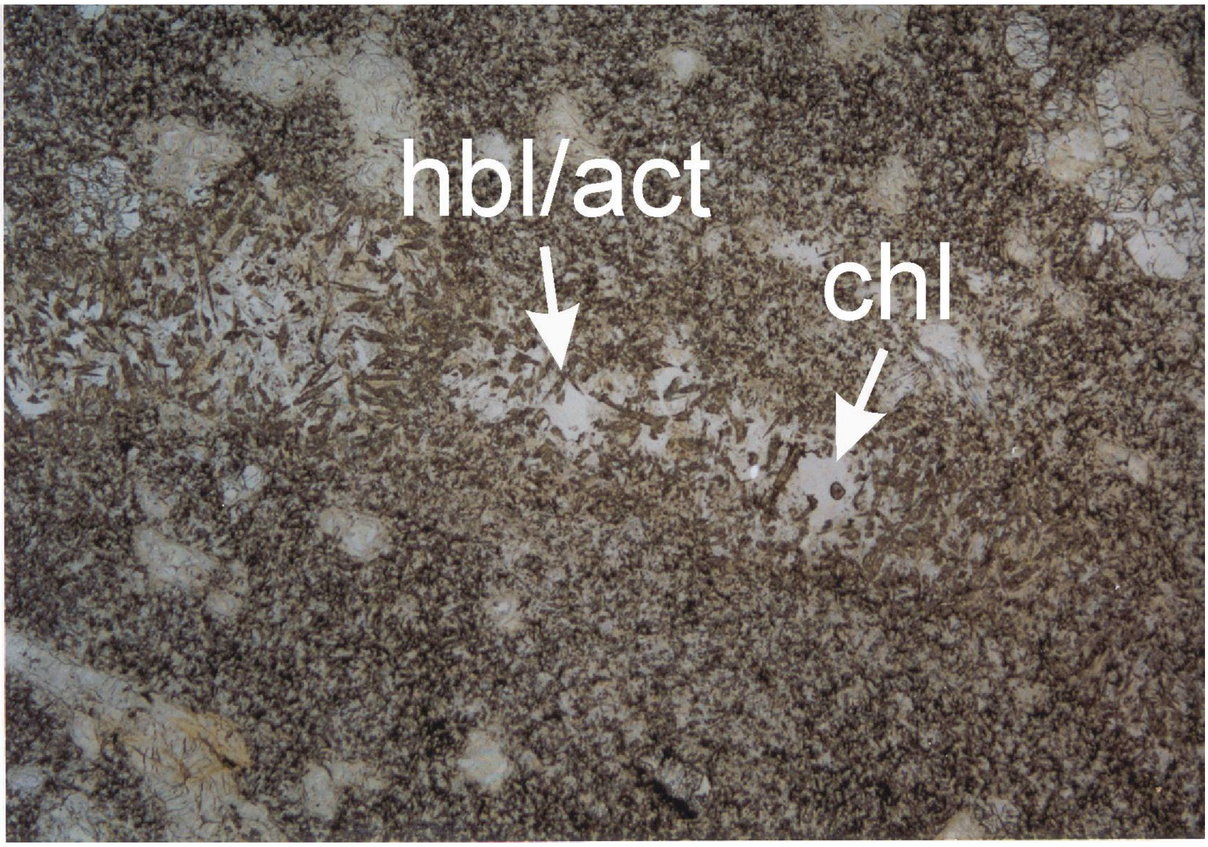

Figure 4.4:

Segregation vein in Manzanillo dike (6013) with hornblende, actinolite and chlorite filling. Long side of photomicrograph 7 mm.

4.1.2 MODAL COMPOSITIONS

Olivine, as mentioned above, is not preserved. Rare, characteristically shaped pseudomorphs of fine Mg-chlorite, however, suggest its earlier presence as a minor phenocryst phase (see Figure 4.1).

Clinopyroxene phenocrysts (generally diopsidic augite) are invariably present, either as single euhedral crystals or glomeroporphyritic aggregates, their sizes reaching up to 0.8 mm and volume percentage up to 15%. Aggregates show irregular, rounded, grain-to-grain contacts, but well-developed crystal faces towards the groundmass. Occasional twinning and optical zonation of single phenocrysts has been observed (Figure 4.5).

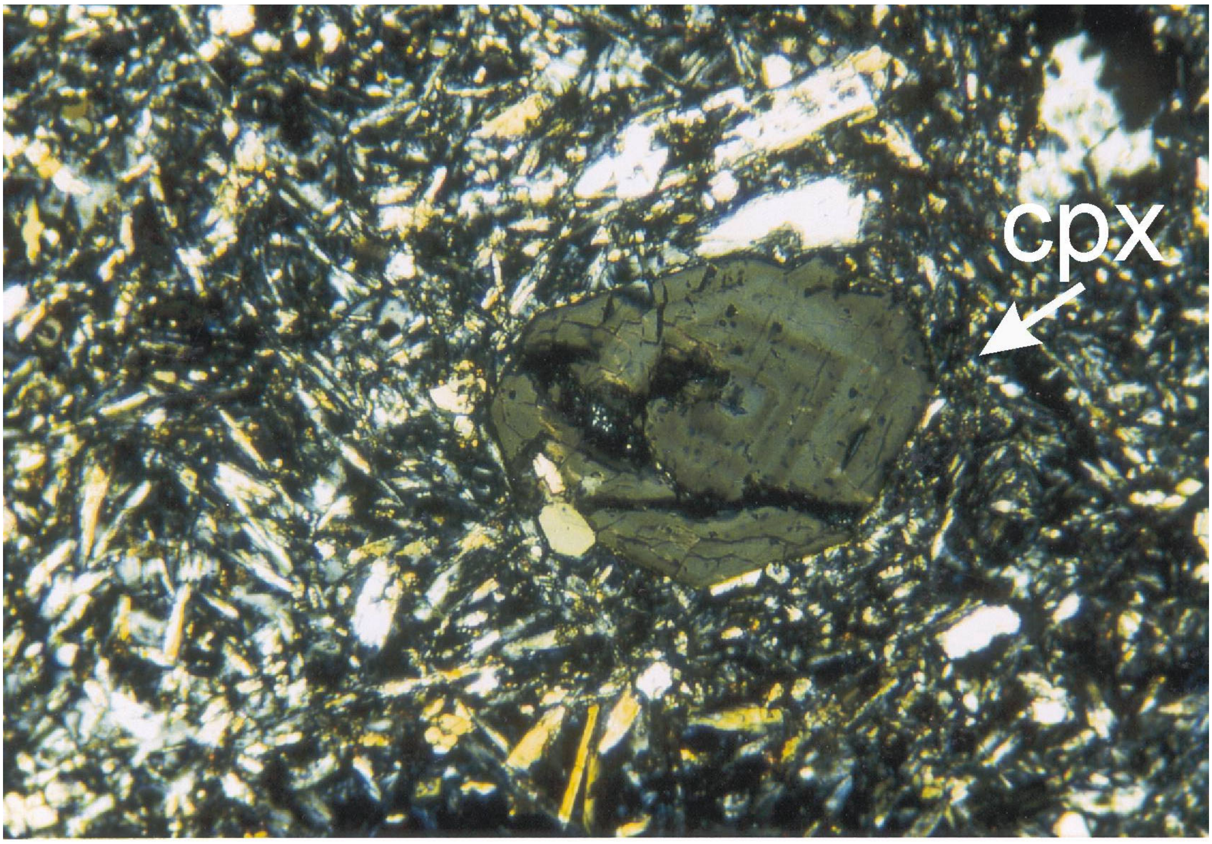

Figure 4.5:

Photomicrograph of multiply zoned clinopyroxene phenocryst in dike (6003) from Manzanillo. Long side of photomicrograph 1.75 mm.

Clinopyroxene phenocrysts show rims of fibrous amphibole, in most cases consisting of pale green actinolite (Figure 4.6). Groundmass pyroxene is augite with a volume proportion reaching 20% and grain size up to 120 µm. Within the higher differentiated samples, pyroxene becomes subordinate to hornblende, both in size and abundance and can even be absent as a phenocryst.

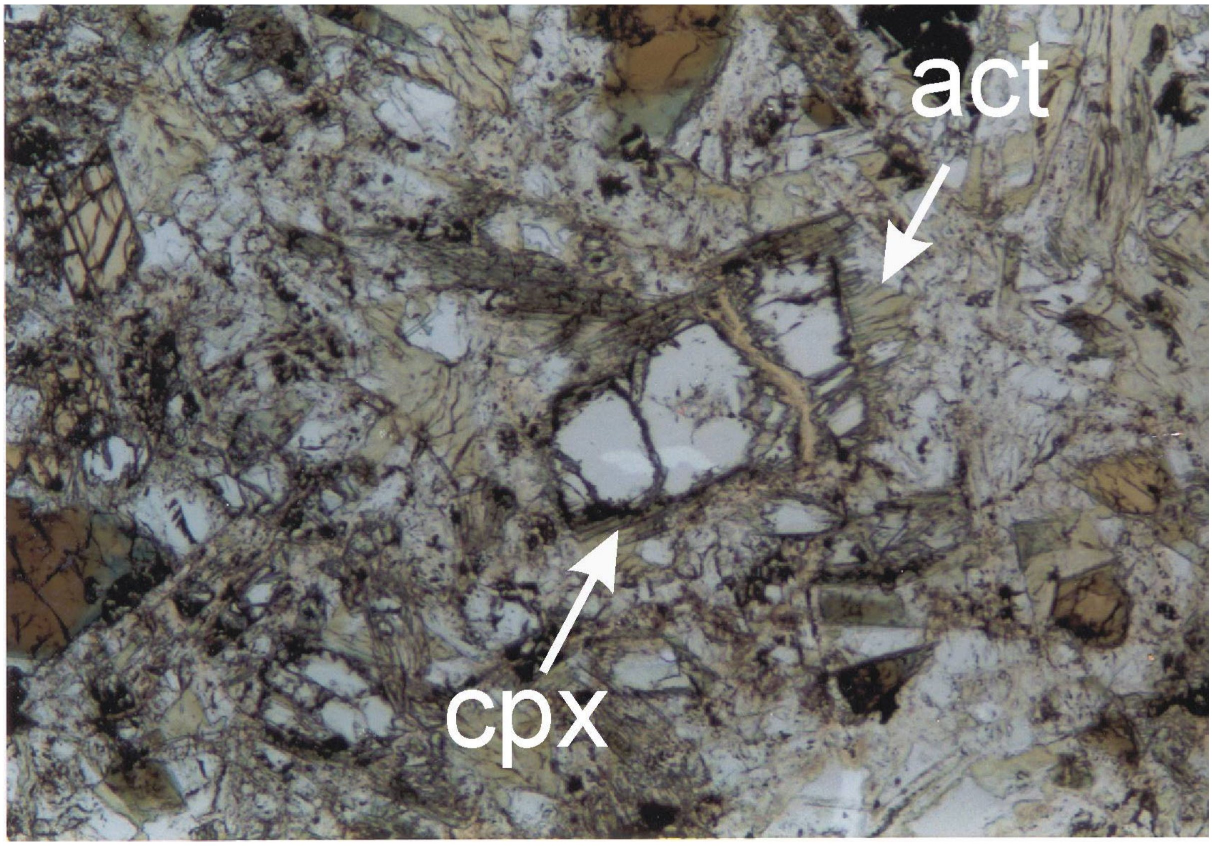

Figure 4.6:

Photomicrograph of clinopyroxene with actinolite rim in dike (6008) from Manzanillo. Long side of photomicrograph 3.5 mm.

Plagioclase is the dominant groundmass phase with a total volume ranging from 48% to 75%. The grain size of groundmass plagioclase reaches up to 160 µm. Rare, sub- to euhedral plagioclase phenocrysts, or plagioclase inclusions in hornblende, reach sizes up to 0.5 mm and vary in composition from An_{16} to An_{84}. Plagioclase phenocrysts are occasionally pristine and show evidence of oscillatory zoning, but are usually cloudy due to sericitic alteration (Figure 4.7).

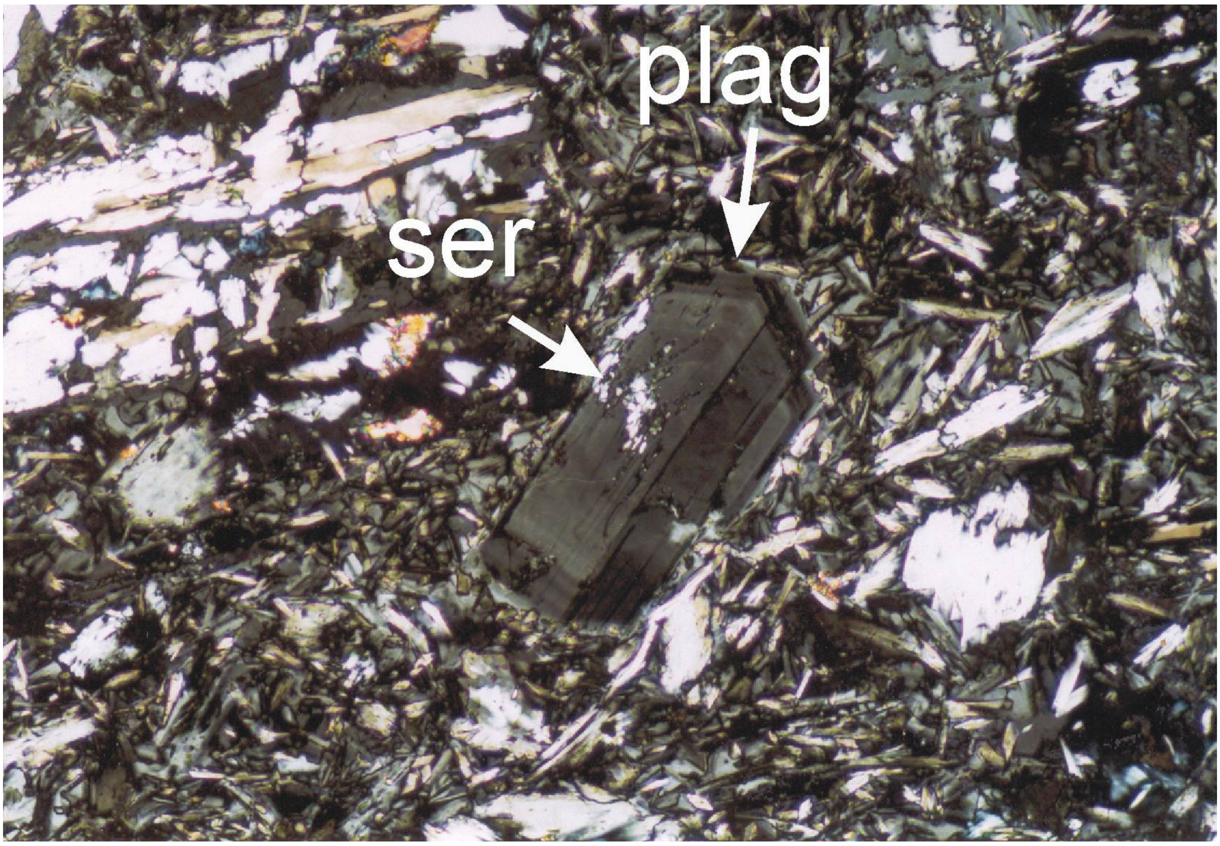

Figure 4.7:

Photomicrograph of twinned and multiply zoned plagioclase phenocryst, partly altered to sericite, in dike (6009) from Manzanillo. Long side of photomicrograph 1.75 mm.

Euhedral amphibole is light to dark brown hornblende, present as phenocryst and groundmass phase. Amphibole often contains inclusions of pyroxene and plagioclase, indicating that it was a late crystallizing phenocryst phase. Rims of heterogeneous composition, such as greenish actinolite or colorless tremolite, occur on hornblende phenocrysts and reach grain sizes up to 0.5 mm (Figure 4.8). Amphibole phenocrysts lack semi-opaque (opacite) reaction rims which are usually attributed to rapid magma ascent when amphibole passes out of the stability field at low pressures (e.g. Gill, 1981). Total amphibole content reaches up to 23 vol%. Amphibole is the only phenocryst phase that contains clinopyroxene as inclusion.

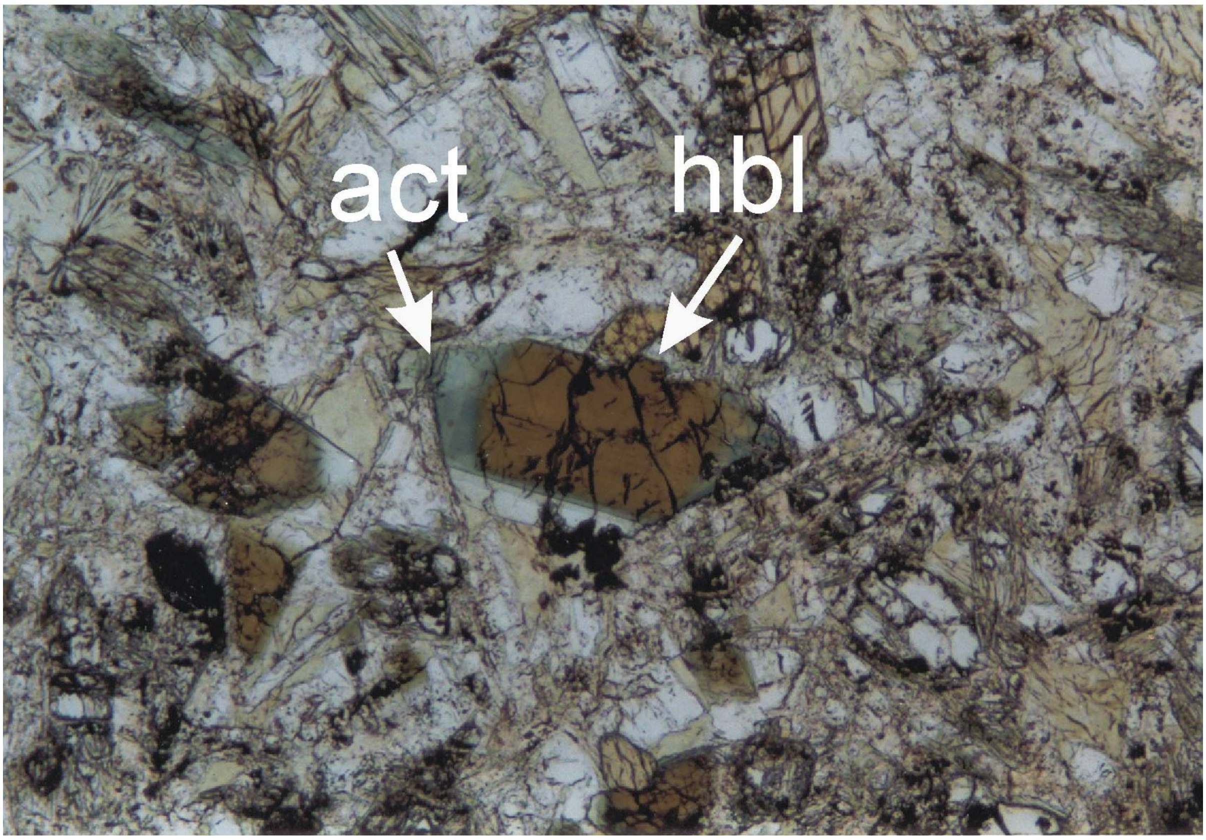

Figure 4.8:

Photomicrograph of hornblende phenocryst mantled with actinolite in dike (6008) from Manzanillo. Long side of photomicrograph 3.5 mm.

Ilmenite is present as a subordinate phenocryst phase reaching 2-3 vol% in a small number of samples of the Cabo Negro dike suite, but is not a widespread phase in other dike samples.

Chromite is present amongst the accessory mineral phases in the most basic samples, frequently as euhedral inclusion in clinopyroxene with <50 µm or as sub- to anhedral, strongly embayed phenocryst reaching 500 µm in diameter (Figure 4.9).

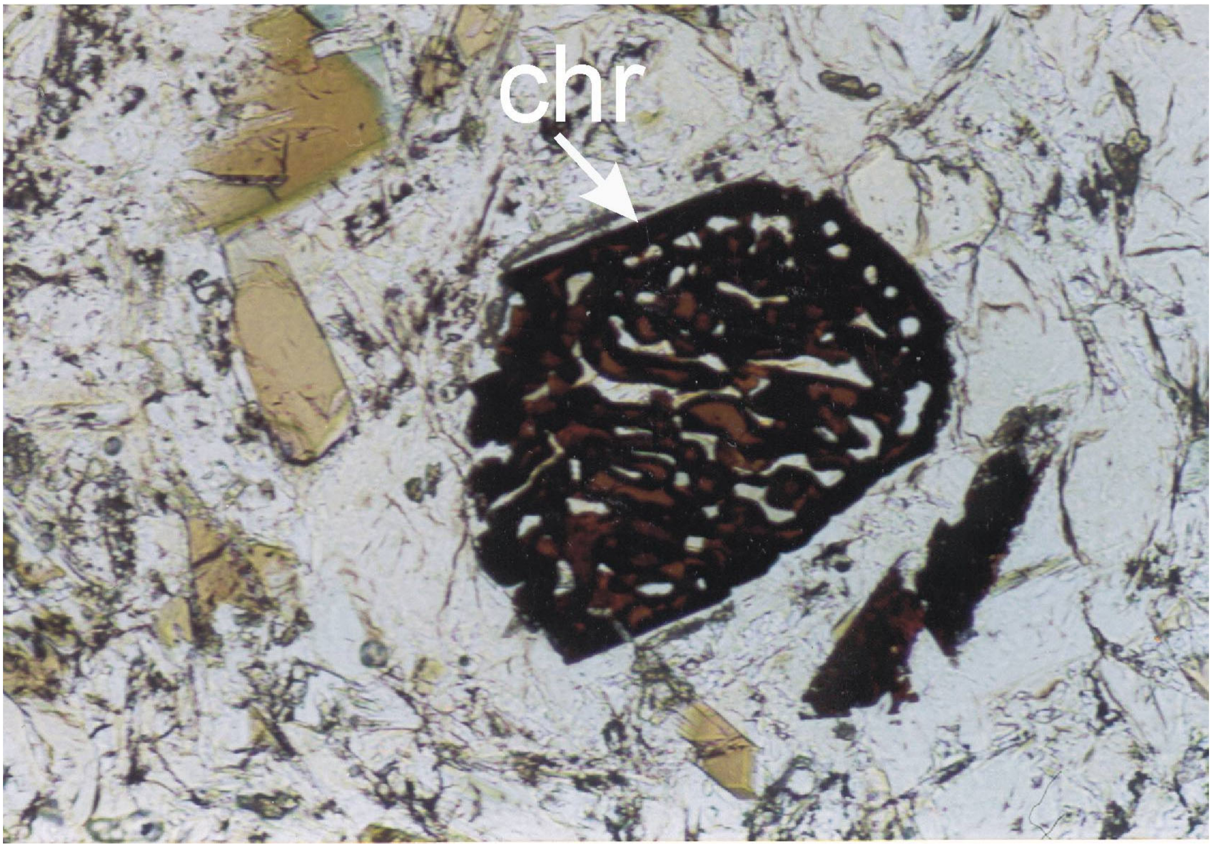

Figure 4.9:

Photomicrograph of partly euhedral, partly resorbed chromite phenocryst in dike (6049) from Cabo Negro. Long side of photomicrograph 1.75 mm.

Galena is an accessory sub- to anhedral constituent with a grain size <80 µm.

Late stage, subsolidus or hydrothermal alteration products replacing phenocrysts and groundmass minerals are common and include actinolite (5-25%), albite (5-30%), chlorite (3-15%), epidote (0-4%), quartz (0-4%), carbonate (0-5%), hematite (1-3%) and accessory leucoxene, rutile and muscovite (sericite) (Figure 4.10).

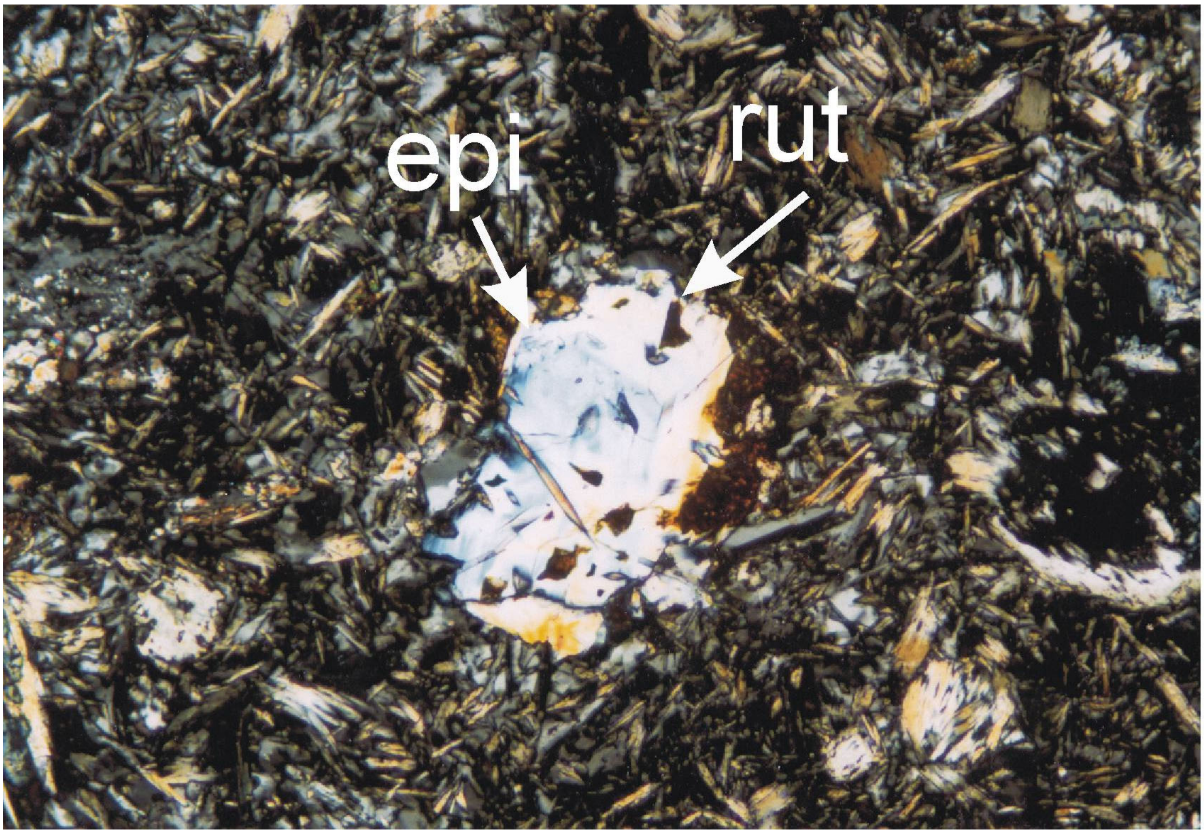

Figure 4.10:

Epidote and rutile in actinolite groundmass in dike (6009) from Manzanillo. Long side of photomicrograph 1.75 mm.

As noted above, even the "freshest" samples are variably altered, usually to chlorite, actinolite, epidote or carbonate. This is especially the case in the finer grained matrices. Otherwise granular pyroxene with interstitial feldspar plus opaque dust can be discerned.

4.2 SMALL GABBROIC INTRUSIONS

4.2.1 TEXTURES AND MODAL COMPOSITIONS

The gabbroic intrusions display cumulate texture with plagioclase, amphibole and clinopyroxene as the dominating constituents. Subhedral plagioclase is the dominant mineral phase with variations in content between 55 and 72 vol%. Grain sizes vary between 0.4 and 5 mm. Plagioclase compositions range from An_7 to An_{88}. Sericitization of plagioclase in gabbroic rocks was also observed, but generally plagioclase crystals are better preserved in the gabbroic intrusions than in dikes. Plagioclase inclusions up to 0.15 mm in size occur in amphiboles. The composition of these inclusions ranges from An_{81} to An_{86}.

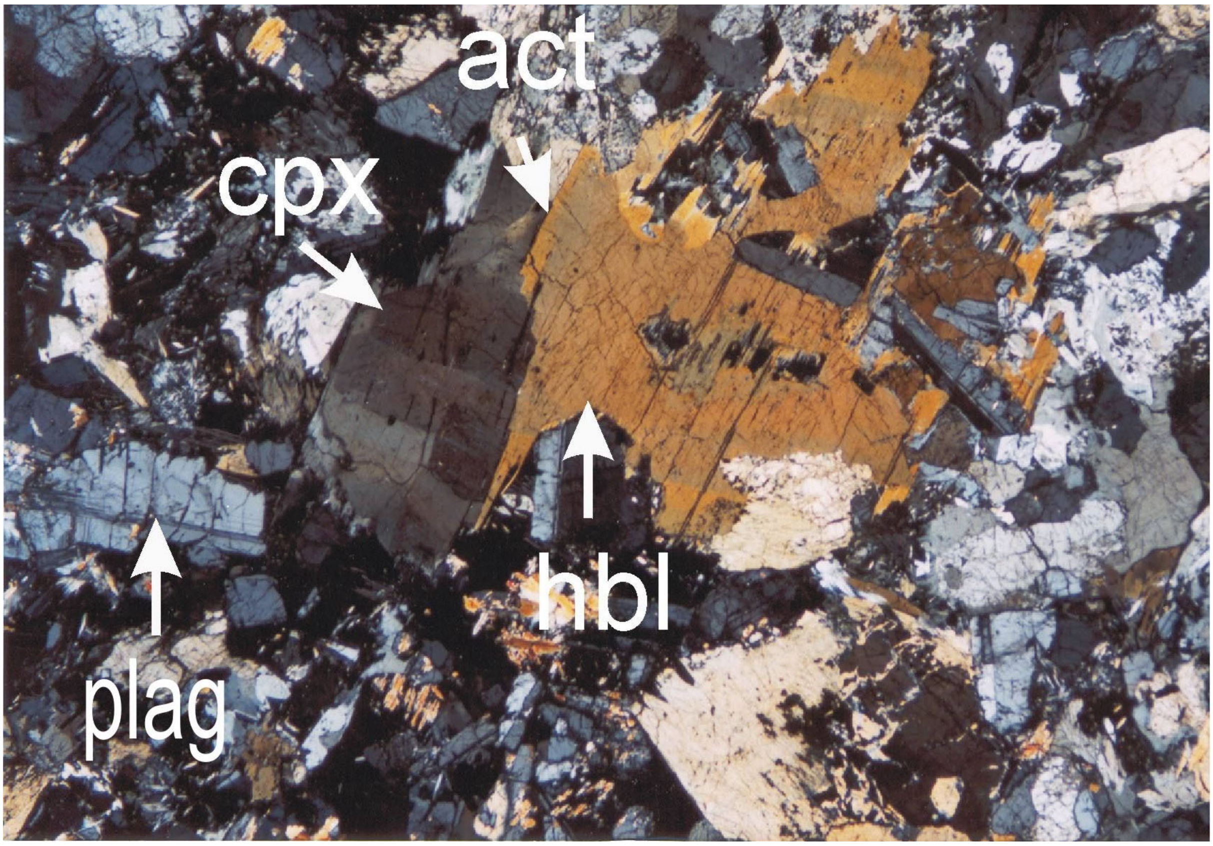

Figure 4.11:

Photomicrograph of Cabo Negro gabbro (6058) with clinopyroxene (grey), hornblende (brown) mantled by actinolite (yellow) and plagioclase. Note plagioclase inclusions in hornblende and sericitization of plagioclase below. Long side of photomicrograph 7 mm.

Amphiboles have maximum grain sizes of 2.5 mm and their total content reaches 30-45 vol%. The gabbroic amphiboles are, similar to amphiboles in dikes, present as composite grains of hornblende cores and actinolite rims (Figure 4.11). Different textural relationships of hornblende are found in the gabbroic rocks: a) poicilitic to ophitic with inclusions of plagioclase; b) replacement or intergrowth with diopsidic augite (uralitization). The total content of clinopyroxene in gabbroic intrusions does not exceed 15 vol%. Similar to amphiboles in dikes, those in gabbros lack opacite rims.

Accessory mineral phases include euhedral sphene (Figure 4.12) and sub- to anhedral and occasionally strongly embayed chromite with grain sizes up to 250 µm.

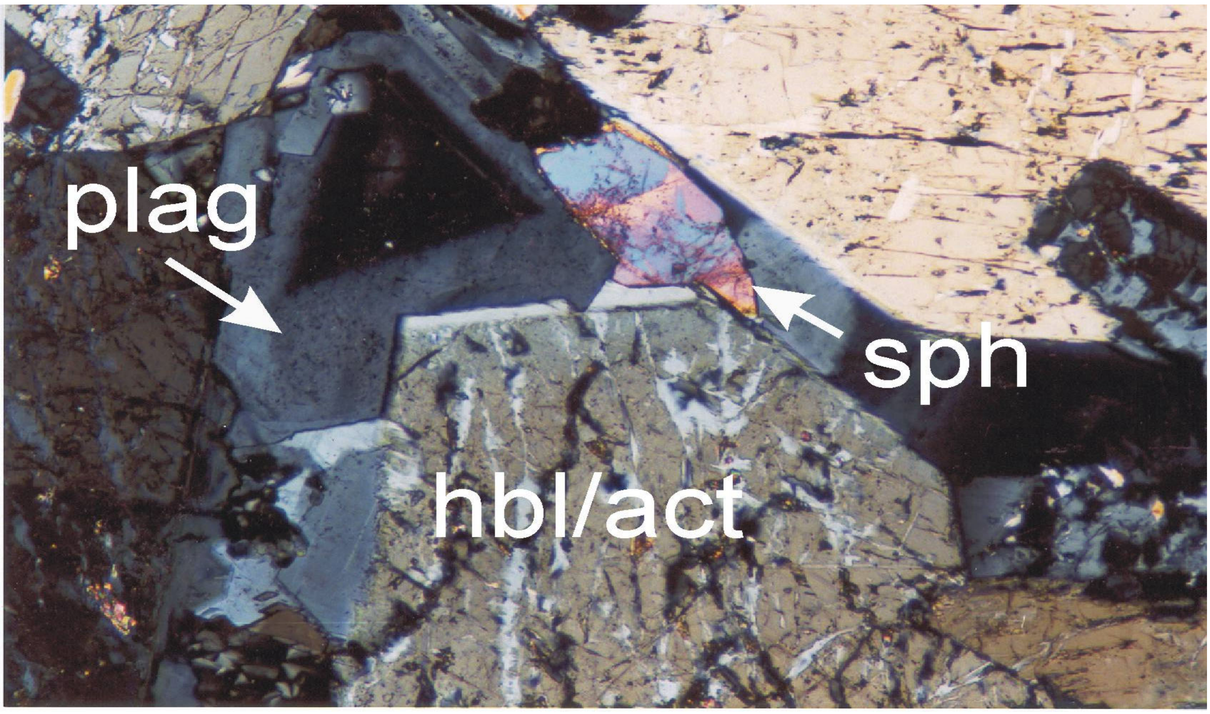

Figure 4.12:

Interstitial sphene between amphibole (hbl/act) and plagioclase in gabbro (6055). Long side of photomicrograph 1.75 mm.

Chlorite is the major constituent of the secondary mineral assemblage. It is present in interstices between amphibole and plagioclase as radiating aggregate with light green pleochroism. Epidote and muscovite (sericite) occur as minor secondary components in or next to plagioclase grains.

4.3. METAGABBROS

4.3.1 TEXTURES AND MODAL COMPOSITIONS

The original mineralogy and igneous texture of the Cabo Blanco metagabbros has been variously modified under greenschist-facies metamorphism.

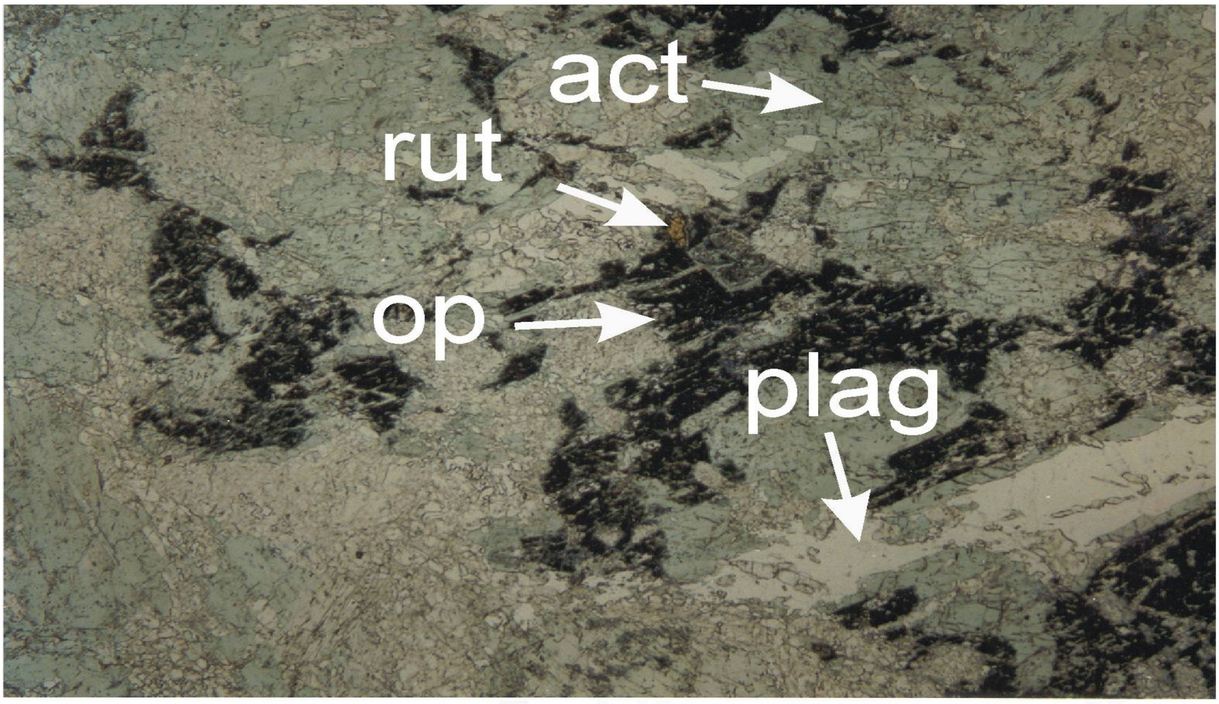

Figure 4.13:

Photomicrograph of metagabbro (6208) from Cabo Blanco with green amphibole (actinolite), opacite, plagioclase and rutile. Long side of photomicrograph 3.5 mm.

The texture produced during shearing shows a foliated granular groundmass of plagioclase, chlorite, epidote, zoisite, muscovite (sericite), quartz, rutile and sphene. Magmatic amphibole is replaced by large porphyroblastic actinolite with grain sizes between 80 and 400 µm. Actinolite appears as brittle, disaggregated phase with abundant plagioclase inclusions with up to 40 µm in size. Pleochroism from light to medium green is characteristic of actinolite, as well as the abundant occurrence of opacite (Figure 4.13).

Sub- to euhedral ilmenite with grain sizes between 30 and 100 µm and fine opaque dust are present as accessory mineral phases.

5.

MINERAL COMPOSITIONS

5.1 ANALYTICAL TECHNIQUES

The composition of igneous minerals and secondary alteration products has been examined in 14 thin sections at the Ruhr-Universität Bochum (RUB), FRG. Thin sections were examined by electron microprobe, using the automated wavelength dispersive system camebax (Cameca).

Standardization was made against jadeite, topaze, pyrope, andradite, spessartine, Cr_2O_3, Ba-glass, NiO, K-glass, NaCl, rutile and anhydrite. Operating conditions were 15 kV acceleration voltage, defocussed beam and beam currents of 12 and 10 nA for primary and secondary minerals, respectively, and 20 s counting time. Na and K were measured first to minimize loss due to volatilization. Qualitative mineral analyses were made using the Kevex energy dispersive system. Results are given in Tables 12.3-12.12 (Appendix).

5.2 COMPOSITION OF IGNEOUS MINERALS

5.2.1 CHROMITE

The occurrence of chromite as single, strongly resorbed phenocryst or inclusion in clinopyroxene is restricted to the basic members of the Margarita suite. Single chromite phenocrysts differ from chromite inclusions in being higher in Cr and lower in Al content, with highest Cr in the Playa Caribe suite. The Cr-Al relation does not correlate with the chemical composition of corresponding bulk rocks, in that chromite with higher Cr content is found in bulk rocks with lower chromium concentration and vice versa. Variable Cr content between chromite and host rocks has also been reported by Allan et al. (1988), in contrast to the results of Irvine (1976).

Chemical compositions of chromite display oxide variations of Cr_2O_3 from 35.7 to 47.4 wt%, Fe_2O_3 from 3.2 to 6.2 wt%, MgO from 11.0 to 15.2 wt% and Al_2O_3 from 17.9 to 26.1 wt%. Mg-numbers from 52 to 70 ($Mg\# = Mg*100/(Mg+Fe^{2+})$) (e.g. Dick & Bullen, 1984; Bednarz, 1988; Zhou et al, 1996) show considerable variation and correlate positively with Cr-numbers from 50 to 63 ($Cr\# = Cr*100/(Cr+Al)$) (e.g. Dick & Bullen, 1984; Bednarz, 1988; Zhou et al., 1996). A large compositional variation in chromite has been regarded to be indicative for different melt composition, temperature, pressure and *f*O2 (e.g. Dick & Bullen, 1984; Allan et al., 1988). Chromites from different suites of Margarita can be distinguished by their Cr#'s, reaching lowest but most variable values in the Cabo Negro suite. They cover the range of Mg#'s from 53 to 69.

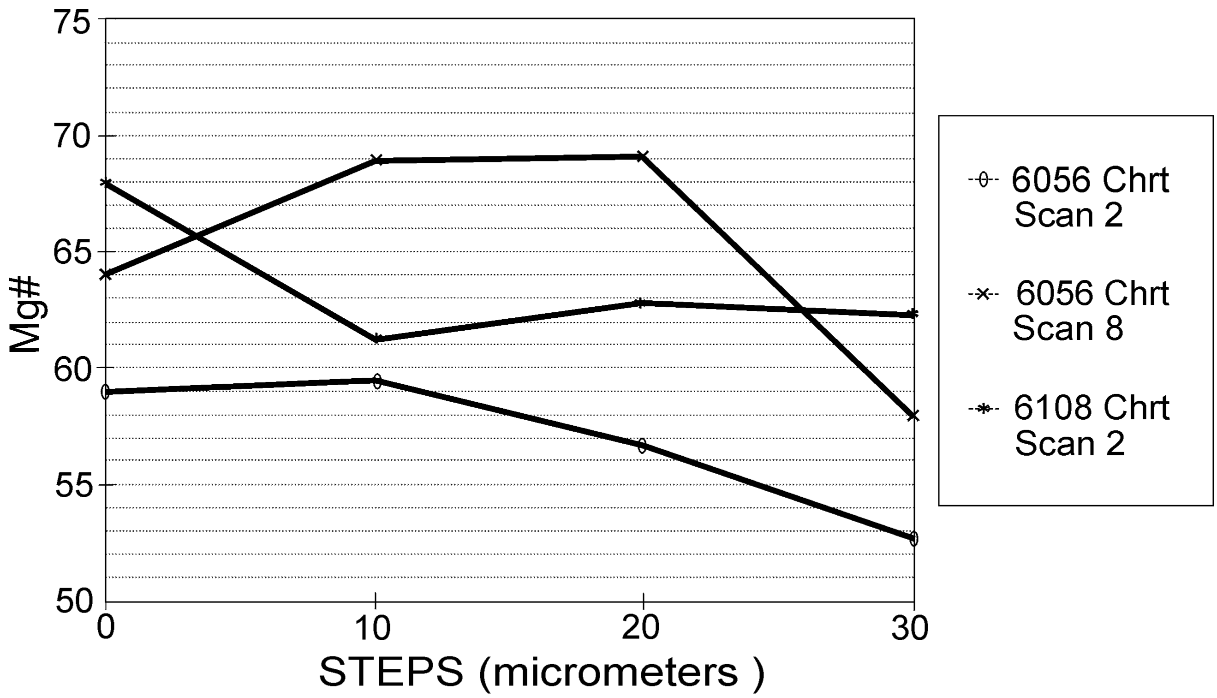

Figure 5.1:

Variations of Mg#'s (molecular ratios =(Mg*100)/(Mg+Fe^{2+})) in profiles across chromite phenocrysts of dike samples (6056) from Cabo Negro and (6108) from Playa Caribe.

Profiles across chromite phenocrysts from samples 6056 (Cabo Negro) and 6108 (Playa Caribe) show, however, with minor oscillation, decreasing Mg#'s from core to rim and are interpreted to reflect the fractional crystallization trend in the Margarita suite (Figure 5.1).

Chromite crystallizes early with olivine in most igneous melts, terminating shortly after the appearance of plagioclase and clinopyroxene (Dick & Bullen, 1984; Deer et al, 1992). A small portion (1%) of chromite preceded and/or coprecipitated with olivine and clinopyroxene in the Margarita suite, where it occurs as a minor phenocryst phase or as tiny inclusion in clinopyroxene. The effect of olivine fractionation is the decrease of the Mg#'s in the melt and liquidus phases. The variation of the Cr#'s in spinels with fractional crystallization, however, is complex. Irvine (1976) has shown that Cr#'s increase with increasing silica content in the fractionating magmas, except for melts with high alumina, where Cr#'s decrease systematically with the degree of crystallization. Accordingly, chromites with high Cr#'s from island arc lavas may thus reflect the high silica and low-alumina content of the parental lavas. The compilation of chromites from Margarita with those from Guam (Reagan & Meijer, 1984), Okmok Volcano (Nye & Reid, 1986), Manam Island (Johnson et al., 1985), Mariana Trough and Lau Basin (Hawkins & Melchior, 1985) indicates intermediate composition of Margarita chromites between arc-related lavas (Guam, Okmok, Manam) and MORB from Dick & Bullen (1984) (Figure 5.2).

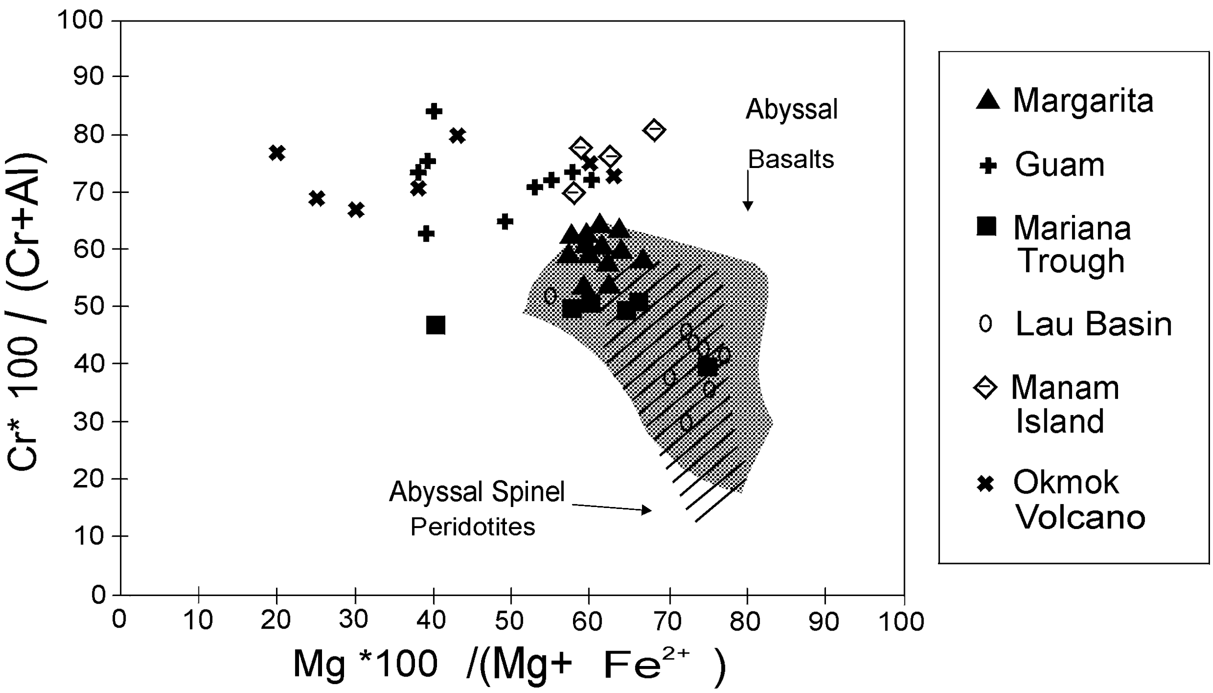

Figure 5.2:

Variation of Mg# (Mg*100)/(Mg+Fe^{2+}) vs. Cr# (Cr*100)/(Cr+Al) (molecular ratios) for chromite from Margarita. For comparison chromite compositions from Guam (Reagan & Meijer, 1984), Mariana Trough and Lau Basin (Hawkins & Melchior, 1985), Manam Island (Johnson et al., 1985), and the Aleutian Okmok Volcano (Nye & Reid, 1986) are also plotted. Fields for MORB and spinel peridotites" from Dick & Bullen (1984).

5.2.2 CLINOPYROXENE

Clinopyroxenes were recalculated to endmember compositions and classified in the system $Ca_2Si_2O_6$-$Mg_2Si_2O_6$-$Fe_2Si_2O_6$. Clinopyroxenes in dikes and in gabbroic intrusions from Margarita vary slightly in average composition (En_{40-51}, Wo_{37-46}, Fs_{7-16}). They plot in the diopside-endiopside-salite-augite quadrilateral into the compositional field of clinopyroxenes from calc-alkaline lamprophyres given by Rock (1991) (Figure 5.3).

Compositional variation of clinopyroxenes (cpx) in single thin sections or even single crystals can be as great as variations between cpx from different samples from Margarita. Mg#'s of clinopyroxenes range from 53 to 75 and are strongly dependent on bulk rock composition (see section 6.5).

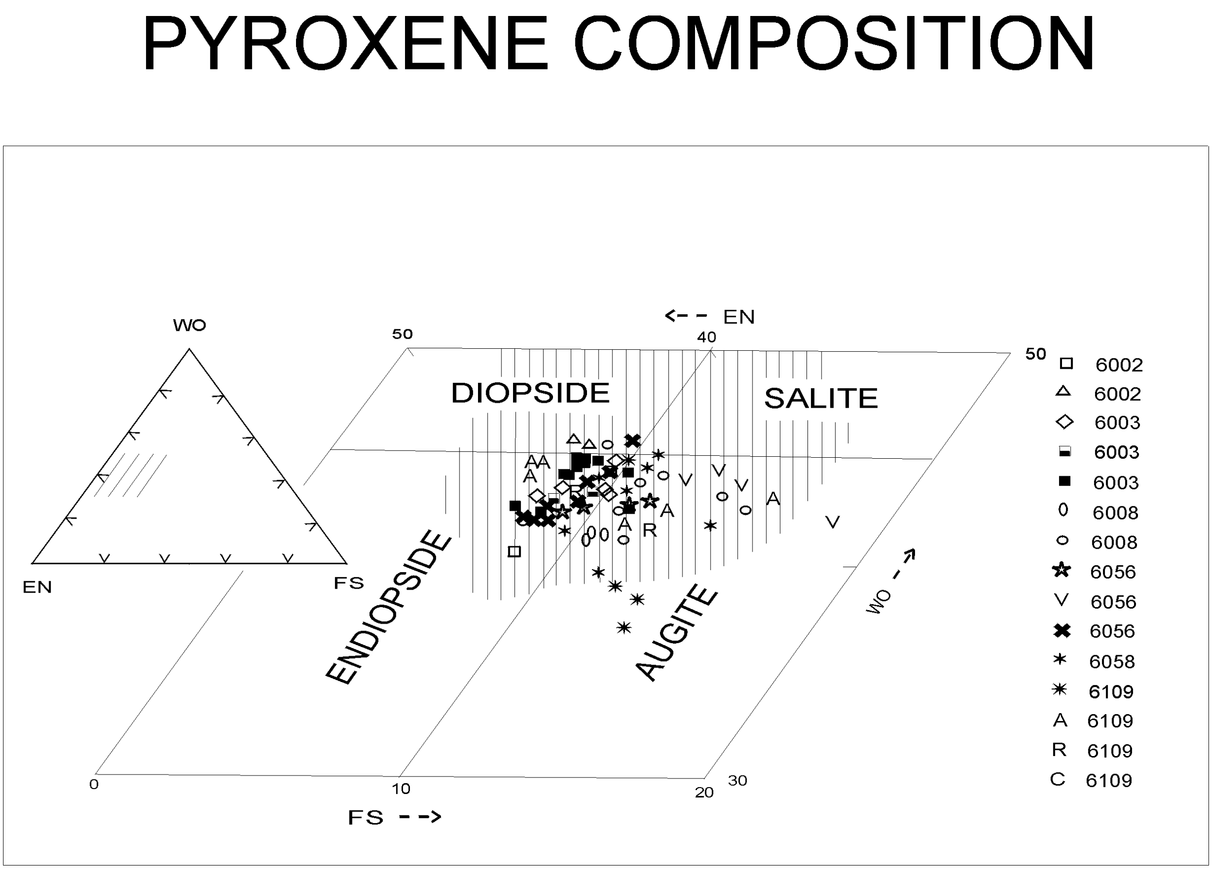

Figure 5.3:

Projection of clinopyroxenes from lamprophyric dikes and gabbroic intrusions from Isla Margarita into the Enstatite-Ferrosilite-Diopside-Hedenbergite quadrilateral. Hatched area represents field of clinopyroxene composition from calc-alkaline lamprophyres (Rock, 1991).

The clinopyroxenes are overall rich in calcium, with variations from 20.56 to 23.22 wt% CaO in phenocrysts and 19.02 to 21.91 wt% CaO in groundmass crystals. Calcium-rich clinopyroxenes from gabbroic intrusions have also been reported by Deer & Abbot (1965), Best & Mercy (1967), Kreher (1992) and in basaltic andesitic lava flows by Pe (1973) where they were attributed to high P_{H2O}.

Al and Ti in the clinopyroxenes correlate well, with Al ranging from 0.10 to 0.37 p.f.u. and Ti from 0.0076 to 0.0417 p.f.u. (Figure 5.4). The nonquadrilateral components Al, Na and Ti in clinopyroxenes are generally interpreted to reflect the temperature, cooling rate, $a\mathrm{SiO_2}$ and coexisting mineral assemblage, as well as pressure. Al_2O_3 contents of <3 wt%, TiO_2 contents of <0.75 wt% and Na_2O contents of <0.5 wt% have been interpreted to indicate crystallization of clinopyroxenes in tholeiitic magmas at crustal level or at least preclude pressures of >10kb (Green, 1972; Gill, 1981). Clinopyroxenes from Margarita are significantly higher in Al_2O_3 (2.4 - 7.4 wt%) and TiO_2 (0.27 - 1.46 wt%) content, but very similar in their overall composition to clinopyroxenes coexisting with amphiboles from the Aegean Arc, Greece (Pe, 1973, 1974).

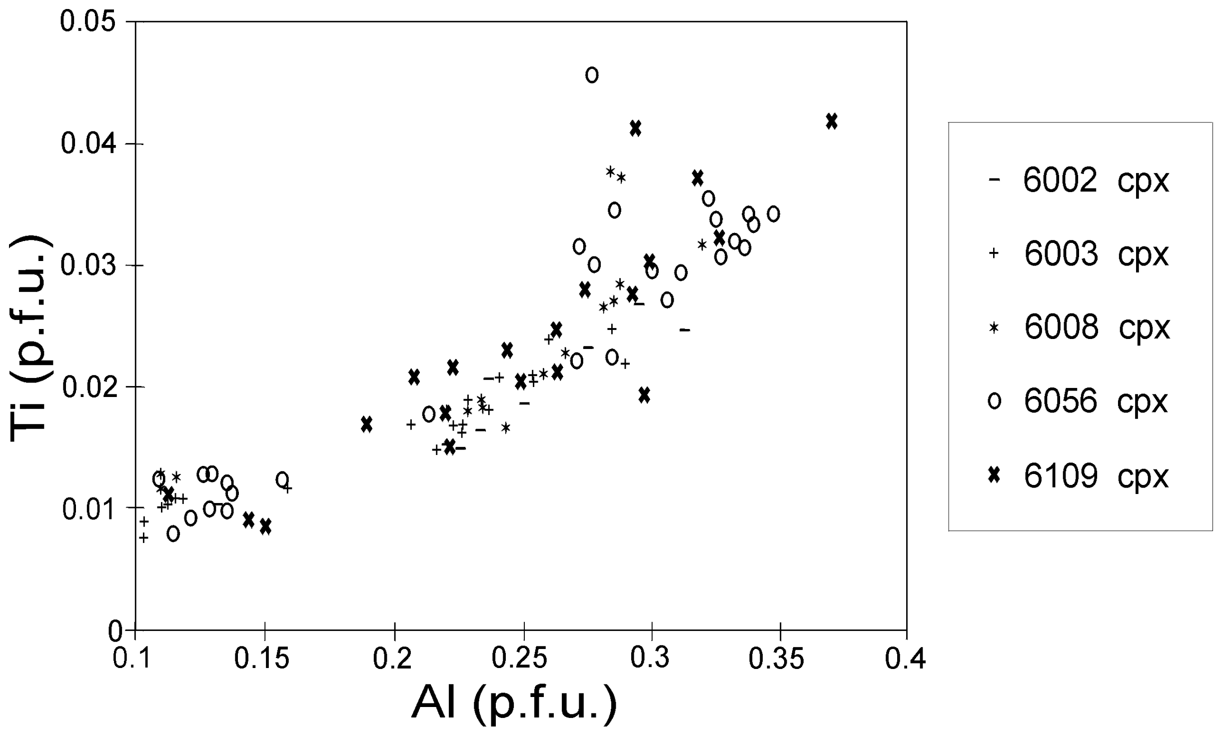

Figure 5.4:

Al-Ti (molecular proportions) variation diagram of clinopyroxenes from Isla Margarita.

Aoki & Kushiro (1968) characterized clinopyroxenes from various rock types with regard to $Al^{(VI)}$ vs. $Al^{(IV)}$ (Figure 5.5). Accordingly, the Margarita clinopyroxenes do not plot within the field for cpx from igneous rocks, but for cpx from intermediate rocks between igneous and granulitic rocks, such as inclusions in basalts. This may also indicate that clinopyroxenes in the Margarita basalts crystallized at high pressure.

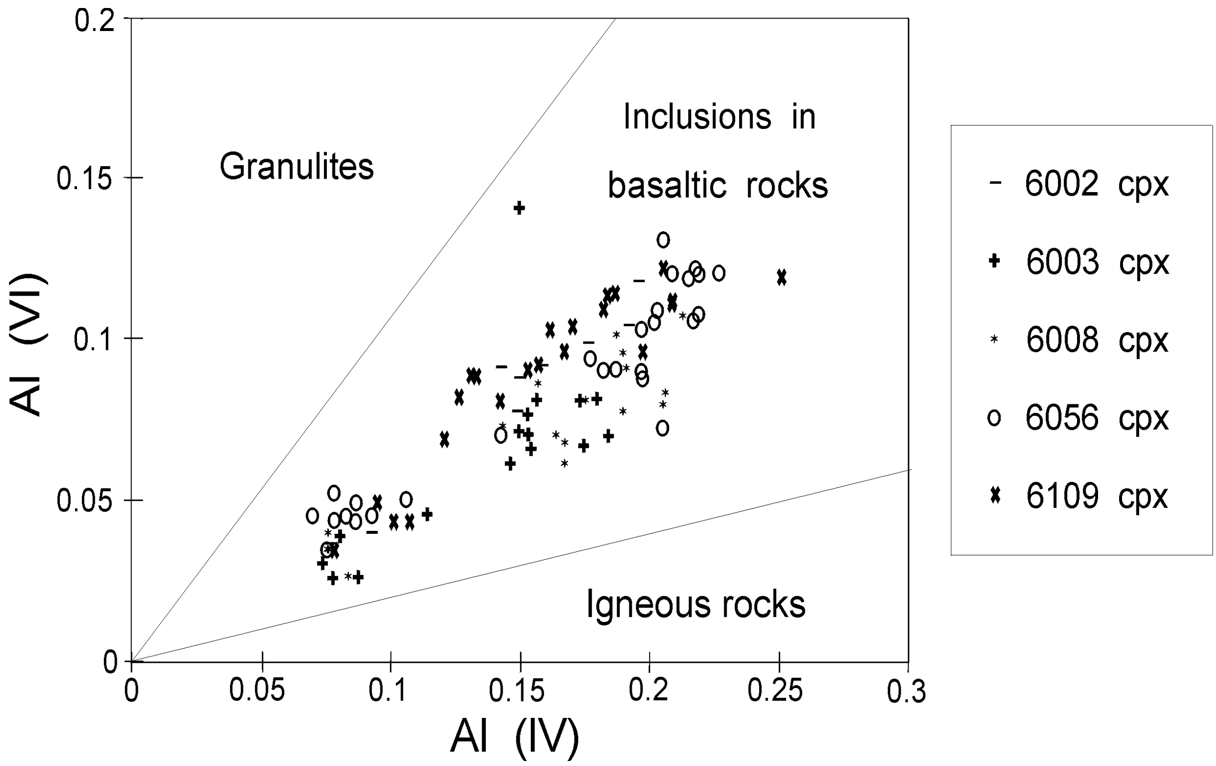

Figure 5.5:

$Al^{(VI)}$ vs. $Al^{(IV)}$ (molecular proportions) variation diagram of clinopyroxenes from Isla Margarita. Dividing lines for clinopyroxenes in granulites and inclusions in basaltic and igneous rocks after Aoki & Kushiro (1968).

Crystallization of clinopyroxene at relatively high PH_2O, however, is in accordance with the absence of orthopyroxene in the Margarita suite, since the augite stability is enhanced relative to orthopyroxene by increased pressure and/or increased water content in andesites (Maksimov et al., 1978). Consequently, decreasing pressure during magma ascent can cause subsequent amphibole crystallization instead of clinopyroxene (Gill, 1981).

The pyroxenes show, much alike their bulk rocks, moderate FeO content (4.0 to 10.0 wt%, averaging around 5.5 wt% FeO*.). An exception is groundmass clinopyroxene from the Playa Caribe dike suite, which shows more ferrous and less calcic composition. A limited range of Fe in pyroxenes from calc-alkaline suites is generally considered to be due to factors limiting concentrations of Fe such as high oxygen fugacity (Gill, 1981). The main condition in the Margarita magmas that restricted the Fe content in the high Ca-clinopyroxenes, however, might have been their hydrous state. Best & Mercy (1967) discuss Ca-rich pyroxenes with limited Fe from the Guadeloupe Complex and state that magmas leave the field of stable pyroxene when only moderately enriched in Fe, with hornblende and biotite taking over as the dominant ferromagnesian minerals.

5.2.3 PLAGIOCLASE

Plagioclase is the most ubiquitous and abundant mineral phase in the dike and gabbro suites of Margarita, typically constituting between 50 and 65 vol% of the rocks. Plagioclase phenocrysts are frequently altered to a large degree with patchy-zonation and sieve-like appearance. Plagioclase cores frequently contain sericite. A compilation of plagioclase compositions is given in Figure 5.6.

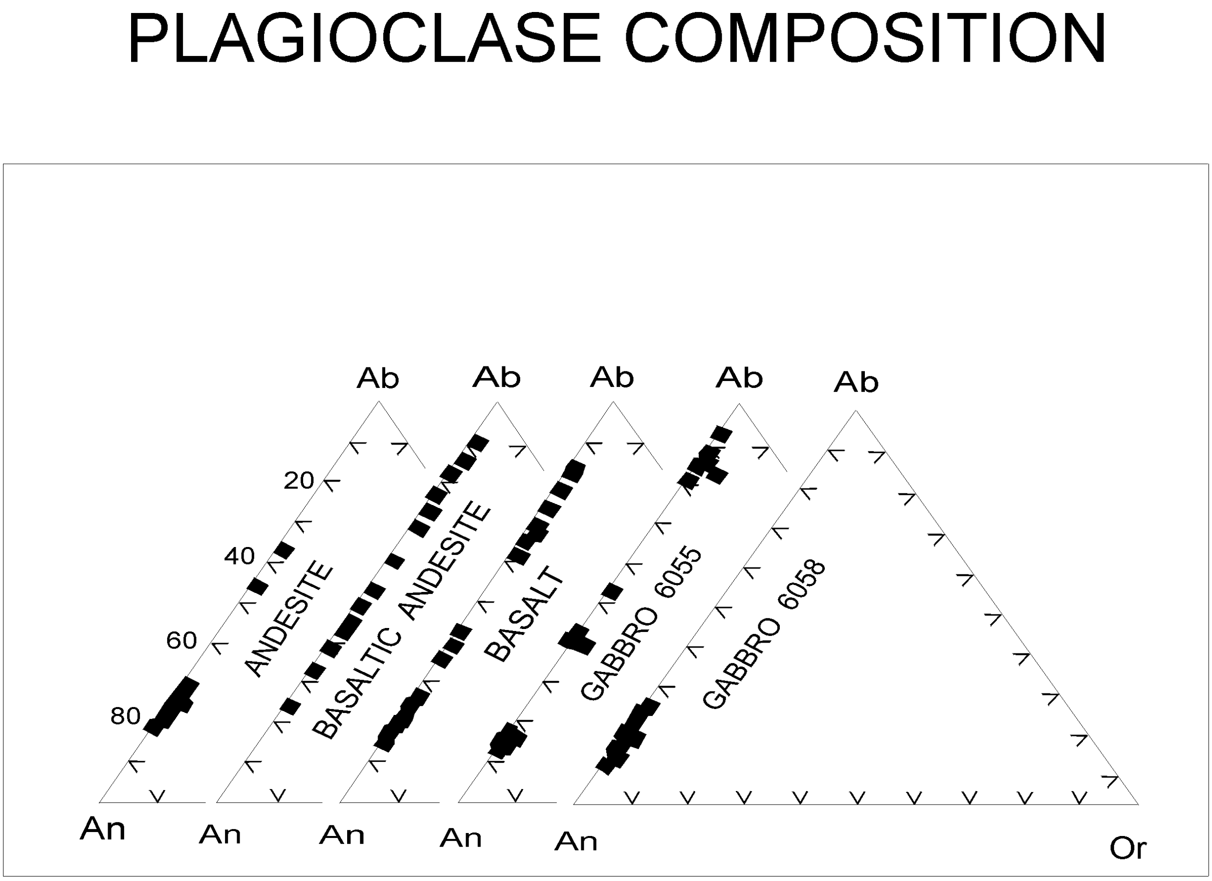

Figure 5.6:

Projection of plagioclase composition from Isla Margarita into the feldspar triangle Ab-An-Or.

Plagioclase composition within thin sections or even single crystals from dike rocks is as variable as within suites. The correlation of average An content in plagioclase with silica concentration of the bulk rocks is poor. The composition of zoned plagioclase phenocrysts in the most acidic sample (6009 with 58.90 wt% SiO_2, Figure 5.7-a) ranges from An_{73} to An_{79}, whereas phenocrysts in the most basic sample (6056 with 48.00 wt% SiO_2, Figure 5.7-b) range from An_{10} to An_{84}. Individual crystals display broad and complex variations with up to 60 mol% An. The broad variation in An content is unsystematic and likely to represent alteration effects (Deer et al., 1992),(see section 5.6).

Rock (1991) reported overall ranges of plagioclase composition in lamprophyres spanning An_{5-90} and variations in individual grains which exceed 50% An. Compositional zoning of unaltered plagioclase in one andesitic and basaltic dike sample from Margarita is displayed in Figures 5.7-a and -b. Microprobe scans of optically and chemically zoned phenocrysts from andesite sample 6009 show relatively constant composition from core to rim, with variations in An content between 79 and 72 mol%. More complex zonation is displayed in plagioclase microphenocrysts from basaltic sample 6056, with core compositions of An_{73} and An_{61} respectively and oscillatory zoning of the rims between An_{72} and An_{43}.

Two compositionally different plagioclase inclusions have been observed in dike amphiboles with ranges in An content between 52-62 and 81-84 mol%. The composition of groundmass plagioclase varies in An content from 17 to 75 mol%, occasionally exceeding An contents of corresponding phenocrysts.

Compositional variation of plagioclase in gabbro 6058 is from An_{74} to An_{88} and in 6055 from An_7 to An_{59} respectively. Plagioclase inner cores from gabbro 6055 vary from An_{14} to An_{19}, outer cores have An_{57} and rims vary from An_7 to An_{14}. Plagioclase inclusions in gabbroic amphibole (sample 6055) vary from An_{81} to An_{86}, thus corresponding well with plagioclase compositions of gabbro 6058, but being significantly different from inner phenocryst cores of their bulk rock.

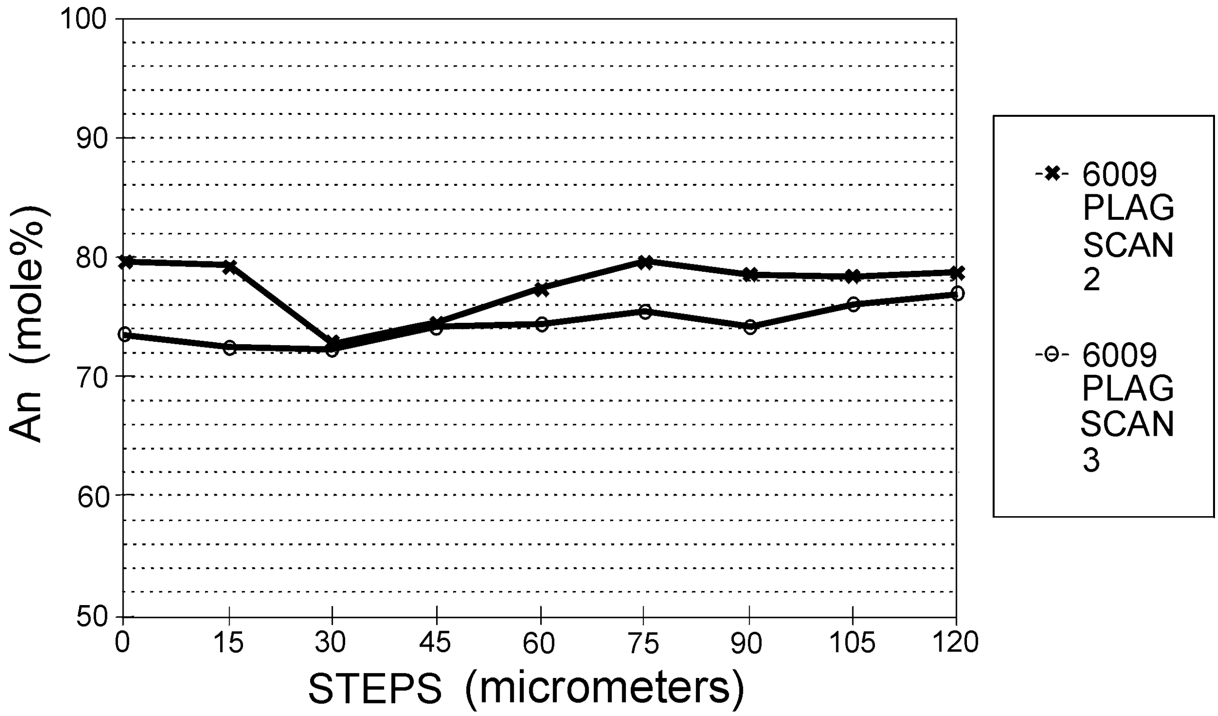

Figure 5.7-a:

Variation in An-content in profiles across plagioclase phenocrysts from dike 6009 (Manzanillo suite).

Gabbroic plagioclase from Margarita also suffered sericitization, which makes assessment of primary and alteration affected portions of the minerals difficult. However, increase in An from inner to outer portions of the mineral generally results from input of fresh magma into the differentiating magma-chamber. The opposite effect is consistent with prograde magmatic differentiation and uprise of the magma in the crust, with increasing Na_2O/CaO in the melt and decreasing temperature. According to the plagioclase-liquid geothermometer of Kudo & Weil (1970), however, fluctuations in PH_2O in crustal levels may also contribute to changing An content with up to 15 mol%.

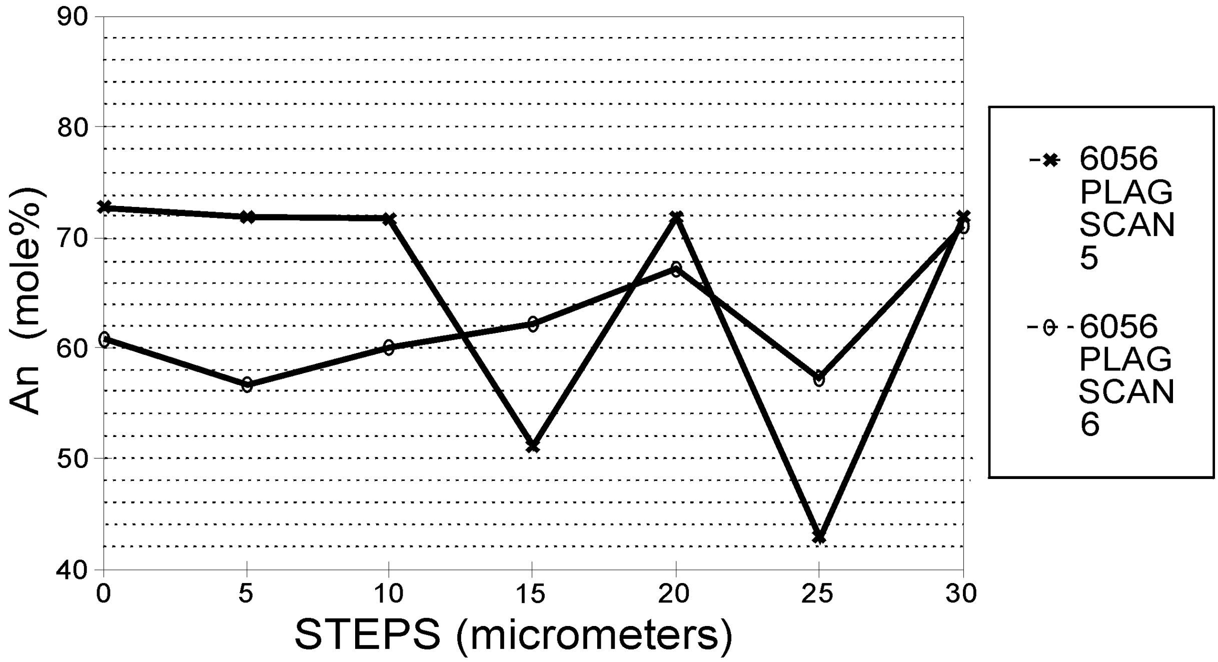

Figure 5.7-b:

Variation in An-content in profiles across plagioclase phenocrysts from dike 6056 (Cabo Negro). Note different step size in Figures 5.7-a and 5.7-b.

5.2.4 AMPHIBOLE

Amphibole is an important, and sometimes the only ferromagnesian mineral phase in the Margarita lamprophyric dikes. The amphibole formulae were recalculated by normalizing the number of cations to 13.000. Corresponding to the nomenclature of Leake et al. (1997) the amphiboles correspond to the calcic suite and the majority of the compositionally different calcic amphiboles ($Ca_B \geq 1.50$; $(Na+K)_A < 0.50$) has been identified as Mg-hornblende (Figure 5.8). They are considered to represent the primary magmatic amphibole suite. A second group of amphiboles is of actinolitic composition and reflects a late stage crystallization and/or hydrothermal alteration product.

The primary magmatic amphibole occurs as a single phenocryst or phenocryst core but also as a groundmass mineral. Actinolite mantles or completely replaces magmatic amphibole phenocrysts; it also occurs in the groundmass.

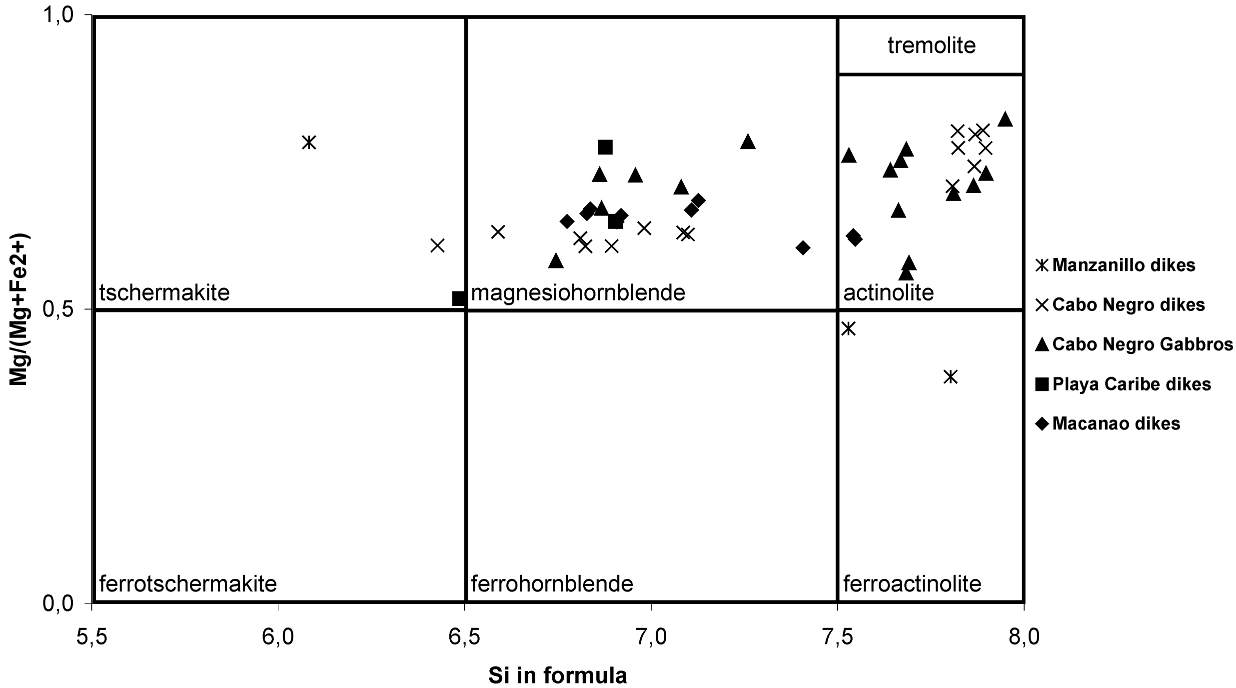

Figure 5.8:

Projection of amphibole composition of the calcic group $Na+K_{(A)}<0.5$, $Ti<0.5$ from Isla Margarita into the $Mg/(Mg+Fe^{2+})$ vs. Si (molecular ratios and proportions) variation diagram, after Leake (1997).

A second group of primary magmatic amphiboles belongs to the suite of calcic amphiboles with $Ca_B \geq 1.50$; $(Na+K)_A \geq 0.50$; Ti<0.50 and are pargasites and edenites (Figure 5.9).

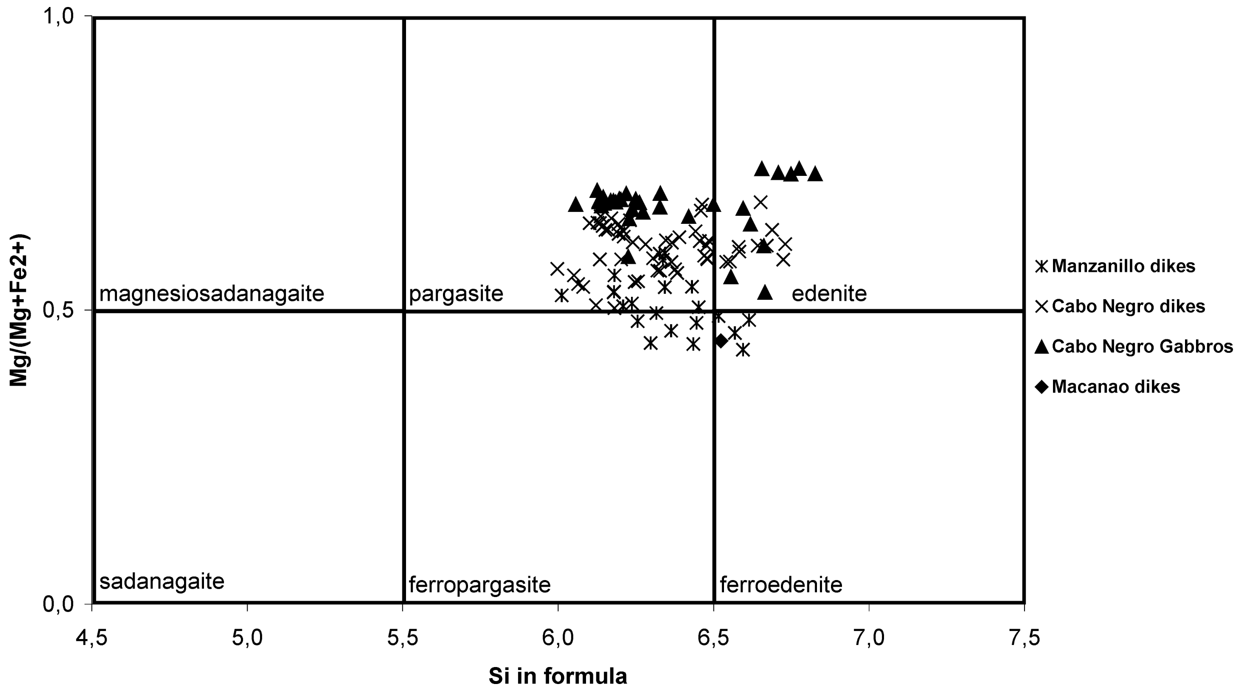

Figure 5.9:

Projection of amphibole composition of the calcic group $Na+K_{(A)}>0.5$, Ti<0.5, $Fe^{3+}>Al^{(VI)}$ from Isla Margarita into the $Mg/(Mg+Fe^{2+})$ vs. Si (molecular ratios and proportions) variation diagram, after Leake (1997)

Compositional zoning occurs within amphibole phenocrysts with Si and Fe increasing and Al and Mg decreasing as well as reverse zoning with Mg increasing and Fe decreasing from core to rim. These compositional changes, as discussed by various authors (Engel & Engel, 1962; Binns 1965; Leake, 1965; Spear 1981; Schuhmacher, 1991), were attributed to changing metamorphic grades. Helz (1973, 1979) and Hammarstrom & Zen (1986) also reported increasing $Al^{(IV)}$ and alkali content in amphiboles with increasing temperature and pressure. The edenite substitution plays an important role in the Ca-rich amphiboles with increasing *P*/T conditions, the pargasite substitution is essentially a combined edenite and Al-tschermakite substitution.

The primary magmatic amphiboles from Margarita rocks have relatively low silica content (39.4 to 47.5 wt% SiO_2), consequently, their crystallization was an efficient means to increase silica and normative qz in the magma during differentiation. Silica content in actinolite is significantly higher with values from 49.6 to 55.9 wt% SiO_2.

The amphibole crystallization played an important role in the differentiation trend of magmas derived from MgO-rich basalts in the Margarita (this study) and the Lesser Antilles province (Arculus, 1976, 1978; Devine, 1995). In contrast, the differentiation processes of magmas in other volcanic arcs do not involve extensive amphibole crystallization, but instead develop to two-pyroxene andesites (Gill, 1981). Sigurdson & Shepherd (1974) reported the occurrence of amphibole in high-MgO basaltic magmas and Cawthorn et al. (1973) suggested that amphibole crystallization plays a major role in production of the calc-alkaline, versus tholeiitic, differentiation trend.

Amphibole phase relationships suggest that amphibole is a product of late-stage and sub-liquidus water-enrichment, rather than a liquidus phase. Reaction relationships, however, affecting the appearance of amphibole are complex (Best & Mercy, 1967; Gill; 1981, Devine & Sigurdsson, 1995) but it is implicit that amphibole appears at the expense of pyroxene or olivine due to (1) increased PH_2O, (2) increased alkali content or (3) decreased temperature or all three. Overgrowth of amphibole on clinopyroxene (uralitization) in Margarita dikes or almost complete replacement of clinopyroxene by amphibole in gabbros is unequivocal evidence for this reaction. It has also been observed in basic intrusions such as the Skaergaard, the Bushveld, the Palisades Sill and the Frankenstein/Odenwald (Bown & Gay, 1959; Papike et al., 1969; Smith, 1977; Veblen & Buseck, 1977; Kreher, 1992).

5.2.5 ILMENITE

Ilmenite is not an abundant mineral phase in the Margarita suite, it occurrs only in a small number of samples (6037, 6038, 6043, 6044) of the Cabo Negro dike suite. Its former presence, however, may be indicated in a large number of samples by abundant leucoxene.

Compositional variation in ilmenite is low, with oxide variations of TiO_2 from 50.3 to 50.7 wt% and of FeO* from 43.5 to 45.6 wt% respectively. MnO content in ilmenites is relatively constant with up to 2.2 wt%. Variations in MnO have been interpreted to be strongly dependent on fO_2 and crystallization temperature by Buddington & Lindsley (1964) and Czamanske & Mihalik (1972), who noted decreasing Mn-content in ilmenites with increasing temperature.

5.2.6 SPHENE

Sphene is the dominant Ti-bearing mineral phase in gabbroic intrusions, with TiO_2 content varying from 23.4 to 38.4 wt%. Other major oxide constituents vary from 29.7 to 42.3 wt% (SiO_2) and 22.1 to 29.3 wt% (CaO). Al_2O_3 content in sphene reaches 6.8 wt%. Sphene may also have been present in lamprophyric dikes as indicated by very fine grained aggregates, resembling leucoxene.

5.3 DISCUSSION OF CRYSTALLIZATION AND EQUILIBRIUM CONDITIONS

The phase assemblages studied contain a number of potential indicators that are characteristic of the conditions under which the Margarita rocks crystallized. It can be reasonably assumed that the zoned phenocryst phases represent changing equilibrium conditions and that the groundmass assemblage reflects subsequent, frozen-in equilibria. The simple, near binary olivine-clinopyroxene, orthopyroxene-clinopyroxene, magnetite-ilmenite or plagioclase-liquid calculation models cannot be applied to determine accurate temperature and pressure conditions, due to lack or alteration of the necessary coexisting phases in the Margarita magmatic suite. Common solution assumptions, however, can be applied so that relative values of *P,T,f* could be significant. The crystallization sequence present further allows conclusions on the depth and the H_2O conditions.

Olivine, clinopyroxene and minor amounts of chromite constitute the early fractionating phases in the Margarita magmatic suite. Plagioclase followed in the crystallization sequence and clearly precedes amphibole, which implies less than 2 to 4 wt% H_2O in the early crystallization history of the magma (Gill, 1981). On the other hand, absence of plagioclase phenocrysts post-dating the appearance of amphibole is interpreted to be related to the subsequent increase *of* PH_2O. Kudo & Weill (1970) demonstrated that increasing PH_2O decreases the plagioclase proportion relative to mafic phases in the crystallization assemblage of basic magmas.

Hornblende is a key mineral in explaining the genesis of the Margarita magmatic suite, since it is restricted to silica-, alkali- and water-enriched magmas in the upper portions of magma reservoirs, and not a widespread liquidus phase. Green (1972) and Eggler & Burnham (1973) state that water content >3 wt% is necessary for crystallization of amphibole at all. Experimental work on a wide range of basaltic compositions has shown that amphibole is a hypersolidus phase under water-saturated conditions at pressures greater than 800-1000 bars (Yoder & Tilley, 1962; Eggler, 1972; Gilbert et al., 1982). The relationship between the upper-temperature stability limit of amphibole and the basalt solidus is a function of basalt composition and oxyen fugacity, but under all conditions studied, if the melt is water saturated, amphibole crystallizes if P_{H2O} exceeds 2 kbar. The maximum temperatures for amphibole stability in basic andesites over a range of f_{H2O} and f_{CO2} are defined with up to 1000°C (Cawthorn et al., 1973; Helz, 1973, 1979; Arculus & Wills, 1980; Gilbert et al., 1982), The upper limit of pressure for formation of primary magmatic hornblende is given by Olsen (1984), Grissom et al. (1985) and Hammarstrom & Zen (1986) with <8kb.

The texture of hornblendes in Margarita dikes and gabbroic intrusions (i.e. replacement of clinopyroxene) suggests that they formed at conditions just above and, perhaps, below the solidus (Wones & Gilbert, 1982). Their late appearance in the dikes and gabbros is consistent with low-pressure crystallization. Subsequent breakdown of amphibole to opacite (plag+opx+cpx+mt) has not been observed in the Margarita dike and gabbroic amphiboles. The breakdown of amphibole generally indicates that amphibole is being resorbed at shallow depths during magma ascent and eruption - related decompression (Gill, 1981; Rutherford &

Hill, 1993; Devine & Sigurdsson, 1995), resulting in the absence of groundmass amphibole. These criteria do not apply to the Margarita amphiboles, since opacite rims are absent and groundmass amphibole does occur. This implies that amphibole was stable until crystallization of the magma was complete and is in accordance with a crystallization depths of 2-5 km and pressures of ca. 2-3 kb.

5.4 COMPOSITION OF SECONDARY MINERALS

5.4.1 CHLORITE

Chlorite is the most abundant secondary mineral phase besides actinolite in the Margarita rocks. The replacement of the igneous mineral suite by secondary alteration products can be characterized by the following reaction:

ol±cpx+plag±hbl->chl+ep+mus±act

Oxide variations of MgO and FeO* in chlorites show similar ranges, with values from 11.2 to 24.4 wt% and from 11.0 to 20.3 wt%, respectively. Silica content varies between 26.1 and 36.2 wt% and alumina content between 17.0 and 26.9 wt%.

The Margarita chlorites are characterized by variable Mg#'s, with values reaching 77, thus being dependent on Mg#'s of bulk rocks and corresponding clinopyroxenes (Mg#'s 53-75). No general correlation between Mg#'s and Al content in chlorites exists. Thus, Al does not seem to be controlled by bulk-rock composition, instead increase of Al in chlorite is dependent on the pressure in which equilibration occurred (Cooper, 1972; Kuniyoshi & Liou, 1976; Beddoe-Stephens, 1981))

5.4.2 EPIDOTE

Epidote is the secondary calcium - aluminum mineral phase and occurs in most cases in association with plagioclase. Variation in chemical composition such as in SiO_2 from 35.8 to 38.7 wt% and in CaO from 20.7 to 24.6 wt% is rather small. Al_2O_3, however, varies from 20.3 to 31.7 wt% and Fe_2O_3 shows considerable variation from 2.3 to 14.6 wt%.

Chemical zonation of epidote minerals has not been observed. Variations in Al and Fe^{3+} content are rather obvious between different mineral grains of the same rock sample. Fe-rich epidote is interpreted as a reaction product of Ca-Al silicates with Fe-bearing phases such as actinolite and strongly influenced by oxygen fugacity (Liou, 1973; Beddoe-Stephens, 1981). This suggests that fO_2 was an important variable during alteration of the Margarita rock suite.

5.4.3 MUSCOVITE

Small flakes of muscovite (sericite) are commonly dispersed within plagioclase. Their SiO_2 content varies from 45.2 to 57.0 wt% and Al_2O_3 content from 26.5 to 37.8 wt%. Potassium content ranges between 3.6 and 11.3 wt%.

5.4.4 HEMATITE

Overall replacement of magnetite (see p. 33) by hematite is characteristic of the Margarita dike suite. The compositional variation in hematite is from 83.7 to 93.5 wt% Fe_2O_3. Considerable amounts of SiO_2 from 3.9 to 7.9 wt% are incorporated in hematite and represent impurities, possibly due to the alteration process.

5.4.5 CALCITE

Calcite occurs as a minor constituent in ocelli but also in secondary veins. Chemical analyses of calcite have not been performed.

5.5 HYDROTHERMAL ALTERATION

The above described secondary mineral phases and alteration products allow restrictions on the temperatures prevailing during alteration of the lamprophyres and gabbros. The most widespread secondary mineral phase is actinolite, but the petrographic indicators also include albitization and sericitization of plagioclase. Furthermore, the abundance of epidote and chlorite indicates replacement of plagioclase and ferromagnesian phases. Alteration of Fe-Ti oxides is recorded by the presence of sphene or leucoxene. The occurrence of galena as fine dust throughout the rock or small aggregates as well as the above described secondary mineral suite strongly indicate hydrothermal alteration.

The alteration assemblage is comparable to oceanic suites (Alt et al., 1986; Gillis & Thompson, 1993; Gillis, 1995) and extrapolation of experimental data from Stakes & O'Neil (1982) suggests that the mineral assemblage present has been altered under low pressure and greenschist-facies conditions. The lower temperature limits are given with ca. 250-300°C for actinolite and 230-275°C for chlorite stability, the maximum temperatures are defined with ca. 350°C.

The occurrence of spheroidal structures and segregation veins in the lamprophyres with actinolite, chlorite and carbonate indicate autometasomatism and late stage crystallization with pneumatolytic action of the residual water-enriched fluids on the earlier crystallized amphibole and clinopyroxene. Calcite precipitated after chlorite, indicating that calcite formation took place during more oxidizing conditions. The formation of primary and secondary phases in the Margarita lamprophyres, however, was rather a gradational process, thus the textural distinction between primary and secondary phases is blurred.

6.

WHOLE ROCK GEOCHEMISTRY

6.1 ANALYTICAL TECHNIQUES

Bulk rock chemical analyses were carried out on 72 samples by X-ray fluorescence on fused glass discs, using an automated Phillips PW 1400 Spectrometer at the Institut für Mineralogie, Ruhr-Universität Bochum (RUB), FRG. U.S.G.S. standards were measured with the sample suite. The precision of XRF major and trace element data is estimated to be better than 3%, except for low Nb (<12 ppm) concentrations, which are near the detection level (Kubbilun, pers. comm).

Fe^{2+} was determined by potentiometric titration of the hydrofluoric acid-silver perchlorate digested samples, with standard potassium bromide solution. CO_2 was determined by closed-system coulometric titration of barium perchlorate solution. H_2O was measured by closed-system coulometric titration of a nonaqueous Karl-Fischer reagent, using N_2 as carrier gas. Water was stripped by heating the sample in a Pt crucible to 1300^{o}C.

The procedures used are described in more detail in Flower et al. (1983) and Bednarz (1988). The data in plots and those used for calculation of normative mineralogy were recalculated on a volatile-free basis. Major element concentrations are given in weight percent, trace elements in parts per million.

6.2 COMPOSITIONAL MODIFICATION BY ALTERATION

Petrographic studies of the Margarita basaltic-andesitic suite indicate that hydrothermal alteration processes severely affected the primary igneous constituents of the rock series and imply changes in chemical composition.

Major and trace elements are frequently liberated during alteration and weathering processes. The element mobility is dependent on the physicochemical conditions of percolating liquids and on the chemical properties of the elements (van der Weijden & van der Weijden, 1995; Gillis, 1995). The enrichment or depletion of an element during alteration, relative to its concentration in the "fresh" parent rock, can be calculated on the basis of the assumed immobility of some elements (e.g. Ti, Zr), which are effectively immobile (Nesbitt, 1979; Middleburg et al., 1988; Mongelli, 1993). The H_2O content has also been used as a simple index for alteration (Mehl et al, 1991; van der Weijden & van der Weijden, 1995). Initial H_2O content in lamprophyres, however, is usually variable and often high (Rock, 1991) which disqualifies it as a useful alteration index for this study. Compositional changes in the Margarita rocks have instead been assessed by using an unaltered sample as a normalizer against the most altered samples, following the method of Mehl et al. (1991). In Figures 6.1 a-d the "freshest" basalt sample (6050) from Cabo Negro, containing unaltered magmatic hornblende, clinopyroxene and plagioclase, is used as a normalizer. The resulting spidergrams allow a quantitative estimate of compositional changes related to alteration, assuming a roughly similar initial composition of the fresh and altered sample. This is inferred from ratios of immobile elements such as Zr, Nb and Y.

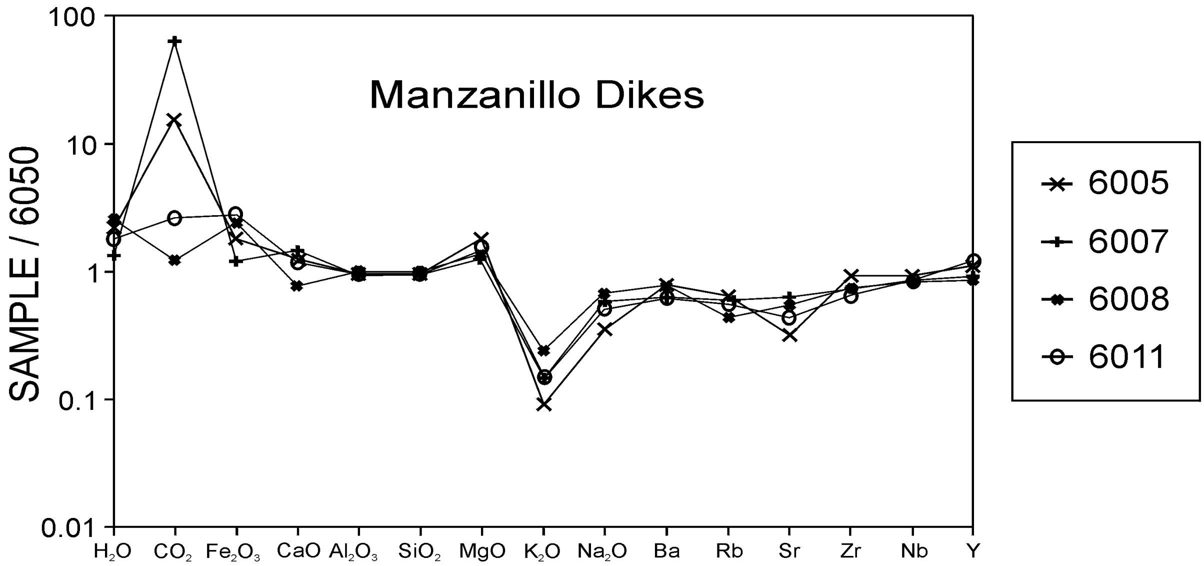

Figure 6.1-a:

Spidergrams of altered Manzanillo dikes. Concentrations are normalized against unaltered dike sample 6050 from Cabo Negro.

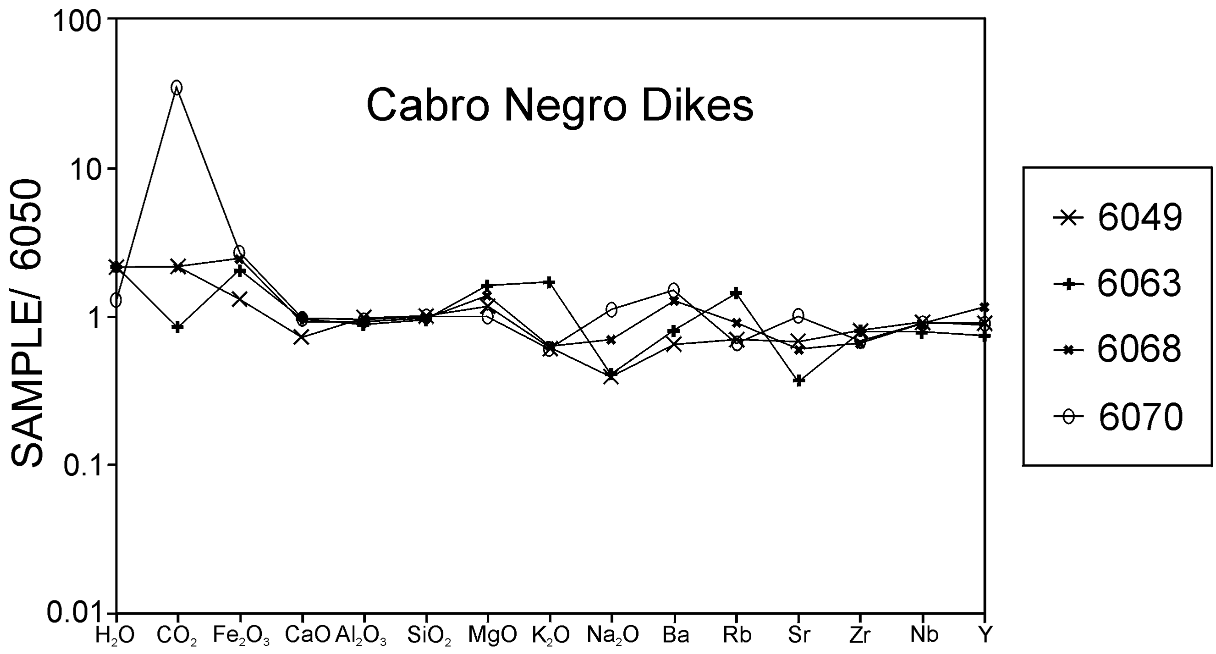

Figure 6.1-b:

Spidergrams of altered Cabo Negro dikes. Concentrations are normalized against unaltered dike sample 6050 from Cabo Negro.

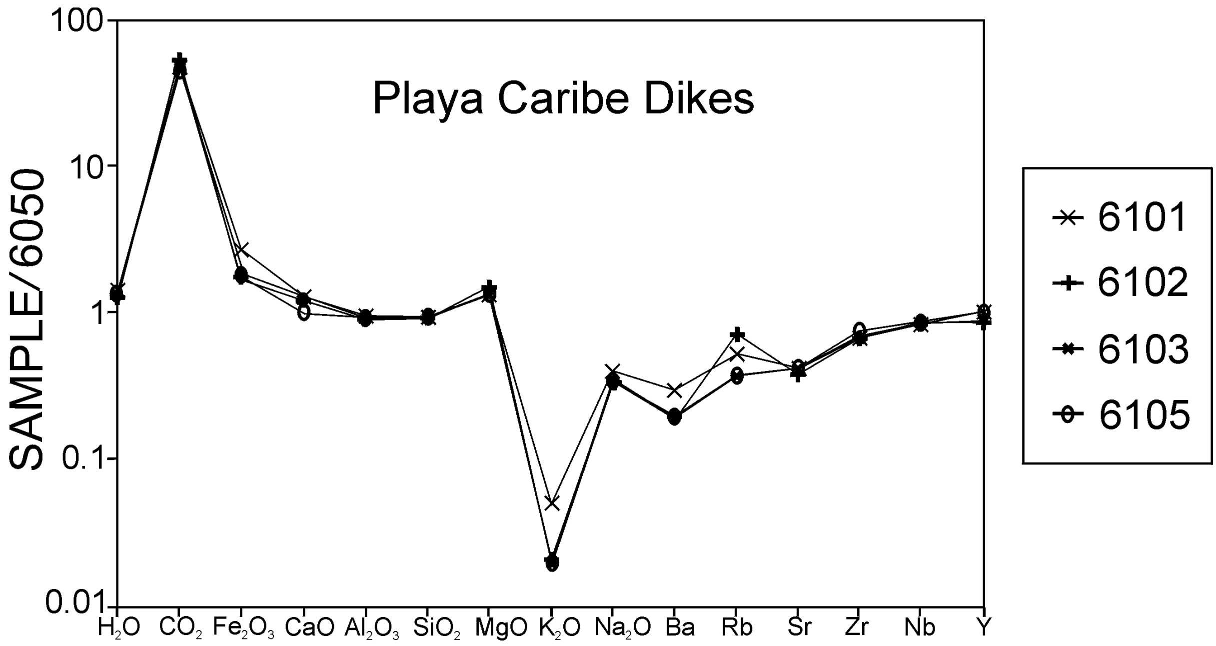

Figure 6.1-c:

Spidergrams of altered Playa Caribe dikes. Concentrations are normalized against unaltered dike sample 6050 from Cabo Negro.

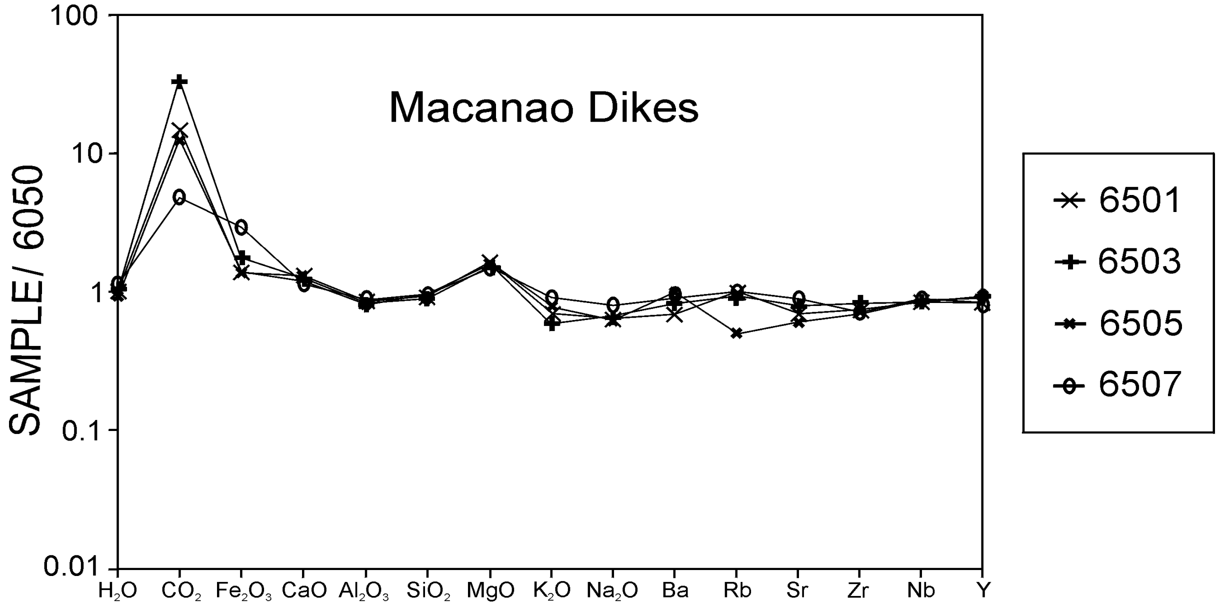

Figure 6.1-d:

Spidergrams of altered Macanao dikes. Concentrations are normalized against unaltered dike sample 6050 from Cabo Negro.

Even allowing for the variations in basaltic composition, it is obvious that the alteration is characterized by a ten-fold increase in CO2 and a two- to three- fold increase in H_2O, Fe_2O_3 and MgO. CaO shows a twofold increase as well as decrease. The increase of CaO, CO_2, H_2O, MgO and Fe_2O_3 can be correlated in thin section with the occurrence of the secondary minerals calcite, chlorite, actinolite and hematite, respectively. Some of the Ca released from the altered rocks responsible for the Ca depletion/enrichment is redistributed locally and incorporated into epidote or calcite vein fillings. Variations in the chemistry of the circulating fluids may be decuced from the progressive filling in occelli and veins, where calcite formed after the precipitation of actinolite and chlorite. This indicates that the secondary minerals changed from Mg-rich to Ca-rich composition during hydrothermal alteration.

Most characteristic of the elemental changes is the locally almost complete depletion of K_2O (most significantly in the Cabo Negro and Playa Caribe dike suites) which can be strongly related to the alteration of magmatic hornblende to actinolite. Ba, Rb, Sr and Na_2O, however, display only slight depletion. Accordingly, the group of large ion lithophile elements (LILE), most prominently K_2O, was removed whereas CO_2, H_2O and MgO were gained from percolating liquids during high-temperature, hydrothermal alteration processes. Subsequent surficial oxidation as indicated by high Fe_2O_3/FeO ratios together with low potash content (Gill, 1981) played an additional role in the Margarita rock suite (Figure 6.2). Usually, Fe is found to be relatively immobile or it shows a slight increase in weathered parts (Middleburg et al., 1988).

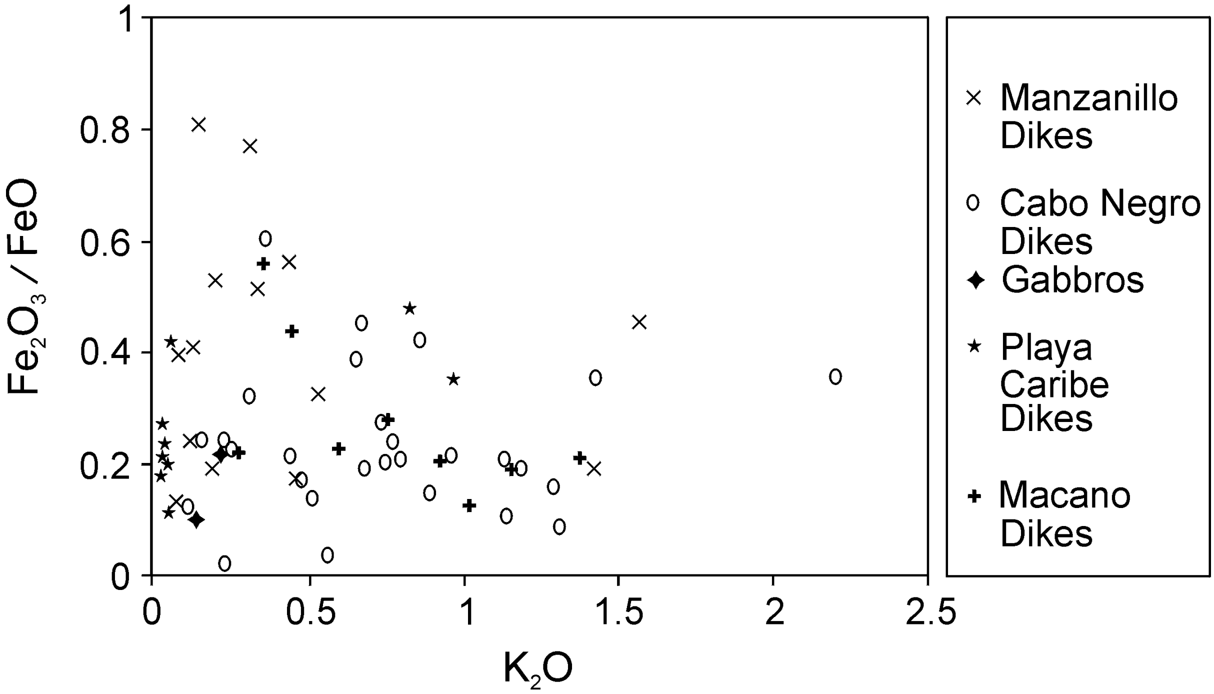

Figure 6.2:

Fe_2O_3/FeO vs. K_2O variation diagram for dikes and gabbroic intrusions from Isla Margarita.

6.3 CIPW NORMATIVE MINERALOGY

CIPW norms represent the idealized anhydrous mineralogy into which magmas would crystallize under uniform conditions (Cross et al., 1903). The normative mineralogy permits comparison of igneous rock suites as it relates complex rocks to simple oxide systems. CIPW norms of Margarita samples were calculated from chemical analyses of whole rocks. To eliminate alteration effects, leading to the occurrence of hematite in the norm, samples with high Fe_2O_3 content were limited to a maximum Fe_2O_3 content of 3 wt%. The remaining Fe_2O_3 was recalculated to FeO.

CIPW

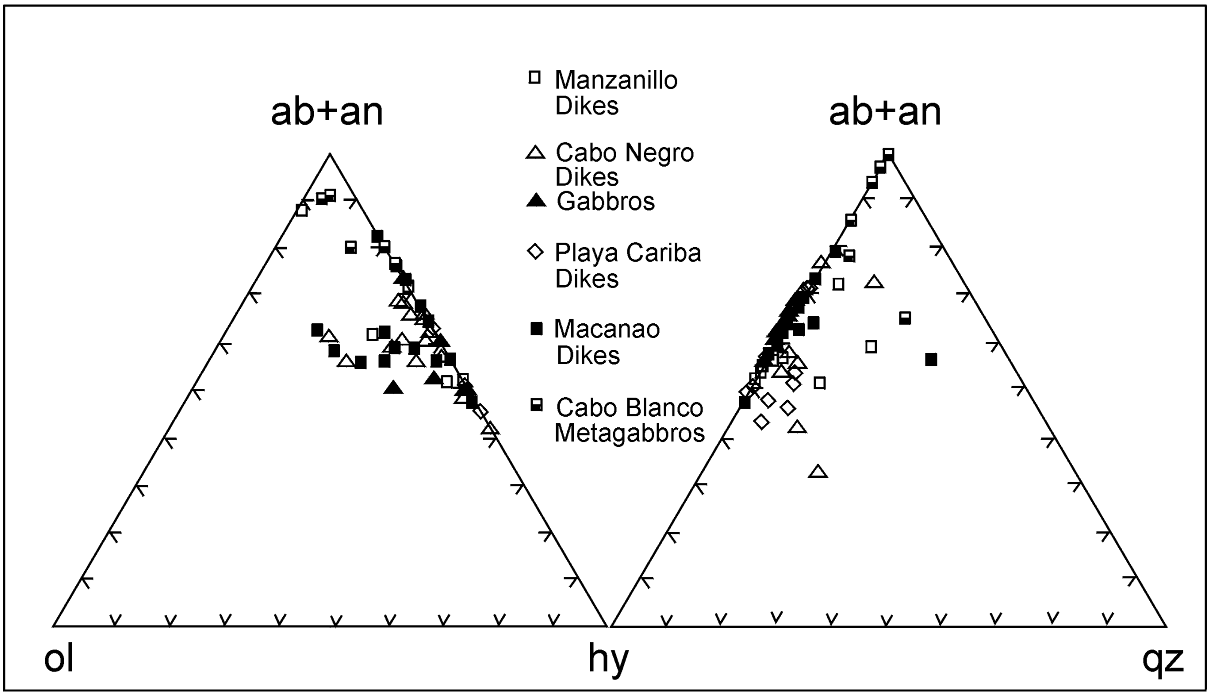

Figure 6.3:

Normative composition of whole rocks from Isla Margarita within the basalt tetrahedrons ab+an-hy-ol and ab+an-hy-qz after Yoder & Tilley (1962).

All rocks, regardless of which series, are hypersthene normative, with variations of Hy_{CIPW} from 13 to 42 within the dikes and of Hy_{CIPW} from 15 to 26 within the gabbroic intrusions, although modal hypersthene is absent. The dikes are partly quartz normative, with maximum values of Q_{CIPW} 17 and partly olivine normative with up to Ol_{CIPW} 16. Gabbroic intrusions are olivine normative, showing a variation of Ol_{CIPW} between 8 and 16 (Figure 6.3). Although olivine frequently occurs in the norm, no modal olivine was found in the Margarita suite. Secondary minerals, such as Mg-chlorite, however, are present and possibly replace former olivine phenocrysts.

The composition of normative plagioclase in the Margarita series varies from An_{CIPW22} to An_{CIPW40}. About 30% of the Margarita rocks studied are corundum normative. This peraluminous character is especially prevalent in the Playa Caribe dike suite. The variable amount of C_{CIPW} from 0.1 to 9.4 can be correlated with the occurrence of modal muscovite, resulting from plagioclase alteration. It may, however, also indicate the degree of assimilation of crustal material.

The Differentiation Index D.I. (D.I. = normative Qz+Or+Ab) after Thornton & Tuttle (1960), ranges from 12 to 42 within the dike suite and from 9 to 23 within the gabbroic intrusions.

6.4 GEOCHEMICAL CLASSIFICATION OF MARGARITA ROCKS

Geochemical characteristics such as silica-, alkali-, iron- and magnesium content are frequently applied for discrimination and nomenclature of igneous rocks (e.g. Macdonald & Katsura, 1964; Miyashiro, 1978). It must be emphasized, however, that the Margarita lamprophyric dike suite is compared and classified in this chapter with chemical (but not mineralogical), plutonic and volcanic equivalents. Total alkali- vs. silica content is applied for discrimination between silica undersaturated (alkalic) and saturated (subalkalic) rocks after Miyashiro (1978). The lamprophyric dikes, gabbroic intrusions and metagabbros plot into the silica saturated, subalkalic field which comprises calc-alkaline and tholeiitic rocks (Figure 6.4).

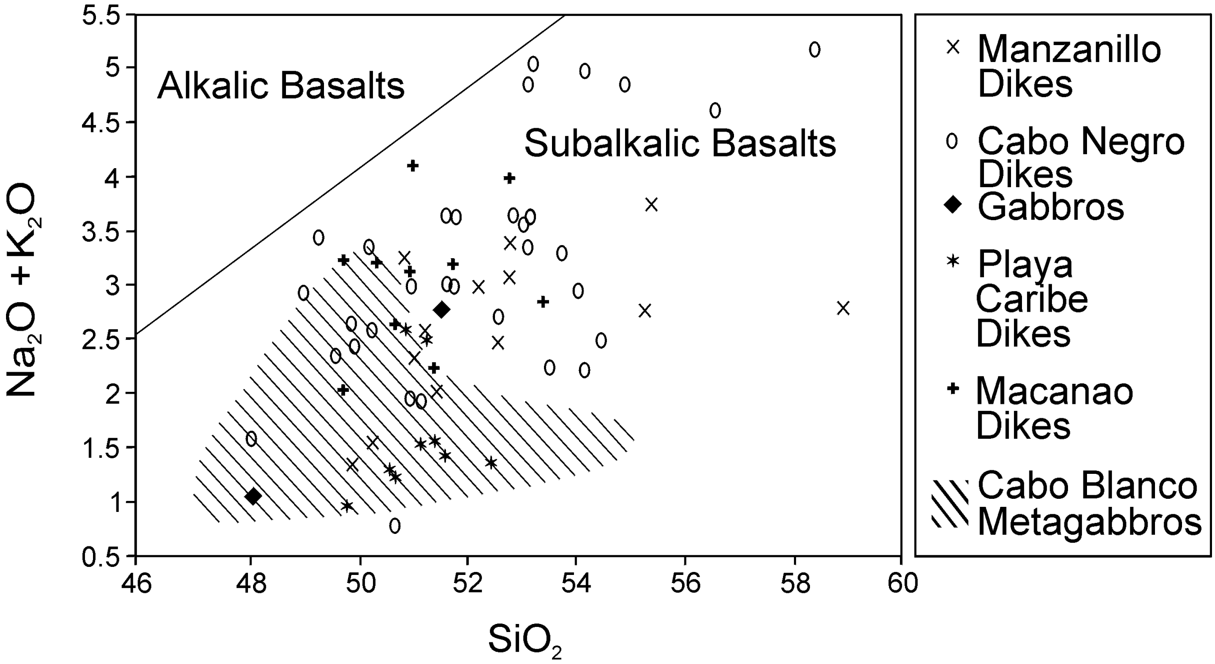

Figure 6.4:

Variation diagram of total alkalies (Na_2O+K_2O) vs. SiO_2 in dikes, gabbroic intrusions and metagabbros from Margarita. Dividing line for alkalic and subalkalic field after Miyashiro (1978). For better resolution of the graphics, the relatively large scatter of the metagabbro suite is displayed with a hatched signature.

The division of Margarita rocks into a series of predominantly basalts (48-52 wt% SiO_2), basaltic andesites (52-57 wt% SiO_2) and few andesites (>57 wt% SiO_2) in Figure 6.5, with low-, medium- and high-K types, is made according to Peccerillo & Taylor (1976).

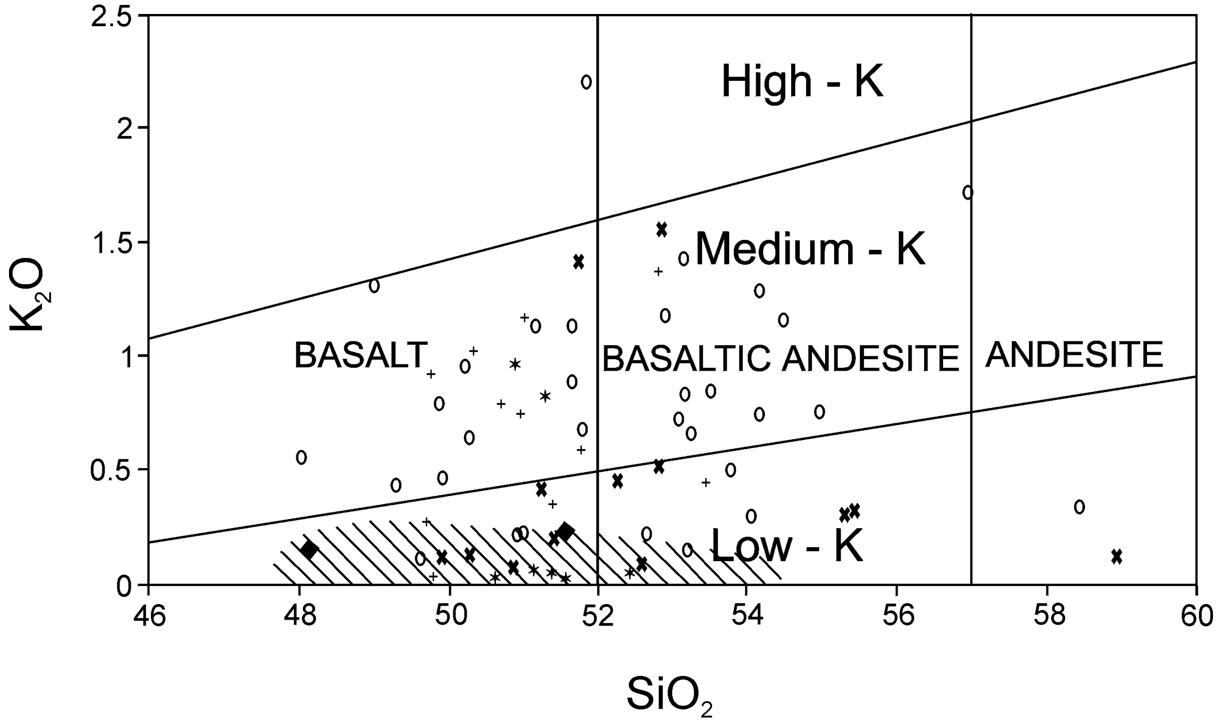

Figure 6.5

K_2O vs. SiO_2 variation diagram for dikes, gabbroic intrusions and metagabbros from Isla Margarita. Division of basalts, basaltic andesites and andesites into low-, medium- and high-K types according to Peccerillo & Taylor (1976). Symbols as in Figure 6.4.

Silica content and the FeO*/MgO-ratio can be used for further discrimination between calc-alkaline and tholeiitic rocks. In the corresponding diagram, the Margarita rock series lacks Fe-enrichment relative to Mg, indicating that calc-alkaline affinity dominates for the entire rock suite (Figure 6.6, after Miyashiro, 1974). On plot of total alkalies vs. iron and magnesium (AFM) in Figure 6.7 (Irvine & Baragar, 1971), the lack of iron-enrichment relative to alkalies and magnesium confirms the calc-alkaline differentiation trend of the Margarita series.

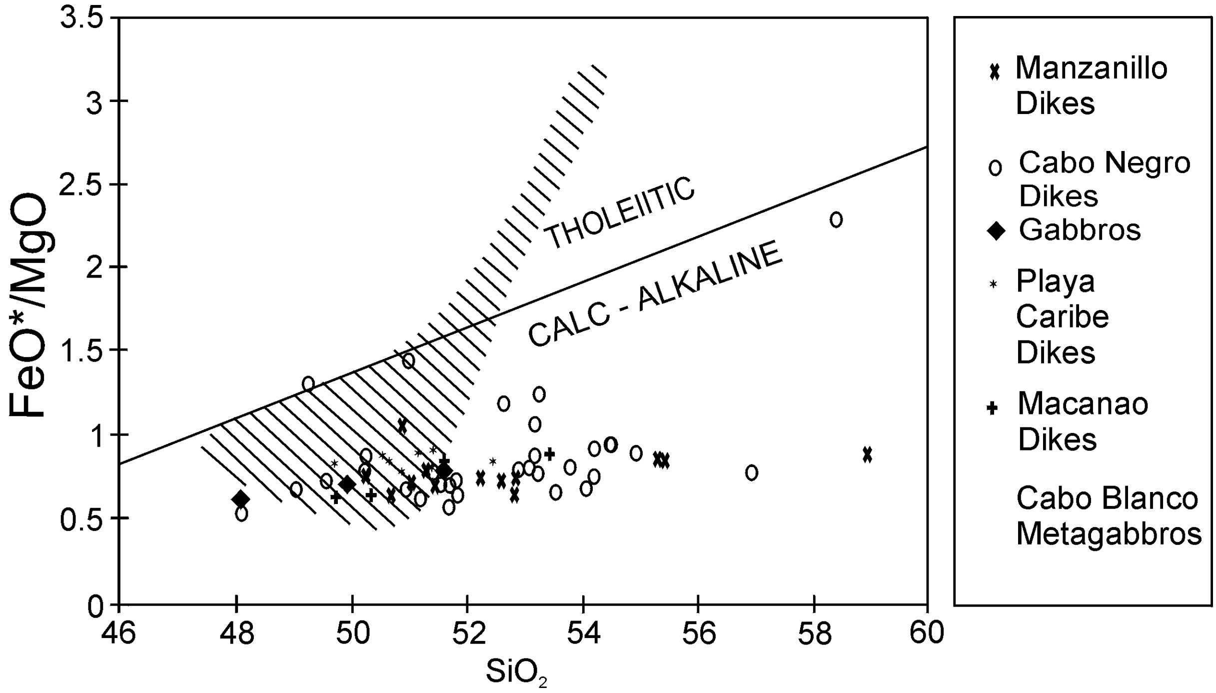

Figure 6.6:

Plot of FeO*/MgO vs. SiO_2 for whole rocks from Isla Margarita used to differentiate tholeiitic from calc-alkaline suites (Miyashiro, 1974).

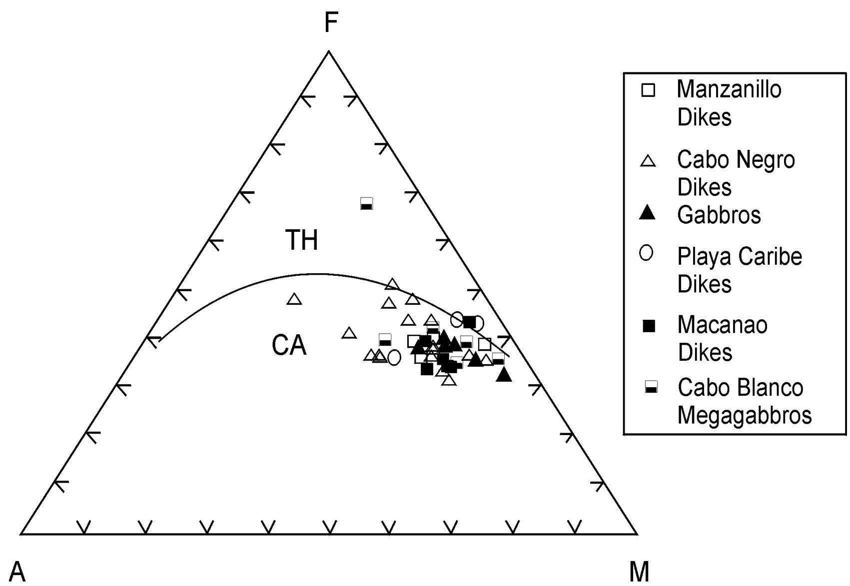

Figure 6.7:

AFM diagramm showing trends of dikes, gabbros and meta- gabbros from Isla Marga-rita. Solid line separates tholeiitic (TH) from calc-alkaline (CA) suites, using the criteria of Irvine & Baragar (1971).

6.5 MAJOR AND TRACE ELEMENT VARIATIONS

6.5.1 SiO_2

The chemical composition of the Margarita lamprophyric dike suite is characterized by a range in SiO_2 content which varies between 48.0 to 59.0 wt%. SiO_2 in gabbroic intrusions and metagabbros varies from 48.1 to 51.6 and 47.8 to 54.2 wt% respectively.

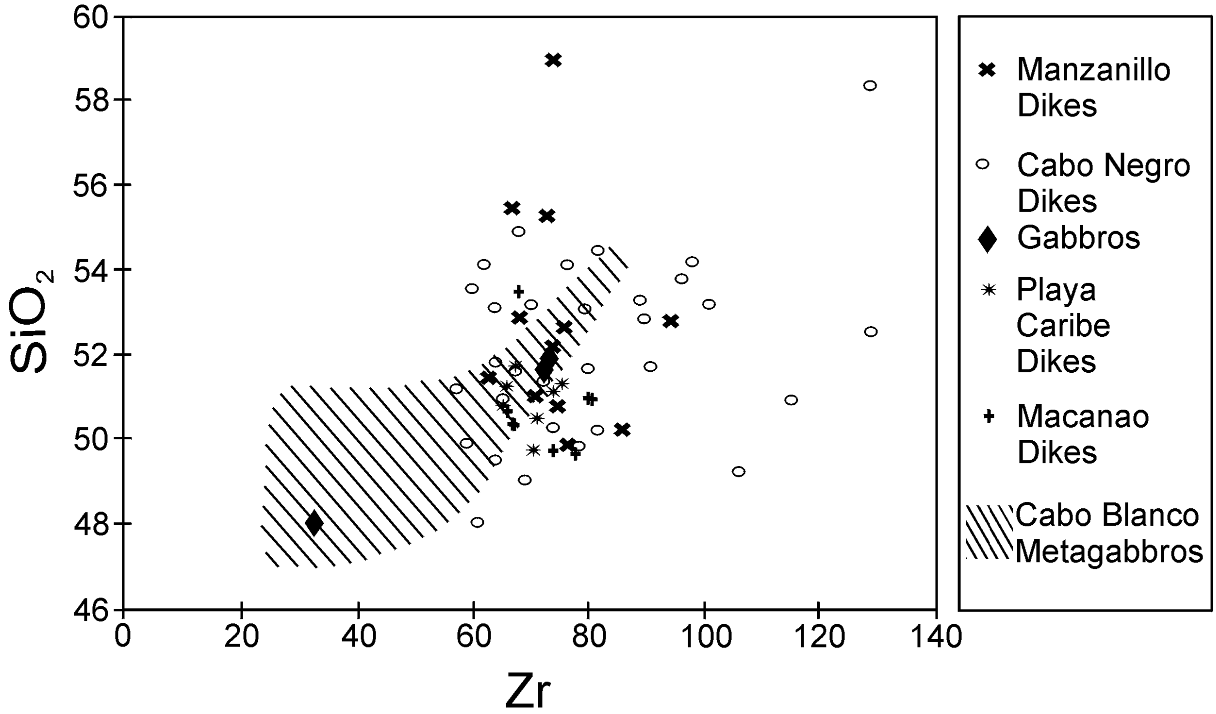

Figure 6.8:

SiO_2 vs. Zr variation diagram of whole rocks from Isla Margarita.

Similar SiO_2 concentrations in the rocks from the different suites do not necessarily imply similar degrees of differentiation, since large variations of compatible element concentrations at given SiO_2 concentrations were observed. Inter-suite comparisons, made on the basis of silica variations, may mask differentiation-dependent differences, whereas within-suite comparisons on this basis may be profitable. The element variations of the majority of other oxides of the Margarita rocks are shown graphically vs. Zr instead of SiO_2 or MgO, as Zr is generally regarded to be unaffected by alteration (e.g. Pearce & Cann, 1973; Meschede, 1986).

6.5.2 CaO, Al_2O_3

The CaO content increases with considerable scatter towards higher differentiated composition and thus higher Zr content. CaO increases in the Cabo Negro dikes from 3.5 to 11.1 wt%, in gabbros from 8.7 to 12.8 wt%. CaO shows no systematic variation with Zr in the Manzanillo suite (5.11 to 15.3 wt%), in the Playa Caribe suite (7.0 to 10.4 wt%) and in the Macanao suite (7.5 to 10.1 wt%) as well as in the metagabbro suite (12.2 to 16.4 wt%) (Figure 6.9).

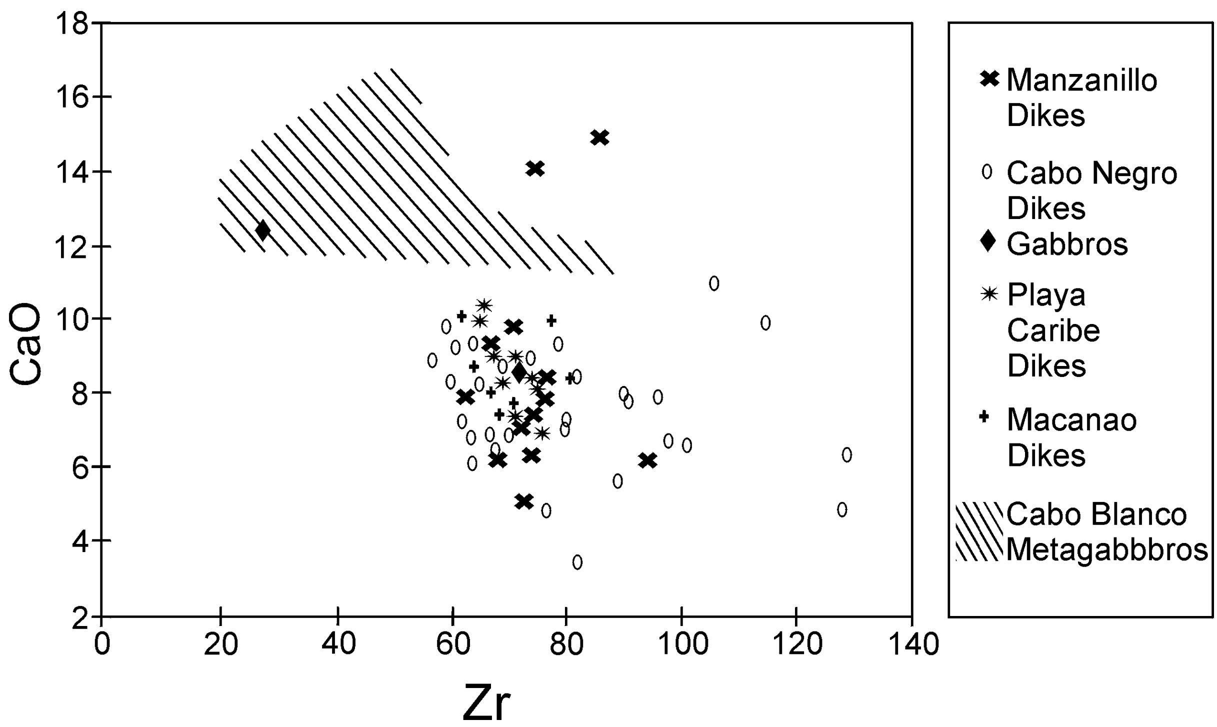

Figure 6.9:

CaO vs. Zr variation diagram of whole rocks from Isla Margarita.

A large variation in Al_2O_3 concentration is observed in the metagabbros (14.8-18.7 wt% Al_2O_3, besides one erratic sample with 9.8 wt%) and in the dikes (14.1 to 19.0 wt% Al_2O_3). The Al_2O_3 range in gabbroic intrusions is small from 14.4 to 16.5 wt%. The majority of samples varies between 14 and 18 wt% Al_2O_3. This is comparable in composition with low-alumina rocks (14-16 wt% Al_2O_3) from island-arc tholeiitic suites of the Izu, Tonga and South Sandwich arcs (Gill, 1981) and the average of lamprophyric spessartites with an Al_2O_3 content of 15 wt% (Rock, 1991).

The CaO/Al_2O_3 ratios of all suites decrease with differentiation (Figure 6.10). This is generally observed in island arc magmas, for which the differentiation trend is determined by fractionation of olivine+clinopyroxene. The CaO/Al_2O_3 ratio in MORB, however, increases with differentiation, which can be attributed to the fractionation of olivine+plagioclase (Bence et al., 1979; Perfit et al., 1980).

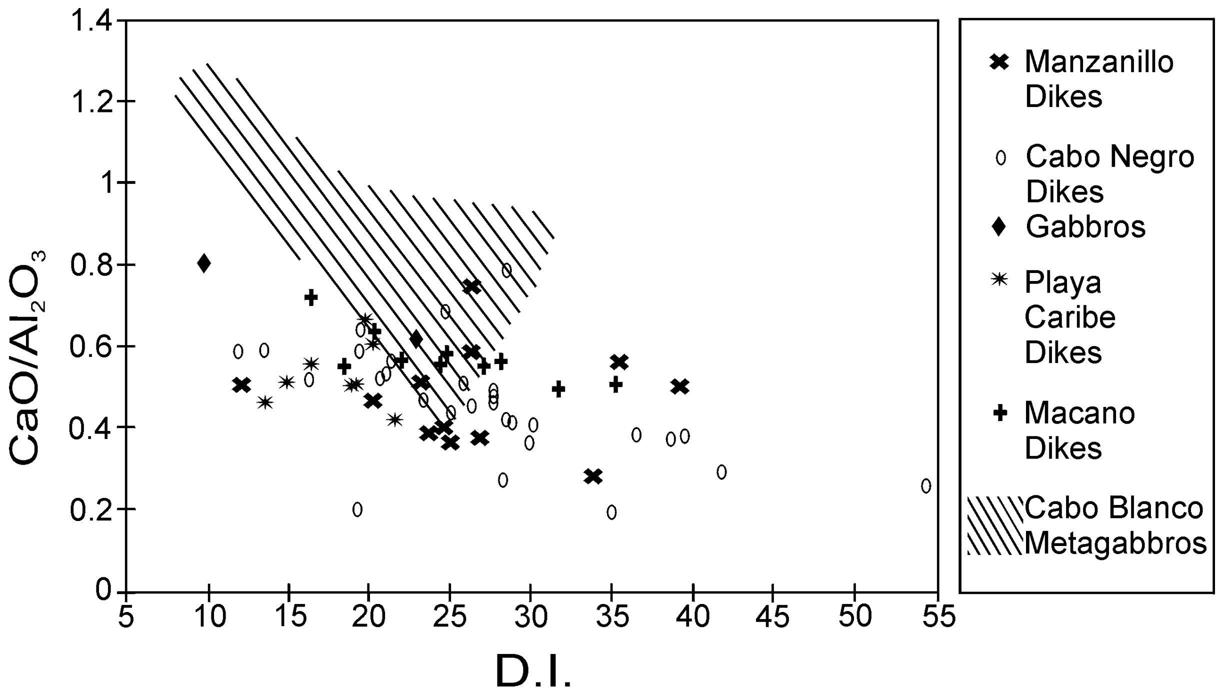

Figure 6.10

CaO/Al2O3 ratios vs. D.I. (Differentiation Index (= normative Q+Or+Ab) after Thornton & Tuttle, 1960) of whole rocks from Isla Margarita.

6.5.3 ALKALIES: Na_2O, K_2O

The Na_2O content in dikes increases from 0.8 to 4.8 wt%, in gabbroic intrusions from 1.0 to 2.5 wt% and in metagabbros with broad scatter from 0.9 to 3.1 wt% towards more differentiated compositions. The Na_2O variation at a given Zr content is considerable and reaches up to 2.5 wt% (Figure 6.11).

K_2O has been proven to be most sensitive to alteration (see section 6.2) and consequently, it shows broadest scatter in concentration. The ranges are from 0.03 to 1.6 wt% K_2O in dikes and from 0.13 to 0.25 wt% in gabbroic intrusions; the range in metagabbros is small between 0.07 and 0.12 wt% K_2O (Figure 6.12).

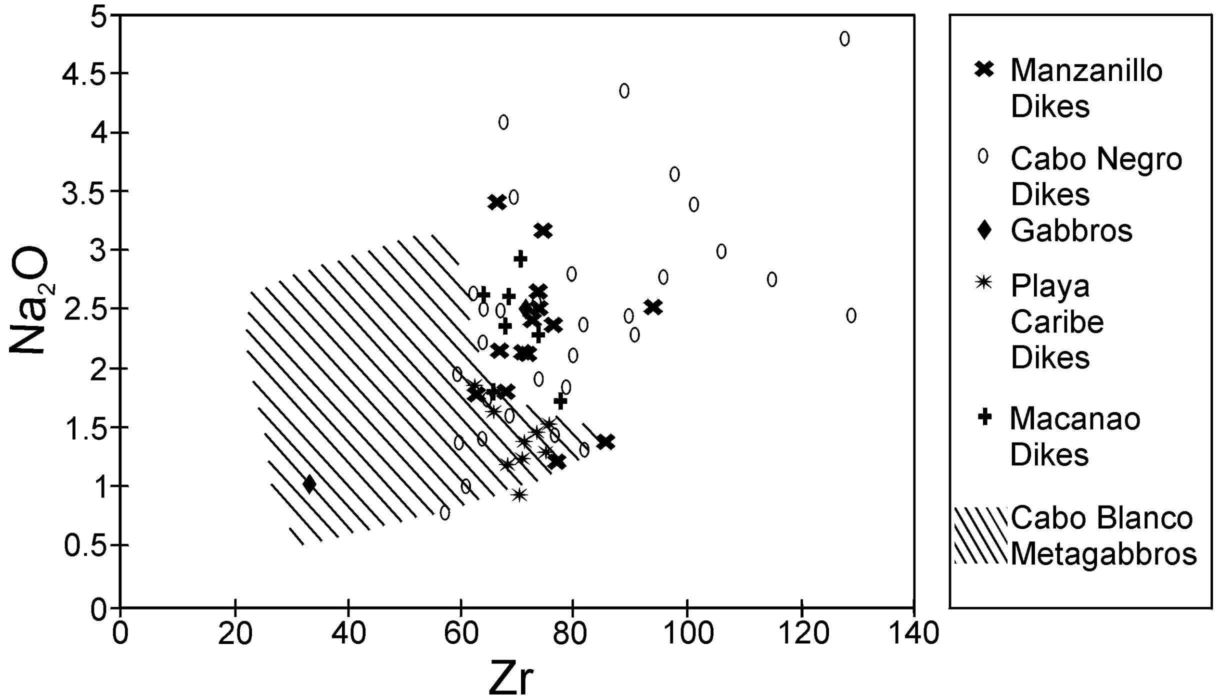

Figure 6.11:

Na_2O vs. Zr variation diagram of whole rocks from Isla Margarita.

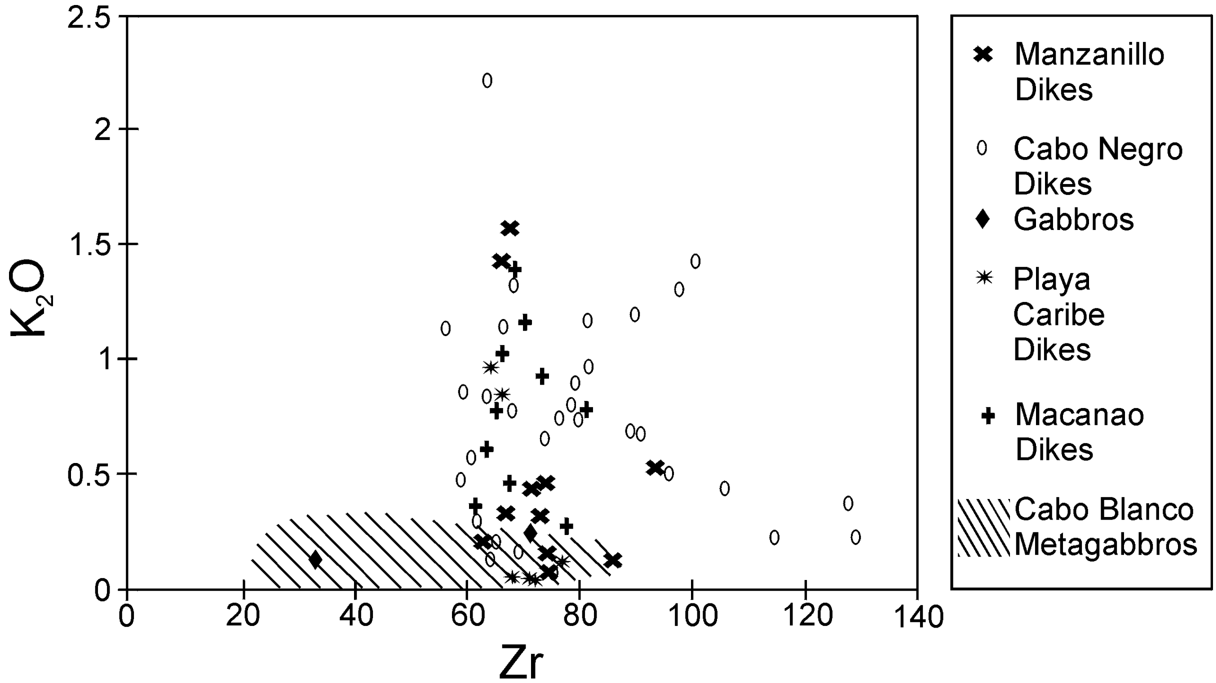

Figure 6.12:

K_2O vs. Zr variation diagram of whole rocks from Isla Margarita.

6.5.4 COMPATIBLE ELEMENTS: Mg, Ni, Cr, Co

Compatible elements correlate negatively with Zr, whereas correlation between compatible elements is positive. Given these criteria, the overall high MgO contents in the Margarita rocks reflect primary compositions, although strongly altered samples may also have gained Mg during hydrothermal alteration processes (see section 6.2).

The dikes display overall broad variation in MgO concentration decreasing with differentiation from 14.5 to 3.4 wt%, with a majority of samples between 14 and 6 wt%. MgO in gabbroic intrusions varies towards higher evolved compositions from 13.9 to 12.4 wt%, in metagabbros from 15.1 to 3.4 wt% (Figure 6.13).

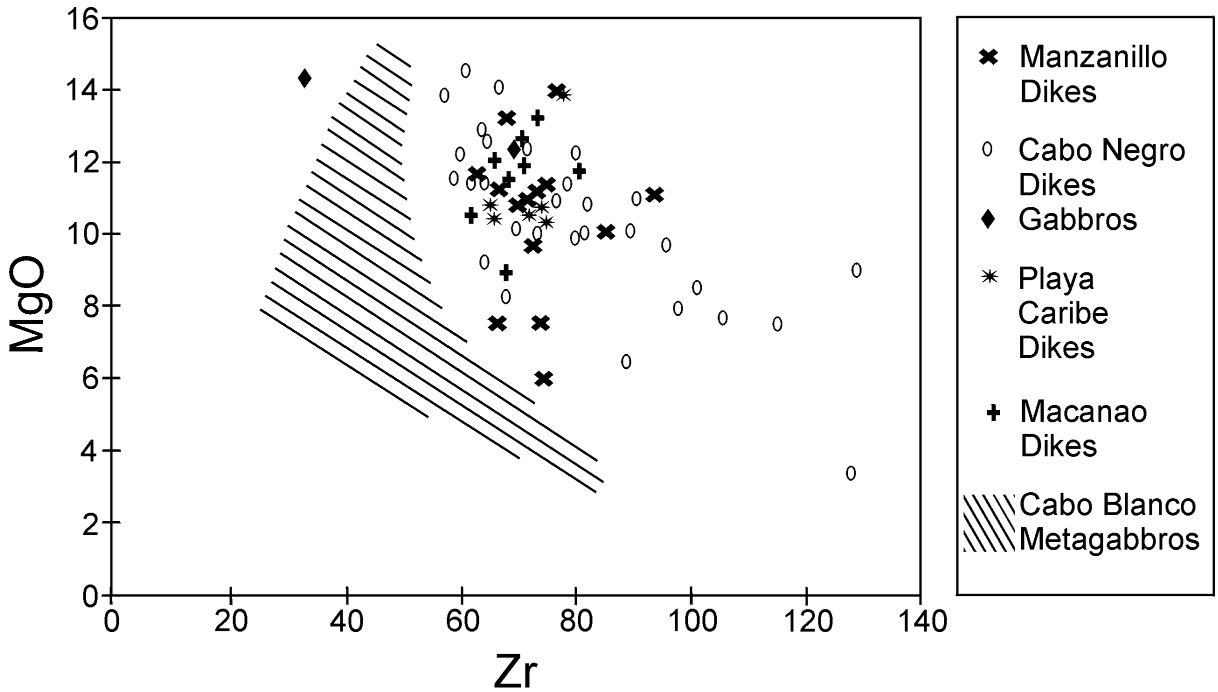

Figure 6.13:

MgO vs. Zr variation diagram of whole rocks from Isla Margarita.

Ni decreases systematically towards higher differentiated samples from 396 to 12 ppm in dikes and from 263 to 206 ppm in gabbroic intrusions (Figure 6.14). The range of Ni in metagabbros is low from 126 to 16 ppm. A positive correlation of Mg and Ni in the Margarita suite is compatible with fractionation of olivine. Absolute Ni concentrations of Margarita rocks are significantly higher (up to 400 ppm) than values of Ni in other basaltic-andesitic suites (Gill, 1981), and in spessartites (Rock, 1991) with up to 100 ppm Ni.

Cr decreases with differentiation from 953 to 18 ppm in dikes and from 681 to 608 ppm in gabbroic intrusions (Figure 6.15), indicating chromite fractionation. Metagabbros show broad scatter with a decrease from 427 to 27 ppm. Cr contents in Margarita rocks are considerably high, also exceeding the concentrations of average spessartites with 330 ppm (Rock, 1991).

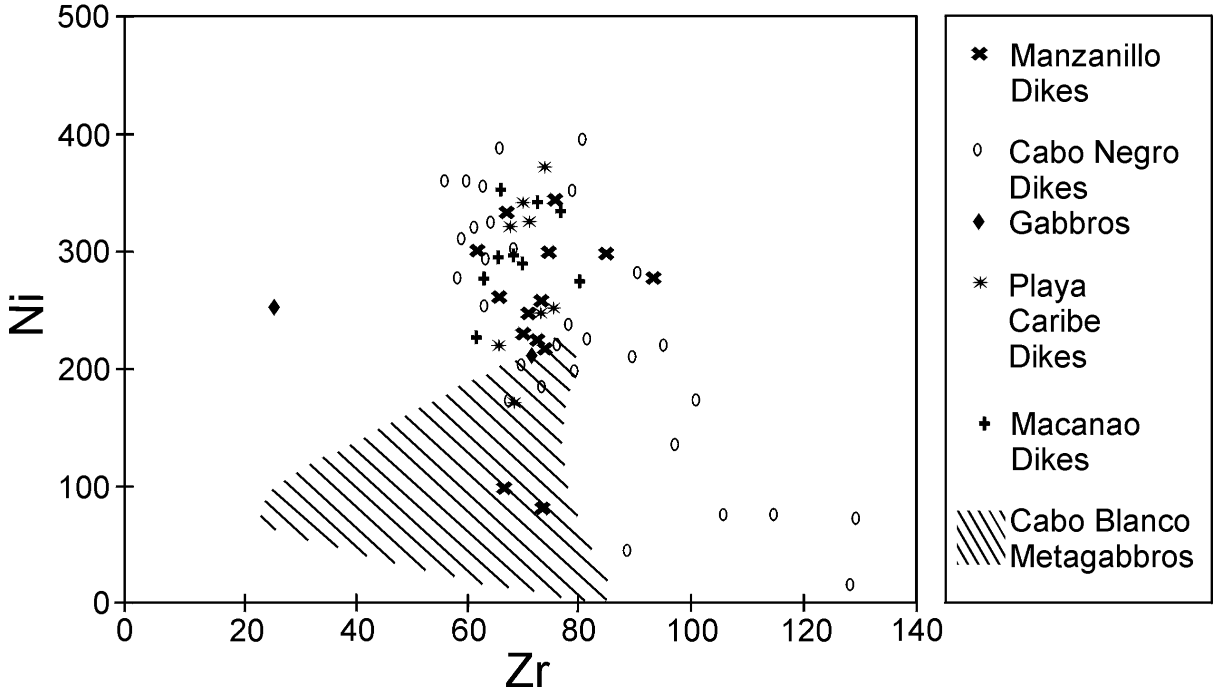

Figure 6.14:

Ni vs. Zr variation diagram of whole rocks from Isla Margarita.

Co contents are less variable than Ni and Cr and decrease systematically with differentiation from 63 to 40 ppm. The Playa Caribe samples 6101 and 6102, however, are considerably higher in Co content with 78 and 96 ppm respectively. Co in gabbroic intrusions decreases from 63 to 58 ppm, whereas metagabbros show a broader variation between 76 and 40 ppm (Figure 6.16). Co contents are, alike Ni contents, higher than in average orogenic suites (Gill, 1981; Wilson, 1988) and spessartites (30-40 ppm) (Rock, 1991) but similar to those of MORB.

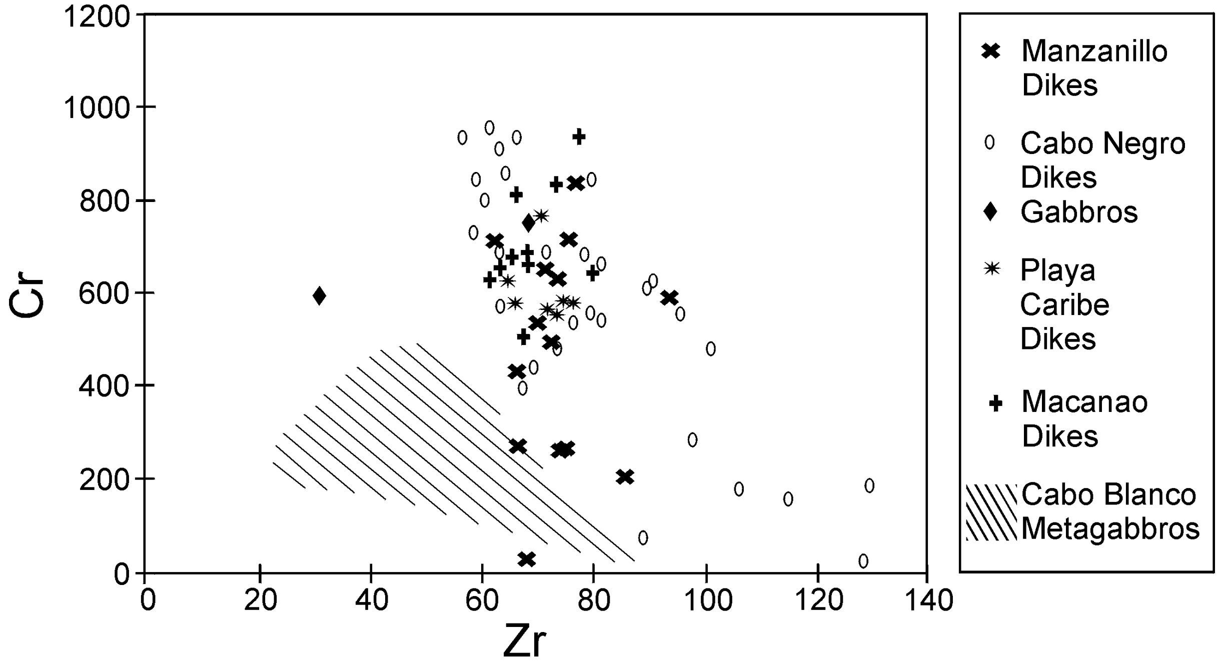

Figure 6.15:

Cr vs. Zr variation diagram of whole rocks from Isla Margarita.

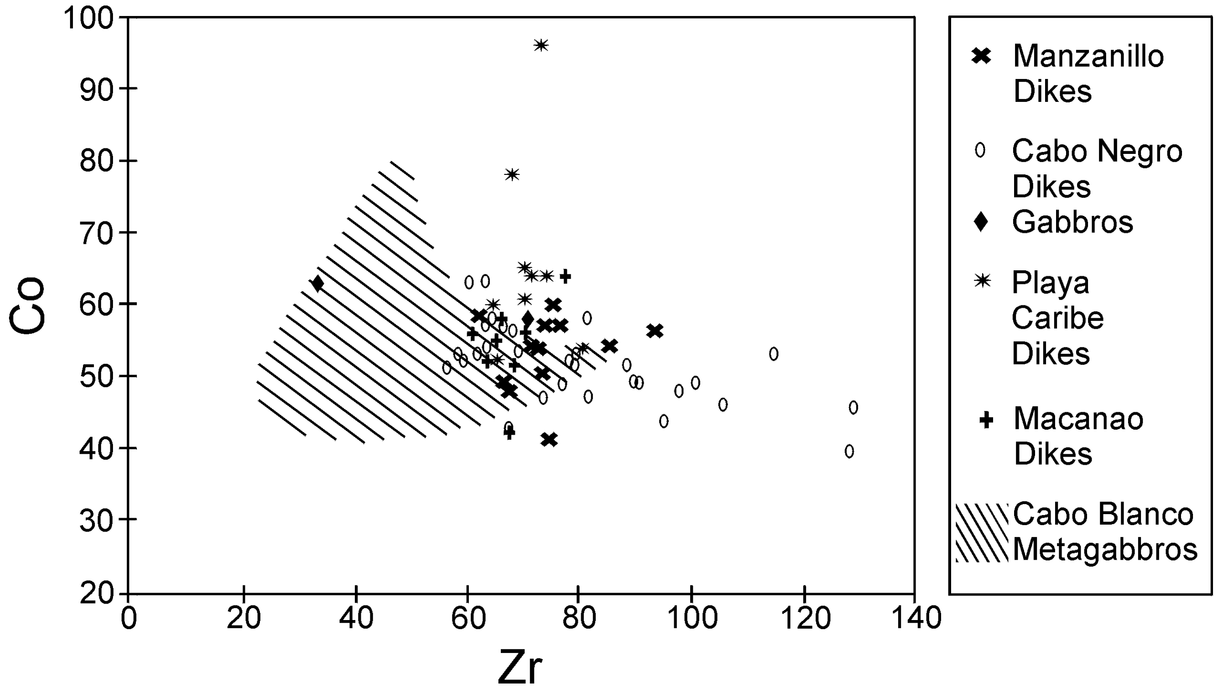

Figure 6.16:

Co vs. Zr variation diagram of whole rocks from Isla Margarita.

The overall high compatible element concentrations lie at levels typical for mafic to ultramafic lamprophyres (Rock, 1977, 1984, 1991; Wimmenauer, 1985) and primitive, high-Mg basalts from the Lesser Antilles (Devine, 1995). The systematic decrease of these elements with differentiation is consistent with partition coefficients >>1 during fractionation of olivine + chromite from parental melts.

5.5 Mg-NUMBER

Variations in basaltic chemistry are often displayed by their Mg-number (Mg# = 100*Mg/(Mg+Fe*)), since decreasing values with differentiation reflect fractionation of ferromagnesian phases. The oxidation state of iron, however, is high in the Margarita suite. Given this criteria, pre-eruption contents of Fe_2O_3 no higher than 3 wt% were estimated when calculating the Mg-numbers (Fe_2O_3 content >3 wt% was recalculated to FeO). Mg#`s in the Margarita suite decrease with differentiation in the dikes from 66 to 35, clustering around 55, in gabbroic intrusions from 62 to 55 and in metagabbros from 78 to 45 (Figure 6.17). In terms of Mg#'s, even the most primitive Margarita basalts do not represent unfractionated equilibrium mantle melts. The requirement that primary mantle melts have Mg# >70, has been widely accepted in discussions of basalt genesis (e.g. Hanson & Langmuir, 1978; Wilson, 1988).

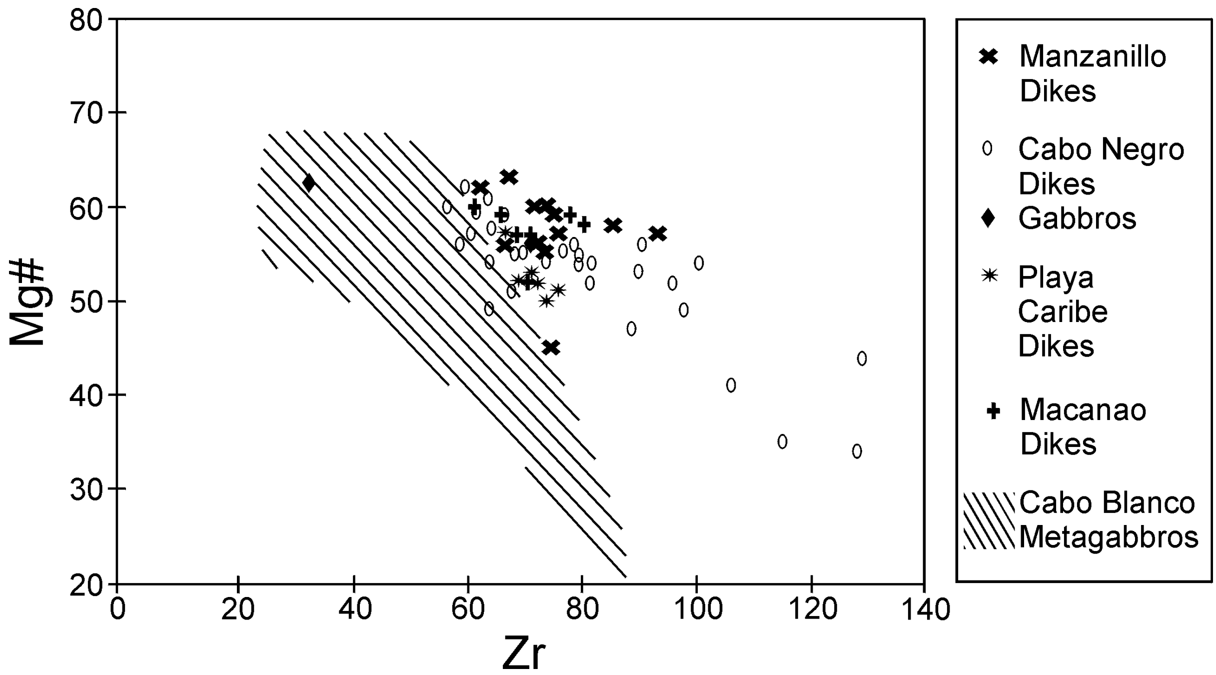

Figure 6.17:

Variation of Mg#'s (100*Mg/(Mg+Fe*)) vs. Zr in whole rocks from Isla Margarita.

Margarita rocks are slightly lower in their Mg#'s than average calc-alkaline lamprophyres, with Mg#'s of 75 (Rock, 1991) and the population of orogenic basaltic-andesitic suites, with average Mg#'s of 60 (Gill, 1981). Amongst the orogenic suite, calc-alkaline rocks display generally higher Mg#'s (lower FeO*/MgO ratios) than tholeiitic rocks at any silica content.

Mg-numbers >60 in calc-alkaline populations are especially common in arcs beneath which young lithosphere is subducted e.g. the Cascades, Mexico and southernmost Chile (Gill, 1981).

6.5.6 FeO*, Fe_2O_3, V

Total iron as FeO* increases with broad scatter from 6.3 to 10.8 wt% towards more differentiated compositions (Figure 6.18). In contrast, the Fe_2O_3/FeO ratios show no systematic trend (Figure 6.19). The latter is considered to be unaffected by differentiation, but rather reflects alteration processes.

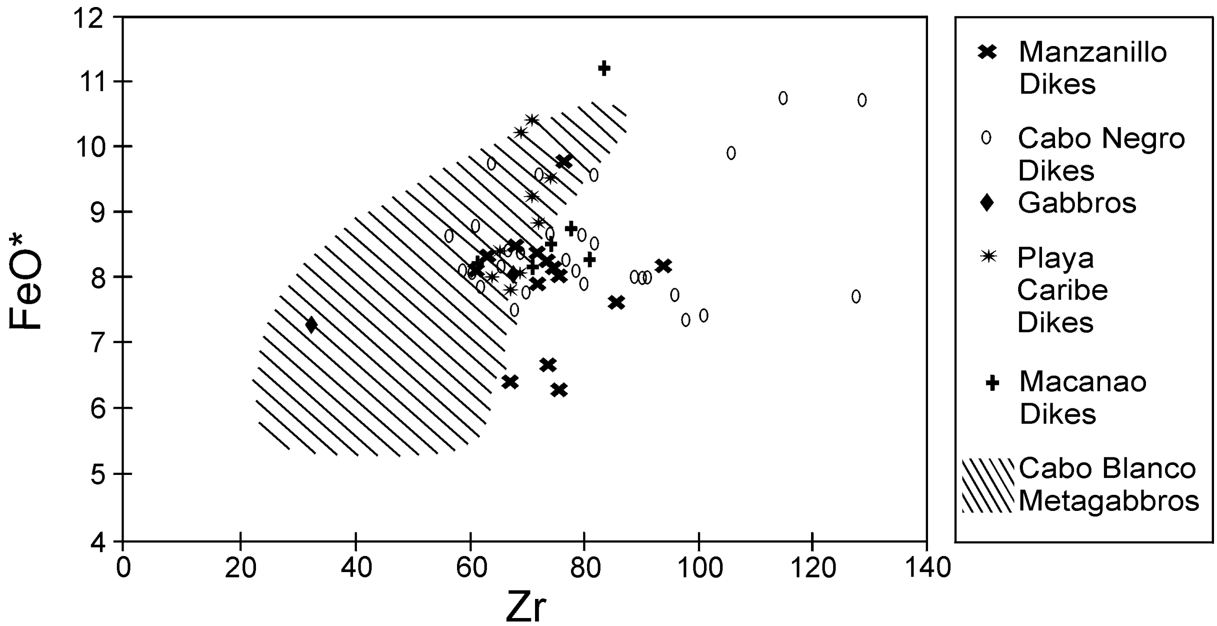

Figure 6.18:

FeO* vs. Zr variation diagram of whole rocks from Isla Margarita.

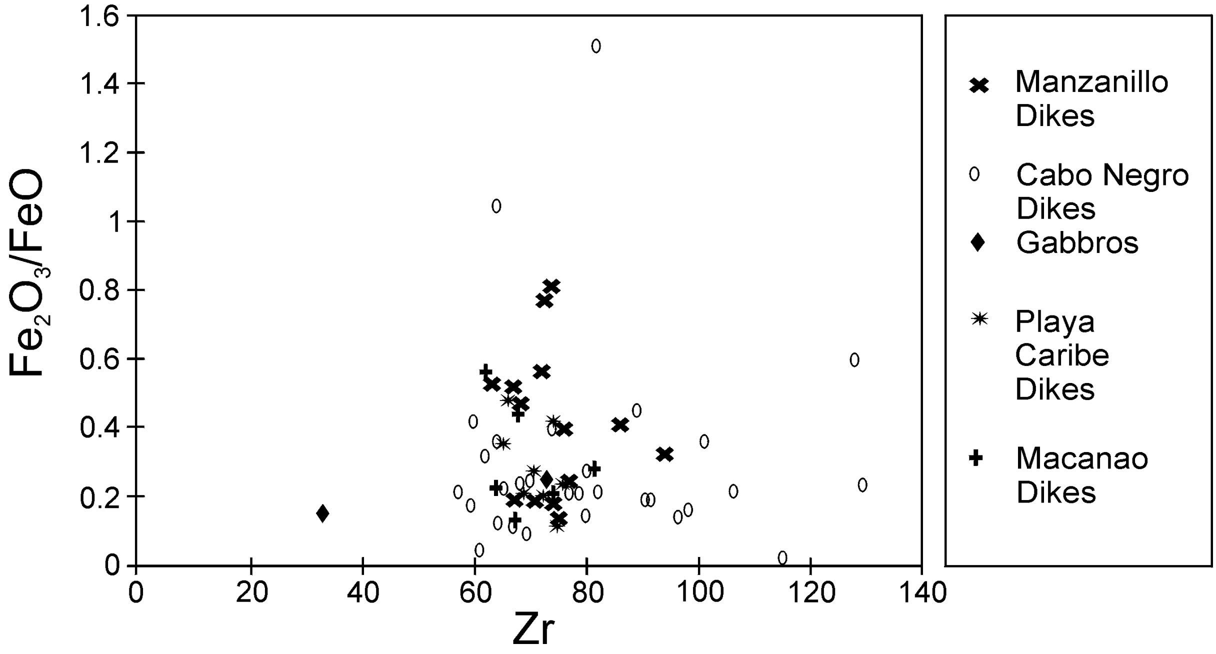

Figure 6.19:

Fe2O3/FeO vs. Zr variation diagram of whole rocks from Isla Margarita.

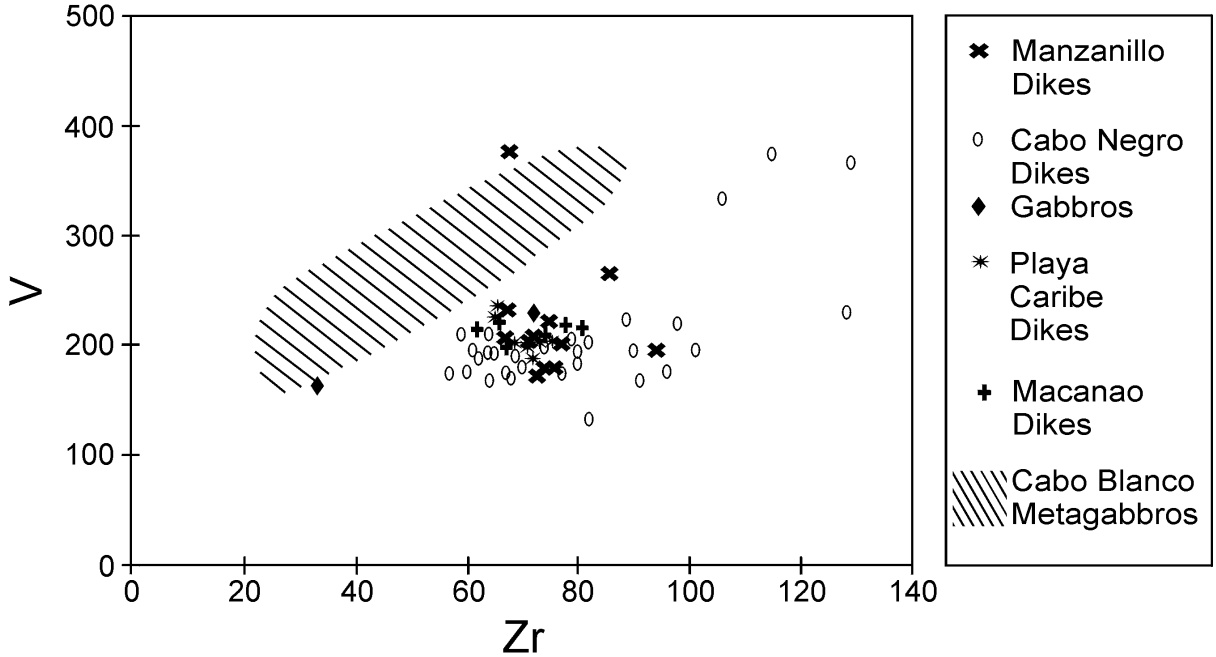

Figure 6.20:

V vs. Zr variation diagram of whole rocks from Isla Margarita.

V shows slight increase with differentiation (132 to 230 ppm, Figure 6.20) except for three dike samples from Cabo Negro which contain ilmenite and thus relatively high V (334 to 376 ppm).

FeO is removed early from the melt by crystallization of chromite and clinopyroxene and V by ilmenite, the latter being altered in most cases to leucoxene (see section 5.2.5). Precipitation of magnetite may have occurred during the late stage crystallization of Margarita rocks. However, magnetite is not preserved, but its former existence may be indicated by the presence of hematite (see section 5.6.4).

6.5.7 HIGH FIELD STRENGTH ELEMENTS: Ti, P, Zr

Overall low concentrations of Ti, P and Zr, all belonging to the group of High Field Strength elements (HFSE), are characteristic of the Margarita samples. TiO_2 varies in concentration from 0.41 to 1.1 wt%, except for three dike samples which contain ilmenite and thus relatively higher TiO_2 concentrations with 1.63 to 2.02 wt% (Figure 6.21).

P_2O_5 shows overall variation from 0.04 to 0.21 wt% (Figure 6.22) and corresponds well to other orogenic suites with 0.05 to 0.3 wt% P_2O_5 (Gill, 1981). The Zr content increases systematically towards higher differentiated endmembers and is consistent with processes dominated by fractional crystallization. The concentrations of Zr vary in dikes from 60 to 130 ppm, in gabbroic intrusions from 33 to 72 ppm and in metagabbros from 27 to 84 ppm. The compositional range of Zr in the Margarita dikes corresponds to the range found in other orogenic suites (50-150 ppm Zr, Gill, 1981). High field strength elements (HFSE) are not incorporated appreciably in major rock-forming minerals (except for Ti in magnetite and ilmenite). As a result, these elements correlate positively with each other and with indices of differentiation in silica saturated magmas.

Low concentrations of HFSE are generally attributed to partial melts from a mantle source already depleted by previous melting (Pearce et al., 1981; Duncan & Green, 1987). The overall low TiO_2 contents of Margarita rocks are characteristic of rocks related to convergent plate boundaries, compared to volcanic rocks from intra-plate settings. Arc basalts and andesites in general, rarely have TiO_2 >1.3 wt%. The consistently low titanium trend is an example for the general impoverishment of arc magmas in the Ti-group elements (including Zr and Nb), an impoverishment that has been used to distinguish arc derived rocks from others by Pearce & Cann (1973) and Mullen (1983).

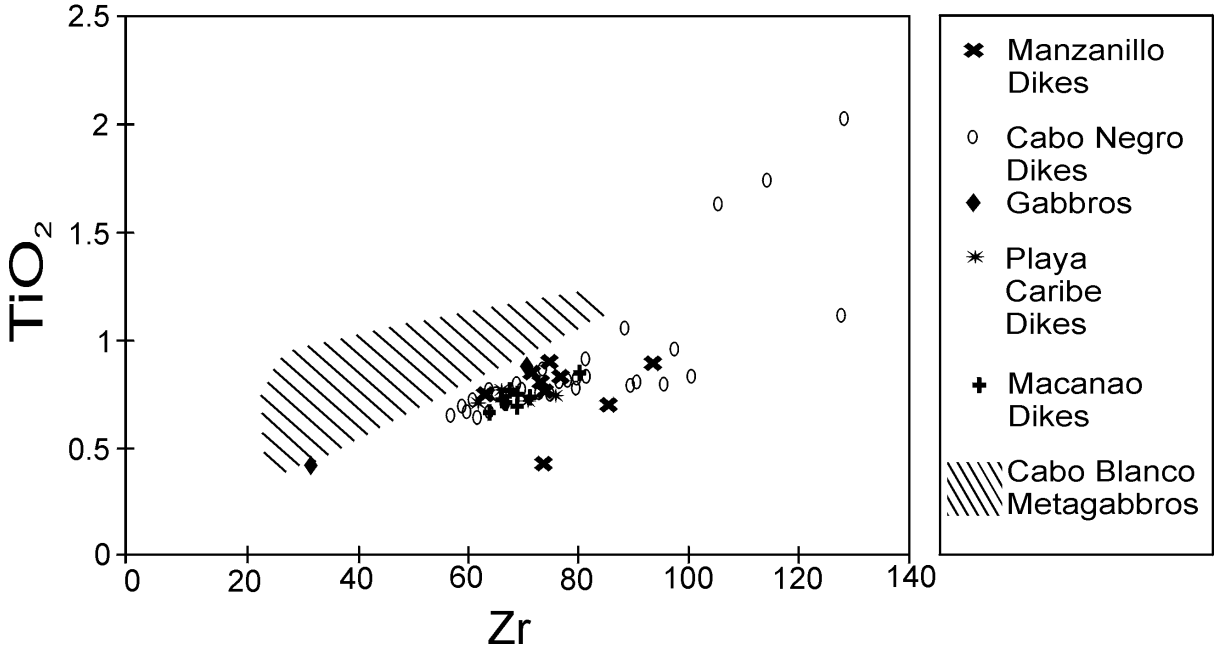

Figure 6.21:

TiO_2 vs. Zr variation diagram of whole rocks from Isla Margarita.

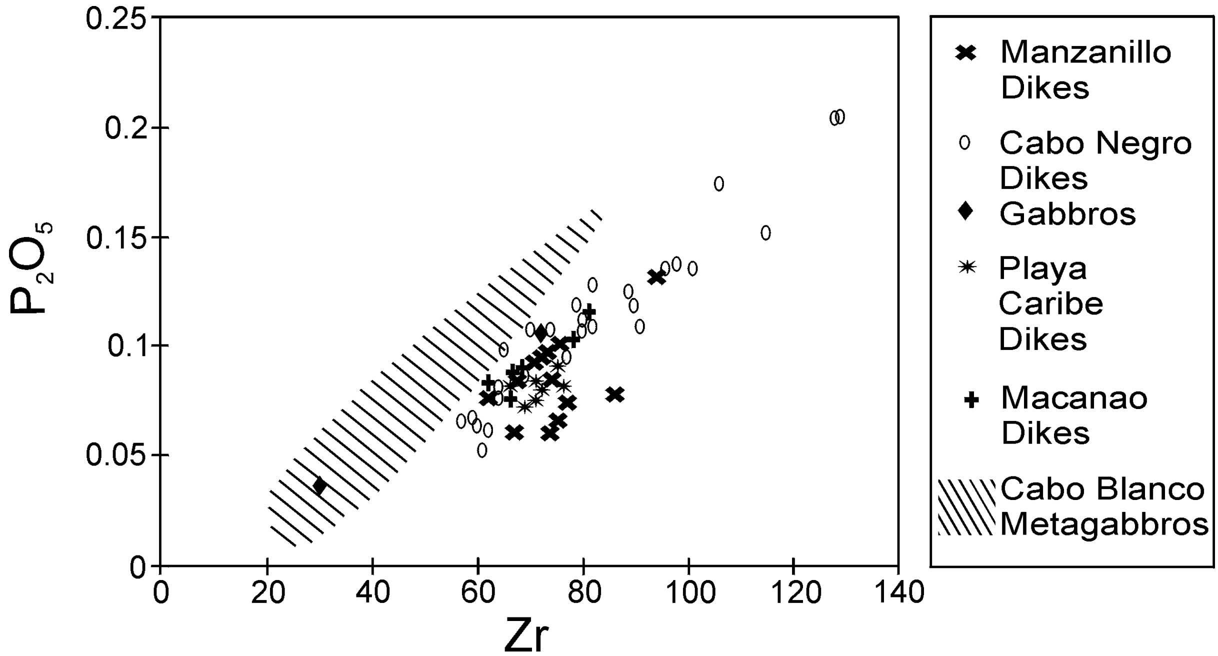

Figure 6.22:

P_2O_5 vs. Zr variation diagram of whole rocks from Isla Margarita.

6.5.8 VOLATILES: H_2O, CO_2, S, H_2O

The role of volatiles in magma generation is a very complex system and especially H_2O affects the subsequent differentiation trend (e.g. Morse, 1980; Sakuyama, 1983; Devine, 1995). Pre-eruptive volatile content can only be accurately estimated in unaltered basaltic glasses, since volatiles can be lost during cooling and degassing, as well as gained by alteration (Gill, 1981; Bednarz & Schmincke, 1989). Few quantitative estimates of the H_2O contents of parental basic magmas exist (e.g. Sisson & Grove, 1993; Devine, 1995; Sobolev & Chaudisson, 1996) and are estimated to be less than 2 wt%. Calc-alkaline rocks in general, but especially calc-alkaline lamprophyres, contain considerably higher concentrations of volatiles and higher CO_2/H_2O ratios than either MORB or Intra Plate basalts, suggesting involvement of a slab-derived volatile component (Rock, 1991).

The Margarita lamprophyres are characterized by a broad variation in H_2O content, ranging from 1.21 to 6.79 wt%, which is regarded to reflect strong alteration. Gabbroic intrusions show relatively small variation in H_2O content, varying from 2.8 to 3.2 wt%. Metagabbros show lowest values between 0.8 and 1.9 wt% (Figure 6.23).

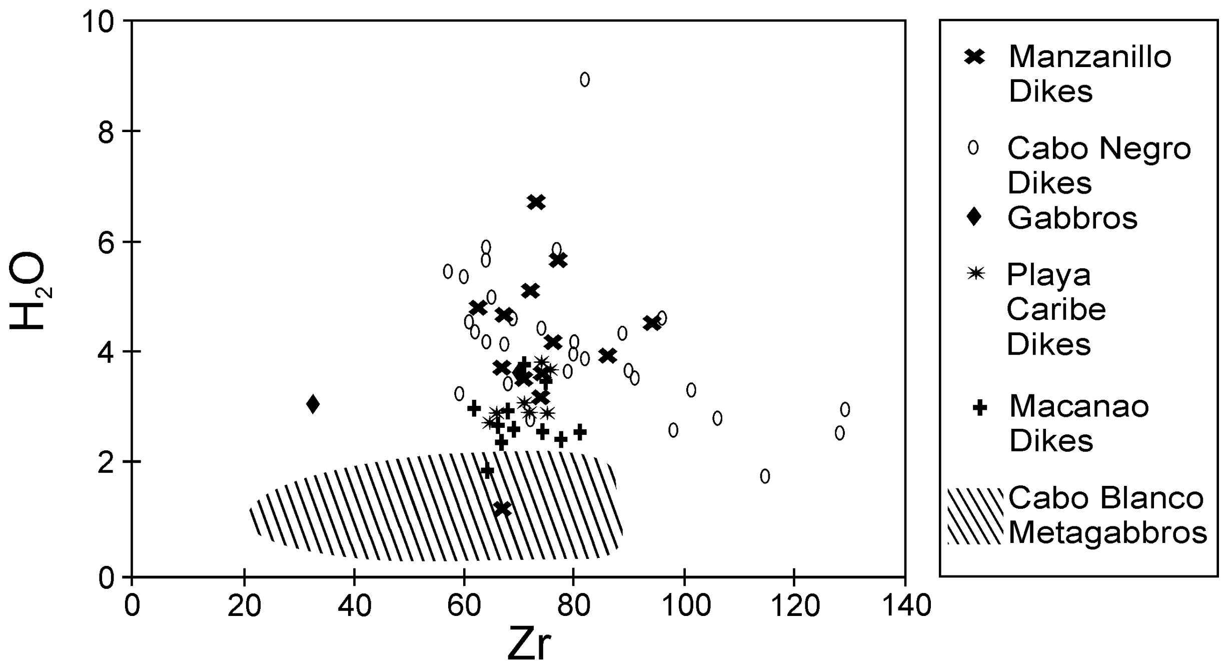

Figure 6.23:

H_2O vs. Zr variation diagram of whole rocks from Isla Margarita.

The pre-eruptive water content of the Margarita magma can be estimated and distinguished from alteration-gained water by comparing the phenocryst crystallization sequence with experimentally determined phase relations in melts with similar compositions. An-rich plagioclase, Wo-rich clinopyroxene and abundant hornblende are classic phase equilibrium indicators of high water pressure (Johnson et al., 1994). A comparison of the phenocryst assemblage in the Margarita rocks, with the respective stability fields for a hornblende-bearing calc-alkaline basic andesite, indicates that the magma contained about 4 wt% H_2O (Burnham, 1979; Merzbacher & Eggler, 1984). Melt water contents as high as 4 wt% further require water pressure to be greater than about 1.5 kb (e.g. Rutherford & Devine, 1988, 1995), corresponding to depths =5 km.

The hydrous state also explains the lamprophyric texture, as it enhances the crystallization of large euhedral amphibole and pyroxene phenocrysts (Smith, 1946; Rock, 1991). In contrast, the crystallization of feldspars is suppressed by the hydrous conditions, which confines their occurrence to the groundmass (Yoder & Tilley, 1962). However, few exceptions exist in the Margarita suite, with a small number of plagioclase phenocrysts occurring in andesitic samples.

The solubility of H_2O in melts is primarily controlled by pressure, whereas temperature and magma composition are relatively unimportant in basalts and andesites (Gill, 1981; Johnson et al., 1994). Thus, water contents affect the depth at which the ascent of magma is arrested and fractionation occurs, with more water-rich magmas fractionating at greater depths. For the Margarita suite this implies that fractionation occurred at depth between 3 and 5 km, when assuming 4 wt% H_2O, as portions of reservoirs deeper than 5 km were water-undersaturated. The crystallization sequence suggests that pyroxenes and/or olivine+plagioclase crystallized early at low H_2O contents (<2 wt%) and temperatures of 1200°C. With increasing H_2O, the liquidus temperature decreased from >1200°C to approximately 1000° and plagioclase crystallization was suppressed relative to crystallization of pyroxenes. Subsequently, amphibole crystallization occurred at 950-1000°C when H_2O in the melt increased to about 4 wt%.

CO_2

The solubility of CO_2 is more dependent on temperature and magma composition than in the case of H_2O. The CO_2 solubility at crustal pressures with T 900°-1100°C is expected to be about 0.5 wt% (Mysen et al., 1975).

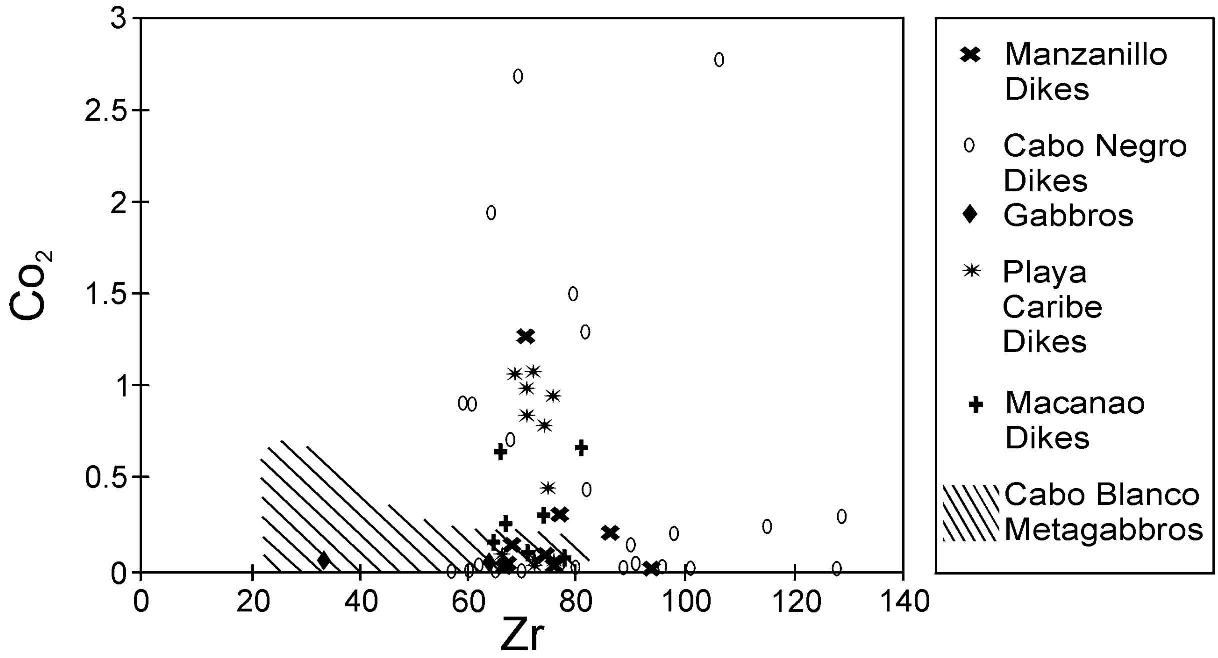

Figure 6.25:

CO_2 vs. Zr variation diagram of whole rocks from Isla Margarita.

CO_2 varies between 0.01 and 2.78 wt% in the Margarita suite (Figure 6.25). The high CO_2 and H_2O values of the dike suite are believed to be partly primary, being characteristic of the lamprophyre rock type (Rock, 1984), and partly related to secondary alteration, as indicated by the occurrence of carbonate. Gabbroic intrusions lack carbonate and show low concentrations of 0.02 and 0.05 wt% CO_2, which is more likely to reflect the initial CO_2 concentrations. CO_2 in metagabbros varies between 0.01 and 0.62 wt%.

Sulfur

The sulfur content in the Margarita samples is low with up to 133 ppm in the lamprophyres. Dikes from Playa Caribe show exceptionally high S contents from 170 to 757 ppm, reflecting the presence of galena. Gabbroic intrusions show low concentrations of 12 and 23 ppm S; metagabbros vary in S content between 17 and 77 ppm (Figure 6.26). The solubility of S is lower in andesites than in basalts and decreases with increasing fO_2 and decreasing temperature and Fe content (Haughton et al., 1974; Mysen, 1977).

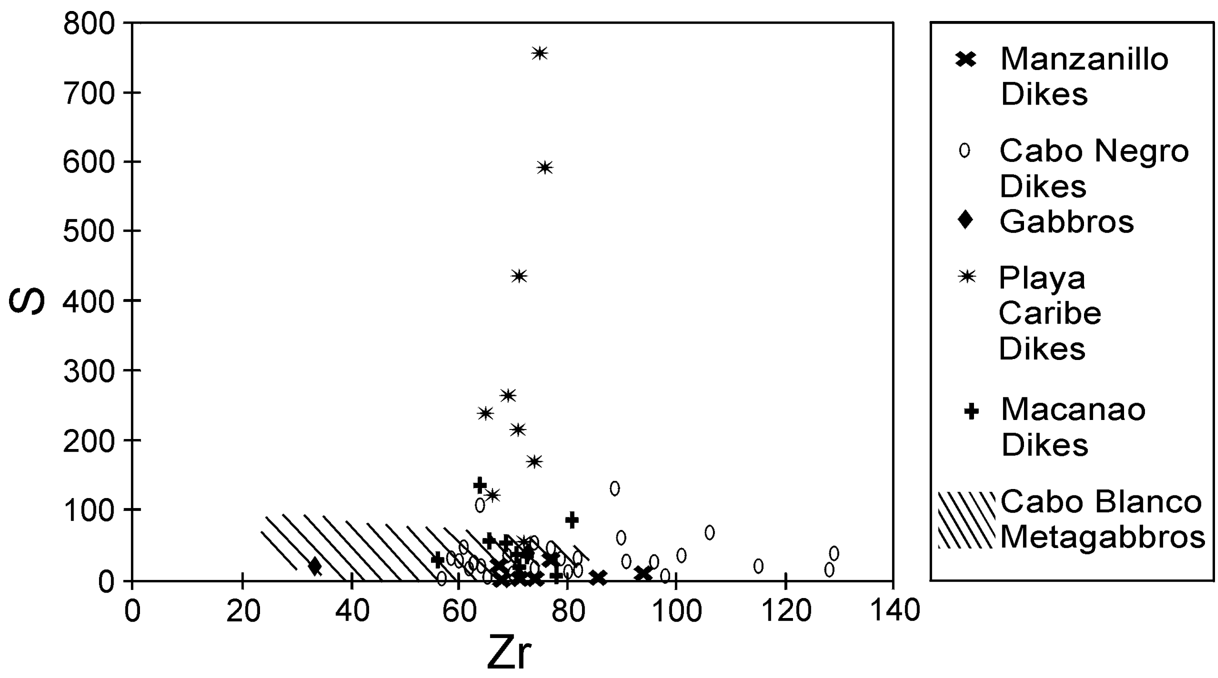

Figure 6.26:

S vs. Zr variation diagram of whole rocks from Isla Margarita.

6.5.9 RARE EARTH ELEMENTS

Rare earth element (REE) concentrations were measured in 20 samples at the Justus-Liebig-Universität, Gießen, FRG. The method used combines a HF-$HClO_4$-attack for sample dissolution with ion-exchange chromatography for separation and concentration. Determination of the REE was made by inductively coupled plasma - atomic emission spectrometry (ICP-AES). The procedure is described in detail by Zuleger & Erzinger (1988). Chondrite normalizing values for REE used in this study were taken from Sun & McDonough (1989).

An important consideration in the application of REE to petrogenetic studies of igneous rocks in general, but especially to the Margarita suite, is the relative immobility of these elements during metamorphism, hydrothermal alteration and weathering. Unless the processes are obviously severe, they do not cause a major change in the patterns or abundances of the REE (Condie et al., 1977; Sun & Nesbitt, 1978; Ludden & Thompson, 1979).

Chondrite normalized rare earth elements of representative samples from distinct dike suites and gabbroic intrusions from Margarita show parallel to subparallel patterns, with variations from light REE (LREE) depleted (La_N (=$La_{Rock}/La_{Chondrite}$) = 8.44) to enriched (La_N = 50.63) concentrations. Metagabbros also vary from LREE depleted (La_N 3.80) to enriched (La_N 31.64) compositions (Figure 6.27). Generally, light REE contents and slopes of REE patterns increase with differentiation, whereas Y and heavy REE hardly change.

The total REE abundances are low and range from 24 to 73 ppm in dikes, from 16 to 37 ppm in gabbroic intrusions and from 13 to 59 ppm in metagabbros. There is no evidence of consistent Eu depletion or enrichment in the total rock rare earth patterns (except for slight positive Eu anomalies in gabbro 6058 and dike 6057).

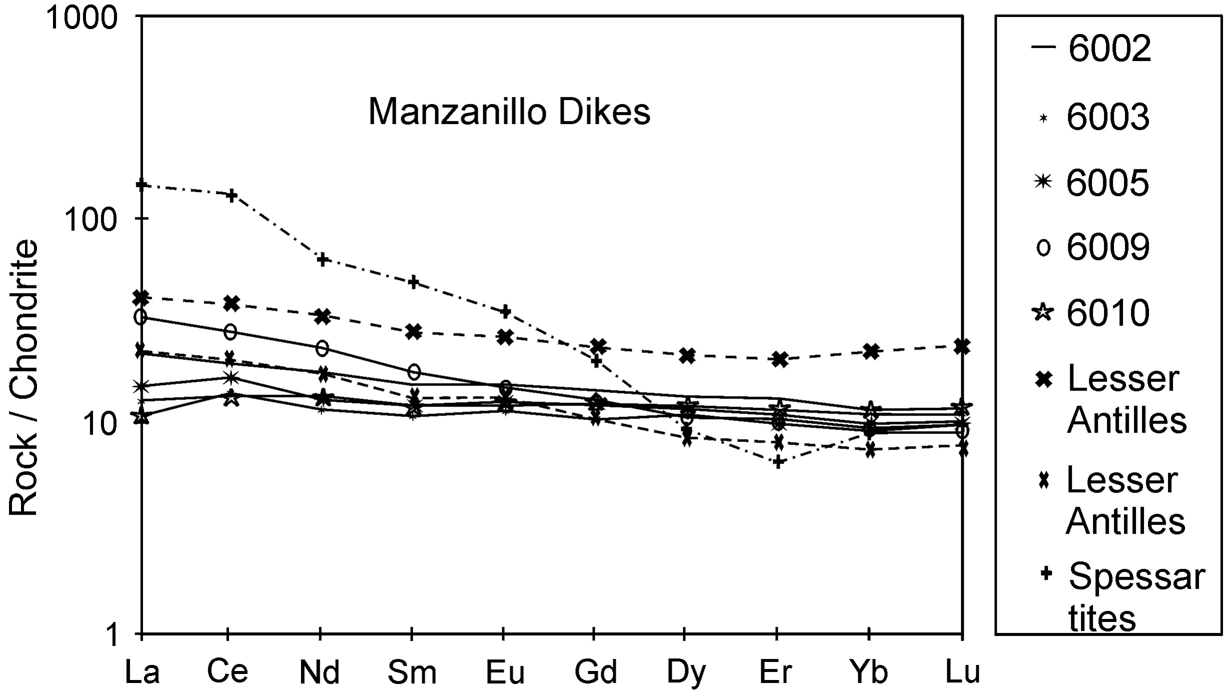

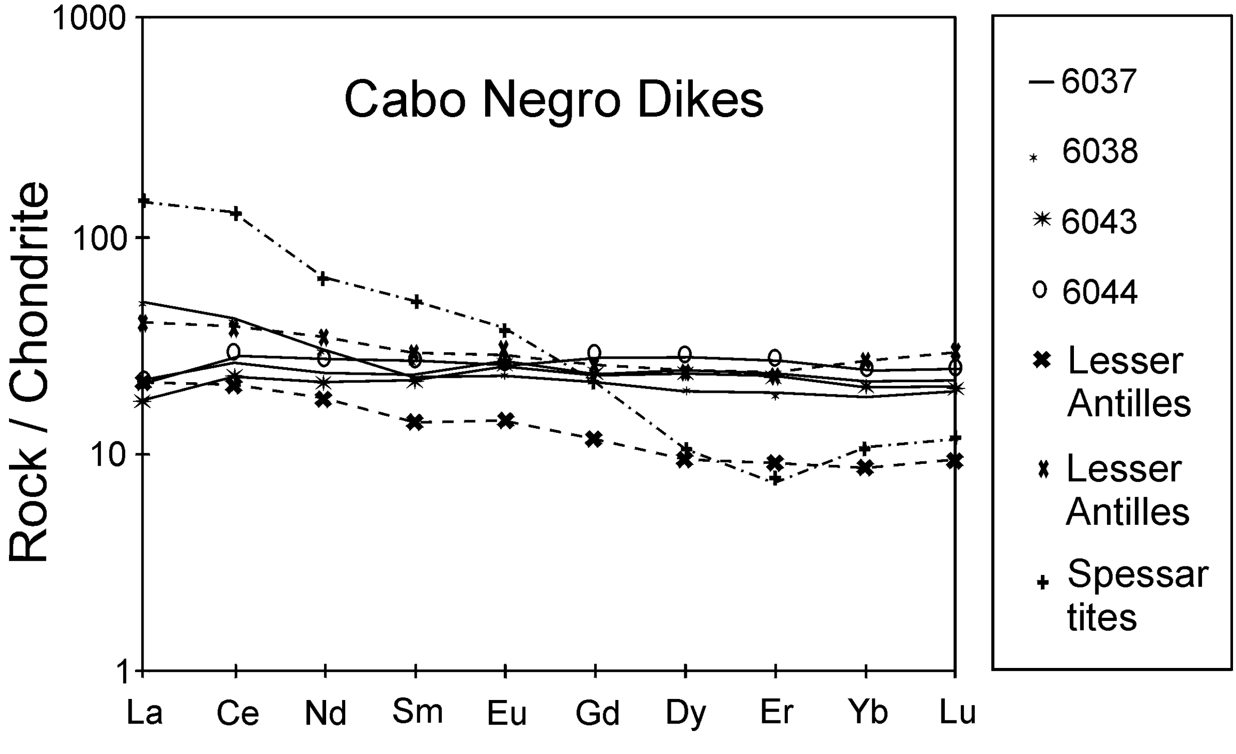

Figure 6.27:

Chondrite-normalized rare earth element patterns of whole rocks from Isla Margarita (solid lines). For comparison, REE patterns of Lesser Antilles basalts (dashed lines) from Davidson (1986) and average spessartites (dot-dashed line) from Rock (1991) are also shown. Normalizing values from Sun & McDonough (1989).

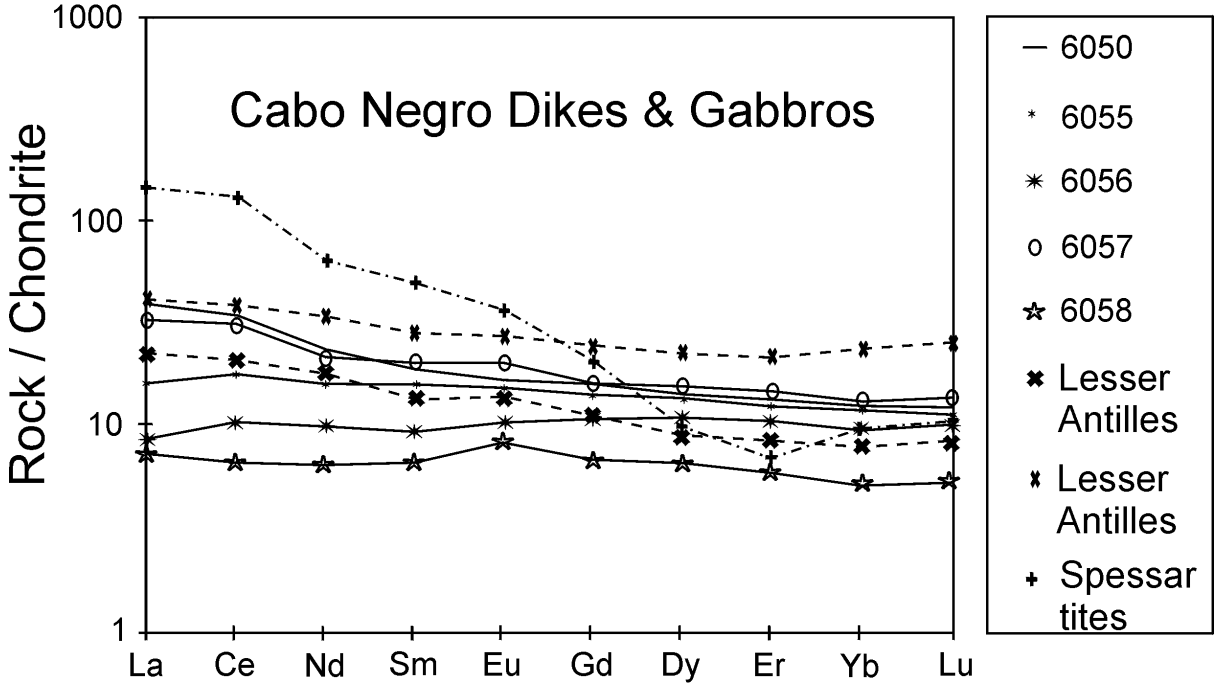

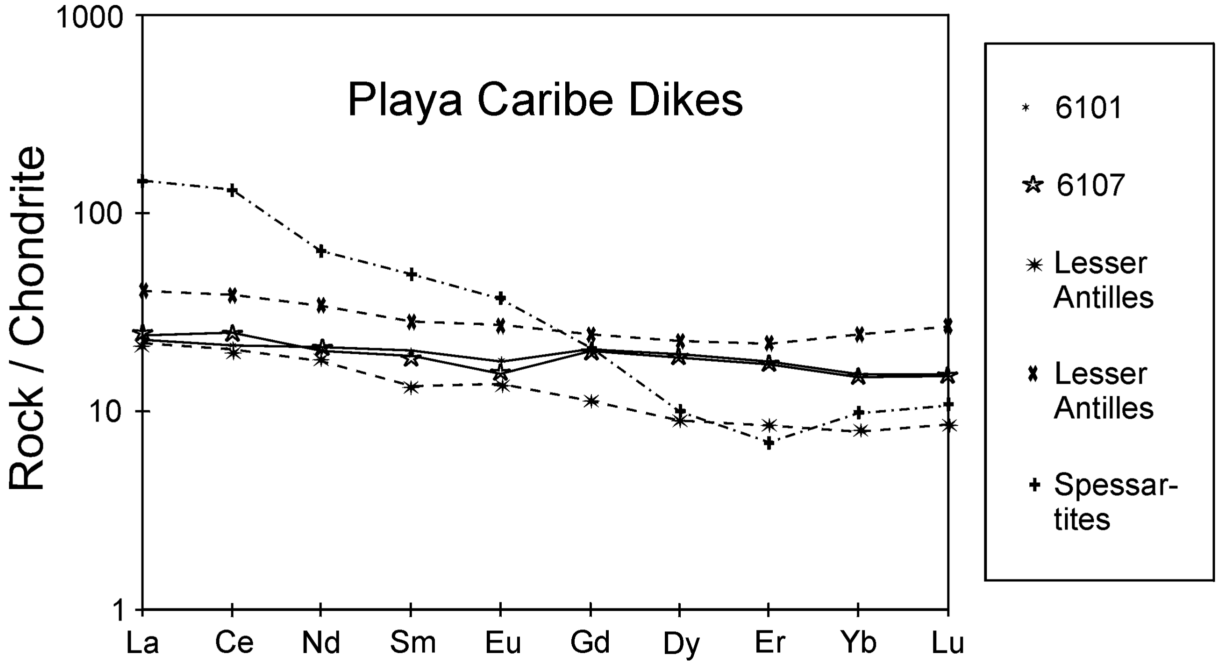

Figure 6.27 (contd.):

Chondrite-normalized rare earth element patterns of whole rocks from Isla Margarita (solid lines). For comparison, REE patterns of Lesser Antilles basalts (dashed lines) from Davidson (1986) and average spessartites (dot-dashed line) from Rock (1991) are also shown. Normalizing values from Sun & McDonough (1989).

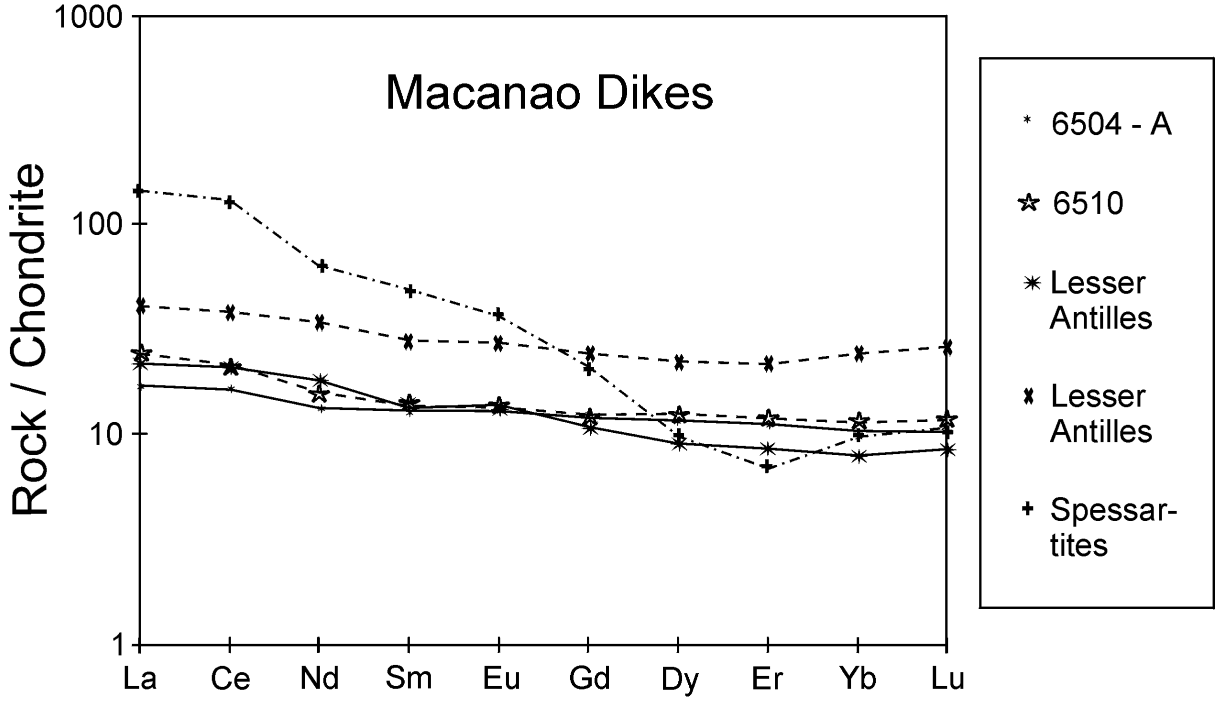

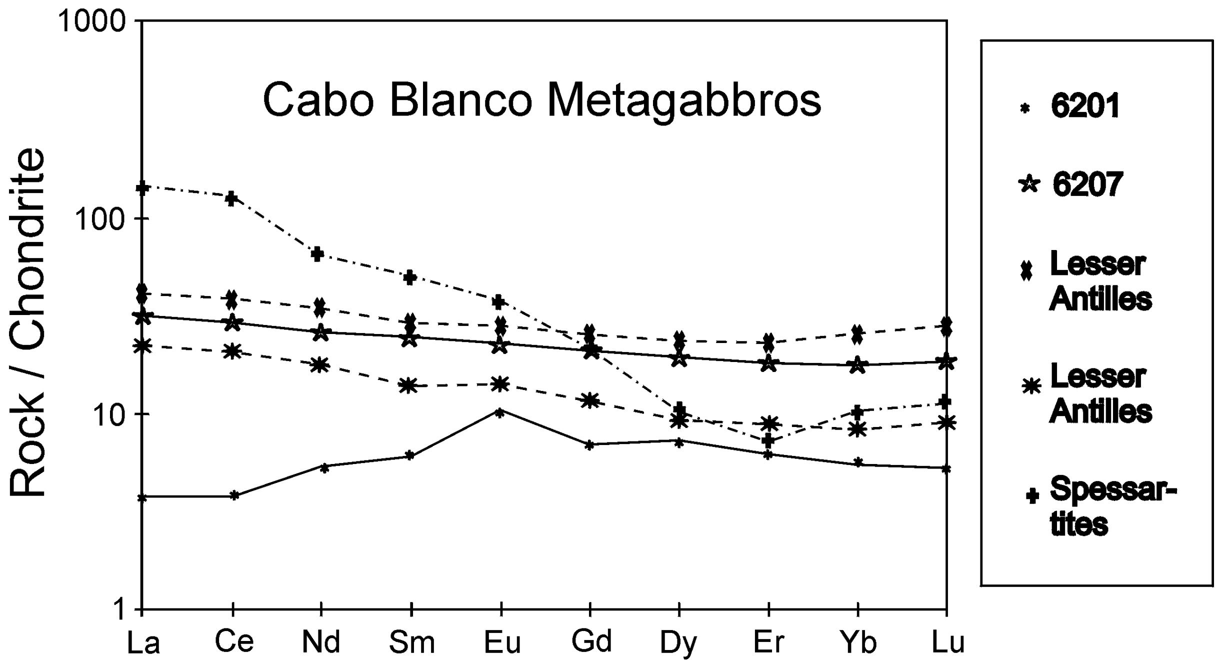

Figure 6.27 (contd.):

Chondrite-normalized rare earth element patterns of whole rocks from Isla Margarita (solid lines). For comparison, REE patterns of Lesser Antilles basalts (dashed lines) from Davidson (1986) and average spessartites (dot-dashed line) from Rock (1991) are also shown. Normalizing values from Sun & McDonough (1989).

A noticeable positive Eu anomaly, as shown in metagabbro 6207, can generally be attributed to plagioclase accumulation (e.g. Pearce, 1983; Wilson, 1988).

Comparison of the REE patterns of the Margarita rock suite with data of basalts and related rocks from the Old Lesser Antilles arc (Davidson, 1986) shows considerable similarity of the REE distribution and overlapping ranges of REE concentration (Figure 6.27). Average spessartites (Rock, 1991) are substantially higher in LREE, but lower in HREE content, compared to Margarita and Lesser Antilles rocks.

Systematic correlation of LREE enrichment with increasing potassium content has not been observed. LREE contents, expressed as the La_{Rock}/La_{Chond} ratio (Figure 6.28) and slopes of REE patterns, as well as total REE contents, however, increase with silica content .

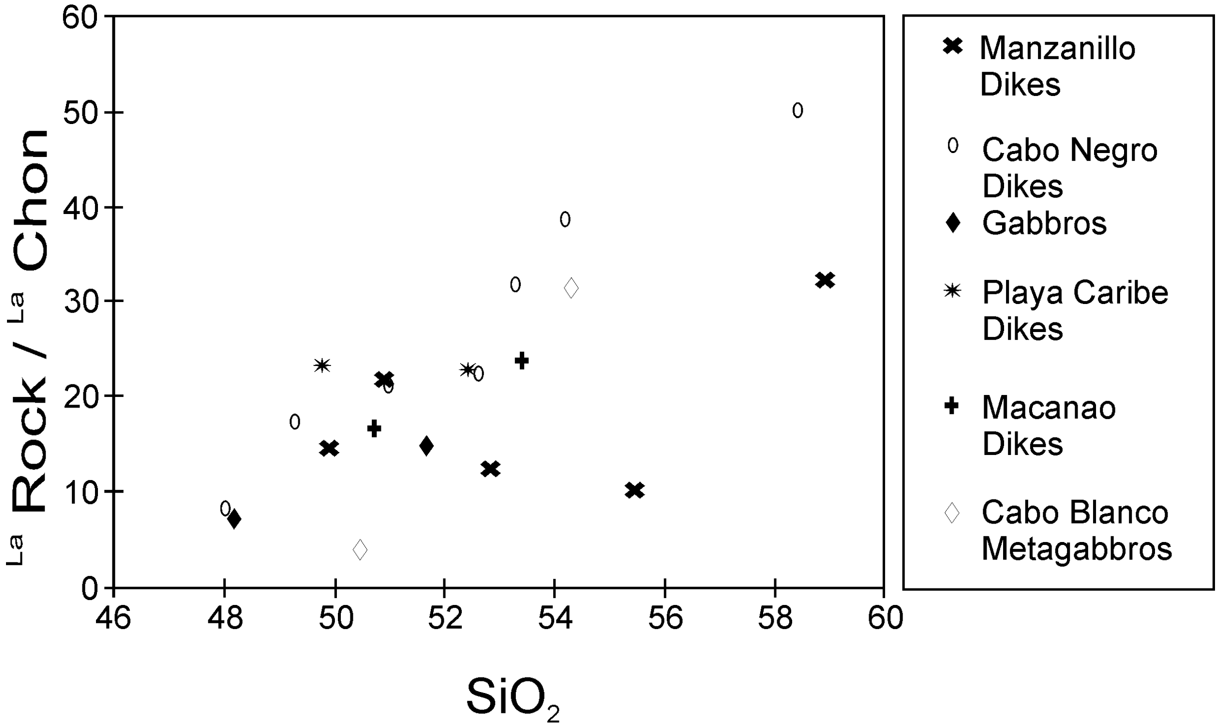

Figure 6.28:

La_{Rock}/La_{Chon} vs. SiO_2 variation diagram of whole rocks from Isla Margarita.

The enrichment of LREE vs. HREE, expressed as the ratio of La_N/Yb_N (= $(La_{Rock}/La_{Chon})/(Yb_{Rock}/Yb_{Chon})$), varies in Mar-garita dikes from 0.85 to 3.03, gabbroic intrusions show little variation from 1.30 to 1.35 and metagabbros vary from 0.72 to 1.86 (Figure 6.29).

Similar La_N/Yb_N values of <3, usually 1-2, occur in the Old Lesser Antilles arc basalts (Davidson, 1986) and were also reported by Jakês & Gill (1979) for the island arc tholeiitic series, whereas the calc-alkaline series has La_N/Yb_N ratios of 5-20, clustering around 6-8.

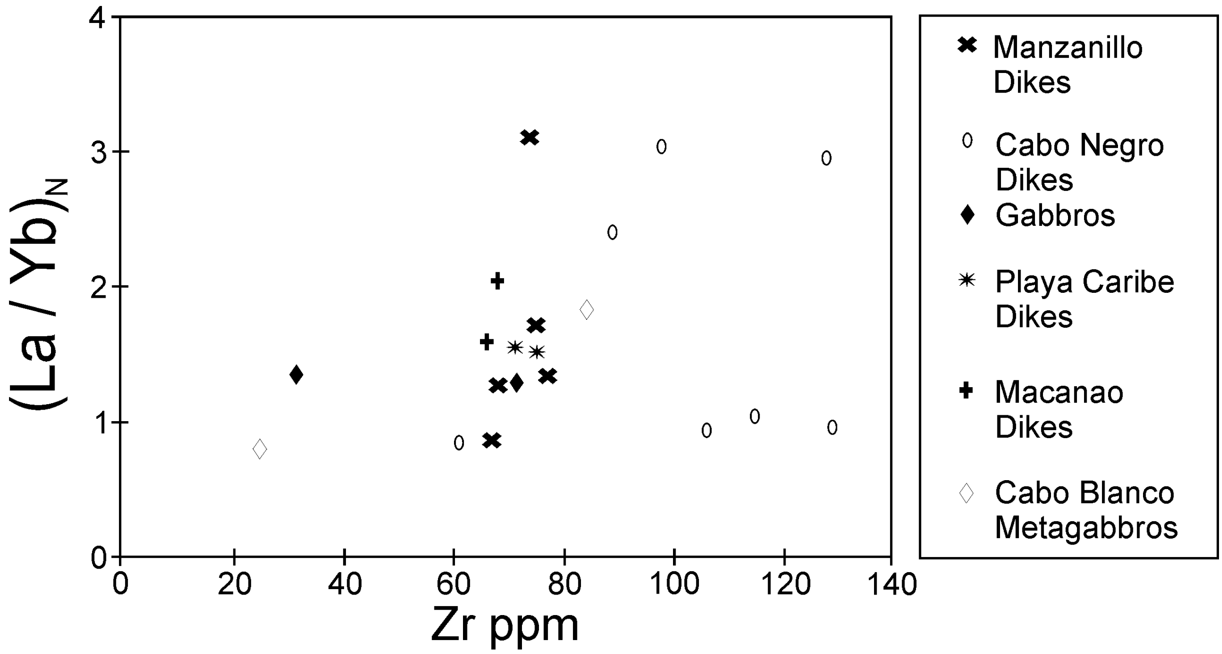

Figure 6.29:

La_N/Yb_N vs. Zr variation diagram of whole rocks from Isla Margarita.

The variations in La_N/Yb_N of Margarita rocks are considered to reflect processes other than fractional crystallization, as none of the phenocryst phases (ol, cpx, hbl, plag) can effectively fractionate La from Yb (Pearce, 1983).

6.5.10 COMPOSITE TRACE ELEMENT PATTERNS (SPIDERGRAMS)

A useful way of comparing the incompatible element geochemistry of basaltic rock suites are normalized trace element variation diagrams ("spidergrams", e.g. Pearce, 1980, 1983; Thompson, 1982; Wilson, 1988; Rock, 1991). The number of elements, as well as normalizing factors, however vary considerably amongst spidergrams in current use. MORB-normalizing values in this study are from Pearce (1983). The order of elements is plotted with decreasing incompatibility from left to right. An exception is Sr, which is compatible with assemblages containing plagioclase.

The Margarita dikes, gabbroic intrusions and metagabbroic intrusions are characterized by enrichment of the mobile LIL elements (Sr, K, Rb, Ba). An exception is K in the Manzanillo and Playa Caribe dike suite and in the Cabo Blanco metagabbro suite, where K has been removed during alteration (see section 6.2). Maximum enrichment amongst the light REE is shown for Rb (7 to 30 fold MORB), relative to the high field-strengh elements (HFSE) P, Zr, Ti; medium REE (Ce, Sm) and heavy REE (Y, Yb) show depleted or MORB-like concentrations (Figure 6.30). A slight depletion of Nb, as typically observed in island arc related rocks, is discernible in andesitic dike 6009 from Manzanillo, all other samples lack this typical depletion. However, a slight and consistent depletion of Ti, also characteristic of subduction related rocks, occurs in all Margarita suites. The Playa Caribe dike suite shows less enrichment of LILE and considerable depletion of Ti. Cabo Blanco metagabbros also display enrichment of LILE, except for K (0.7-0.8 x MORB) and broad variation between MORB-like and strongly depleted medium and heavy REE.

The MORB-normalized spidergram patterns of Margarita rocks are most closely matched by island arc basalts from the Lesser Antilles and Tonga (Pearce, 1983). Average spessartites (Rock, 1991) also exhibit broadly similar patterns with enrichment of the large ion lithophile elements (LILE), but the degree of enrichment varies considerably between the suites. The concentrations of HFSE, medium and heavy REE in spessartites also differ from those in Margarita rocks. Lesser Antilles and Tonga rocks, however, form similar trends, which lie parallel or subparallel to MORB composition, but at lower levels.

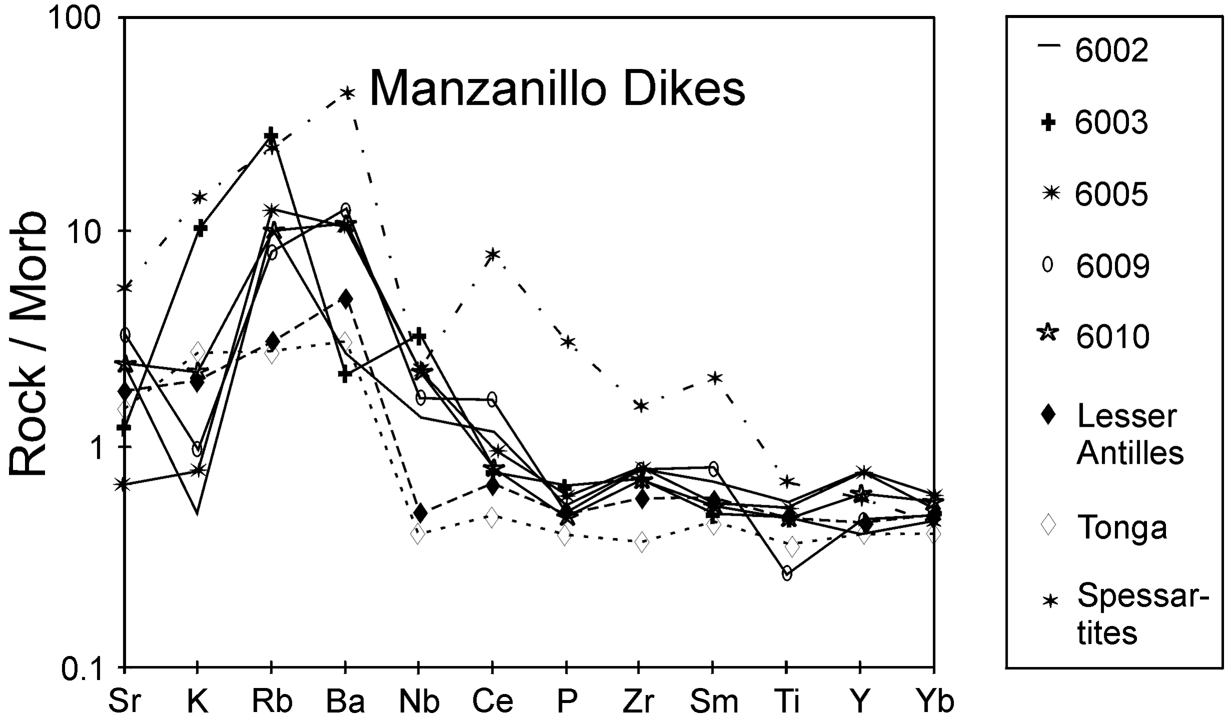

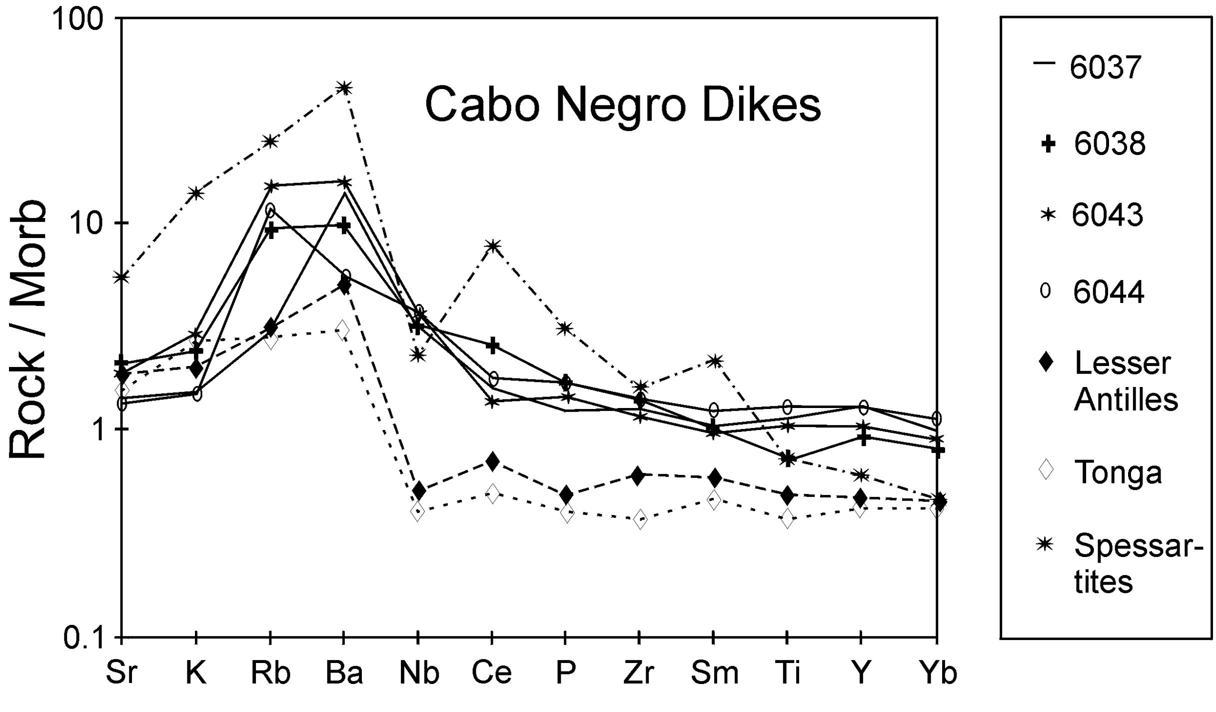

Figure 6.30:

MORB-normalized trace element patterns ("spidergrams") of whole rocks from Isla Margarita. For comparison, trace element patterns of basaltic-andesitic samples from the Lesser Antilles (Pearce, 1983), Tonga (Pearce, 1983) and spessartites (Rock, 1991) are also shown. Normalizing factors are from Pearce (1983).

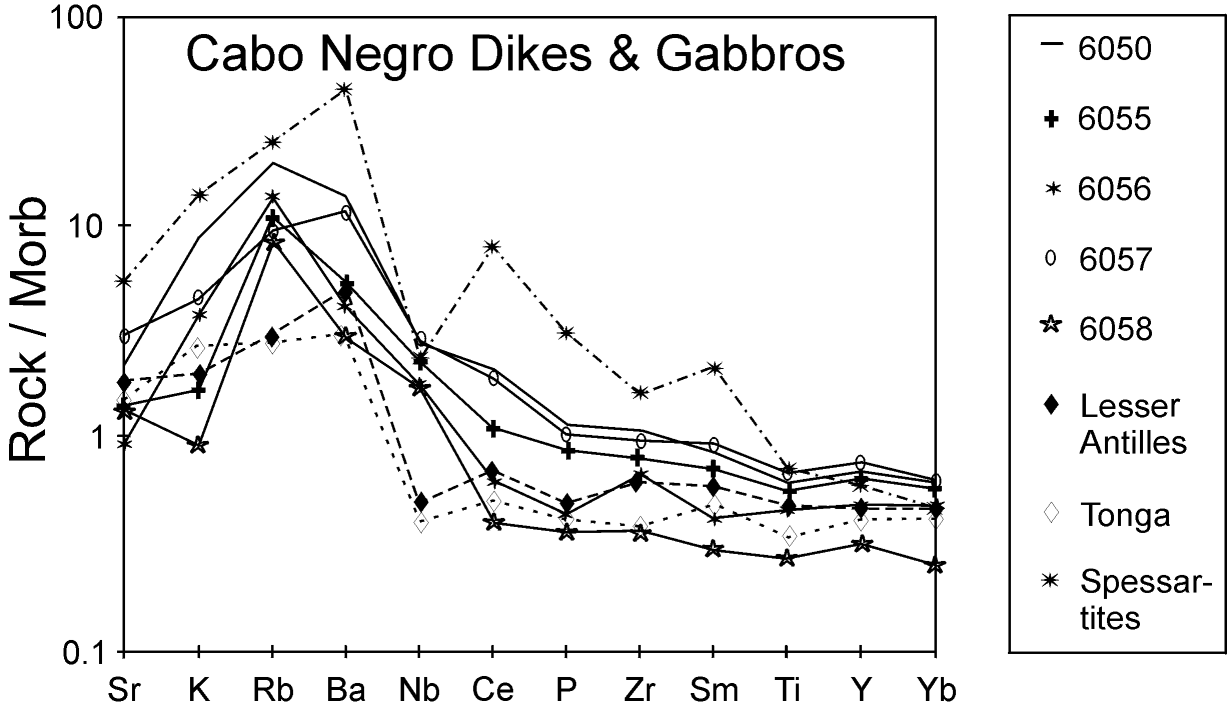

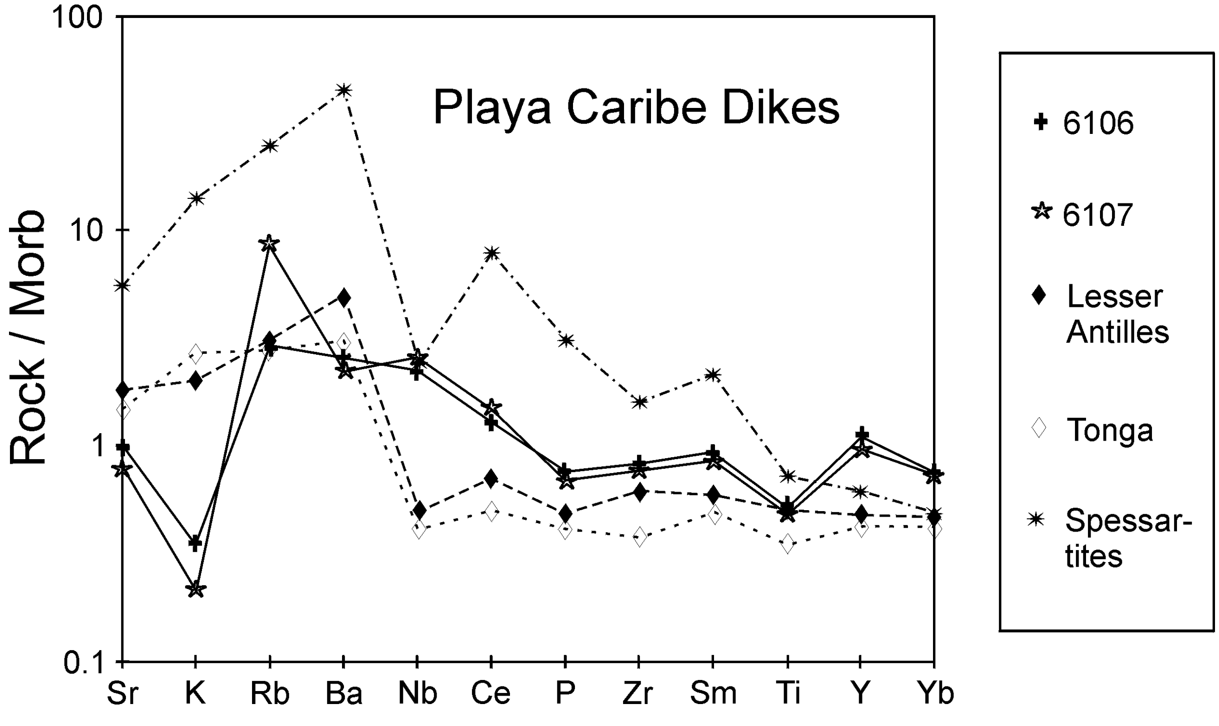

Figure 6.30 (contd.):

MORB-normalized trace element patterns ("spidergrams") of whole rocks from Isla Margarita. For comparison, trace element patterns of basaltic-andesitic samples from the Lesser Antilles (Pearce, 1983), Tonga (Pearce, 1983) and spessartites (Rock, 1991) are also shown. Normalizing factors are from Pearce (1983).

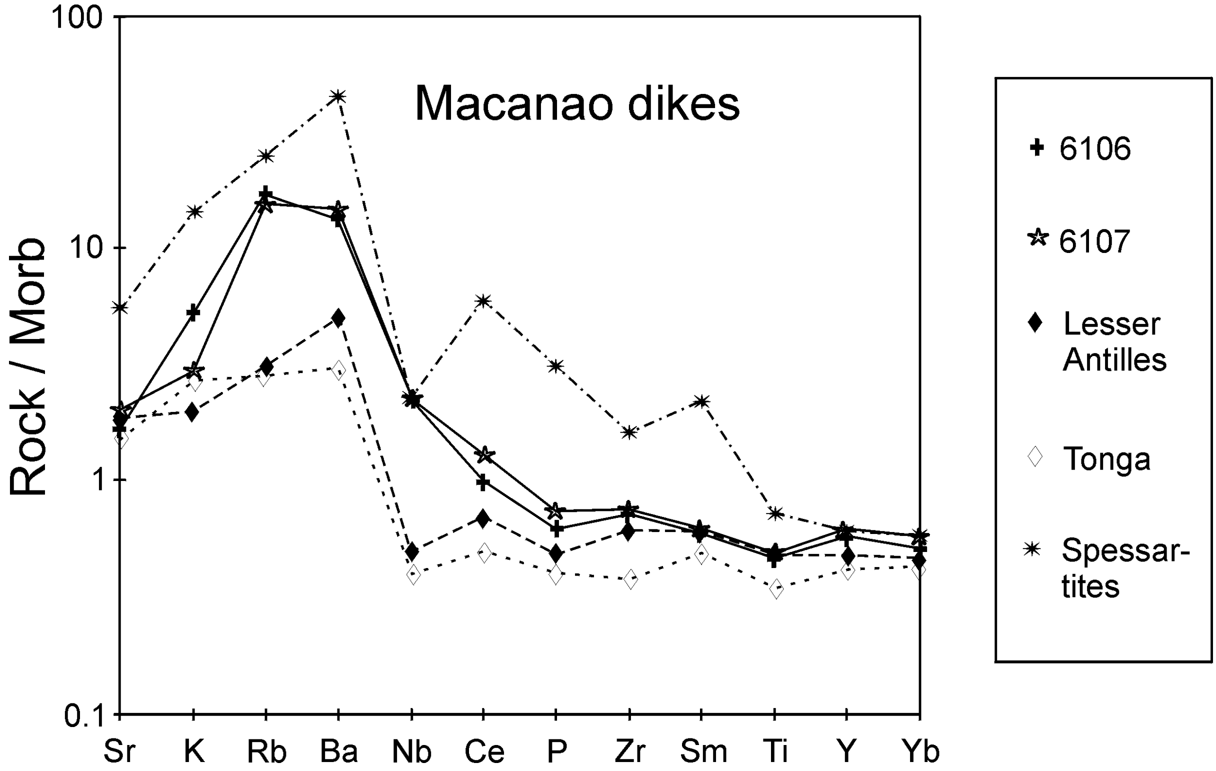

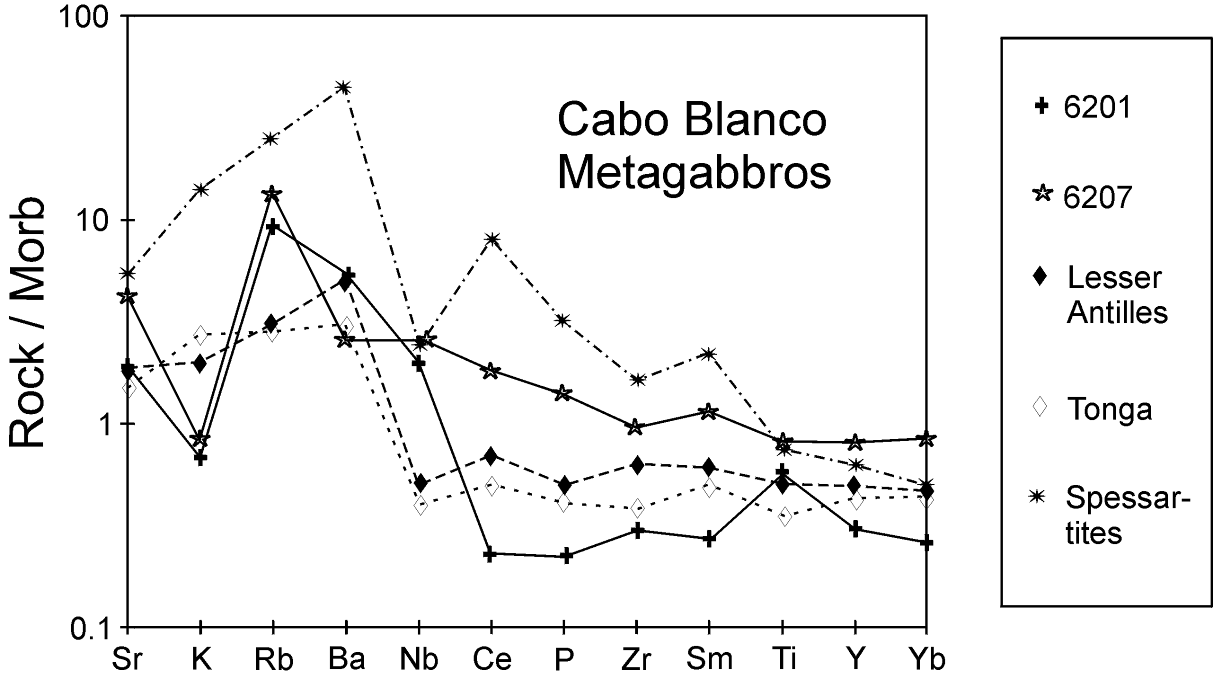

Figure 6.30 (contd.):

MORB-normalized trace element patterns ("spidergrams") of whole rocks from Isla Margarita. For comparison, trace element patterns of basaltic-andesitic samples from the Lesser Antilles (Pearce, 1983), Tonga (Pearce, 1983) and spessartites (Rock, 1991) are also shown. Normalizing factors are from Pearce (1983).

The enrichment in LILE is diagnostic and particularly exemplified by high Ba/La ratios. These vary widely in the Margarita suite from 8.0 to 88 in dikes and from 28 to 34 in gabbroic intrusions. Although Ba may be sensitive to alteration, a systematic decrease in Ba/La ratio with increasing silica content is apparent and may roughly represent the initial concentrations in the Margarita rocks. LILE are more enriched in the Margarita rocks, orogenic basalts and andesites in general than in oceanic basalts, when samples of similar rare earth elements are compared. For example, high and variable Ba/La ratios of 8-88 in the Margarita suite compare to values >15 in most volcanic rocks from convergent plate boundaries. They are in contrast to the extremely low values of 4-10 in N-MORB or 10-15 in E-MORB and most within-plate basalts (Wood et al., 1980). Ba/La ratios are also higher in volcanic arcs than in adjacent backarcs.

Studies by Pearce (1982, 1983) and Bednarz (1989) showed that rock suites, selectively enriched in LILE, can be explained either by derivation from two magma sources, or by a two-stage origin. Pearce (1983) devised an empirical method for evaluating the proportions of the various geochemical components in such rocks, based on the patterns shown by basalts from known tectonic settings. According to Pearce (1983), the enrichment of elements relative to MORB represents the subduction zone component, whereas depletion of elements relative to MORB suggests that either less crystal fractionation or more partial melting of the source(s) took place during magma generation.

6.6 TRACE ELEMENTS AS PETROGENETIC INDICATORS

Trace element ratios have been frequently used to characterize igneous rock suites and to asses a possible genetic relationship between spatially and temporally related samples (e.g. Pearce & Cann, 1973, Pearce & Norry, 1979; Sun & McDonough, 1989, Bednarz, 1988, Devine, 1995). The ratios of high field strength elements (HFSE) are particularly informative, as they are insensitive to variations in the degree of partial melting and fractional crystallization, so that variable ratios can be attributed to source heterogeneity (Pearce & Norry, 1979; Meschede, 1986). This may be due to depletion of HFSE and/or enrichment of LILE in the source, related to systematic variations in the regions of melt generation.

The HFSE ratios Zr/Y, Zr/Ti, and Zr/Nb are critical in this respect and may identify the main components of variation exhibited by basalt magmas (Pearce & Norry, 1979). Within the Margarita rock series, the Playa Caribe dike suite (except for two samples), the Macanao dike suite and the Cabo Blanco metagabbro suite show little variation in Zr/Y ratios (3.2-4.3), whereas the Manzanillo and Cabo Negro dike suites are characterized by larger variation in Zr/Y (3.0-5.5). A discrimination diagram of Zr/Y values of rocks from different tectonic settings (Pearce & Norry, 1979), reveals that Margarita rocks have slightly higher absolute Zr abundances than typical island arc basalts, resulting in an overlap into the field of MORB (Figure 6.31). Absolute Y contents in Margarita rocks range from 5 to 44 ppm in dikes, from 10 to 20 ppm in gabbroic intrusions and from 7 to 24 ppm in metagabbros. The concentrations are comparable to those of orogenic suites, the range of 20 to 25 ppm Y being considered typical (Gill, 1976a). Y contents <15 ppm are restricted to andesites erupted through crust >30 km thick, as in New Zealand and Chile (Ewart & Taylor, 1969).

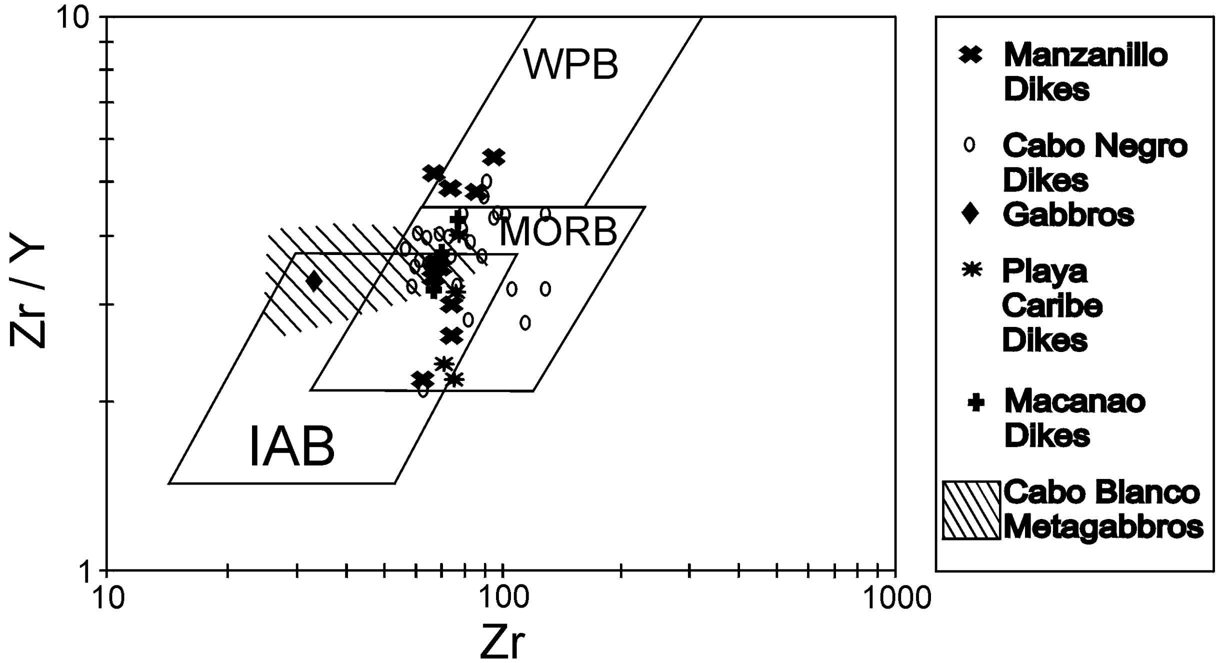

Figure 6.31:

Zr/Y vs. Zr variation diagram of whole rocks from Isla Margarita in relation to within-plate basalts, MORB and island-arc basalts, as defined by Pearce & Norry (1979).

More consistent information about source heterogeneity can generally be attained by the Zr/Nb ratio, since it is insensitive to variations in the degree of partial melting and crystal fractionation. Margarita rocks display considerably low Zr/Nb ratios (Figure 6.32), with values no higher than 9 in metagabbros and 17 in dikes and gabbroic intrusions. These values are rather typical for MORB than for calc-alkaline rocks. However, it must be stressed again that Nb concentrations of Margarita rocks lie near the detection level of XRF and that analytical error in this particular case may be considerably high. More reliable are Zr/Ti ratios (Figure 6.33), with Zr/Ti in dikes and gabbroic intrusions clustering around 100 and in metagabbros around 150. The ratios are comparable to Zr/Ti mean values of other island arc related rocks as defined by Pearce & Cann (1973).

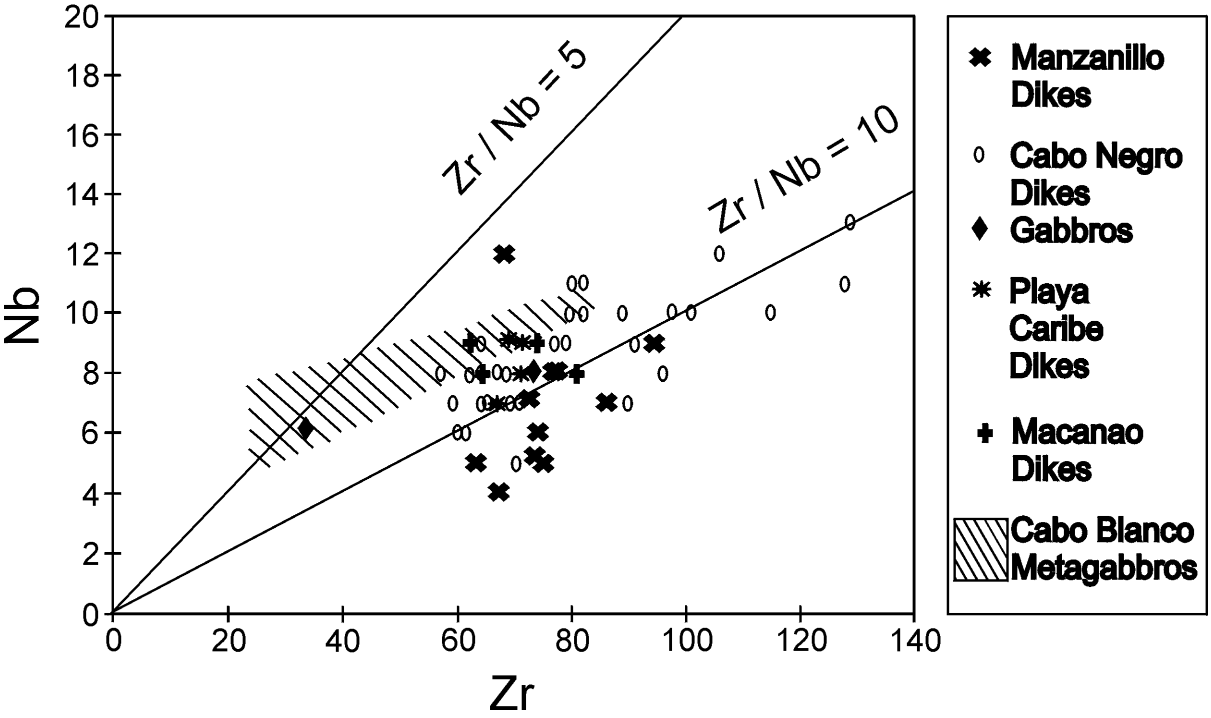

Figure 6.32:

Nb vs. Zr variation diagram of whole rocks from Isla Margarita.

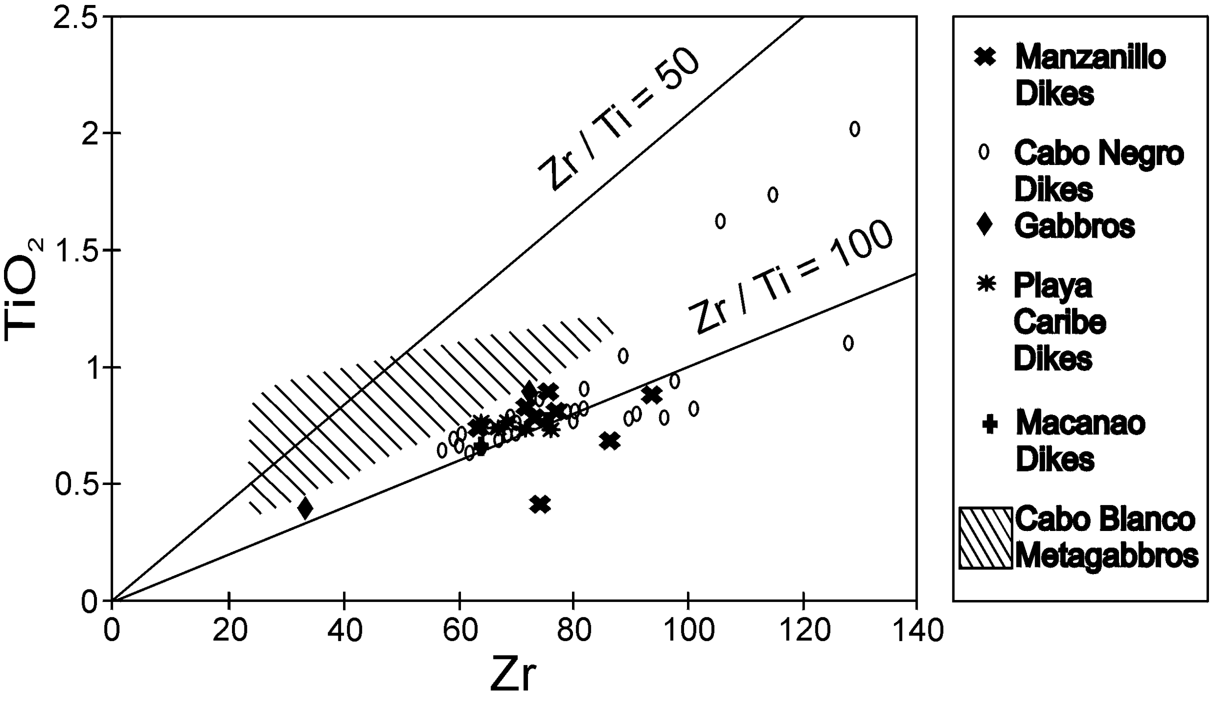

Figure 6.33:

TiO_2 vs. Zr variation diagram of whole rocks from Isla Margarita.

Similar to the behavior of HFSE, the ratios of highly incompatible trace elements are insensitive to fractional crystallization and should differ little amongst genetically related samples (e.g. Pearce & Norry, 1979; Bednarz, 1988). The large ion lithophile elements (LILE), especially K and Rb, are potentially useful monitors of crust-magma interactions because they are concentrated in early crustal anatectic melts. Mineral-melt partition coefficients for these elements in basaltic andesite magmas are very low, approaching zero, for the ferromagnesian minerals olivine, clinopyroxene and amphibole (Arth, 1976).

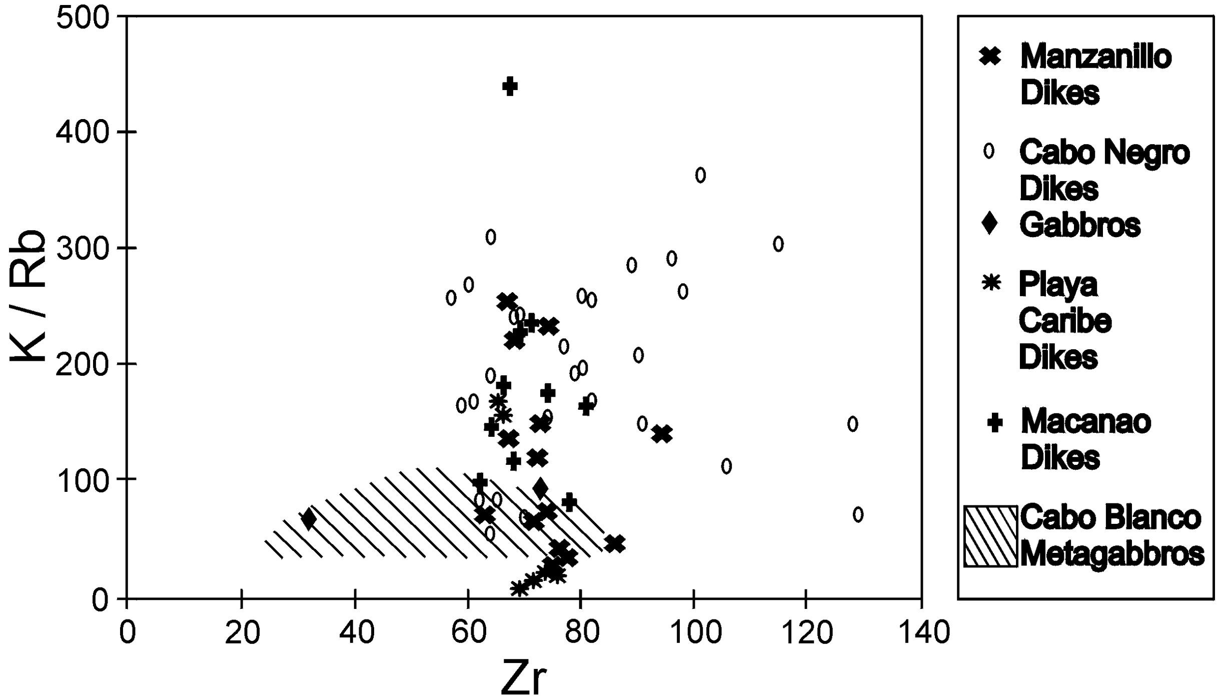

Figure 6.34:

K/Rb vs. Zr variation diagram of whole rocks from Isla Margarita.

K/Rb ratios of Margarita rocks increase roughly with differentiation (Figure 6.34), with the majority of samples reaching a ratio of 300, thus being slightly higher than average continental crust (K/Rb = 250), but significantly lower than N-type MORB with K/Rb up to 1000 (Jakês & White, 1970).

Although caution is required in interpreting K/Rb variations, as LILE, particularly K, have been proven to be mobile and susceptible to alteration, it is obvious that the individual Margarita dike suites display considerable scatter of K/Rb ratios at given Zr contents. This is especially applicable to the Macanao dike suite, where removal of K during alteration has not been observed (see Figure 6.1-d).

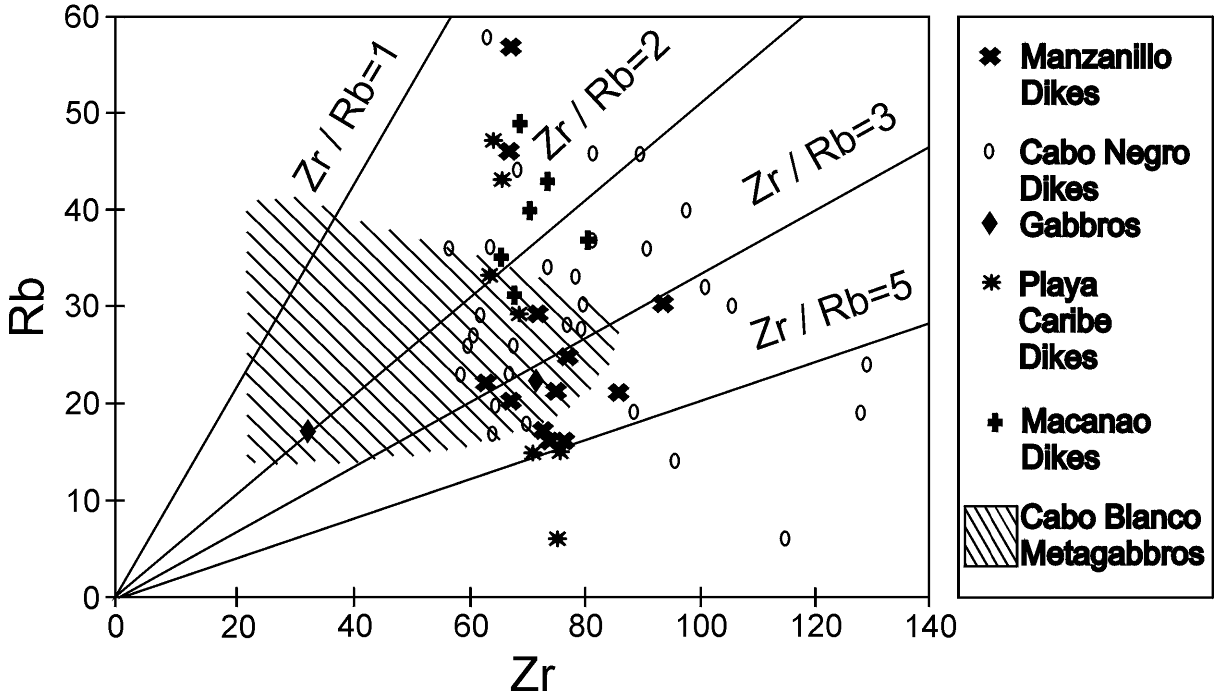

Figure 6.35:

Rb vs. Zr variation diagram of whole rocks from Isla Margarita.

Zr/Rb ratios, used as an example of LILE versus HFSE in Margarita rocks, are consistently low and range from 1.1 to 6.9 in dikes, from 2.0 to 3.3 in gabbroic intrusions and from 0.7 to 3.3 in metagabbros (Figure 6.35). They are significantly lower in all series than the average Zr/Rb ratio of 45 in MORB (Pearce, 1983), but again, comparable to arc related magmas from the Old Lesser Antilles arc (Davidson, 1986), the Tonga-Kermadec arc (Ewart & Hawkesworth, 1987) and Papua New Guinea (Johnson et al., 1985). Values of other incompatible trace element ratios, such as Ba/Zr (0.6-8.4) and Sr/Zr (1.0-9.0) in the Margarita rocks are in excellent agreement with those from the high-Mg basalt-andesite association of Grenada and St. Vincent (Devine, 1995).

6.7 DISCUSSION OF WHOLE ROCK COMPOSITION

The geochemical diagrams display the variations in major, trace and rare earth element concentrations in the Margarita rock series and allow constraints on source composition, crystal fractionation and crustal assimilation processes. While scatter amongst incompatible elements is quite severe, it is apparent that the compatible elements Mg, Ni, Cr, Co also Fe and Ca decrease with differentiation from basaltic to andesitic composition, reflecting substantial olivine, chromite, clinopyroxene and subsequent amphibole fractionation. It is inferred from the overall high concentrations of the compatible elements that the parental magmas of this suite were fairly basic in composition, and that primitive mantle participated to a major degree in magma genesis. This is consistent with higher degrees of melting in the source than is common in island arc-related settings. Compatible element similarities exist between high-Mg andesites from the Bonin-Mariana arc system and Margarita rocks. However, there is little mineralogical resemblance. The boninite suite is also far less enriched in incompatible elements and displays significantly lower LILE/HFSE and CaO/Al_2O_3 ratios. The rarity of olivine and the absence of orthopyroxene in the Margarita suite also marks a fundamental difference and precludes the use of the term "boninite" (Cameron et al., 1979) to describe the present rock suite.

Basaltic to andesitic suites, with high Mg-contents and geochemical affinity to Margarita rocks, have been reported from the southern Antillean islands, such as Grenada and the Grenadines and the northern islands St. Kitts and Saba. Further occurrences have been reported from the southern and central islands Grenada, Martinique and St. Vincent (Maury & Westercamp, 1985; Devine, 1995). High Mg-andesites have been described from other island arcs such as the Aleutians by Kay (1978) and Yogodzinski et al. (1994, 1995), from Cape Vogel, Papua New Guinea by Jenner (1981), from Japan by Tatsumi (1982) and the Kamchatka arc by Hochstaedter et al. (1996).

The Margarita series is further characterized by enrichment in large ion lithophile elements (LILE) and light rare earth elements (LREE) relative to other incompatible elements. This is perhaps the most consistent feature confirming the affinity of these rocks to island arc volcanics, rather than to any other volcanic rock suite erupted in different tectonic settings. This enrichment component is regarded to be independent of the nature of the mantle wedge, but assumed to be subduction-derived (Pearce, 1983). Experimental work by You et al. (1996) demonstrates mobilization of the incompatible elements in hydrothermal fluids at relatively low temperatures (ca. 300°C), whereas the high-field strength elements (Nb, Ta, Ti and Zr) are immobile. This is consistent with the proposal that the addition of subduction zone hydrous fluids to the subarc mantle can produce these unique characteristics of arc magmas. The degree of LILE and LREE enrichment in the Margarita rocks, however, is variable, implying that the subduction component contributed to variable degrees to magma genesis.

The Margarita magmatic suite shows merely slight depletion of Nb in one andesitic sample, whereas consistent depletion of Nb is commonly observed in island arc or subduction related magmas, such as those from the Lesser Antilles (Hawkesworth, unpubl. data in: Pearce, 1983), Tonga (Pearce et al., 1981), Fiji (Gill, 1970), New Hebrides (Gorton, 1977), Marianas

(Wood et al., 1980) and subduction related lavas in general e.g. Central Chile (Pearce, 1983), Iran (Dostal & Zerbi, 1978), and Western USA (Ewart, 1982). However, a slight depletion of Ti occurs consistently and is indicative for a relation of the Margarita magma source to the subduction process in the Aves/Proto-Antillean region. Hildreth & Moorbath (1988) concluded that the most likely process to produce Nb- and Ti-depleted compositions in subduction-related magmas is partial melting of the lower crust, resulting in the generation of magmas of andesitic to rhyolitic composition, but with otherwise high concentrations of incompatible elements. According to Green & Pearson (1986) and Brenan et al. (1996), Ti-rich phases such as rutile, ilmenite, sphene, titanomagnetite, Ti-bearing amphibole and garnet could all be important as sinks for Ti and Nb (also for Ta). Ionov & Hofmann (1995) concluded that amphibole and mica are important hosts for Nb and Ta and reported partition coefficcients for Nb and Ta ranging between 10 to 85.

The HFSE relations of Margarita magmas do not unequivocally prove genetic relationship between spatially related dikes and gabbro suites, but broadly similar source characteristics can be inferred. The correlation between incompatible element contents and ratios indicates that source magmas underwent slightly different paths of open system evolution. Accordingly, variations in these ratios are generated, at least in part, during differentiation in the crust.

7.

RADIOGENIC ISOTOPES

7.1 ANALYTICAL TECHNIQUES

Radiogenic isotopes were measured at the Deptartment of Geological Sciences at the University of California, Santa Barbara (UCSB). Eight representative samples, six of which were also selected for $^{40}Ar/^{39}Ar$ dating, were analyzed for isotopic ratios under clean-lab conditions. Isotopes were analyzed in plagioclase mineral separates. Separation was made by electro-magnetic and heavy liquid methods followed by hand-picking. Feldspar separates were estimated to be 99% pure. The separates were acid-washed with 2N HCl to remove any surface contaminants and were then soaked to remove alteration products and decomposed with HF. A total procedure blank was run with every batch of samples.

All samples measured at UCSB were total spiked with two mixed spikes, ^{205}Pb-^{235}U-^{230}Th and ^{87}Rb-^{87}Sr. Elements were separated by column chemistry in the sequence Pb, U, Th, Rb, Sr (for a more detailed discussion of the column chemistry see Tilton et al., 1989). Pb, U, Th, Rb and Sr were run using single Re filaments, and isotopic ratios were measured on a multi-collector Finnigan MAT 261 mass spectrometer, operating in static mode. Replicate standards were NBS 981 (Pb), U 500 (U), Th-Mix (Th), NBS 987 (Sr) and Rb Shelf (Rb). The two sigma reproducibility is <0.02% per mass unit for Pb, <1.0% for U and Th, <0.002% for Sr and <1% for Rb isotopic ratios, based upon multiple analyses of the standards (Tilton, pers. comm).

Rb and Sr isotopes of one dike and country rock sample from Playa Caribe and a second gabbro were analyzed in whole rocks at the Institut für Geologie, Ruhr-Universität Bochum. Rb and Sr were separated by column-chemistry, but samples were not spiked. Isotopes were measured on a multi-collector Finnigan MAT 262 mass spectrometer using single Re filaments. NBS 987 was also used as a reference standard and produced agreeable results to NBS 987 measurements at UCSB with $^{87}Sr/^{86}Sr$ of 0.710200±20.

Sr ratios are corrected for the decay of Rb, lead ratios are corrected for the decay of U and Th respectively. Accordingly, the isotope data presented in this study represent initial isotopic ratios. Decay corrections were based on results from $^{39}Ar/^{40}Ar$ age dating.

7.2 ISOTOPE RELATIONS

The isotopic compositions of lead and strontium in volcanic rocks are sensitive tracers of any contribution to the magmas. They are used primarily to evaluate the extent to which certain elements come from the upper mantle versus other sources, such as sediments or crust. The bulk of island arc volcanic rocks shows a quite restricted range of isotopical composition, reflecting their source chemistry (see below). Additionally, contamination has an overprinting effect on the composition of the original magmatic liquid.

In order to characterize the island arc sources, isotopic ratios, together with selected major and trace elements and REE, can reasonably assess the possible roles of enrichment and contamination.

7.2.1 STRONTIUM

Margarita basalts and basaltic andesites span a considerably wide range of initial $^{87}Sr/^{86}Sr$ isotopic ratios with values from 0.70401 to 0.70615. Lamprophyric dikes from the western peninsula Macanao are noticeably higher in $^{87}Sr/^{86}Sr$ ratios (0.70523-0.70615) than those from the eastern peninsula Paraguachoa (0.70401-0.70499). Gabbroic samples from Paraguachoa (Cabo Negro) correspond well to adjacent dikes, with ratios of 0.70472 and 0.70431 respectively. A graphite schist country rock sample from Playa Caribe yields a $^{87}Sr/^{86}Sr$ ratio of 0.71391. Margarita rocks show slightly lower initial Sr ratios than average calc-alkaline lamprophyres with values of $^{87}Sr/^{86}Sr = 0.7068$ (Rock, 1991), but higher $^{87}Sr/^{86}Sr$ ratios than average orogenic andesites and related rocks (see below). Margarita rocks, however, correspond well in isotopic composition to rocks from the Lesser Antilles arc (Figure 7.1) and are significantly displaced towards higher $^{87}Sr/^{86}Sr$ ratios from fresh MORB, with an average value of 0.70265 (Hart, 1976) and from oceanic islands with an average ratio of 0.70386 (Faure, 1986).

The $^{87}Sr/^{86}Sr$ isotopic ratios of most island-arc andesitic suites at modern convergent plate boundaries lie between 0.7030 and 0.7040. Within this range are andesites from Tonga, Fiji, and Vanuatu (Gill & Compston, 1973; Gill, 1976b), New Britain (Peterman et al., 1970), the Mariana and Izu Islands (Pushkar, 1968; Hart et al., 1970; Meijer, 1976; Masuda et al., 1976), the South Sandwich Islands (Hawkesworth et al., 1977) and the Northern Lesser Antilles (Hedge & Lewis, 1971; Hawkesworth & Powell, 1980; Davidson, 1986). Higher $^{87}Sr/^{86}Sr$ ratios occur in volcanic arc zones overlying crust which is >30 km thick and pre-Mesozoic in age: New Zealand (Ewart & Stipp, 1968), Papua New Guinea (Page & Johnson, 1974) and Peru and Chile (Pichler & Zeil, 1972; McNutt et al., 1975; Briqueu & Lancelot, 1979). Exceptional instances of high ratios, despite thin crust, include eastern Indonesia (Whitford et al., 1977) and the Antilles from Dominica to Grenada (Hedge & Lewis, 1971; Hawkesworth & Powell, 1980; Davidson, 1986).

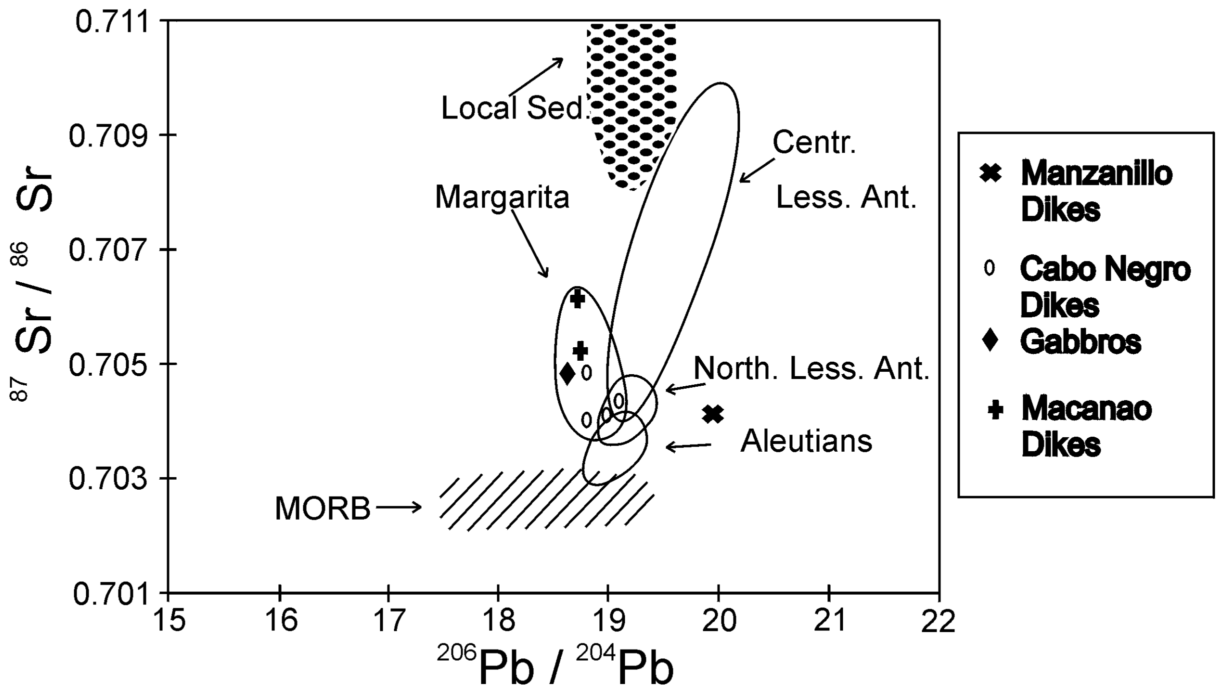

Figure 7.1:

$^{87}Sr/^{86}Sr$ vs. $^{206}Pb/^{204}Pb$ initial isotope ratio correlation diagram for Margarita basalts and oceanic basalt suites. Data sources: MORB from Sun et al. (1975), Church & Tatsumoto (1975), Tatsumoto (1978); Antilles from Donnelly et al. (1971), Davidson (1986, 1987), White & Dupré (1986); Aleutians from Kay et al. (1978); local sediments from White et al. (1985).

The Margarita $^{87}Sr/^{86}Sr$ isotopic compositions are presented along with mid-ocean ridge basalts (Sun et al., 1975; Church & Tatsumoto, 1975; Tatsumoto, 1978), calc-alkaline volcanic rocks from the Northern and Central Lesser Antilles arc (Donnelly et al., 1971; Davidson, 1986, 1987; White & Dupré, 1986), the Aleutians (Kay et al., 1978) and local sediments (White et al., 1985). In this diagram, Margarita data are confined between the isotopic composition of MORB and the field of local sediments (Figure 7.1). Variations in $^{87}Sr/^{86}Sr$ isotopic ratios within samples from both peninsulas exhibit positive trends with SiO_2, but negative trends with their Mg# and $K_2O/(K_2O+Na_2O)$ ratios (Figures 7.2 - 7.4), reflecting assimilation - fractional crystallization (contamination concomitant with fractionation). Rb correlates positively with K content in whole rocks, whereas the Rb content vs. $^{87}Sr/^{86}Sr$ shows no definite trend (Figure 7.5), further indicating that the $^{87}Sr/^{86}Sr$ isotopic ratios do not represent the primary source compositions. Sr ratios do not correlate positively with CO_2 and H_2O content, making secondary alteration-related effects on the Sr isotopic compositions of the Margarita series unlikely.

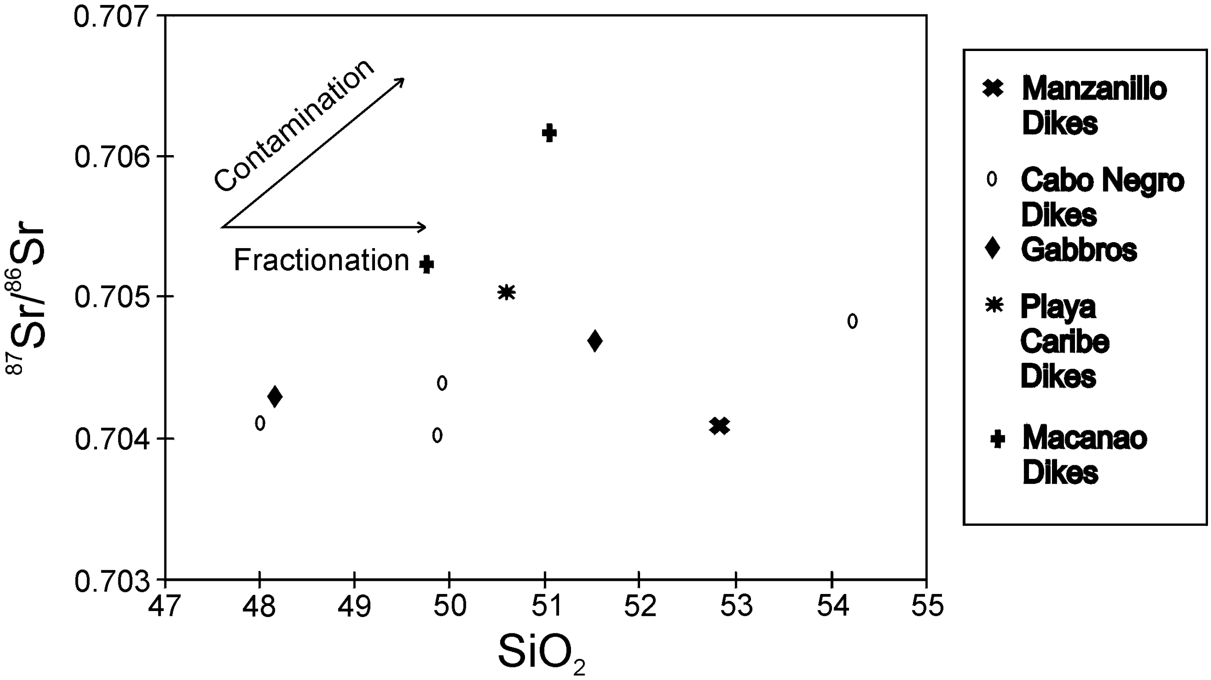

Figure 7.2:

$^{87}Sr/^{86}Sr$ initial isotope ratios vs. SiO_2 in Margarita dikes and gabbroic intrusions as a function of differentiation.

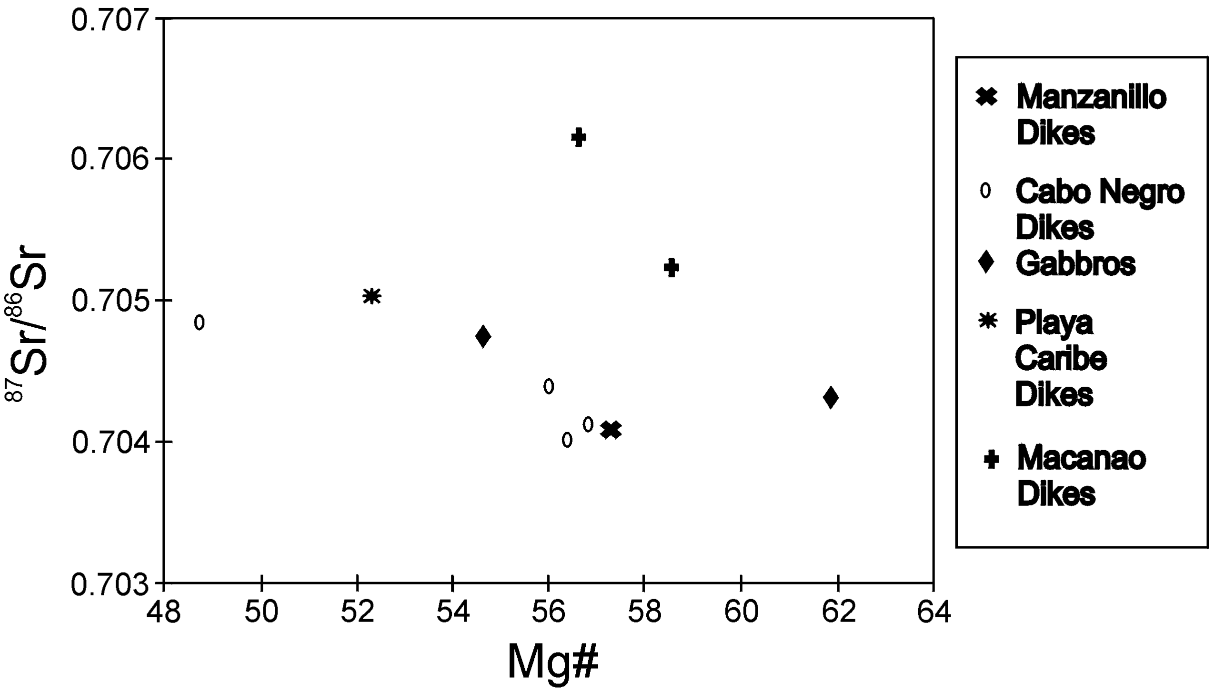

Figure 7.3:

$^{87}Sr/^{86}Sr$ initial isotope ratios vs. Mg# in Margarita dikes and gabbroic intrusions as a function of differentiation.

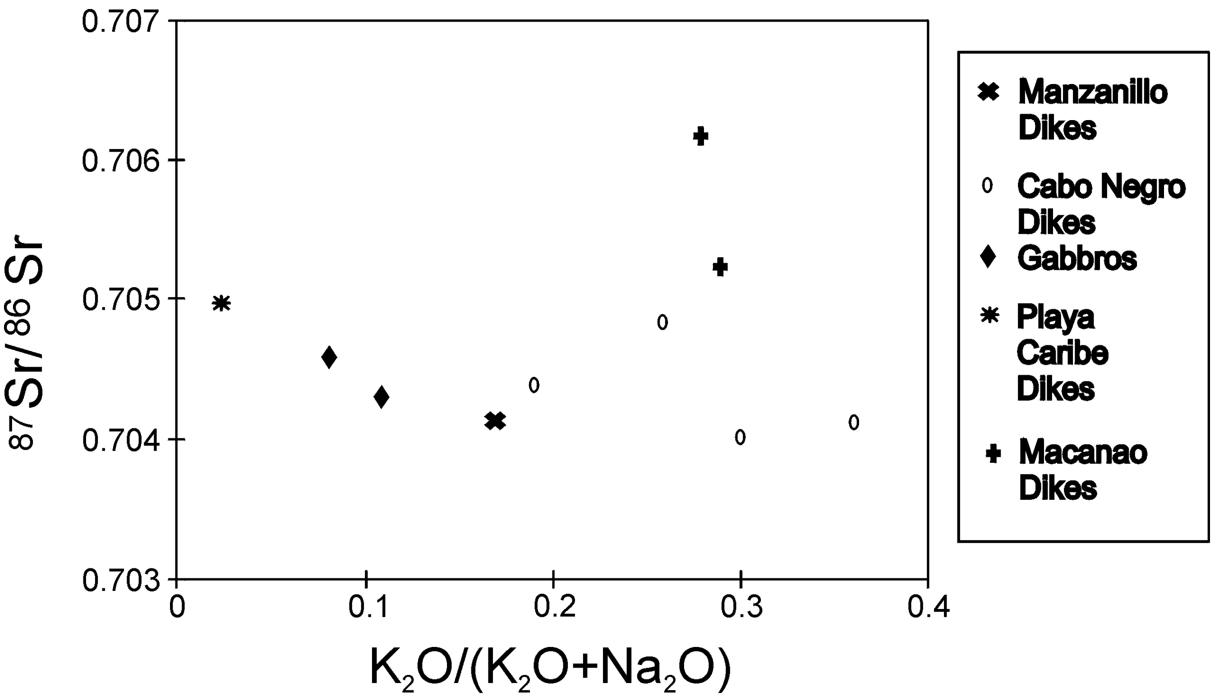

Figure 7.4:

$^{87}Sr/^{86}Sr$ initial isotope ratios vs. K_2O/K_2O+Na_2O in Margarita dikes and gabbroic intrusions as a function of differentiation.

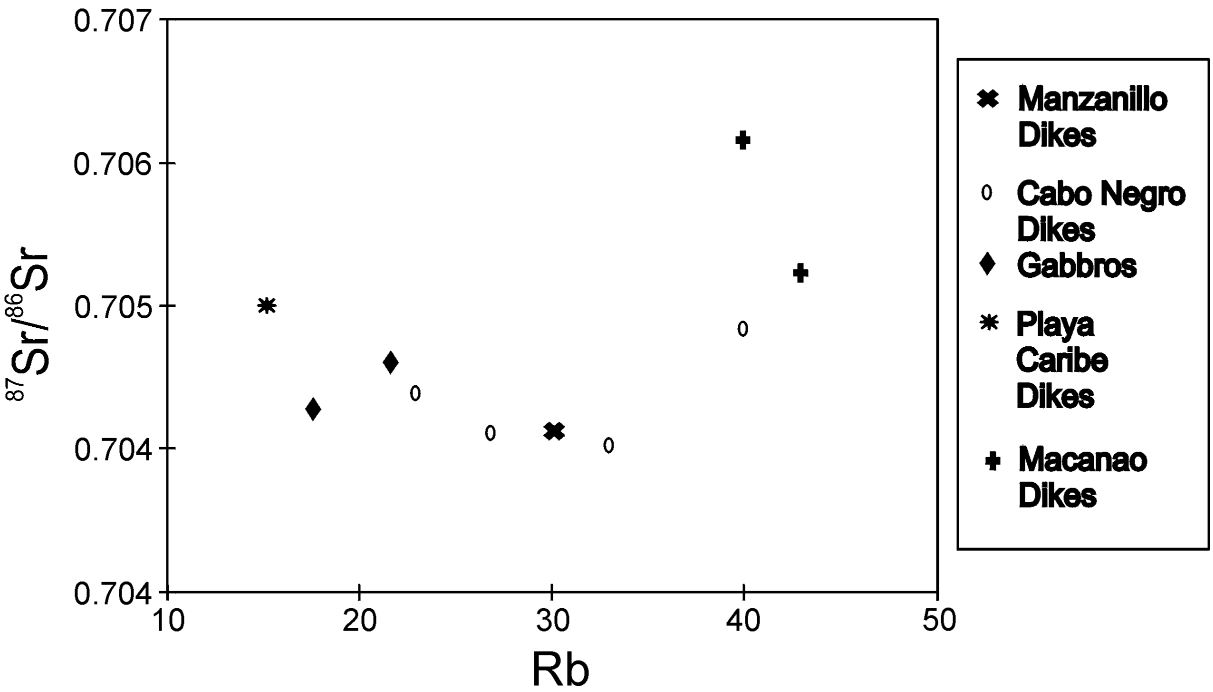

Figure 7.5:

$^{87}Sr/^{86}Sr$ initial isotope ratios vs. Rb in plagioclase mineral separates of dikes and gabbroic intrusions from Isla Margarita.

7.2.2 LEAD

The Pb isotopic data of the Margarita volcanic rocks define a rough linear correlation of $^{206}Pb/^{204}Pb$, from 18.657 to 19.913 and of $^{208}Pb/^{204}Pb$ ratios from 38.476 to 39.337 (Figure 7.6). They slightly overlap into the compositional field of MORB from Thirwall & Graham (1984).

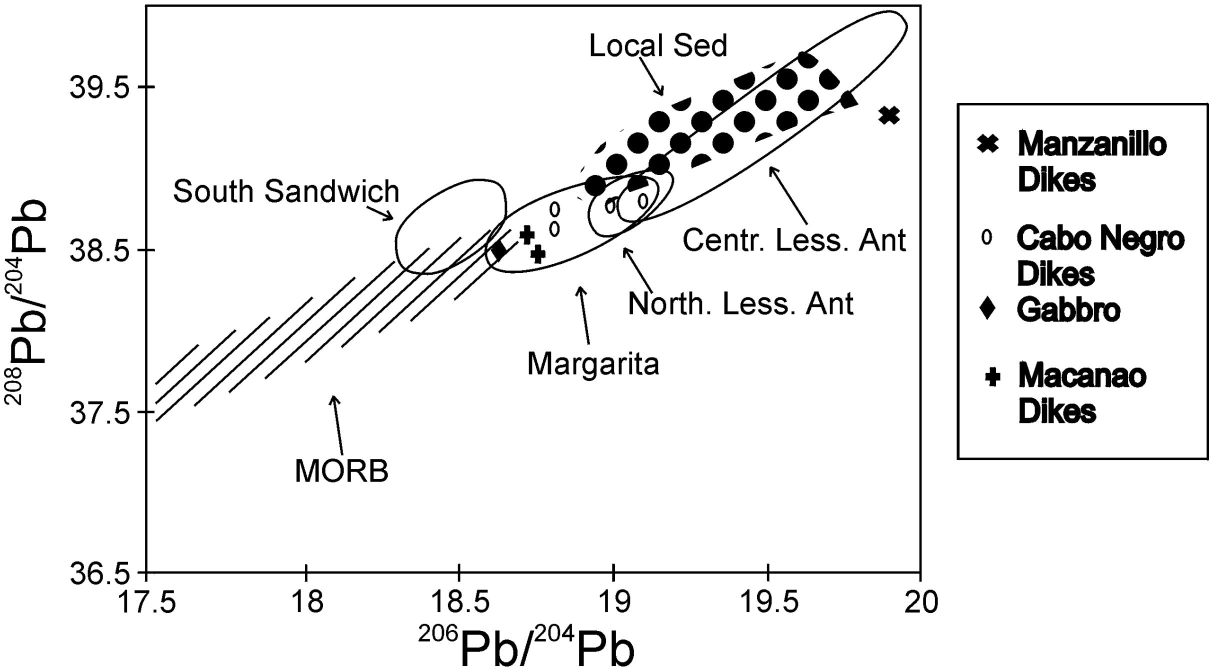

Figure 7.6

$^{208}Pb/^{204}Pb$ vs. $^{206}Pb/^{204}Pb$ initial isotope ratio systematics of Margarita rocks. MORB field is for Atlantic basalts (Thirwall & Graham, 1984). Sediment composition from DSDP samples reported by White et al. (1985). Data fields for calc-alkaline rocks from the Central and Northern Lesser Antilles from Donnelly et al. (1971), Davidson (1986, 1987), White & Dupré (1986); Aleutians from Kay et al. (1978); South Sandwich from Hickey et al. (1986); Marianas from Meijer (1976) and Hickey et al. (1986).

The isotopic ratios of $^{207}Pb/^{204}Pb$, however, are higher than MORB and vary from 15.634 to 15.792. Samples from the Paraguachoa peninsula have in average more radiogenic Pb than those from Macanao, with sample 6012 showing significantly higher radiogenic Pb than all other samples. The high Pb ratios are most likely due to small impurities of galena resulting from the hydrothermal alteration processes.

The lead isotope ratios of Margarita volcanic rocks form a linear array, similar to the results of other island arc volcanics. The similarity of Pb isotope ratios of the Margarita and Northern Lesser Antilles rocks (Davidson, 1987) and local sediments from the adjacent Atlantic Ocean floor (White et al., 1985) must be emphasized.

The Pb isotopic ratios of Margarita and other island arc volcanic rocks such as the South Sandwich (Hickey et al., 1986) and Aleutian islands (Kay et al., 1978) are displaced from the MORB $^{207}Pb/^{204}Pb$ correlation towards higher $^{207}Pb/^{204}Pb$. However, the degree of displacement of the $^{207}Pb/^{204}Pb$ lead ratio from that of MORB is relatively higher in the Margarita volcanic rocks than in those from the South Sandwich and Aleutian arc. The lead ratios from Margarita are also presented together with average calc-alkaline lamprophyres (Rock, 1991), calc-alkaline rocks of the Central Lesser Antilles (Davidson, 1987; White & Dupré, 1986), the Marianas frontal and remnant arc (Meijer, 1976; Hickey et al., 1986), as well as with ratios from local sediments from the Lesser Antilles frontal arc (White et al., 1985). The Margarita lead compositions are confined between sediment and MORB and correspond to average lead isotopic compositions of middle and upper crustal rocks (Bacon et al., 1984).

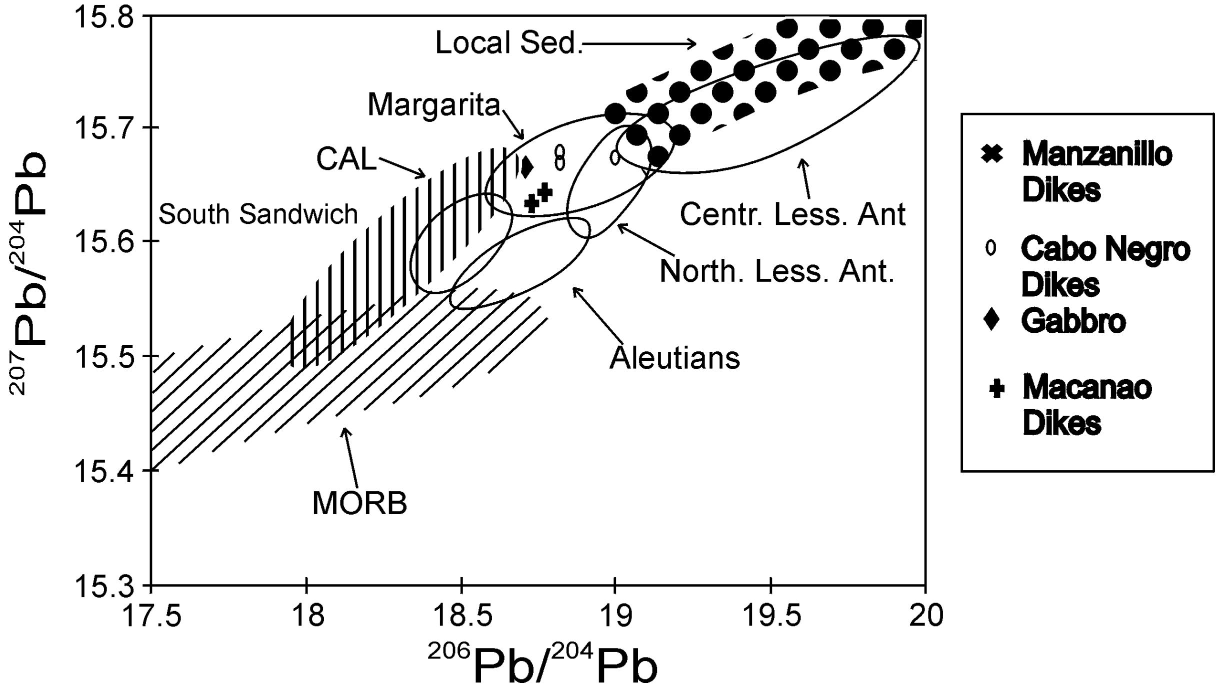

Figure 7.7:
$^{207}Pb/^{204}Pb$ vs. $^{206}Pb/^{204}Pb$ initial isotope ratio systematics of Margarita rocks. Initial isotope ratio systematics of Margarita rocks. MORB field is for Atlantic basalts (Thirwall & Graham, 1984). Sediment composition from DSDP samples reported by White et al. (1985). Data fields for calc-alkaline rocks from the Central and Northern Lesser Antilles from Donnelly et al. (1971), Davidson (1986, 1987), White & Dupré (1986); Aleutians from Kay et al. (1978); South Sandwich from Hickey et al. (1986); Marianas from Meijer (1976) and Hickey et al. (1986); CAL = calc-alkaline lamprophyres from Rock (1991).

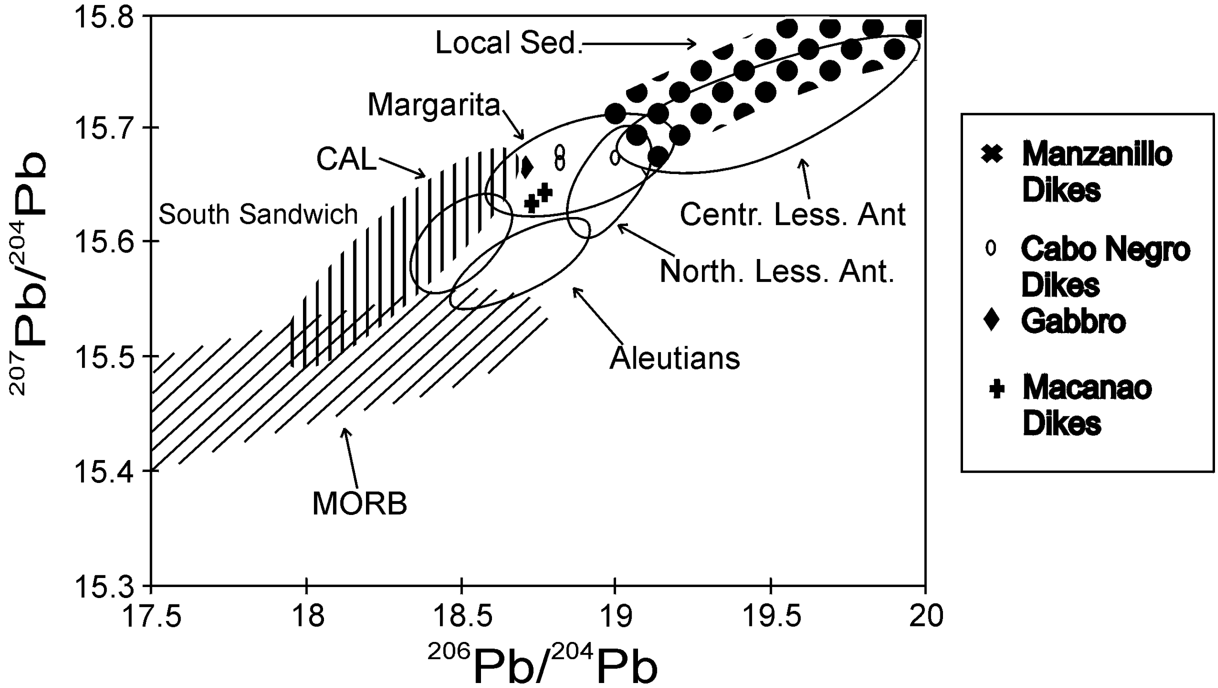

Figure 7.8:

$^{208}Pb/^{204}Pb$ vs. $^{207}Pb/^{204}Pb$ initial isotope ratio systematics of Margarita rocks. Initial isotope ratio systematics of Margarita rocks. MORB field is for Atlantic basalts (Thirwall & Graham, 1984). Sediment composition from DSDP samples reported by White et al. (1985). Data fields for calc-alkaline rocks from the Central and Northern Lesser Antilles from Donnelly et al. (1971), Davidson (1986, 1987), White & Dupré (1986); Aleutians from Kay et al. (1978); South Sandwich from Hickey et al. (1986); Marianas from Meijer (1976) and Hickey et al. (1986); CAL = calc-alkaline lamprophyres from Rock (1991).

The Margarita Pb and Sr variations are also shown in relation to geochemically distinct mantle components (Figure 7.9), established by Zindler & Hart (1986). The mantle components are defined there as "depleted" N-type MORB (DMM-A, -B), which is identifiable along ridge segments, with low $^{87}Sr/^{86}Sr$ and low $^{206}Pb/^{204}Pb$, a mantle component enriched in U and Th relative to Pb (HIMU), with very high $^{206}Pb/^{204}Pb$ and low $^{87}Sr/^{86}Sr$, the enriched mantle (EM I), the prevalent mantle (PREMA) with relatively constant $^{87}Sr/^{86}Sr$ (0.7033) and the bulk silicate earth (BSE).

In the $^{87}Sr/^{86}Sr$ vs. $^{206}Pb/^{204}Pb$ diagram shown below, the Margarita data fall outside the DMM-HIMU-BSE mixing triangle and are shifted towards the field of local sediments. The simplest model for explaining these isotopic variations involves the mixing of two components. Accordingly, the Margarita magmas would reflect interaction of MORB-like source material with local sediments. Considering the complexity of other geochemical characteristics of the Margarita magmas, however, suggests that this binary model is too simple.

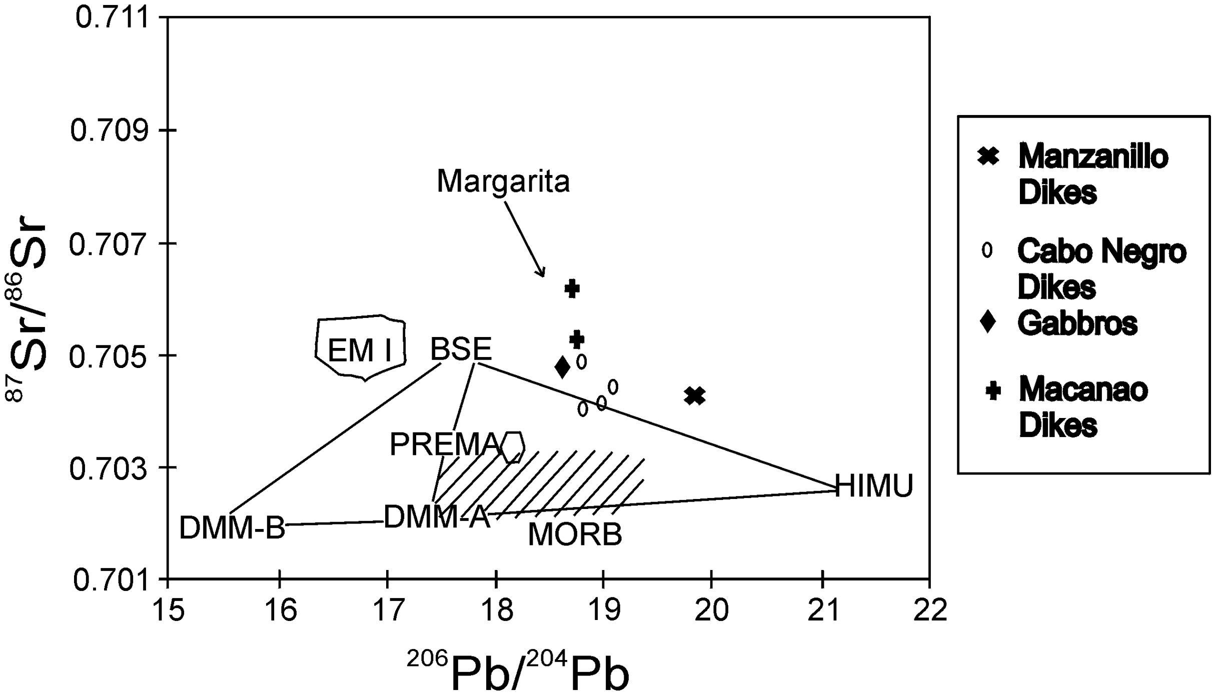

Figure 7.9:

$^{87}Sr/^{86}Sr$ vs. $^{206}Pb/^{204}Pb$ initial isotope ratio correlation diagram in relation to the geochemically distinct mantle compents DMM-A and -B (depleted N-type MORB), HIMU (Th- and U-enriched mantle relative to Pb), EM (enriched mantle), PREMA (prevalent mantle) and BSE (bulk silicate earth) after Zindler & Hart (1986). See discussion in text.

The corresponding trends of increasing radiogenic Sr with differentiation, as observed in plots of $^{87}Sr/^{86}Sr$ vs. SiO_2 and Mg#, respectively, are not so well established by Pb isotopes; although negative correlation of $^{207}Pb/^{204}Pb$ with Mg# confirms the observed Sr trend, the Pb ratios do not clearly increase with SiO_2. The variations illustrated in Figures 7.10 and 7.11, however, are thought to be due to effects of crustal contamination, rather than to mantle heterogeneity.

No significant trend of increasing isotopic ratios of Pb or Sr with increasing ages of the rocks is defined by the present data, which would confirm the possible role of assimilation during crystal fractionation. It must be stressed, however, that the obtained $^{40}Ar/^{39}Ar$ age data (see section 8.2) are approximate values, and the number of samples might not be representative.

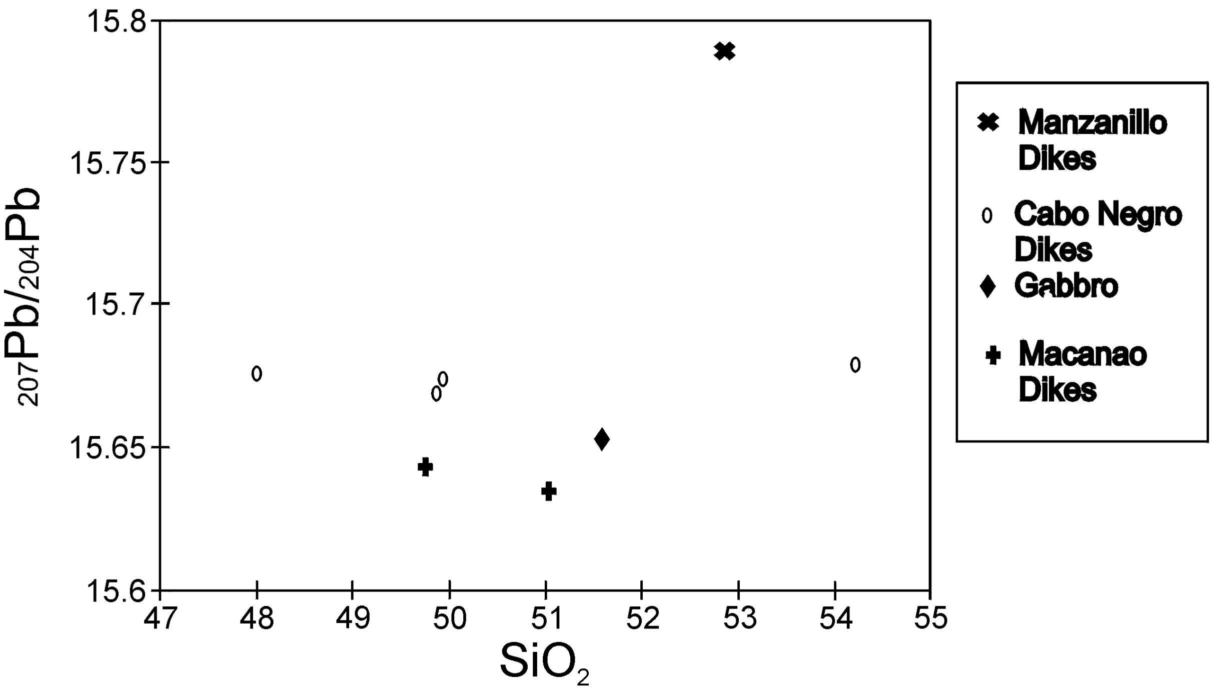

Figure 7.10:
$^{207}Pb/^{204}Pb$ initial isotope ratios vs. SiO_2 in Margarita dikes and gabbroic intrusions as a function of differentiation.

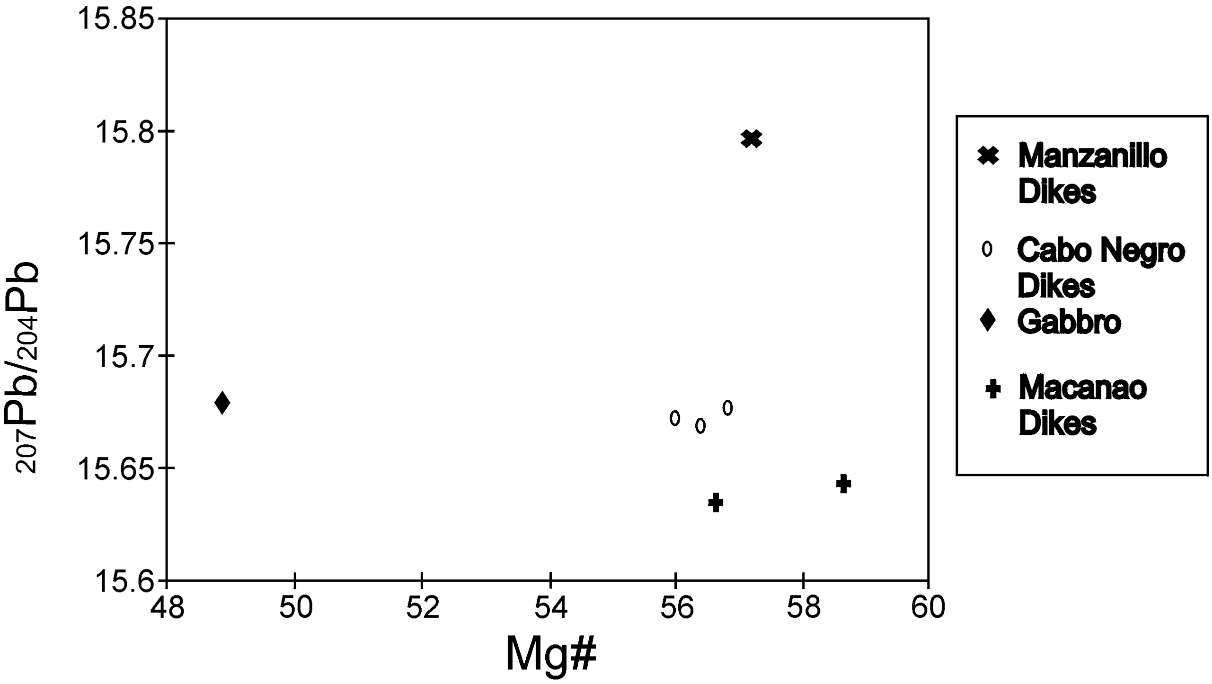

Figure 7.11:
$^{207}Pb/^{204}Pb$ initial isotope ratios vs. Mg# in Margarita dikes and gabbroic intrusions as a function of differentiation.

7.3 DISCUSSION

Source materials and evolutionary processes for basalts, related to orogenic provinces, can be distinguished from rocks of other tectonic provinces on the basis of isotopic ratios together with bulk rock composition. The final melt product of orogenic magmas may represent some confused average of large vertical sections of crust and mantle. However, significant isotopic heterogeneity also occurs within mantle domains, as observed in samples of MORB from a single dredge haul (LeRoex et al., 1983) and within the eruptives of a single small seamount (Zindler et al., 1984). At the other extreme, large areas of the earth show coherent and characteristic isotopic signatures (Dupré & Allegre, 1983), thus providing useful constraints defined by the extreme ends of the scale-length spectrum. Source contamination (=reflux of subducted sedimentary material into the mantle source of magmas) - versus crustal contamination (=assimilation of crustal material) cannot be conclusively assessed using radiogenic isotopes alone. Differences in $^{87}Sr/^{86}Sr$ isotopic ratio may also result from differences in the Rb/Sr ratio of the source region in the mantle, or assimilation, or isotope exchange of the basalt magma with rocks in the continental or oceanic crust, including pelagic sediments. Lithosphere age also exerts control on the isotopic ratio. Finally, alteration of basalt by seawater may as well lead to elevated $^{87}Sr/^{86}Sr$ ratios.

Isotopic ratios, together with various differentiation indices, such as the Mg# and SiO_2 content and trace element concentrations, may contribute to meaningful correlations and reduce the number of possible alternatives. Three principal components may be defined as contributing to the isotopic and trace element compositions of the Margarita magmas: the subducted slab, the overlying mantle wedge and a crustally derived contaminant.

Partial melting of eclogite, derived from a subducted slab, alone cannot generate the isotopic and chemical compositions of most island arc magmas (Gill, 1974; Wyllie, 1982). Melting of unaltered MORB is incapable of changing its isotopic composition and also unable to produce the large range in radiogenic isotope ratios displayed by the Margarita data and island arc volcanics in general. However, interaction of oceanic crust with seawater may variably elevate the Sr isotopic composition (Menzies & Seyfried, 1979). Successive dehydration of basaltic oceanic crust may involve slab-derived fluids as responsible factors for the geochemical characteristics of island arc volcanic rocks. Trace elements, derived by dehydration mechanisms, in particular LILE and LREE, would be concentrated relative to HFSE and HREE.

A subduction-modified mantle wedge source requires at least 20% partial melting to generate island arc magmas (Dupuy et al., 1982). Consequently, such high degrees of melting cannot fractionate LREE from HREE and generate the LREE-enriched patterns of Margarita and other island arc magmas. The REE and isotopic patterns rather reflect contamination or mixing of the mantle source with melt or equilibrated fluid from crustal sediment. It may then be appropriate to consider mixing, involving a mantle component enriched in LILE including radiogenic Sr, rather than "pristine" MORB or MORB-like mantle as source material for the Margarita magmas.

White & Dupré (1986) suggested that subducted oceanic sediment contributes to the magma source of most, if not all arcs. It is more obvious, however, in the Aves/Lesser Antilles region because the sediments being subducted have a much higher Pb radiogenic isotopic composition than most oceanic sediments. Radiogenic Pb ratios in the Antilles arc are regarded as strong evidence for a terrigenous component, derived from the Archaean shield area of South America. Lead isotopic analyses of gneisses from the Imataca series of the Guayana shield area in Venezuela range in $^{206}Pb/^{204}Pb$ ratios from 17.70 to 24.58, in $^{207}Pb/^{204}Pb$ from 15.36 to 19.18 and in $^{208}Pb/^{204}Pb$ from 34.92 to 46.77 (Montgomery, 1979).

If sediment subduction can be proven, it is important to determine the proportion of this component involved in magmagenesis. Davidson (1986) calculated a maximum of 2% bulk sediment mixed into the mantle source, which is required to generate the entire range of isotopic compositions from the Lesser Antilles; White & Dupré (1986) calculated mixing of 3% or less subducted sediment with a depleted mantle source to explain the geochemistry of most arc magmas. The complete absence of an accretionary sediment wedge at some arcs, such as the Marianas (Hussong et al., 1981), may explain the similarity in isotopic composition to MORB, whereas involvement of sediment with a strong contrast in isotopic and trace element concentration is reflected in large shifts in $^{87}Sr/^{86}Sr$ and most prominently in ^{206}, ^{207} and $^{208}Pb/^{204}Pb$ in the southern Caribbean province. It is, however, more realistic to consider a partial melt derived from the sediment as a contaminant, rather than bulk sediment. This effect becomes more important as the degree of partial melting decreases, and Sr or Pb may be concentrated in accessory phases.

Crustal thickness, the density contrast between crust and melt as well as the physical properties of the conduits play important roles, as they influence the ascent velocity of magmas. A strong compositional contrast between the ascending liquid and the crustal rocks will cause the magma to assimilate crustal material, resulting in chemically and isotopically modified compositions. Crustal thickness of the Northern Venezuela - Southern Caribbean region varies between 20-35 km (Bowin, 1976; Bonini et al., 1977; Bonini, 1978). A heterogeneous crystalline basement, with metasedimentary and metavolcanic components, is present in the Margarita Block. A realistic mechanism for contamination within the crust involves the combined effect of assimilation and crystal fractionation (AFC). In comparison to their ascent through the mantle, the Margarita magmas may have experienced a much slower ascent through the heterogeneous and more silicic crust. The degree of contamination at higher crustal level, resulting from the heterogeneous country rock suite, might be reflected in the variable isotopic composition of Margarita magmas. Basaltic dikes from Macanao, intrusive into the metasedimentary Los Robles group display the highest Sr-isotopic ratios (0.70523-0.70615) of the entire suite, followed by a Playa Caribe dike (0.70499) intrusive into a metasedimentary graphite schist. Gabbro and dike rocks, intrusive into the intermingled metavolcanic and metasedimentary Manzanillo Formation and into the metavolcanic La Rinconada group, display moderate to low values (0.70401-0.70483).

The trends in isotope plots show increasing $^{87}Sr/^{86}Sr$ with decreasing Rb/Sr ratios, decreasing Rb and K, but increasing SiO_2 content. These criteria do not favor the possibility of increasing radiogenic ^{87}Sr during fractional crystallization, but strongly support the hypothesis of contamination by sediments and/or by continental crust, reflecting an assimilation-fractional crystallization (AFC) trend. This implies that changes in isotopic composition are being produced during differentiation, while magma is residing in the crust. The $^{87}Sr/^{86}Sr$ isotopic ratio of 0.71391 in a Playa Caribe country rock indicates a significantly higher isotopic ratio than those of Margarita magmas and may well serve as a contaminant. Country rock xenoliths from the Manzanillo Formation of Margarita, found in lamprophyric dikes, indicate that country rock material can be a high-level contaminant of the ascending magma. The degree of contamination is reflected by the isotopic composition which correlates with indices of fractionation, such as the SiO_2 content and Mg#.

8.

GEOCHRONOLOGY

8.1 ANALYTICAL TECHNIQUES

Five dike and one gabbro sample were dated using mineral separates of magmatic hornblende. Separates were obtained by heavy-liquid and magnetic separation, followed by hand-picking to attain the highest possible purity. Grain sizes of hornblende separates are 50-100µm, except for hornblendes from dike samples 6012 and 6056 which have grain sizes of <50µm. Identification of intergrowths with actinolite and removal by handpicking was difficult in these samples.

Hornblende separates were packaged in aluminum foil and loaded into a quartz vial with Taylor Creek Sanidine flux monitors. Vials were irradiated at the USGS-TRIGA reactor in Denver for 8 hours in October 1993. Samples were analyzed 6 months later, when activity had dropped to optimum levels, at the Department of Geological Sciences at UCSB. Gas was purified continuously during extraction in a metal extraction line by two SAES type ST-172 porous getters and analyzed on a MAP (Mass Analyzer Products) mass spectrometer, fitted with a Baur Signer source and a Johnston MM1 multiplier.

$^{40}Ar/^{39}Ar$ age spectra were obtained by conventional step heating, using a Staudacher type resistance furnace. Flux monitors used were Taylor Creek Sanidine (85G003) with an assigned age of 27.92 Ma (Dalrymple & Duffield, 1988).

8.2 ^{39}AR/^{40}AR AGE SPECTRA

The ^{40}Ar/^{39}Ar age spectra of hornblendes from the Margarita dikes and gabbro differ significantly from model age spectra (e.g. McDougall & Harrison, 1988). The spectra yield more complex age patterns which lack discernible plateaus, but display irregular, saddle-shaped patterns, resulting in considerably different ages for the different incremental heating steps. In addition to the conventional display of ^{40}Ar/^{39}Ar data in age spectra (Figure 8.1), the associated variations in K/Ca for each heating step are also shown. The antipathetic variations between ages and K/Ca ratios are consistent with complex release patterns. Initial gas increments of hornblendes from Macanao dikes (6501, 6507) and the Cabo Negro gabbro (6055) give apparent ages very much older than the successive increments, whereas the Manzanillo dike (6012), the Cabo Negro dike (6050) and (6056), the latter crosscuts Cabo Negro gabbro (6055), yield the oldest apparent ages in the last increments. Age minima occur at intermediate amounts of ^{39}Ar released. The Manzanillo dike (6012) shows the least consistent data, characterized by a relatively large error for each heating step and, similar to dike sample 6056, considerable age differences over the entire spectrum. The resulting ages range from 26.8 to 78.3 Ma (6012) and 55.9 to 140.7 Ma (6056) respectively. As mentioned above, the hornblende separates of these samples have grain sizes <50µm, which made detection of impurities and intergrowth with actinolite difficult. Apparrently, this may be one reason which contributes to the more complex age spectra. Given these discrepancies, the total fusion ages and weighted mean plateau ages have to be treated with caution, since they are likely to be too high and do not represent the crystallization ages of the minerals.

The irregularly shaped age spectra share the same characteristics as those found by previous workers (Lanphere & Dalrymple, 1976; Claesson & Roddick, 1983; Kirsch et al., 1988) for igneous rocks and minerals known to contain excess ^{40}Ar. Lanphere & Dalrymple (1976) found that excess ^{40}Ar is released both in the first and the last increment, but state that the minima in the saddle-shaped spectra roughly approaches the crystallization age of the minerals; similar results were obtained by Harrison & McDougall (1980) and Berger & York (1981). Given that a plateau is not formed, this would mean maximum ages of 38-40 Ma for the Macanao Dikes, 55-43 Ma for the Cabo Negro and Manzanillo Dikes, and 61 Ma for the Cabo Negro gabbro.

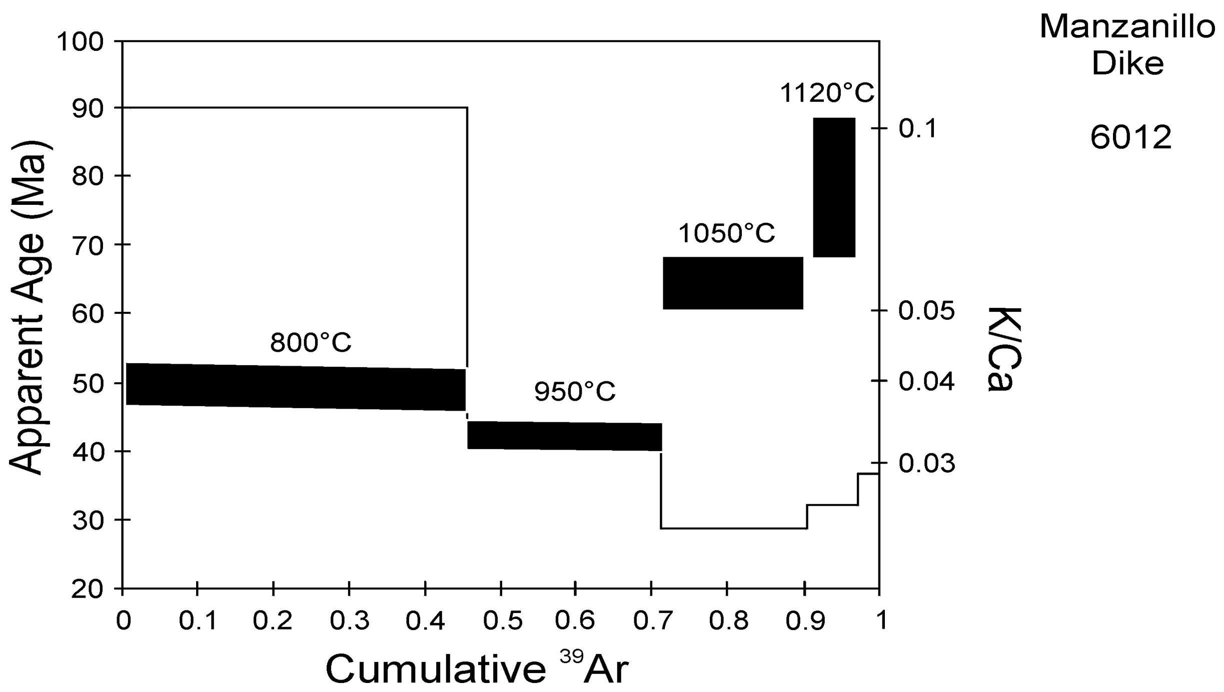

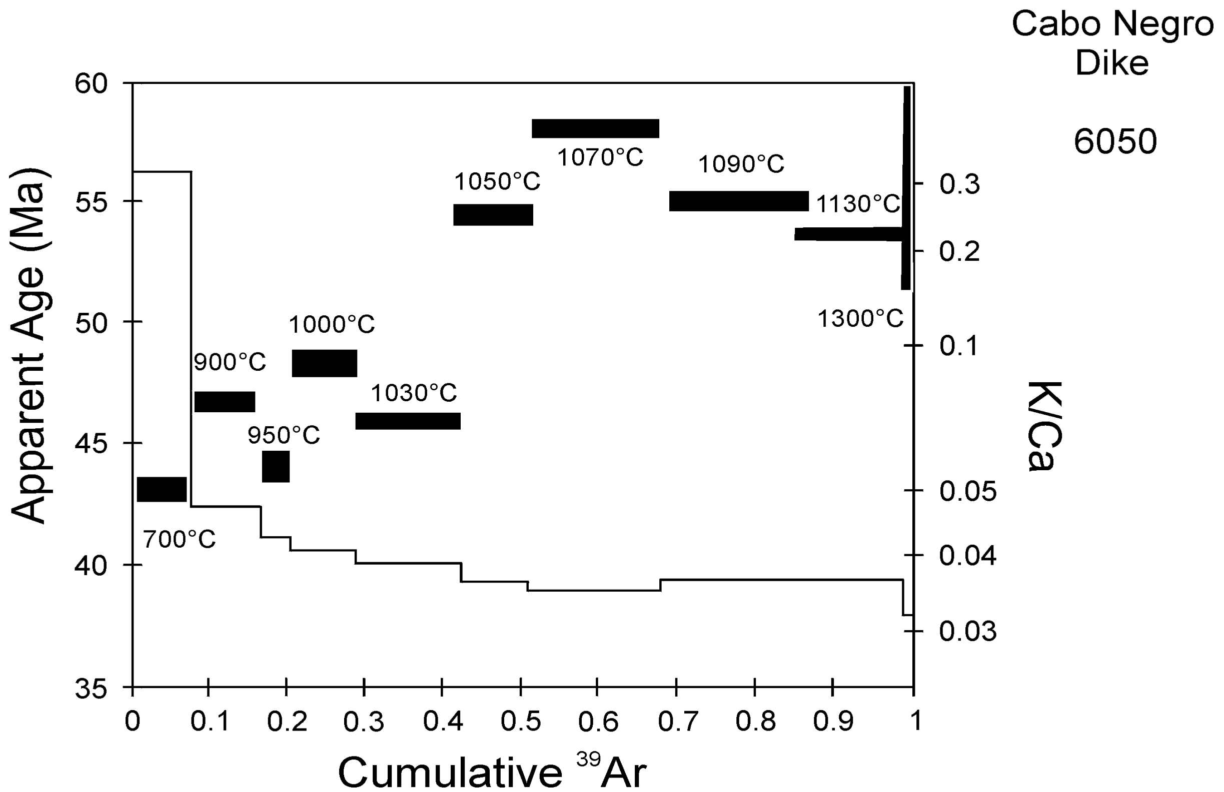

Figure 8.1:

$^{40}Ar/^{39}Ar$ apparent age spectra of six stepwise degassed hornblende mineral samples from Isla Margarita. The stippled band indicates the ± 1 sigma deviation. Solid line shows the K/Ca ratio for each step of the hornblende age spectrum.

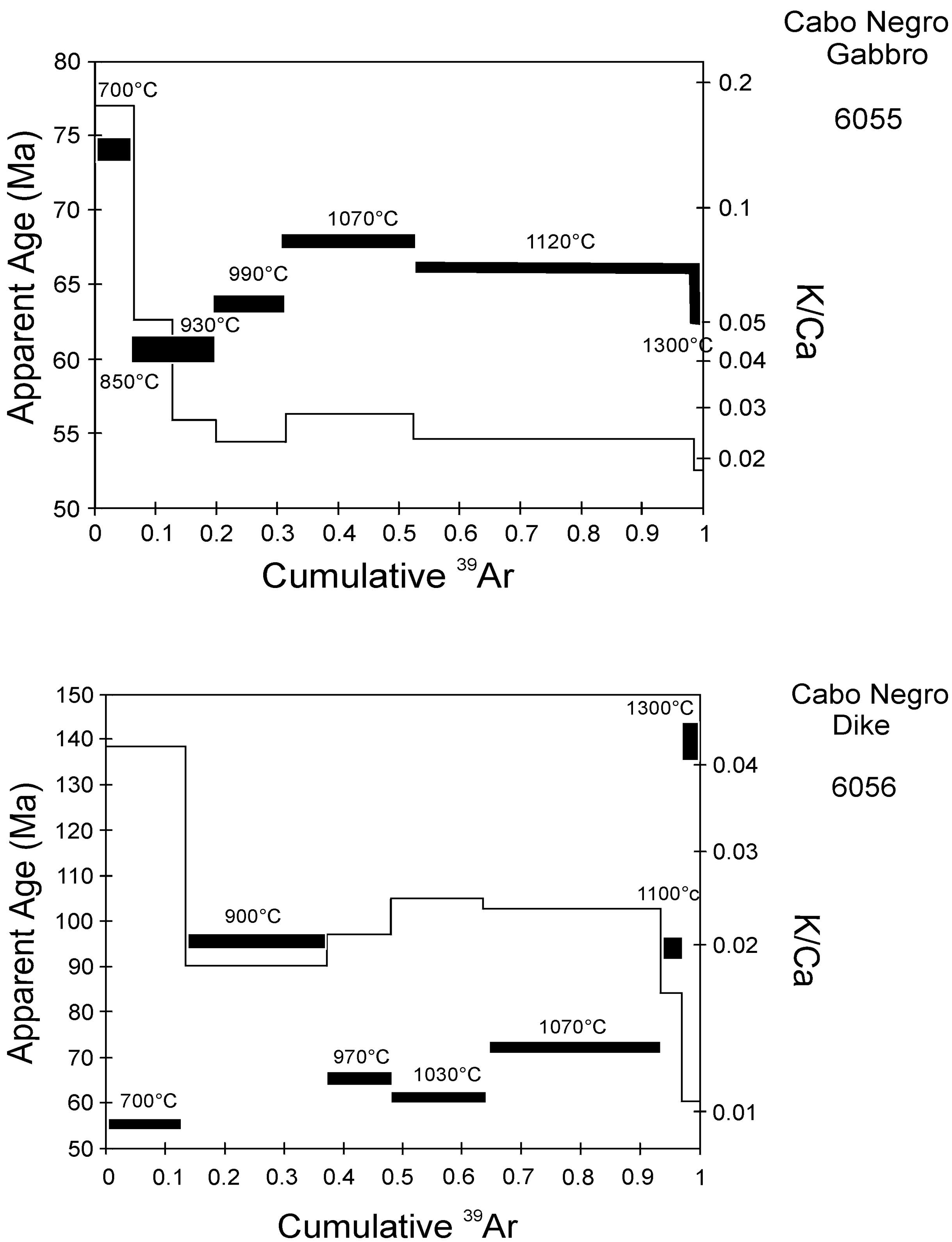

Figure 8.1 (contd.):

40Ar/39Ar apparent age spectra of six stepwise degassed hornblende mineral samples from Isla Margarita. The stippled band indicates the ± 1 sigma deviation. Solid line shows the K/Ca ratio for each step of the hornblende age spectrum.

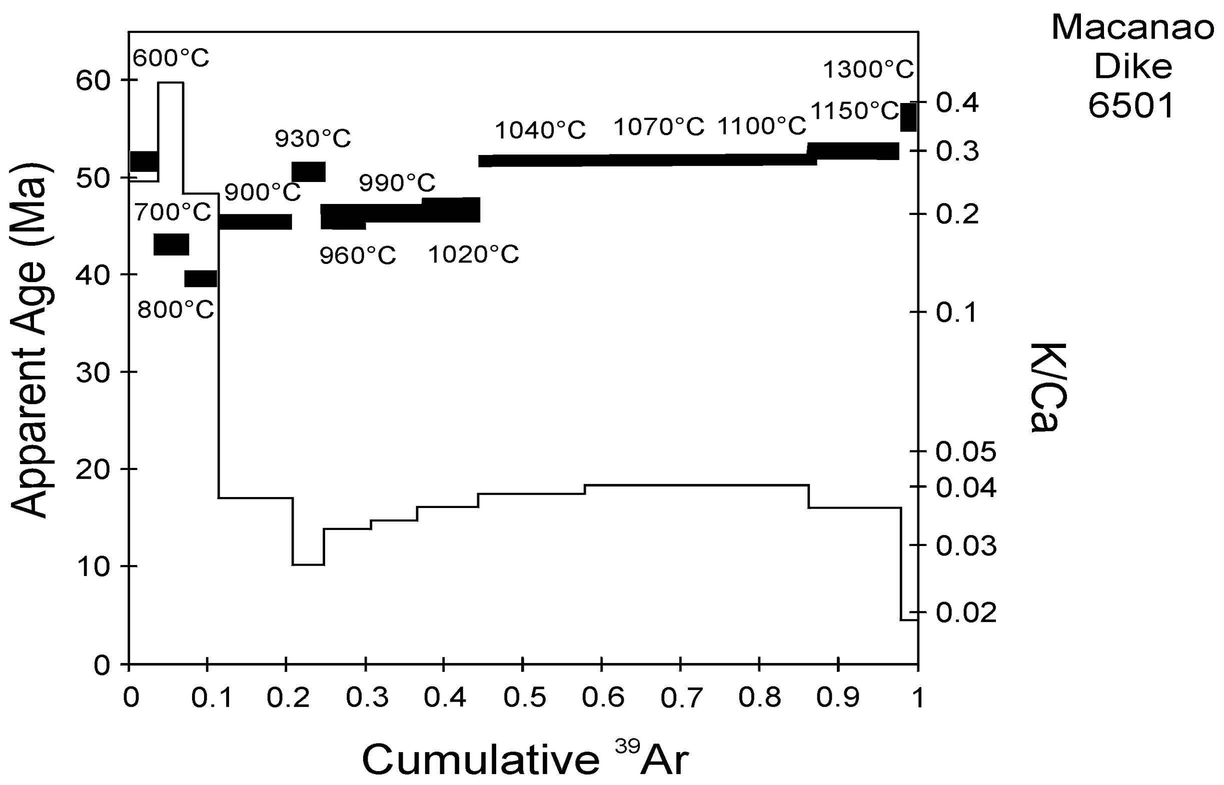

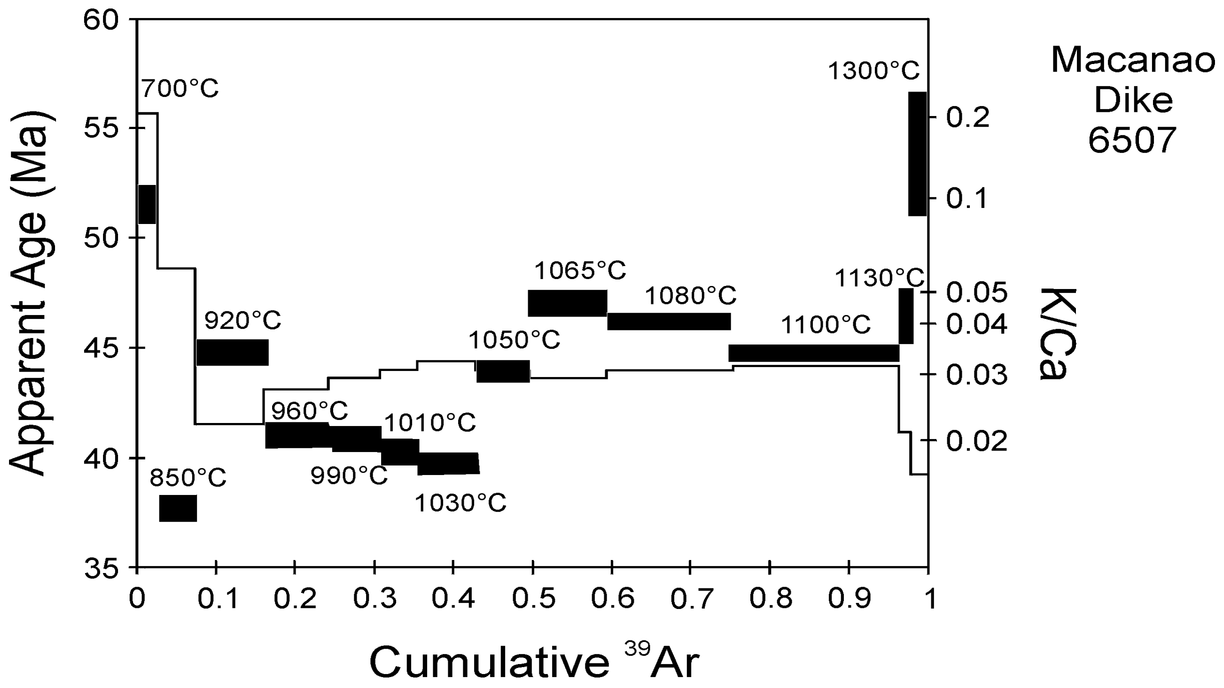

Figure 8.1 (contd.):

40Ar/39Ar apparent age spectra of six stepwise degassed hornblende mineral samples from Isla Margarita. The stippled band indicates the ± 1 sigma deviation. Solid line shows the K/Ca ratio for each step of the hornblende age spectrum.

Table 8.1 shows a section of the complex age data, the complete data are given in Table 12.9 (Appendix).

TABLE 8.1:

SAMPLE	TFA*1)	WMPA*2)	IIA*3)	$^{40}Ar/^{36}Ar$
6012	51.66±19.60	49.39±49.39	45.35±12.74	305.8±33.5
6050	51.15± 0.10	51.54± 0.09	94.69±90.41	5607 ±2825
6055	66.09± 0.15	66.26± 0.15	64.29± 3.29	330.9±58.5
6056	75.28± 0.22	71.04± 0.20	55.83± 8.48	446.5±78.0
6501	48.97± 0.12	49.56± 0.11	45.86± 3.34	344.9±49.7
6507	45.34± 0.10	45.22± 0.10	43.41± 1.41	329.0±23.8

TFA*1) = Total Fusion Age, WMPA*2)= Weighted Mean Plateau Age

IIA*3) = Inverse Isochron Age

8.3 ISOCHRON DIAGRAMS

The scatter in $^{40}Ar/^{36}Ar$ vs. $^{39}Ar/^{40}Ar$ isochron diagrams can be used as an unambiguous indicator of samples for which the basic K/Ar systems are disturbed (Lanphere & Dalrymple, 1976) and in this case, the isochron plots have been considered to roughly represent the crystallization ages of samples that contain excess argon.

Isochron plots of Margarita rocks have been considered to yield useful ages, however, with some restrictions. Whereas Cabo Negro dike (6050) allows no isochron fit, the isochron diagram of dike (6056) with an inverse isochron age of 55.83±8.48 Ma reveals more reliable data than the total fusion and weighted mean plateau age, with 75.28 and 71.04 Ma respectively. The latter are considered to be incorrect, as this dike crosscuts gabbro (6055) with an age of 64.3 Ma.

Given these restrictions, the $^{40}Ar/^{39}Ar$ data of hornblendes from Margarita can be summarized to approximate ages of 64 Ma for the Cabo Negro gabbro (6055) followed by coexisting dike (6056) with 56 Ma. A significantly younger dike (6050) from the same suite was dated with 47 Ma, comparable to dike (6012) from Manzanillo, which yields an age of 44 Ma. The Macanao dikes (6501 and 6507) are in the same age range with 46 and 43 Ma respectively.

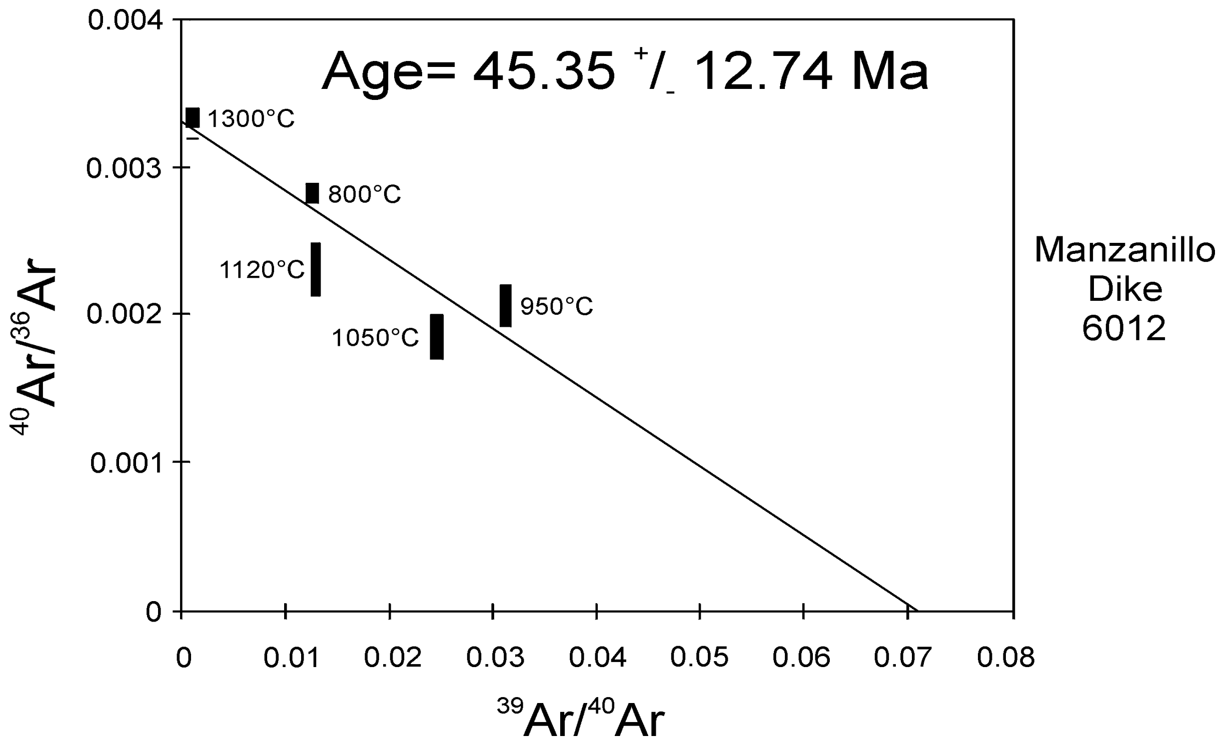

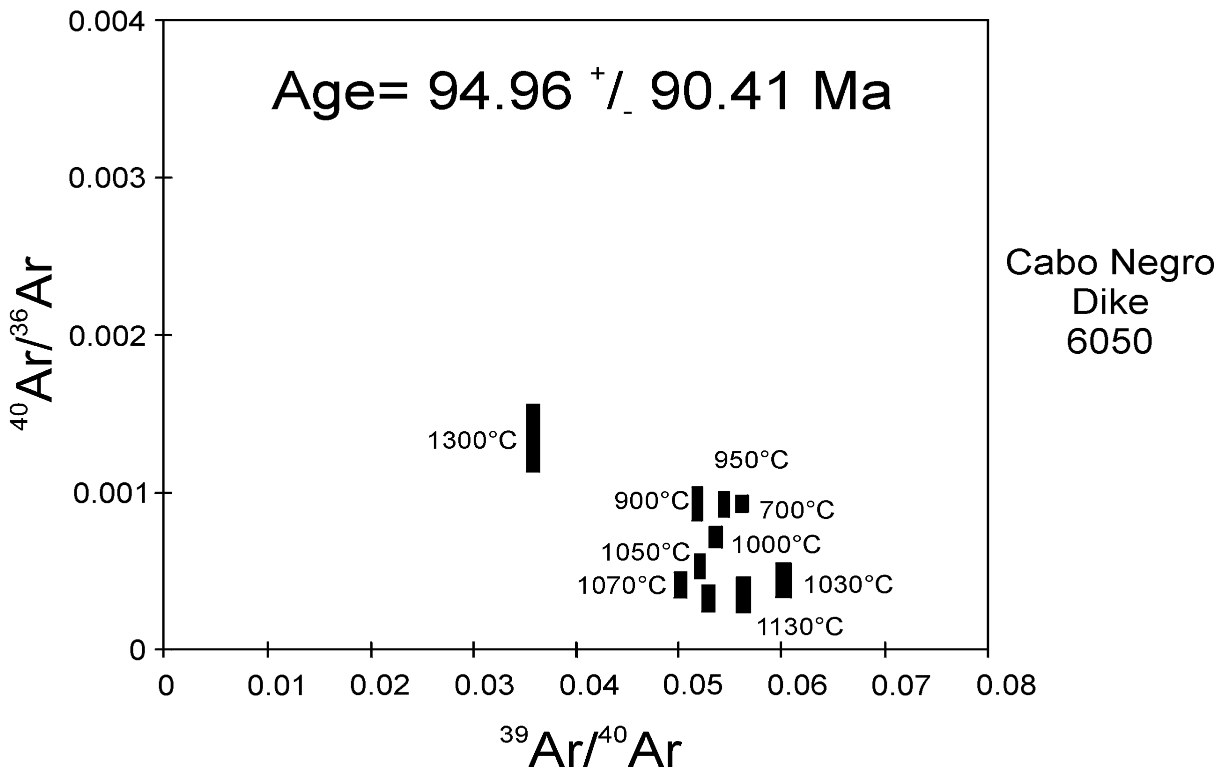

Figure 8.2:

$^{36}Ar/^{40}Ar$ vs. $^{39}Ar/^{40}Ar$ isotope correlation diagram showing isochron fit to selected gas fractions of hornblendes from Isla Margarita. The bar signature indicates the ± 1 sigma deviation.

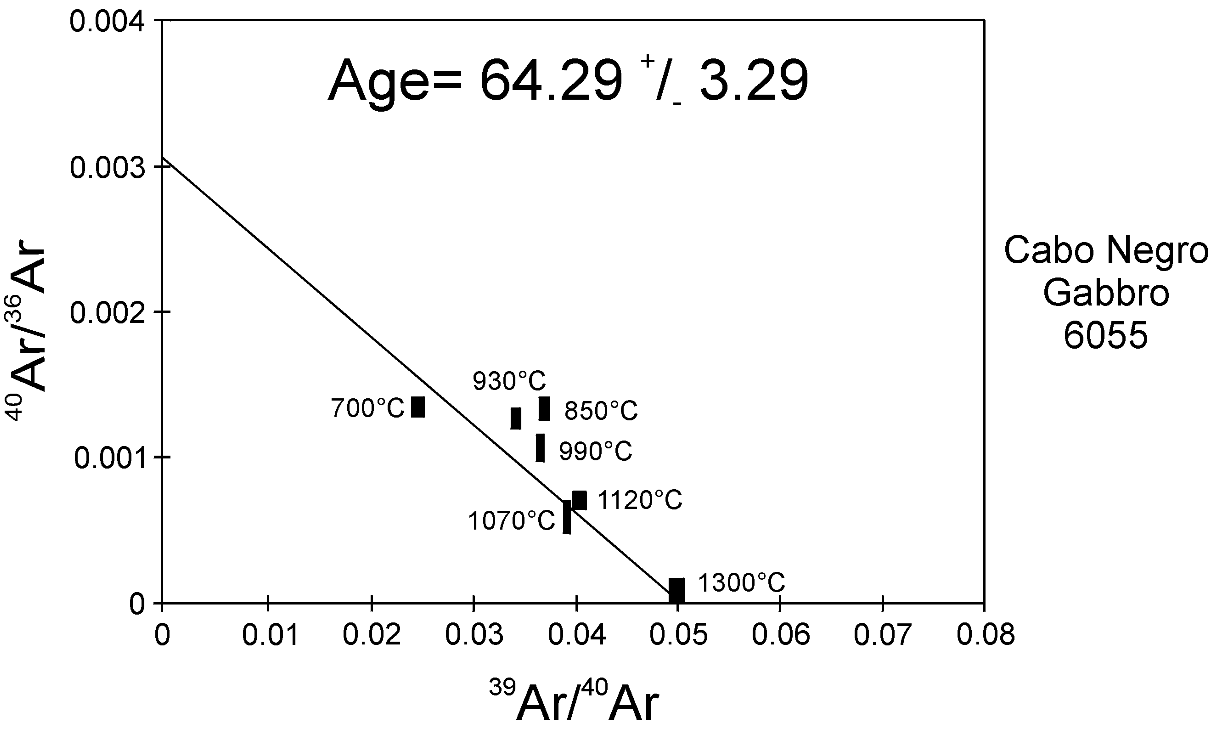

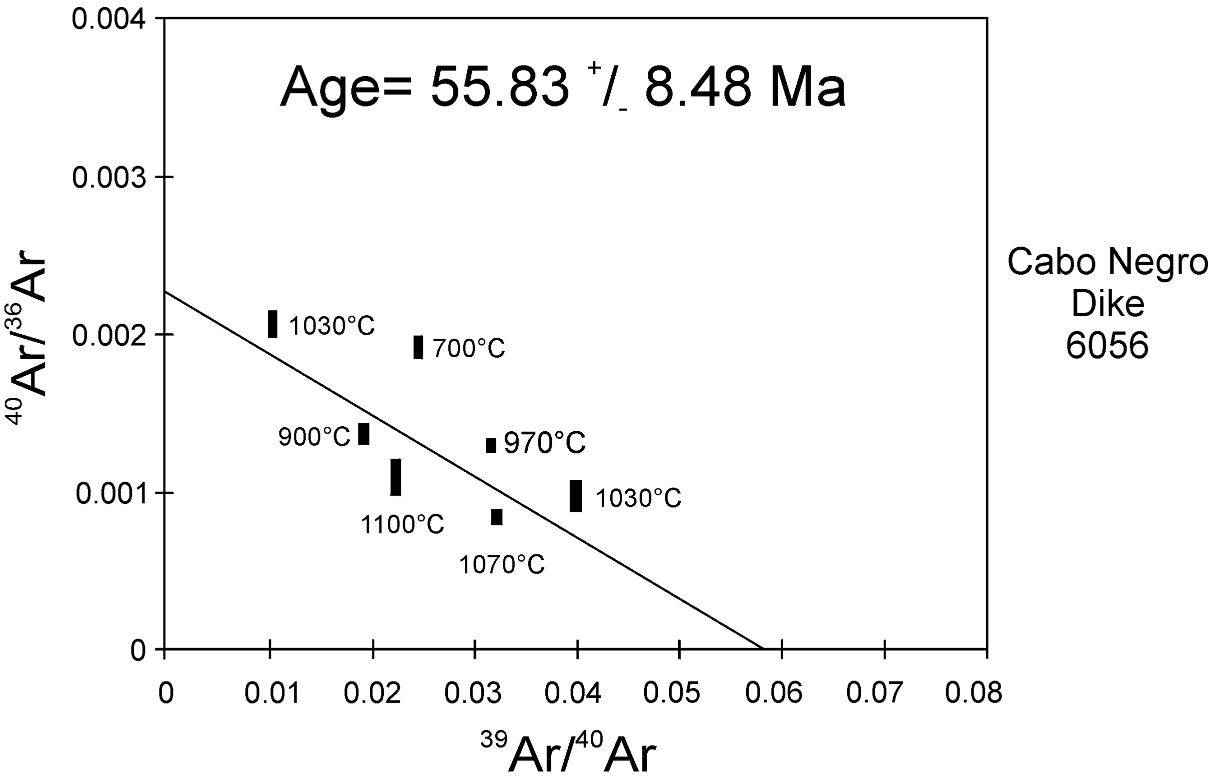

Figure 8.2 (contd):

$^{36}Ar/^{40}Ar$ vs. $^{39}Ar/^{40}Ar$ isotope correlation diagram showing isochron fit to selected gas fractions of hornblendes from Isla Margarita. The bar signature indicates the ± 1 sigma deviation.

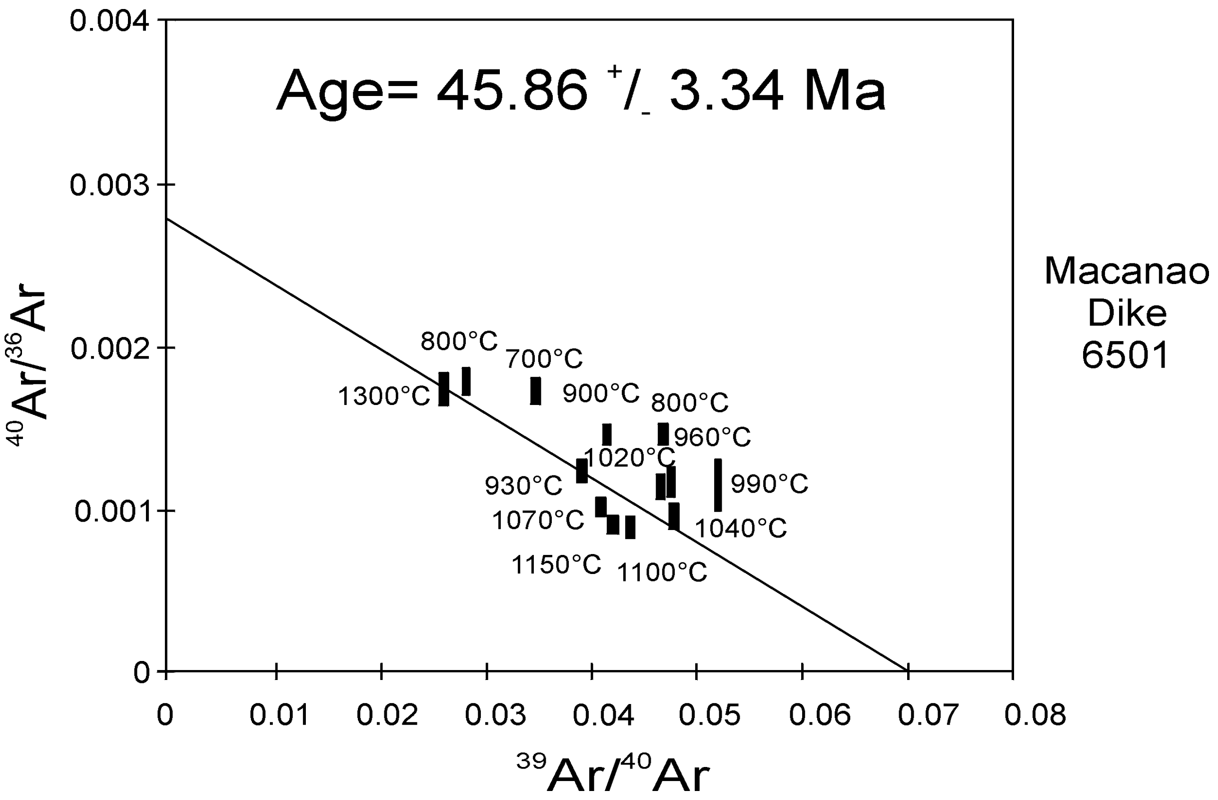

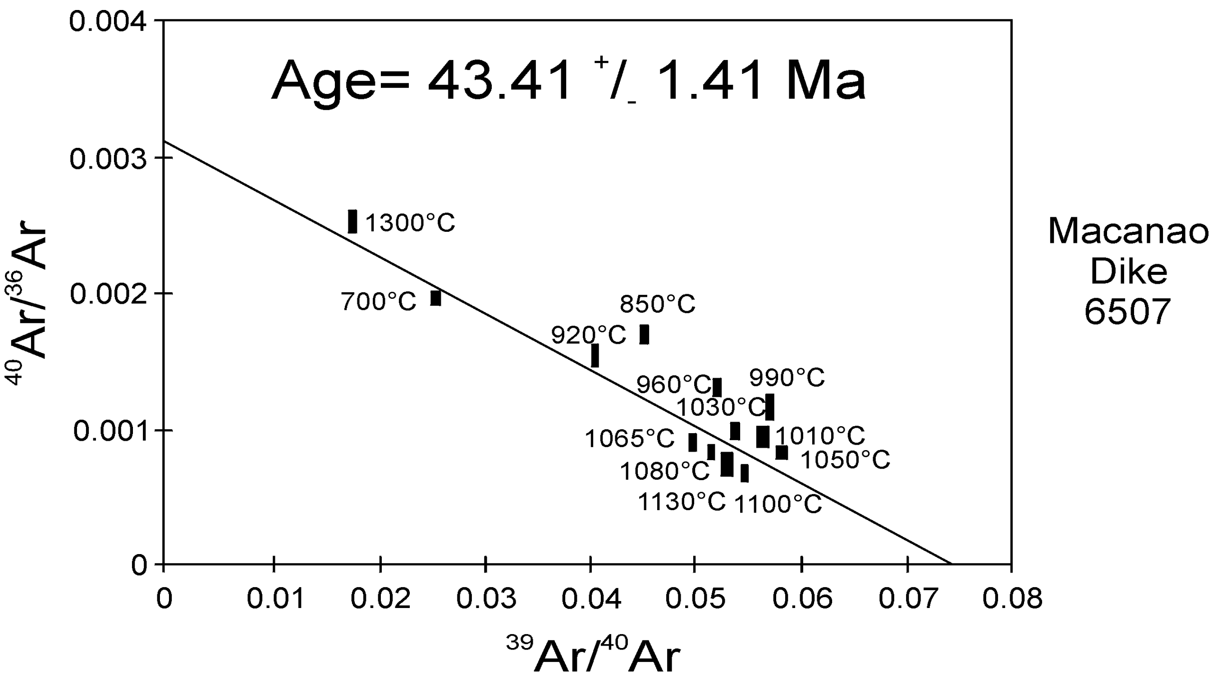

Figure 8.2 (contd):

$^{36}Ar/^{40}Ar$ vs. $^{39}Ar/^{40}Ar$ isotope correlation diagram showing isochron fit to selected gas fractions of hornblendes from Isla Margarita. The bar signature indicates the ± 1 sigma deviation.

8.4 DISCUSSION

The age information resulting from $^{40}Ar/^{39}Ar$ spectra of hornblendes from the Margarita intrusive series is inhomogeneous over large parts of the release spectra, indicating disturbed K-Ar systems. Given this fact, the present study takes up, on the example of Margarita rocks, the problem of excess argon, but also the question whether to interpret the $^{40}Ar/^{39}Ar$ age results as intrusion or slow cooling ages. If magma intrudes into a shallow and cold crustal level, it cools down rapidly and the ages obtained should correspond to the time of intrusion. However, if the intrusion takes place in a crustal level with increased temperatures, the closure temperatures of the minerals will be reached successively during cooling of the intrusive body on the one hand and cooling of the country rocks on the other hand, and the ages will represent "cooling ages".

The intrusion of the lamprophyric dikes on Margarita along preexisting fracture zones provides geological evidence that the dikes intruded after the post-metamorphic cooling event of the Margarita country rock, which had already passed from a lower ductile to an upper brittle crustal environment (Stöckhert et al., 1993, 1995). In this case, the country rock had cooled down to a sufficiently low temperature ($<300^{o}C$) and allowed rapid cooling of the intruding dikes. Consequently, the radiometric ages obtained should correspond to the time of intrusion.

The saddle-shaped release spectra, however, indicate that the primary argon isotopic systems are disturbed and are diagnostic of excess ^{40}Ar. The minima in the age spectra approach the crystallization age, and the $^{36}Ar/^{40}Ar$ versus $^{39}Ar/^{40}Ar$ isochron diagrams may roughly reveal the crystallization age of the Margarita dikes and gabbro.

The obtained age information of Margarita rocks is geologically meaningful and can be compared with data of volcanic rocks occurring on other Venezuelan offshore islands in the immediate vicinity.

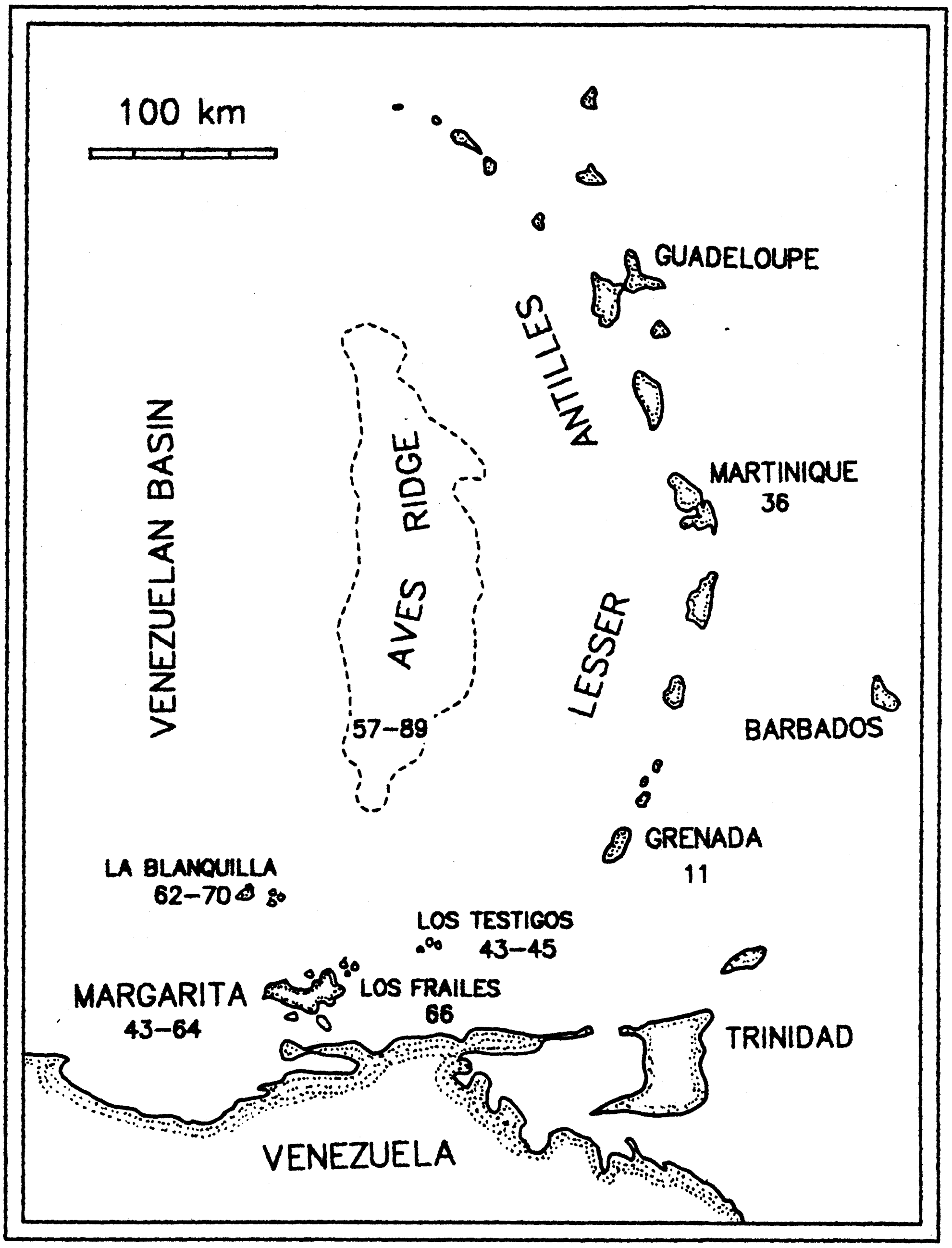

Figure 8.3:

Index map showing the geochronology of Margarita (this study), the neighboring Venezuelan offshore islands Los Frailes, Los Testigos and La Blanquilla (Santamaria, 1972; Santamaria & Schubert, 1974), the Aves Ridge (Fox et al., 1971; Nagle, 1972) and the Lesser Antilles Grenada and Martinique (Nagle et al., 1976).

The correlation of Ar/Ar age data from Margarita with K/Ar age data from the island groups Los Frailes, Los Testigos and La Blanquilla (Santamaria, 1972) show close agreement (Figure 8.3). Margarita dike rocks agree with ages of diabases and granodiorites from the Los Testigos islands, which range between 43 and 45 Ma; within the age spectrum of the gabbroic and corresponding dike sample from Margarita are diabases from the Los Frailes islands with 66 Ma.

8.

CONCLUSIONS

9. CONCLUSIONS

GEOCHEMICAL AND GEODYNAMIC SIGNIFICANCE OF EOCENE MAGMATISM ON ISLA MARGARITA

Isla Margarita represents a piece of crust close to the southern boundary of the Caribbean plate. Peridotites and high-pressure metamorphic units were juxtaposed at a convergent plate boundary, subsequently intruded by various magmatic rock suites, exhumed and finally covered by sediments. Structural relations and P-T paths reflect a complicated tectonic history. The latest magmatic activity is represented by small gabbroic intrusions and dikes which crosscut all units with the exception of the sedimentary cover. Geochemistry and geochronology of these magmatic rocks have been studied in this work to reconstruct the source, the magmatic evolution and the tectonic setting during this igneous activity. The rocks are pyroxene and amphibole-phyric lamprophyric dikes and small gabbroic intrusions, corresponding in chemical composition to basaltic-andesitic rocks. They are partially altered under lower greenschist-facies conditions with the secondary mineral assemblage of actinolite, chlorite, epidote and calcite. The rocks are rich in compatible elements which indicates a high degree of partial melting of the mantle source. Depletion of high field strength elements (HFSE Ti, P, Zr) indicates that melts had already been extracted from this mantle source before. Enrichment in large ion lithophile elements (LILE Ba, Rb, K, Sr) and light rare earth elements (REE La, Ce) is attributed to interaction with continental or sedimentary material. The isotopic composition spans considerable ranges, from values close to those characteristic of mid-ocean ridge basalts to compositions more characteristic of continental material. There is a broad trend with differentiation towards more contaminated compositions, but no correlation with the rock ages. The isotopic and combined trace element characteristics cannot distinguish unequivocally between a contaminated mantle source above a subduction zone and contamination of the melt during uprise through the continental crust. However, the contrasting isotopic compositions appear to be more consistent with a model based upon variable degrees of assimilation of compositionally heterogeneous continental material, rather than derivation from a strongly heterogeneous mantle source. An AFC model (the combined effect of assimilation and crystal fractionation) seems to be a realistic mechanism for the evolution of the magmas.

On the other hand, increasing radiogenic lead isotopic ratios along the Lesser Antilles island arc from north to south has been reported by Hawkesworth & Powell (1980) and White & Dupré (1986). This may be attributed to subducted sediments derived from the South American craton. Since the isotopic, REE and trace element characteristics of the Margarita and Lesser Antilles volcanic rocks overlap, suggesting similar processes of magma evolution, the high lead isotopic ratios of the Margarita rocks may originate from a similar source region.

Alltogether, the magmas have originated from a subduction-modified mantle source and have been contaminated to a considerable degree during uprise through the thin continental crust. The occurrence of calc-alkaline lamprophyres is characteristic for the terminal stage of magmatism at convergent plate boundaries.

The reconstruction of the tectonic position during this magmatism is based on its age. Despite some uncertainty inherent to the disturbed $^{39}Ar/^{40}Ar$ age spectra, the data indicate a Paleocene/Eocene age, with the undeformed gabbro (64 Ma) being somewhat older than the dikes (56-43 Ma). This spread in ages overlaps with that found for the latest igneous activity on the Aves ridge, dated with 89-57 Ma (Fox et al., 1971; Nagle, 1972). On the other hand the Margarita magmatic rocks are significantly older than the earliest igneous rocks exposed on the Lesser Antilles, which have been dated as 35-40 Ma old (Nagle et al., 1976; Mattinson et al., 1980). This supports the concept chosen by Stöckhert et al. (1995) to fix Margarita at the southern tip of the Aves ridge for the reconstruction of the displacement path of the Margarita block in the Caribbean plate tectonic framework (Figure 9.1).

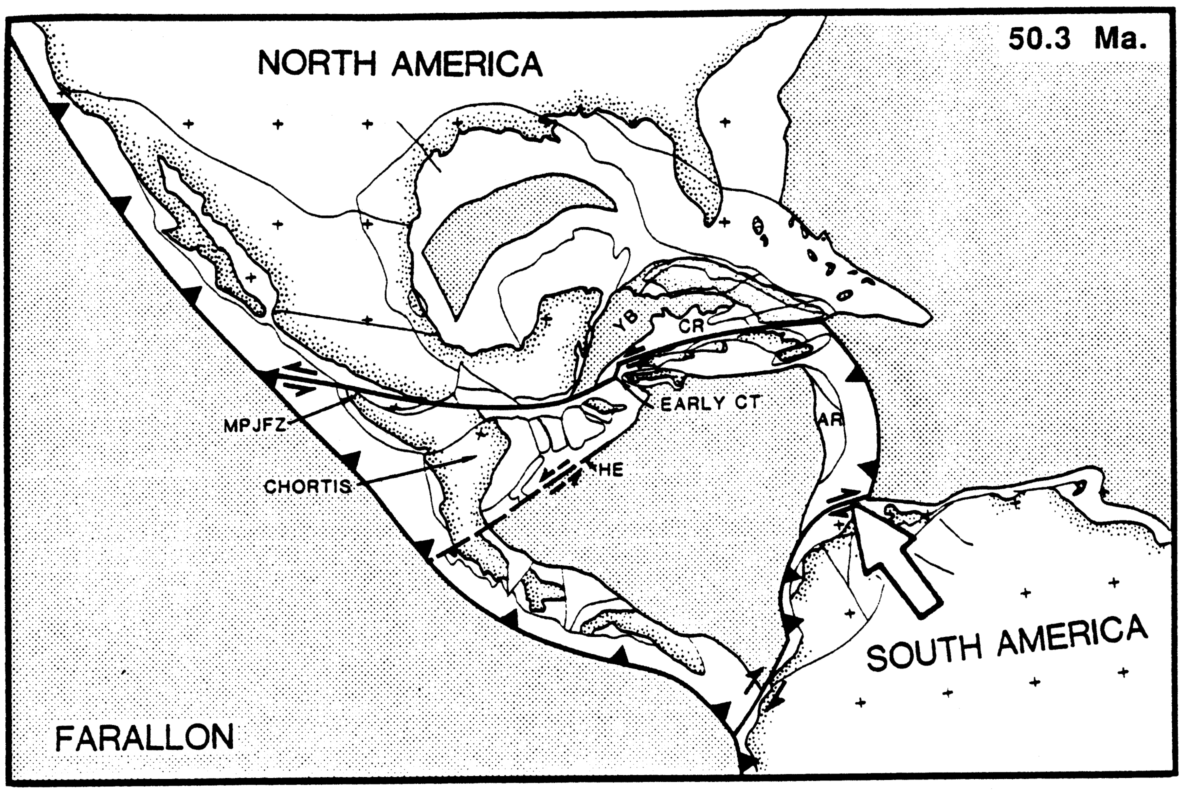

Figure 9.1:

Plate-tectonic reconstruction of the Caribbean for the Middle Eocene (Ross & Scotese, 1988) with presumed location of Isla Margarita (Stöckhert et al., 1995).

In comparison to other Venezuelan offshore islands, the age of the Margarita gabbro corresponds to the age of magmatic rocks exposed on the Los Frailes islands, located ca. 15 km NE of Margarita (66 Ma, Santamaria, 1972). The similarity of Margarita and Los Frailes rocks (Moticska, 1972) suggests a close genetic relationship between both suites, which belong to the youngest igneous series on the Venezuelan offshore islands. Together with the Eocene magmatic rocks from Los Testigos (43-45 Ma, Santamaria, 1972) and the latest Cretaceous/Paleocene rocks from La Blanquilla (62-70 Ma, Santamaria, 1972), they fill the gap in igneous activity between the extinct Aves ridge and the still-active Lesser Antillean arc in both time and space. During this period, subduction at the Aves ridge ceased and the new subduction zone at the Lesser Antilles was created further to the east.

The structural position and age of the dikes and gabbroic intrusions provide a reference system for the Tertiary tectonic evolution of Margarita and allow a correlation with plate tectonic reconstructions. The emplacement of the dikes along preexisting conjugate shear fractures indicates that the country rock resided in a shallow crustal level and had already suffered brittle extensional deformation prior to the intrusions. As evident from the brittle deformation of the dikes themselves, several compressional and extensional stages followed while Margarita was displaced to the east with respect to South America along the conservative plate boundary at the southern border of the Caribbean plate (Erlich & Barrett, 1990).

A summary of the entire deformation-temperature-time history of the crustal block exposed on Margarita (Figure 9.2, Stöckhert et al., 1995) comprises (1) accretion and high-pressure metamorphism in the deep level of a fore-arc, (2) intrusion of calc-alkaline magmas in an intermediate level of a volcanic arc, (3) strike-slip deformation in an intermediate crustal level along a transform plate margin and (4) shallow crustal setting close to a transform plate margin. The Paleocene/Eocene magmatic activity coincides with the transition from (3) to (4), which comprises the rapid displacement of Margaritan crust into the brittle upper crust due to a major tectonic reorganization. The depth of intrusions is estimated to be about 5 km with a prevailing country-rock temperature in the order of 250-300 °C as inferred from the secondary mineral assemblage.

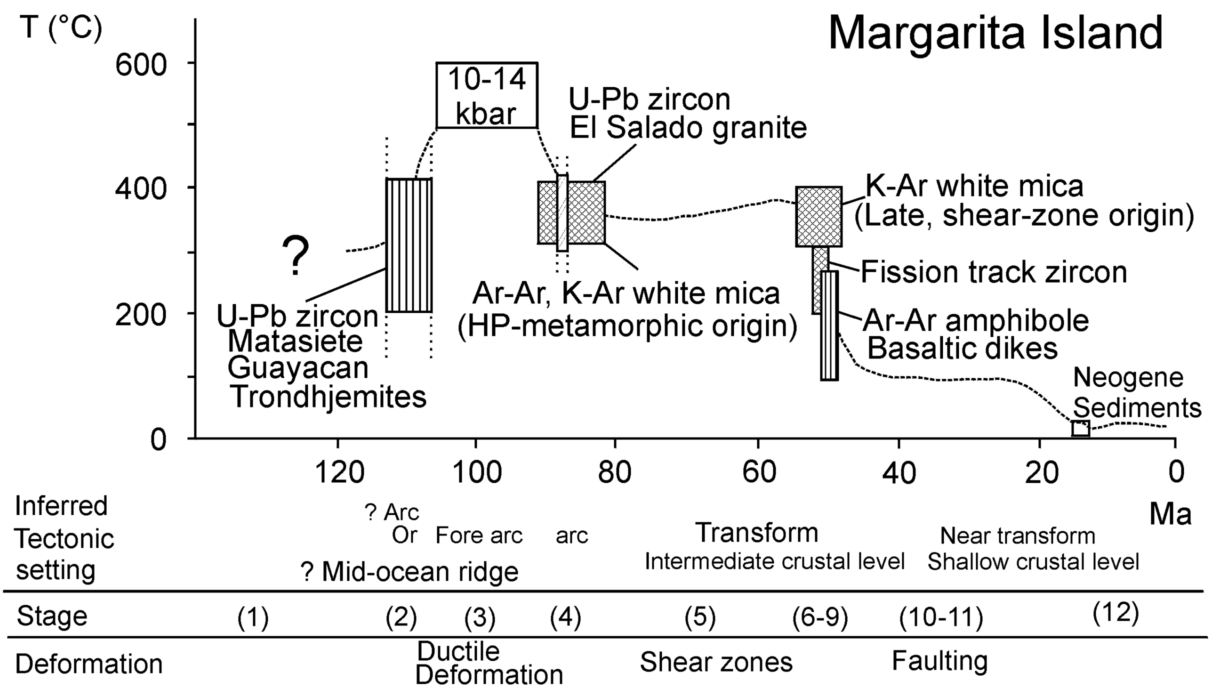

Figure 9.2:

Summary of the time-temperature history of the Marga-rita Complex by (Stöckhert et al., 1995)

The Paleocene/Eocene magmatic activity of Margarita is one of the fundamental keystones for the reconstruction of the crustal history of Margarita presented by Stöckhert el al., 1993, 1995). This reconstruction appears to be in perfect accordance with plate-tectonic scenarios developed by Pindell et al. (1988), Ross & Scotese (1988), Pindell & Barrett (1990) and Pindell (1993) and supports a Pacific origin of the Caribbean plate.

10.

ACKNOWLEDGEMENTS

10. ACKNOWLEDGEMENTS

This work was carried out at the Institut für Geologie, Ruhr-Universität Bochum (RUB), Germany and the Department of Geology, University of California, Santa Barbara (UCSB) under supervision of Prof. Bernhard Stöckhert (RUB) and Prof. George Tilton (UCSB), to whom the author is most grateful for encouragement, helpful criticism, advice and funding.

Helpful advice in laboratory techniques at UCSB for radiogenic isotope analyses came from Leslie Ames, Massimo D'Antonio and Dave Parkinson. Andy Calvert and Phil Gans supported $^{40}Ar/^{39}Ar$ age dating. Walter Köhler and Horst Kubbilun assisted in multiple microprobe and XRF sessions at RUB. Rb and Sr isotope data for three Margarita samples were kindly provided for three samples by D. Buhl, RUB. REE concentrations were measured at the Institut für Geologie (Prof. J. Erzinger), Justus Liebig Universität Gießen, which is highly appreciated.

Fruitful discussions with Peter Bitschene are greatly acknowledged. Proof-reading of the manuscript by Ian Bray is also appreciated.

Studies at UCSB were supported by a one-year research scholarship from DAAD; my special thanks go to Christiane Gabriel, Gaby Parmentier-Dienst and Nancy Bennett.

11. LIST OF ABBREVIATIONS

Ab	= albite
act	= actinolite
AFC	= assimilation-fractional crystallization
AFM	= alkalies, iron, magnesium
An	= anorthite
$a SiO_2$	= silica activity
BSE	= bulk silikate earth
C	= corundum
CAL	= calc-alkaline lamprophyres
CIPW	= Cross, Iddings, Pirsson, Washington
chl	= chlorite
cpx	= clinopyroxene
Cr#	= Cr-number (Cr*100/(Cr+Al))
DMM	= depleted mantle
D.I.	= differentiation index
DSDP	= deep sea drilling project
E-MORB	= enriched mid-ocean ridge basalt
EMP	= electron microprobe
En	= enstatite
ep	= epidote
FeO*	= total iron
$f O_2$	= oxygen fugacity
Fs	= ferrosilite
hbl	= hornblende
HFSE	= high field-strength elements
HIMU	= U and Th enriched mantle
HREE	= heavy rare earth elements
hy	= hypersthene
IIA	= inverse isochron age
ICP-AES	= inductively coupled plasma - atomic emission spectrometry
LILE	= large-ion lithophile elements
LREE	= light rare earth elements
MORB	= mid-ocean ridge basalte
Mg#	= Mg-number (Mg*100/(Mg+Fe^{2+})
mus	= muscovite
mt	= magnetite
N-MORB	= normal mid-ocean ridge basalt

ol	= olivine
opx	= orthopyroxene
Or	= orthoclase
P	= pressure
p.f.u.	= per formula unit
$pH2_O$	= partial pressure of water
plag	= plagioclase
PREMA	= prevalent mantle
qz	= quartz
REE	= rare earth elements
T	= temperature
TFA	= total fusion age
vol%	= volume percent
WMPA	= weigted mean plateau age
Wo	= wollastonite
wt%	= weight percent
XRF	= X-ray fluorescence

12.

REFERENCES

Allan JF, Sack RO, Batiza R (1988) Cr-rich spinels as petrogenetic indicators: MORB-type lavas from the Lamont sea chain, Eastern Pacific. Amer Mineral 73:741-753

Alt JC, Honnorez J, Laverne C, Emmerman R (1986) Hydrothermal alteration of a 1 km section trough the upper oceanic crust, Deep Sea Drilling Project Hole 504B: Mineralogy, chemistry and evolution of seawater-basalt interaction. J Geophys Res 91:10309-10335

Aoki K, Kushiro I (1968) Some clinopyroxenes from ultramafic inclusions in Dreiser Weiher, Eifel. Contrib Mineral Petrol 18:326-337

Arculus RJ (1976) Geology and geochemistry of the alkali basalt-andesite association of Grenada, Lesser Antilles island arc. Geol Soc Amer Bull 87:612-624

Arculus RJ (1978) Mineralogy and petrology of Grenada, Lesser Antilles island arc. Contrib Mineral Petrol 65:413-424

Arculus RJ, Wills KJA (1980) The petrology of plutonic blocks and inclusions from the Lesser Antilles island arc. J Petrol 21:243-299

Arth JG (1976) Behavior of trace-elements during magmatic processes - a summary of theoretical models and their applications. US Geol Surv J Res 4:41-47

Avé Lallemant HG (1991) The Caribbean-South American plate-boundary, Araya Peninsula, eastern Venezuela. In: Larue DK, Draper G (eds) Transactions, 12th Caribbean Geological Conference, St. Croix, US Virgin Islands, South Miami, Florida. Miami Geol Soc:461-471

Bacon CR, Kurasawa H, Delevaux MH, Kistler RW, Doe BR (1984) Lead and strontium isotopic evidence for crustal interaction and compositional zonation in the source regions of Pleistocene basaltic and rhyolitic magmas of the Coso volcanic field, California. Contrib Mineral Petrol 85:366-375

Beddoe-Stephens B (1981) Metamorphism of the Rossland volcanic rocks, southern British Columbia. Can Mineral 19:631-641

Bednarz U (1988) Volcanological, geochemical and petrological evolution and sub-seafloor alteration in the northeastern Troodos ophiolite, Cyprus. Ph.D. Dissertation, Ruhr-Universität Bochum, Germany:295 pp

Bednarz U, Schmincke HU (1989) Mass transfer during sub-seafloor alteration of the upper Troodos crust (Cyprus). Contrib Mineral Petrol 102:93-101

Beets DJ, Maresch WV, Mottana A, Bocchio R, Beunk FF, Monen HP (1984) Magmatic rock series and high-pressure metamorphism as constraints on the tectonic history of the southern Caribbean. In: Bonini WE et al. (eds) The Caribbean-South American plate boundary and regional tectonics. Geol Soc Amer Mem 162:95-130

Bence AE, Baylis DM, Bender JF, Grove TL (1979) Controls on the major and minor element chemistry of mid-ocean ridge basalts and glasses. In: Talwani M, Harrison CG, Hayes DE (eds) Deep Drilling Results in the Atlantic Ocean: Ocean Crust. Amer Geophys Union:331-341

Berger GW, York D (1981) Geothermometry from $^{40}Ar/^{39}Ar$ dating experiments. Geochim Cosmochim Acta 45:795-811

Best MG, Mercy ELP (1967) Composition and crystallization of mafic minerals on the Guadalupe igneous complex, California. Amer Mineral 52:436-474

Binns RA (1965) The mineralogy of metamorphosed basic rocks from the Willyama Complex, Broken Hill district, New South Wales, part 1: hornblendes. Mineral Mag 35:306-326

Bonini WE (1978) Anomalous crust in the eastern Venezuela Basin and the Bouger gravity anomaly field of northern Venezuela and the Caribbean borderland. Geol Mijnbouw 57 (2):117-122

Bonini WE, Acker C, Buzan G (1977) Gravity studies across the western Caribbean Mountains, Venezuela. In: Memoria Congreso Latino-Americano de Geología, IV, Caracas 1977: Venezuela Ministerio de Minas e Hidrocarburos, Boletín de Geología, Publicacíon Especial 7(4):2300-2323

Bowin CO (1976) Caribbean gravity field and plate tectonics. Geol Soc Amer Spec Paper 169:79 pp

Bown MG, Gay P (1959) The identification of oriented inclusions in pyroxene crystals. Amer Mineral 44:592-692

Brenan JM, Shaw HF, Ryerson FJ, Phinney DL (1996) Experimental determination of trace element partitioning between pargasite and a synthetic hydrous andesitic melt. Earth Planet Sci Lett 135:1-11

Briqueu L, Lancelot JR (1979) Rb-Sr systematics and crustal contamination models for calc-alkaline igneous rocks. Earth Planet Sci Lett 43:385-396

Buddington AF, Lindsley DH (1964) Iron-titanium oxide minerals and synthetic equivalents. J Petrol 5:310-357

Burke K (1988) Tectonic evolution of the Caribbean. Ann Rev Earth Planet Sci 16:201-230

Burke K, Cooper C, Dewey JF, Mann P, Pindell JL (1984) Caribbean tectonics and relative plate motions. In: Bonini WE et al. (eds) The Caribbean-South American plate boundary and regional tectonics: Geol Soc Amer Memoir 162:31-63

Burnham CW (1979) Magmas and hydrothermal fluids. In: Barnes HL (ed) Geochemistry of hydrothermal ore deposits. Holt, Rinehart and Winston:34-76

Cameron WE, Nisbet EG, Dietrich VJ (1979) Boninites, komatiites and ophiolithic basalts. Nature 280:550-553

Cawthorn RG, O'Hara MJ (1976) Amphibole fractionation in calc-alkaline magma genesis. Amer J Sci 276:309-329

Cawthorn RG, Curran EB, Arculus RJ (1973) A petrogenentic model for the origin of calc-alkaline suites of Grenada, Lesser Antilles. J Petrol 14:327-337

Chevalier Y (1987) Les zones internes de la chaîe sud caraibe sur le transect: Ile de Margarita-Péninsule d´ Araya (Venezuela). Ph.D. Dissertation, Université de Bretagne occidentale, Brest, France:464 pp

Church SE, Tatsumoto M (1975) Lead isotope relation in oceanic ridge basalts from the Juan de Fuca - Gorda Ridge area, NE Pacific Ocean. Contrib Mineral Petrol 53:253-279

Claesson S, Roddick JC (1983) $^{40}Ar/^{39}Ar$ data on the age and metamorphism of the Ottfjället dolerites, Särv Nappe, Swedish Caledonides. Lithos 16:61-73

Condie KC, Viljoen MJ, Kable EJD, (1977) Effect of alteration on element distribution in Archaean tholeiites from the Barberton greenstone belt, South Africa. Contrib Mineral Petrol 64:75-89

Cooper AF (1972) Progressive metamorphism of metabasic rocks from the Haast Schist Group of southern New Zealand. J Petrol 13:457-492

Cooper AF (1979) Petrology of ocellar lamprophyres from Western Otago, New Zealand. J Petrol 20:139-163

Cross W, Iddings JP, Pirsson LV, Washington HS (1903) Quantitative classification of igneous rocks. Univ Chicago Press, Chicago.

Czamanske GK, Mihalik P (1972) Oxidation during magmatic differentiation. Finnmarka Complex, Oslo area, Norway: Part I, the opaque oxides. J Petrol 13:493-509

Dalrymple GB, Duffield WA (1988) High precision $^{40}Ar/^{39}Ar$ data of Oligocene rhyolites from the Mogollon-Datil volcanic field using a continuous laser system. Geophys Res Lett 15:463-466

Davidson JP (1986) Isotopic and geochemical constraints on the petrogenesis of subduction-related lavas from Martinique, Lesser Antilles. J Geophys Res 91:5943-5962

Davidson JP (1987) Crustal contamination versus subduction zone enrichment: Examples from the Lesser Antilles and implications for mantle source compositions of island arc volcanic rocks. Geochim Cosmochim Acta 51:2185-2198

Deer WA, Abbot D (1965) Clinopyroxenes of the gabbro cumulates of the Kap Edvard Holm complex, East Geenland. Mineral Mag Tilley Vol:177-193

Deer W, Howie RA, Zussman J (1992) An introduction to the rock forming minerals (2nd ed). Longman Group Ltd, London:696 pp

DeMets DC, Gordon RG, Argus DF, Stein SA (1990) Current plate motions. R Astron Soc Geophys J 101:425-478

Devine JD (1995) Petrogenesis of the basalt-andesite-dacite association of Grenada, Lesser Antilles island arc, revisited. J Volc Geother Res 69:1-33

Devine JD, Sigurdsson H (1995) Petrology and eruption styles of Kick`em Jenny submarine volcano, Lesser Antilles island arc. J Volc Geother Res 69:35-58

Dick JB, Bullen T (1984) Chromite as a petrogenetic indicator in abyssal and alpine-type peridotites and spatially associated lavas. Contrib Mineral Petrol 86:54-76

Donnelly TW Rogers JJW, Pushkar P, Armstrong RL (1971) Chemical evolution of the igneous rocks of the West Indies: an investigation of thorium, uranium and potassium distributions and lead and strontium isotopic ratios: Geol Soc Amer Mem 130:181-224

Donnelly TW, Beets D, Carr MJ, Jackson T, Klaver G, Lewis J, Maury R, Schellekens H, Smith AL, Wadge G, Westercamp D (1990) History and tectonic setting of Caribbean magmatism. In: Dengo G, Case JE (eds) The Caribbean region. Boulder, Colorado, Geol Soc Amer. The Geology of North America H:339-374

Dostal J, Zerbi M (1978) Geochemistry of the Savalan volcano (northwestern Iran). Chem Geol 22:31-42

Duncan RA, Green DH (1987) The genesis of refractory melts in the formation of oceanic crust. Contrib Mineral Petrol 96:326-342

Dupré B, Allegre C (1983) Pb-Sr isotopic variations in Indian Ocean basalts and mixing phenomena. Nature 303:142-146

Dupuy C, Dostal G, Marcelot G, Bogault H, Joron L, Treuil M (1982) Geochemistry of basalts from central and southern New Hebrides arc: Implications for their source rock composition. Earth Planet Sci Lett 60:207-225

Eggler DH (1972) Water-saturated and undersaturated melting relations in a Paricutin andesite and an estimate of water content in the natural magma. Contrib Mineral Petrol 34:261-271

Eggler DH, Burnham CW (1973) Crystallization and fractionation trends in the system andesite-H_2O-CO_2-O_2 at pressures to 10 kb. Geol Soc Amer Bull 84:2517-2532

Engel AEJ, Engel CG (1962) Hornblendes formed during progressive metamorphism of amphibolites, northwest Adirondack Mountains, New York. Geol Soc Amer Bull 73:1499-1514

Erlich RN, Barrett SF (1990) Cenozoic plate tectonic history of the northern Venezuela-Trinidad area. Tectonics 9:161-184

Ewart A (1982) The mineralogy and petrology of Tertiary-Recent orogenic volcanic rocks: with special reference to the andesitic-basaltic compositional range. In: Thorpe RS (ed) Orogenic Andesites and related rocks:22-95

Ewart A, Stipp JJ (1968) Petrogenesis of the volcanic rocks of the Central North Island, New Zealand, as indicated by a study of $^{87}Sr/^{86}Sr$ ratios and Sr, Rb, K U and Th abundances. Geochim Cosmochim Acta 32:699-736

Ewart A, Taylor SR (1969) Trace element geochemistry of the rhyolite volcanic rocks, Central North Island, New Zealand, Phenocryst data. Contrib Mineral Petrol 22:127-146

Ewart A, Hawkesworth CJ (1987) The Pleistocene-Recent Tonga-Kermadec Arc Lavas: Interpretation of new isotopic and rare earth data in terms of a depleted mantle source model. J Petrol 28:495-530

Faure G (1986) Principles of isotope geology. John Wiley & Sons, New York-Toronto-Singapore:589 pp

Flower MFJ, Pritchard RG, Schmincke H-U, Robinson PT (1983) Geochemistry of basalts: deep dea drilling project sites 482, 483, and 485 near the Tamayo fracture zone, Gulf of California. In: Initial Reports of DSDP, US Gov Printing Office 65:559-578

Fox PF, Schreiber E, Heezen BC (1971) The geology of the Caribbean crust: Tertiary sediments, granitic and basic rocks from the Aves Ridge: Tectonophysics 12:89-109

Gilbert MC, Helz RT, Popp RK, Spear FS (1982) Experimental studies of amphibole stabiltiy. Reviews in Mineralogy 9B, Mineral Soc Amer:229-278

Gill JB (1970) Geochemistry of Viti Levu, Fiji and its evolution as an island arc. Contrib Mineral Petrol 27:179-203

Gill JB (1974) Role of underthrust oceanic crust in the genesis of a Fijian calc-alkaline suite. Contrib Mineral Petrol 43:29-45

Gill JB (1976a) Composition and age of Lau Basin and ridge volcanic rocks: Implications for evolution of an inter-arc basin and remnant arc. Geol Soc Amer Bull 87:1384-1395

Gill JB (1976b) From island arc to oceanic islands: Fiji, southwestern Pacific: Geology 4:625-626

Gill JB (1981) Orogenic andesites and plate tectonics. Minerals and rocks. Springer Verlag, Berlin-Heidelberg-New York:390 pp

Gill JB, Compston W (1973) Strontium isotopes in island arc volcanic rocks. In: Coleman P (ed) The Western Pacific-island arcs, marginal seas, geochemistry:483-496

Gillis KM (1995) Controls of hydrothermal alteration in a section of fast-spreading oceanic crust. Earth Planet Sci Lett 134:473-489

Gillis KM, Thompson (1993) Metabasalts from the Mid-Atlantic Ridge: new insights into hydrothermal systems in slow-spreading crust. Contrib Mineral Petrol 113:502-523

Gonzalez de Juana C (1974) Elements of diastrophic history of northeastern Venezuela. Geol Soc Amer Bull 82:2383-2396

Gonzalez de Juana C, Vignali M (1971) Rocas metamórficas e igneas en la Peninsula de Macanao, Margarita, Venezuela. Proc VI Caribb Geol Conf Venezuela:63-68

Gorton MP (1977) The geochemistry and origin of Quarternary volcanism in the New Hebrides. Geochim Cosmochim Acta 41:1257-1270

Green TH (1972) Crystallization of calc-alkaline andesite under controlled high-pressure hydrous conditions. Contrib Mineral Petrol 34:150-166

Green TH, Pearson NJ (1986) Ti-rich accessory phase saturation in hydrous mafic-felsic compositions at high P,T. Chem Geol 54:185-201

Grissom GC, Peters EK, Sisson VB, Stowell HH, Hollister LS (1985) Pressure of crystallization of plutons in the Coast Mts., BC and Alaska, based on aluminum content of hornblende. Geol Soc Amer Abstracts with Programs 17:358

Guth LR, Avé Lallemant HG (1991) A kinematic history for eastern Margarita Island, Venezuela. In: Larue DK, Draper G (eds) Transactions, 12th Caribbean Geological Conference, St. Croix, US Virgin Islands (1989): South Miami, Florida. Miami Geol Soc: 472-480

Hamilton DL, Burnham CW, Osborn EF (1964) The solubility of water and effects of oxygen fugacity and water content on crystallization in mafic magmas. J Petrol 5:21-39

Hammarstrom JM, Zen E-An (1986) Aluminum in hornblende: an empirical igneous geobarometer. Amer Mineral 71:1297-1313

Hanson GN, Langmuir CH (1978) Modelling of major elements in mantle-melt systems using trace element approaches. Geochim Cosmochim Acta 42:725-741

Harrison TM, McDougall I (1980) Investigations of an intrusive contact, northwest Nelson, New Zealand-II. Diffusion of radiogenic and excess ^{40}Argon in hornblende revealed by $^{40}Ar/^{39}Ar$ age spectrum analyses. Geochim Cosmochim Acta 44:2005-2020

Hart SR (1976) LIL-element geochemistry of Leg 34 basalts. Initial Reports of DSDP, US Gov Printing Office 34:283-288

Hart SR, Brocks C, Krogh TE, Davis GL, Nava D (1970) Ancient and modern volcanic rocks: a trace element model. Earth Planet Sci Lett 10:17-28

Haughton DR, Roeder PL, Skinner J (1974) Solubility of sulfur in mafic magmas. Econ Geol 69:451-467

Hawkesworth CJ, Powell M (1980) Magma series in the Lesser Antilles island arc. Earth Planet Sci Lett 51:297-308

Hawkesworth CJ, O'Nions RK, Pankhurst RJ, Hamilton PJ, Evensen NM (1977) A geochemical study of island arc and back arc tholeiites from the Scotia Sea. Earth Planet Sci Lett 36:253-262

Hawkins JW, Melchior JT (1985) Petrology of Mariana Trough and Lau Basin basalts. J Geophys Res 90:11431-11468

Hedge CE, Lewis JF (1971) Isotopic composition of strontium in three basalt-andesite centers along the Lesser Antilles Arc. Contrib Mineral Petrol 32:39-47

Helz RT (1973) Phase relations of basalts in their melting ranges at PH_2O = 5kb as a function of oxygen fugacity. J Petrol 14:249-302

Helz RT (1979) Alkali exchange between hornblende and melt: a temperature-sensitive reaction. Amer Mineral 64:953-965

Helz RT (1982) Phase relations and compositions of amphiboles produced in studies of the melting behaviour of rocks. In: Amphiboles: Petrology and experimental phase relations. Reviews in Mineralogy 9B, Mineral Soc Amer:279-346

Hess HH, Maxwell JC (1949) Geological reconnaissance of the Island of Margarita (I). Geol Soc Amer Bull 60:1837-1868

Hickey RL, Frey FA, Gerlach DC, Lopez-Escobar L (1986) Multiple sources for basaltic arc rocks from the Southern Volcanic Zone of the Andes (34^o-41^oS): Trace element and isotopic evidence for contributions from subducted oceanic crust, mantle and continental crust. J Geophys Res 91:5963-5983

Hildreth W, Moorbath S (1988) Crustal contributions to arc magmatism in the Andes of Central Chile. Contrib Mineral Petrol 98:455-489

Hochstaedter AG, Kepezhinskas P, Defant M (1996) Insights into the volcanic arc mantle wedge from magnesian lavas from the Kamchatka arc. J Geophys Res 101:697-712

Hunter VF (1978) Notes on the stratigraphy of Margarita Island. Geol Mijnbouw 57 (2):189-192

Hussong DM et al. (1981) Initial Reports of DSDP, US Gov Printing Office 60:929 pp

Ionov DA, Hoffman AW (1995) Nb-Ta-rich mantle amphiboles and micas: Implications for subduction-related metasomatic trace element fractionations. Earth Planet Sci Lett 131:341-356

Irvine TN (1976) Chromite crystallization in the join Mg_2SiO_4 - $CaMgSi_2O_6$ - $CaAl_2Si_2O_8$ - $MgCr_2O_4$ - SiO_2. Carnegie Inst Wash Yearb 76:465-472

Irvine TN, Baragar WRA (1971) A guide to the chemical classification of the common volcanic rocks. Can J Earth Sci 8:532-584

Jakês P, White AJR (1970) K/Rb ratios of rocks from island arcs. Geochim Cosmochim Acta 34:849-856

Jakês P, Gill J (1979) Rare earth elements and the island arc tholeiitic series. Earth Planet Sci Lett 9:17-28

Jenner GA (1981) Geochemistry of high Mg-andesites from Cape Vogel, Papua New Guinea. Chem Geol 33:307-332

Johnson RW, Jaques AL, Hickey RL, McKee CO, Chappell BW (1985) Manam Island, Papua New Guinea: Petrology and geochemistry of a Low-TiO_2 basaltic island arc volcano. J Petrol 26:283-323

Johnson MC, Anderson AT, Rutherford MJ (1994) Pre-eruptive volatile content of magmas. In: Carroll MR, Holloway JR (eds) Volatiles in magmas. Reviews in Mineralogy 30, Mineral Soc Amer:281-330

Kay RW (1978) Aleutian magnesian andesites: melts from subducted Pacific ocean crust. J Volc Geother Res 4:117-132

Kay RW, Sun SS, Lee-Hu CN (1978) Pb and Sr isotopes in volcanic rocks from the Aleutian Islands and Pribof Islands, Alaska. Geochim Cosmochim Acta 42:263-273

Kirsch H, Kober B, Lippolt HJ (1988) Age of intrusion and rapid cooling of the Frankenstein gabbro (Odenwald, SW Germany) evidenced by $^{40}Ar/^{39}Ar$ and single-zircon $^{207}Pb/^{206}Pb$ measurements. Geol Rundschau 77(3):693-711

Kluge R, Baumann A, Maresch WV, Krückhans G (1992) U-Pb zircon ages of leucocratic plutons on the island of Margarita (Venezuela). VIII Congr Latinoamer Geol, Salamanca. Actas Sessiones Cient Simp 4:184-188

Kreher B (1992) Petrologie und Geochemie der Gabbrointrusion des Frankensteins (Odenwald) Ph.D. Dissertation, Universität Würzburg , Germany: 229 pp

Kudo AM, Weill DF (1970) An igneous plagioclase thermometer. Contrib Mineral Petrol 25:52-65

Kugler HG (1957) Contribution to the geology of the islands of Margarita and Cubagua, Venezuela. Geol Soc Amer Bull 68:555-566

Kuniyoshi S, Liou JG (1976) Contact metamorphism of the Karmutsen volcanics, Vancouver Island, British Columbia. J Petrol 17:73-99

Lanphere MA, Dalrymple GB (1976) Identification of excess ^{40}Ar by the $^{40}Ar/^{39}Ar$ age spectrum technique. Earth Planet Sci Lett 32:141-148

Leake BE (1965) The relationship between tetrahedral aluminium and the maximum possible octahedral aluminium in natural calciferous and sub-calciferous amphiboles. Amer Mineral 50:843-851

Leake BE et al. (1997) Nomenclature of amphiboles. Report of the subcommitte on amphiboles of the international association commision on new minerals and mineral names. Eur J Mineral 9:623-651

LeRoex AP, Dick HJB, Erlank AJ, Reid AM, Frey FA, Hart SR (1983) Geochemistry, mineralogy and petrogenesis of lavas erupted along the Southwest Indian Ridge between the Bouvet Triple Junction and 11 degrees east. J Petrol 24:267-318

Liou JG (1973) Synthesis and stability relations of epidote, $Ca_2Al_2FeSi_3O_{12}(OH)$. J Petrol 14:381-413

Ludden JN, Thompson G (1979) An evaluation of the behaviour of the rare earth elements during the weathering of sea-floor basalt. Earth Planet Sci Lett 43:85-92

Macdonald GA, Katsura T (1964) Chemical composition of Hawaiian lavas. J Petrol 5:82-133

MacDonald WD (1990) Survey of Caribbean paleomagnetism. In: Dengo G, Case JE (eds) The Caribbean region. Boulder, Colorado, Geol Soc Amer. The Geology of North America H:393-432

Maksimov AP, Kadik AA, Korovushkina EY, Ivanov BV (1978) Crystallization of an andesite melt with a fixed water content at pressures up to 12 kbar. Geochim Int 15:20-29

Maresch WV (1971) The metamorphism and structure of northeastern Margarita Island, Venezuela. Ph.D. Dissertation, Princeton University:278 pp

Maresch WV (1972) Eclogitic-amphibolitic rocks on Isla Margarita, Venezuela. Geol Soc Amer Mem 132:429-437

Maresch WV (1975) The geology of northeastern Margarita Island, Venezuela: a contribution to the study of Caribbean Plate margins. Geol Rundschau 64:846-883

Maresch WV, Abraham K (1981) Petrography, mineralogy and metamorphic evolution of an eclogite from the island of Margarita, Venezuela. J Petrol 22:337-362

Masuda Y, Nishimura S, Ikeda T, Katsui Y (1976) Rare-earth and trace elements in the Quaternary volcanic rocks of Hokkaido, Japan. Chem Geol 15:251-271

Mattinson JM, Fink LK Jr, Hopson CA (1980) Geochronologic and isotopic study of the La Désirade Island Basement Complex: Jurassic Oceanic Crust in the Lesser Antilles? Contrib Mineral Petrol 71:237-245

Maury RC, Westercamp D (1985) Variations chronologiques et spatials des basalts neogenes des Petites Antilles; implications sur l`evolution d`arc. In: Mascle A (ed) Géodynamique des Caraibes:77-89

McCann WR, Pennington WD (1990) Seismicity, large earthquakes, and the margin of the Caribbean Plate. In: Dengo G, Case JE (eds) The Caribbean region. Geol Soc Amer. The Geology of North America H:291-306

McDougall I, Harrison TM (1988) Geochronology and thermochronology by the $^{40}Ar/^{39}Ar$ Method. Oxford University press, New York

McNutt RH, Crocket JH, Clark AH, Caelles JS, Farrar E, Haynes SJ, Zentilli M (1975) Initial $^{87}Sr/^{86}Sr$ ratios of plutonic and volcanic rocks of the central Andes between latitudes 26^{o} and 29^{o} south. Earth Planet Sci Lett 27:305-313

Mehl KW, Bitschene PR, Schmincke HU, Hertogen J (1991) Composition, alteration and origin of the basement lavas and volcaniclastic rocks at site 738, southern Kerguelen Plateau. In: Barron J, Larsen B (eds) Proceedings of the Ocean Drilling Program, Scientific Results 119:299-322

Meijer A (1976) Pb and Sr isotopic data bearing on the origin of volcanic rocks from the Marianas Island Arc system. Geol Soc Amer Bull 87:1358-1369

Menzies M, Seyfried WE (1979) Basalt seawater interaction: Trace element and Sr isotope variations in experimentally altered glassy basalts. Earth Planet Sci Lett 44:463-472

Merzbacher CI, Eggler DH (1984) A magmatic geohygrometer: Application to Mount St. Helens and other dacitic magmas. Geology 12:587-590

Meschede M (1986) A Method of discriminating between different types of mid-ocean ridge basalts and continental tholeiites with the Nb-Zr-Y diagram. Chem Geology 56:207-218

Metz HL (1968) Geology of the El Pilar fault zone, State of Sucre, Venezuela. In: Saunders (ed) Fourth Caribb Geol Conf Trans, Caribbean Printers, Arina, Trinidad and Tobago:293-298

Middleburg JJ, Van der Weijden CH, Woittiez JRW (1988) Chemical processes affecting the mobility of major, minor and trace elements during weathering of granitic rocks. Chem Geol 68:253-273

Miyashiro A (1974) Volcanic rock series in island arcs and active continental margins. Amer J Sci 274:321-335

Miyashiro A (1978) Nature of alkalic volcanic rock series. Contrib Mineral Petrol 66:91-104

Molnar P, Sykes LR (1969) Tectonics of the Caribbean and middle American regions from focal mechanisms and seismicity. Geol Soc Amer Bull 80:1639-1684

Montgomery CW (1979) Uranium-Lead geochronology of the Archean Imataca Series, Venezuelan Guayana Shield. Contrib Mineral Petrol 69:167-176

Montgomery H, Pessagno EA jr, Muñoz IM (1992) Jurassic (Tithonian) radiolaria from La Désirade (Lesser Antilles): Preliminary paleontological and tectonic implications. Tectonics 11:1426-1432

Montgomery H, Pessagno EA, Pindell J (1994) A 195 Ma Terrane in a 165 Ma Sea: Pacific Origin of the Caribbean Plate. GSA Today 4(1):1-6

Moticska P (1972) Geologia del archipelago de Los Frailes. VI Conferencia Geologica Del Caribe, Margarita, Venezuela:69-73

Mullen ED (1983) $MnO/TiO_2/P_2O_5$: A minor element discrimination for basaltic rocks of oceanic environments and its implications for petrogenesis. Earth Planet Sci Lett 62:53-62

Mysen BO (1977) Solubility of volatiles in silicate melts under the pressure and temperature conditions of partial melting in the upper mantle. In: Dick HJB (ed) Magma genesis. State Oreg Dep Geol Mineral Bull 96:1-14

Mysen BO, Arculus RJ, Eggler DH (1975) The solubility of carbon dioxide in melts of andesite, tholeiite, and olivine nephelinite composition at 30 kbar pressure. Contrib Mineral Petrol 53:227-239

Nagle F (1972) Rocks from seamounts and escarpments on the Aves ridge. Caribbean Geol Conf Trans VI, Margarita, Venezuela:409-413

Nagle F, Stipp JJ, Fisher DE (1976) K-Ar geochronology of the Limestone Caribbees and Martinique, Lesser Antilles, West Indies: Earth Planet Sci Lett 29:401-412

Nesbitt HW (1979) Mobility and fractionation of rare earth elements during weathering of a granodiorite. Nature 279:206-210

Nye CJ, Reid MR (1986) Geochemistry of primary and least fractionated lavas from Okmok volcano, Central Aleutans: Implications for arc magma genesis. J Geophys Res 91:10271-10287

O'Hara MJ (1968) The bearing of phase equilibria studies in synthetic and natural systems on the origin and evolution of basic and ultrabasic rocks. Earth Sci Rev 4:69-133

Olsen SN (1984) Mass-balance and mass-transfer in migmatites from the Colorado Front Range. Contrib Mineral Petrol 85:30-44

Page RW, Johnson RW (1974) Strontium isotope ratios of Quaternary volcanic rocks from Papua New Guinea. Lithos 7:91-100

Papike JJ, Ross M, Clark JR (1969) Chrystal-chemical characterization of clinoamphiboles based on five new structure refinements. Mineral Soc Amer Spec Paper 2:117-136

Pe GG (1973) Petrology and geochemistry of volcanic rocks of Aegina, Greece. Bull Volcanol 37:491-514

Pe GG (1974) Volcanic rocks of Methana, South Aegean Arc, Greece. Bull Volcanol 38:270-290

Pearce JA (1980) Geochemical evidence for the genesis and eruptive setting of lavas from Thethyan ophiolites. In: Panayiotou A (ed) Ophiolites. Proc Intern Ophiol Symp Cyprus 1979. Geol Surv Dept, Nicosia (Cyprus):261-272

Pearce JA (1982) Trace element characteristics of lavas from destructive plate boundaries. In: Thorpe RS (ed) Orogenic Andesites and related rocks:525-548

Pearce JA (1983) Role of the sub-continental lithosphere in magma genesis at active continental margins. In: Hawkesworth CJ, Norry MJ (eds) Continental basalts and mantle xenoliths. The Open University and University of Leicester, Shiva Publishing Company:230-272

Pearce JA, Cann JR (1973) Tectonic setting of basic volcanic rocks determined using trace element analyses. Earth Planet Sci Lett 19:290-300

Pearce JA, Norry MJ (1979) Petrogenetic implications of Ti, Zr, Y and Nb variations in volcanic rocks. Contrib Mineral Petrol 69:33-47

Pearce JA, Alabaster T, Shelton AW, Searle MP (1981) The Oman ophiolite as a Cretaceous arc-basin complex: evidence and implications. Phil Trans R Soc London (A) 300:299-317

Peccerillo A, Taylor SR (1976) Geochemistry of the Eocene calc-alkaline volcanic rocks from the Kasamonu area, northern Turkey. Contrib Mineral Petrol 58:63-81

Pennington WD (1981) Subduction of the eastern Panama Basin and seismotectonics of northwestern South America. J Geophys Res 86:10753-10770

Pérez OJ, Aggarwal YP (1981) Present-day tectonics of the southeastern Caribbean and northeastern Venezuela. J Geophys Res 86:10791-10804

Perfit MR, Gust DA, Bence AE, Arculus RJ, Taylor SR (1980) Chemical characteristics of Island-Arc Basalts: Implications for mantle sources. Chem Geol 30:227-256

Peterman ZE, Lowder GG, Carmichel ISE (1970) $^{87}Sr/^{86}Sr$ ratios of the Talasea series, New Britain, Territory of New Guinea. Geol Soc Amer Bull 81:39-40

Pichler H, Zeil W (1972) The Cenozoic rhyolite-andesite association of the Chilean Andes. Bull Volcanol 35: 424-452

Pindell JL (1993) Regional synopsis of Gulf of Mexico and Caribbean evolution. In: Pindell JL (ed) Mesozoic and early Cenozoic development of the Gulf of Mexico and Caribbean region (Transactions, Gulf Coast Section SEPM Foundation, 13th Annual Research Conference), Houston SEPM Foundation:251-274

Pindell JL, Barrett SF (1990) Geological evolution of the Caribbean Region: a plate-tectonic perspective in the Caribbean Region. In: Dengo G, Case JE (eds) The Caribbean region. Geol Soc Amer. The Geology of North America H:405-432

Pindell JL, Dewey JF (1982) Permo-Triassic reconstruction of western Pangea and the evolution of the Gulf of Mexico/Caribbean region: Tectonic 1:179-211

Pindell JL, Cande SC, Pitman WC III., Rowley DB, Dewey JF, Labrecque J, Haxby W (1988) A plate kinematic framework for models of Caribbean evolution. Tectonophysics 155:121-138

Pushkar P (1968) Strontium isotope ratios in volcanic rocks of three island arc areas. J Geophys Res 73:2701-2713

Reagan MK, Meijer A (1984) Geology and geochemistry of early arc-volcanic rocks from Guam. Geol Soc Amer Bull 95:701-713

Robertson P, Burke K (1989) Evolution of southern Caribbean plate boundary, vicinity of Trinidad and Tobago. Amer Assoc Pet Geol Bull 73:490-509

Rock NMS (1977) The nature and origin of lamprophyres: some definitions, distinctions and derivations. Earth Sci Rev 13:123-169

Rock NMS (1984) Nature and origin of calc-alkaline lamprophyres: minettes, vogesites, kersantites and spessartites. Trans R Soc Edinburgh, Earth Sci 74:193-227

Rock NMS (1991) Lamprophyres. Blackie and Son, Oxford:285 pp

Ross MI, Scotese CR (1988) Hierarchical tectonic analysis of the Gulf of Mexico and Caribbean region. Tectonophysics 155:139-168

Rutherford MJ, Devine JD (1988) The May 18, 1980 eruption of Mount St. Helens. 3. Stability and chemistry of amphibole in the magma chamber. J Geophys Res 93:11949-11959

Rutherford MJ, Hill P (1993) Magma ascent rates from amphibole breakdown: An experimental study applied to the 1980-1986 Mount St. Helens eruptions. J Geophys Res 98:19667-19685

Rutherford MJ, Devine JD (1995) Pre-eruption P-T conditions and volatiles in the 1991 Pinatubo magma. In: Punongabayan RS, Newhall CG (eds) The 1991 eruptions of Pinatubo Volcano, Phillipines. US Geol Surv Spec Paper

Sakuyama M (1983) Phenocryst assemblages and H_2O content in circum-Pacific arc magmas. In: Hilde TWC, Uyeda S (eds) Geodynamics of the Western Pacific-Indonesian Region. Amer Geophys Union Geodyn Ser 11:143-158

Santamaria JF (1972) Geochemistry and geochronology of the Venezuelan Coast Ranges and southern Caribbean islands and their relation to tectonic evolution. PH.D. Dissertation, Rice University Houston, Texas:112 pp

Santamaria JF, Schubert C (1974) Geochemistry and geochronology of the Southern Caribbean - Northern Venezuela plate boundary. Geol Soc Amer Bull 7:1085-1098

Schellekens JH, Montgomery H, Joyce J, Smith AL (1990) Late Jurassic to Late Cretaceous development of island arc crusts in southwestern Puerto Rico. Transactions 12th Caribbean Geological Conference, St. Croix:153

Schubert C (1971) Geologia de la Peninsula de Araya, Estado Sucre. Mem IV Cong Geo Venez 21, supl 1

Schuchert CA (1935) Historical geology of the Antillean-Caribbean region. J Wiley & Sons, New York:811 pp

Schuhmacher R (1991) Compositions and phase relations of calcic amphiboles in epidote- and clinopyroxene-bearing rocks of the amphibolite and lower granulite facies, central Massachusetts, USA. Contrib Mineral Petrol 108:196-211

Sievers W (1898) Die Inseln vor der Nordküste von Venezuela. Globus 74:163-165, 302-307

Sigurdsson H, Shepherd JB (1974) Amphibole-bearing basalts from the submarine volcano Kickem'-Jenny in the Lesser Antilles island arc. Bull Volcanol 38:891-910

Sisson TW, Grove TL (1993) Temperatures and H_2O contents of low-MgO high-alumina basalts. Contrib Mineral Petrol 113:167-184

Smith HG (1946) The lamprophyre problem. Geol Mag 83:165-169

Smith PPK (1977) An electron microscope study of amphibole lamellae in augite. Contrib Mineral Petrol 59:317-322

Sobolev AV, Chaudisson M (1996) H_2O concentrations in primary melts from supra-subduction zones and mid-ocean ridges: Implications for H_2O storage and recycling in the mantle. Earth Planet Sci Lett 137:45-55

Speed RC (1985) Cenozoic collision of the Lesser Antilles Arc and continental South America and origin of the El Pilar fault. Tectonics 4:40-70

Spear FS (1981) Amphibole-plagioclase equilibria: an empirical model for the relation albite+tremolite=edenite+4quartz. Contrib Mineral Petrol 77:355-364

Stakes DS, O'Neil JR (1982) Mineralogy and stable isotope geochemistry of hydrothermally altered oceanic rocks. Earth Planet Sci Lett 57:285-304

Stöckhert B, Maresch WV, Toetz A, Kluge R, Krückhans G, Kaiser C, Aguilar V, Klier T, Laupenmühlen S, Piepenbreier D, Wiethe I (1993) Tectonic history of Isla Margarita, Venezuela - a record of a piece of crust close to an active plate margin. Zentralbl Geol Paläont 1:485-498

Stöckhert B, Maresch WV, Brix M, Kaiser C, Toetz A, Kluge R, Krückhans-Lueder G (1995) Crustal history of Margarita Island (Venezuela) in detail: Constraint on the Caribbean plate-tectonic scenario. Geology 23:787-790

Sun SS, Nesbitt RW (1978) Petrogenesis of ultrabasic and basic volcanics: evidence from rare earth elements. Contrib Mineral Petrol 65:301-325

Sun SS, McDonough WF (1989) Chemical and isotopic systematics of ocean basalts: implications for mantle composition and processes. In: Saunders AD, Norry MJ (eds) Magmatism in the Ocean Basins. Geol Soc London Spec Publ 42:313-345

Sun SS, Tatsumoto M, Schilling JG (1975) Mantle plume mixing along the Reykjanes Ridge axis: Lead isotopic evidence. Science 190:143-147

Sykes LR, McCann WR, Kafka AL (1982) Motion of the Caribbean Plate during the last 7 million years and implications for earlier movements. J Geophys Res 87:10656-10676

Tatsumi Y (1982) Origin of high-magnesian andesites in the Setouchi volcanic belt, southwest Japan, II. Melting phase relations at high pressures. Earth Planet Sci Lett 60:305-317

Tatsumoto M (1978) Isotopic composition of lead in oceanic basalt and its implication to mantle evolution. Earth Planet Sci Lett 38:63-87

Taylor GC (1960) Geology of the Island of Margarita. Ph.D. Dissertation, Princeton University:121 pp

Thompson RN (1982) Magmatism of the British Tertiary Volcanic Province. Scott J Geol 18:49-107

Thirwall MF, Graham AM (1984) Evolution of high-Ca, high-Sr C-series basalts from Grenada, Lesser Antilles: Contamination in the arc crust. J Geol Soc London 141:427-445

Tilton GR, Schreyer W, Schertl HP (1989) Pb-Sr-Nd isotopic behavior of deeply subducted crustal rocks from the Dora Maira Massif, Western Alps, Italy. Geochim Cosmochim Acta 53:1391-1400

Thornton CP, Tuttle OF (1960) Chemistry of igneous rocks. I: Differentiation Index. Amer J Sci 258:664-684

Van der Weijden CH, Van der Weijden RD (1995) Mobility of major, minor and some redox-sensitive trace elements and rare-earth elements during weathering of four granitoids in central Portugal. Chem Geol 125:149-167

Veblen DR, Buseck PR (1977) Petrologic implications of hydrous biopyriboles intergrown with igneous pyroxene (abstr). EOS 58:1242

White WM, Dupré B, Vidal P (1985) Isotope and trace element geochemistry of sediments from the Barbados Ridge-Demerars Plain region, Atlantic Ocean. Geochim Cosmochim Acta 49:1875-1886

White WM, Dupré B (1986) Sediment subduction and magma genesis in the Lesser Antilles: isotopic and trace element constraints. J Geophys Res 91:5927-5941

Whitford DJ, Compston W, Nicholls JA, Abbott MJ (1977) Geochemistry of Late-Cenozoic lavas from eastern Indonesia; the role of subducted sediments in petrogenesis. Geology 5:571-575

Wilson M (1988) Igneous Petrogenesis. Harper Collins Academic Press:466 pp

Wimmenauer W (1985) Petrographie der magmatischen und metamorphen Gesteine. Enke Verlag Stuttgart:382 pp

Wood DA, Joron JL, Marsh NG, Tarney J, Treuil M (1980) Major and trace element variations in basalts from the North Philippine Sea drilled during DSDP Leg 58: A comparative study of back-arc-basin basalts with lava series from Japan and mid-ocean ridges. Initial Reports of DSDP, US Gov Printing office 58: 873-894

Woodring WP (1954) Caribbean land and sea through the ages. Geol Soc Amer Bull 65:719-732

Wones DR, Gilbert MC (1982) Amphiboles in the igneous environment. Reviews in Mineralogy 9B, Mineral Soc Amer:355-390

Wyllie PJ (1982) Subduction products according to experimental prediction. Geol Soc Amer Bull 93:468-476

Yoder HS, Tilley CE (1962) Origin of basalt magmas: an experimental study of natural and synthetic rock systems. J Petrol 3:342-532

Yogodzinski GM, Volynets ON, Koloskov AV, Seliverstov NI (1994) Magnesian andesites and the subduction component in a strongly calcalkaline series at Piip Volcano, far western Aleutians. J Petrol 34:163-204

Yogodzinski GM, Kay RW, Volynets ON, Koloskov AV, Kay SM (1995) Magnesian andesite in the western Aleutian Komandorsky region: Implications for slab melting and processes in the mantle wedge. Geol Soc Amer Bull 107:505-519

You CF, Castillo PR, Gieskes JM, Chan LH, Spivac AJ (1996) Trace element behaviour in hydrothermal experiments; implications for fluid processes at shallow depths in subduction zones. Earth Planet Sci Lett 140:41-52

Zhou MF, Robinson PT, Malpas J, Zijn L (1996) Podiform Chromitites in the Luobusa Ophiolite (Southern Tibet): implications for melt-rock interaction and chromite segregation in the upper mantle. J Petrol 37:3-21

Zindler A, Hart S (1986) Chemical Geodynamics. Ann Rev Earth Planet Sci Lett 14:493-571

Zindler A, Staudigel H, Batiza R (1984) Isotope and trace element geochemistry of young Pacific seamounts: implications for the scale of upper mantle heterogenity. Earth Planet Sci Lett 70:175-195

Zuleger E, Erzinger J (1988) Determination of the REE and Y in silicate materials with ICP-AES. Fresenius Zeitschr Analyt Chem 332:140-143

12.

APPENDIX

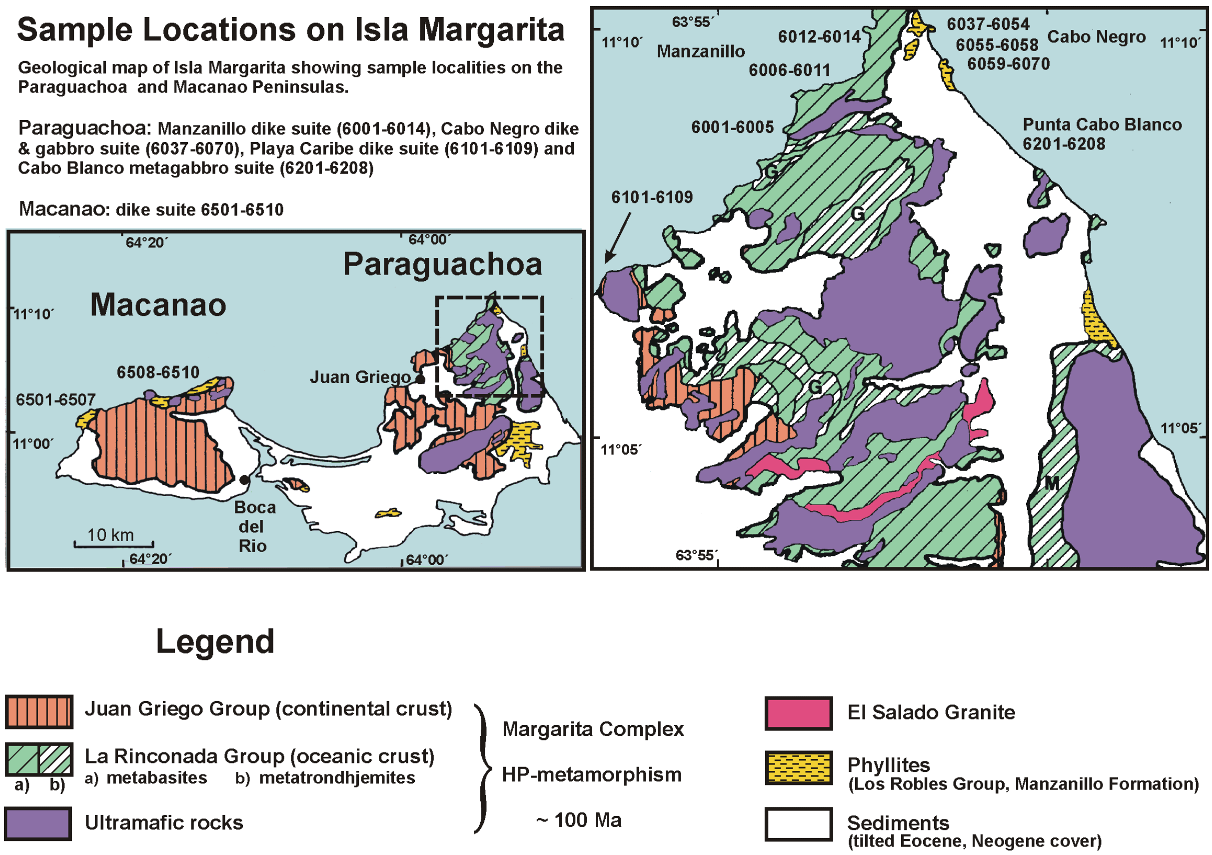

Figure 12.1:

Simplified map of Isla Margarita showing sample localities of the Manzanillo dike suite (6001-6014), the Cabo Negro dike & gabbro suite (6037-6070), the Playa Caribe dike suite (6101-6109), the Cabo Blanco metagabbro suite (6201-6208) and the Macanao dike suite (6501-6510).

Table 12.1:

Sample list from Isla Margarita. TS-Thin section. EMP-Electron microprobe analyses. XRF-X-ray fluorescence analyses. REE-Rare earth element analyses. Sr-i, Pb-i-initial isotopic ratio analyses. Ar/Ar-age determintion.

Sample	Locality	Rock-Type	Thickness	Orientation	Composition	TS	EMP	XRF	REE	Sr-i	Pb-i	Ar/Ar
6001	Playa Porto Viejo	Dike	0.35 m	210/80	Basalt	(+)	(-)	(+)	(-)	(-)	(-)	(-)
6002	Guayacan	Dike	0.30 m	210/70	Basalt	(+)	(+)	(+)	(+)	(-)	(-)	(-)
6003	Guayacan	Dike	0.12 m	240/85	Basaltic Andesite	(+)	(+)	(+)	(+)	(-)	(-)	(-)
6004	Guayacan	Dike	0.36 m	204/85	Basalt	(+)	(-)	(+)	(-)	(-)	(-)	(-)
6005	Guayacan	Dike	0.29 m	205/85	Basalt	(+)	(-)	(+)	(+)	(-)	(-)	(-)
6006	Morros de Constanza	Dike	0.17 m	09/82	Basaltic Andesite	(+)	(-)	(+)	(-)	(-)	(-)	(-)
6007	Morros de Constanza	Dike	0.23 m	198/85	Basalt	(+)	(-)	(+)	(-)	(-)	(-)	(-)
6008	Morros de Constanza	Dike	0.31 m	36/60	Basaltic Andesite	(+)	(+)	(+)	(-)	(-)	(-)	(-)
6009	N of Morros de Constanza	Dike	0.27 m	210/88	Andesite	(+)	(+)	(+)	(+)	(-)	(-)	(-)
6010	N of Morros de Constanza	Dike	0.18 m	216/83	Basaltic Andesite	(+)	(-)	(+)	(+)	(-)	(-)	(-)
6011	N of Morros de Constanza	Dike	0.33 m	217/84	Basalt	(+)	(-)	(+)	(-)	(-)	(-)	(-)
6012	Manzanillo	Dike	0.78 m	210/86	Basaltic Andesite	(+)	(-)	(+)	(-)	(+)	(+)	(+)
6013	Manzanillo	Dike	0.18 m	212/85	Basalt	(+)	(+)	(+)	(-)	(-)	(-)	(-)
6014	Manzanillo	Dike	0.35 m	239/85	Basaltic Andesite	(+)	(-)	(+)	(-)	(-)	(-)	(-)
6037	Cabo Negro	Dike	0.49 m	240/45	Basalt	(+)	(+)	(+)	(+)	(-)	(-)	(-)
6038	Cabo Negro	Dike	0.52 m	228/60	Andesite	(+)	(-)	(+)	(+)	(-)	(-)	(-)
6039	Cabo Negro	Dike	0.50 m	240/45	Basaltic Andesite	(+)	(-)	(+)	(-)	(-)	(-)	(-)
6040	Cabo Negro	Dike	0.50 m	10/90	Basalt	(+)	(-)	(+)	(-)	(-)	(-)	(-)
6041	Cabo Negro	Dike	0.40 m	228/60	Basaltic Andesite	(+)	(-)	(+)	(-)	(-)	(-)	(-)
6042	S of Cabo Negro	Dike	1.00 m	295/85	Basalt	(+)	(-)	(+)	(-)	(+)	(+)	(-)
6043	S of Cabo Negro	Dike	0.20 m	170/80	Basalt	(+)	(+)	(+)	(+)	(-)	(-)	(-)
6044	S of Cabo Negro	Dike	1.50 m	130/70	Basaltic Andesite	(+)	(-)	(+)	(+)	(-)	(-)	(-)
6045	S of Cabo Negro	Dike	0.20 m	168/80	Basalt	(+)	(-)	(+)	(-)	(-)	(-)	(-)
6046	S of Cabo Negro	Dike	0.35 m	295/85	Basalt	(+)	(-)	(+)	(-)	(-)	(-)	(-)
6047	S of Cabo Negro	Dike	0.30 m	05/80	Basaltic Andesite	(+)	(-)	(+)	(-)	(-)	(-)	(-)
6048	N of Punta Cazonero	Dike	0.30 m	05/80	Basaltic Andesite	(+)	(-)	(+)	(-)	(-)	(-)	(-)
6049	N of Punta Cazonero	Dike	0.40 m	192/80	Basaltic Andesite	(+)	(-)	(+)	(-)	(-)	(-)	(-)
6050	N of Punta Cazonero	Dike	1.00 m	05/75	Basaltic Andesite	(+)	(+)	(+)	(+)	(+)	(+)	(+)
6051	N of Punta Cazonero	Dike	0.80 m	193/85	Basalt	(+)	(-)	(+)	(-)	(-)	(-)	(-)
6052	N of Punta Cazonero	Dike	0.45 m	215/60	Basaltic Andesite	(+)	(-)	(+)	(-)	(-)	(-)	(-)
6053	N of Punta Cazonero	Dike	0.20 m	198/90	Basalt	(+)	(-)	(+)	(-)	(-)	(-)	(-)
6054	N of Punta Cazonero	Dike	1.05 m	220/85	Basalt	(+)	(-)	(+)	(-)	(-)	(-)	(-)
6055	Punta Cazonero	Gabbro			Basalt	(+)	(+)	(+)	(+)	(+)	(+)	(+)
6056	Punta Cazonero	Dike	0.25 m	195/88	Basalt	(+)	(+)	(+)	(+)	(+)	(+)	(+)
6057	Punta Cazonero	Dike	0.22 m	175/70	Basaltic Andesite	(+)	(+)	(+)	(+)	(-)	(-)	(-)
6058	Punta Cazonero	Gabbro			Basalt	(+)	(+)	(+)	(+)	(+)	(-)	(-)

Table 12.1 (continued):

Sample	Locality	Rock-Type	Thickness	Orientation	Composition	TS	EMP	XRF	REE	Sr-i	Pb-i	Ar/Ar
6059	S of Punta Cazonero	Dike	0.20 m	41/86	Basalt	(+)	(-)	(-)	(-)	(-)	(-)	(-)
6060	S of Punta Cazonero	Dike	0.40 m	344/75	Basaltic Andesite	(+)	(-)	(+)	(-)	(-)	(-)	(-)
6061	Punta Varadero	Dike	1.55 m	178/88	Basalt	(+)	(-)	(+)	(-)	(+)	(+)	(-)
6062	Punta Varadero	Dike	0.15 m	179/70	Basalt	(+)	(-)	(+)	(-)	(-)	(-)	(-)
6063	Punta Varadero	Dike	0.35 m	204/85	Basalt	(+)	(-)	(+)	(-)	(-)	(-)	(-)
6064	S of Punta Varadero	Dike	0.30 m	191/75	Basalt	(+)	(-)	(+)	(-)	(-)	(-)	(-)
6065	S of Punta Varadero	Dike	0.30 m	206/70	Basaltic Andesite	(+)	(-)	(+)	(-)	(-)	(-)	(-)
6066	S of Punta Varadero	Dike	0.40 m	192/62	Basalt	(+)	(-)	(+)	(-)	(-)	(-)	(-)
6067	N of Playa El Agua	Dike	0.35 m	08/85	Basaltic Andesite	(+)	(-)	(+)	(-)	(-)	(-)	(-)
6068	N of Playa El Agua	Dike	0.35 m	186/78	Basaltic Andesite	(+)	(-)	(+)	(-)	(-)	(-)	(-)
6069	N of Playa El Agua	Dike	0.22 m	183/65	Basaltic Andesite	(+)	(-)	(-)	(-)	(-)	(-)	(-)
6070	N of Playa El Agua	Dike	0.35 m	195/90	Basaltic Andesite	(+)	(-)	(+)	(-)	(-)	(-)	(-)
6101	Playa Caribe	Dike	0.38 m	200/85	Basalt	(+)	(-)	(+)	(+)	(-)	(-)	(-)
6102	Playa Caribe	Dike	0.35 m	210/85	Basalt	(+)	(-)	(+)	(-)	(-)	(-)	(-)
6103	Playa Caribe	Dike	0.60 m	210/85	Basalt	(+)	(-)	(+)	(-)	(+)	(-)	(-)
6104	Playa Caribe	Dike	0.50 m	204/85	Basalt	(+)	(-)	(+)	(-)	(-)	(-)	(-)
6105	Playa Caribe	Dike	0.25 m	195/85	Basalt	(+)	(-)	(+)	(-)	(-)	(-)	(-)
6106	Playa Caribe	Dike	0.28 m	226/85	Basaltic Andesite	(+)	(-)	(+)	(-)	(-)	(-)	(-)
6107	Playa Caribe	Dike	0.40 m	205/86	Basalt	(+)	(-)	(+)	(+)	(-)	(-)	(-)
6108	E of Playa Caribe	Dike	0.18 m	220/82	Basalt	(+)	(-)	(+)	(-)	(-)	(-)	(-)
6109	E of Playa Caribe	Dike	0.10 m	220/82	Basalt	(+)	(+)	(+)	(-)	(-)	(-)	(-)
6201	Punta Cabo Blanco	Metagabbro	0.45 m		Basalt	(+)	(-)	(+)	(+)	(-)	(-)	(-)
6202	Punta Cabo Blanco	Metagabbro	1.20 m		Basalt	(+)	(-)	(+)	(-)	(-)	(-)	(-)
6203	Punta Cabo Blanco	Metagabbro	0.78 m		Basalt	(+)	(-)	(+)	(-)	(-)	(-)	(-)
6204	Punta Cabo Blanco	Metagabbro	1.80 m		Basalt	(+)	(-)	(+)	(-)	(-)	(-)	(-)
6205	Punta Cabo Blanco	Metagabbro	0.80 m		Basalt	(+)	(-)	(+)	(-)	(-)	(-)	(-)
6206	Punta Cabo Blanco	Metagabbro	1.60 m		Basalt	(+)	(-)	(+)	(-)	(-)	(-)	(-)
6207	Punta Cabo Blanco	Metagabbro	0.80 m		Basaltic Andesite	(+)	(-)	(+)	(+)	(-)	(-)	(-)
6208	Punta Cabo Blanco	Metagabbro	1.80 m		Basalt	(+)	(-)	(+)	(-)	(-)	(-)	(-)
6501	Morro del Robledal	Dike	1.00 m	230/75	Basalt	(+)	(-)	(+)	(-)	(+)	(+)	(+)
6502	Morro del Robledal	Dike	0.10 m	230/77	Basalt	(+)	(-)	(+)	(-)	(-)	(-)	(-)
6503	Morro del Robledal	Dike	0.20 m	230/75	Basalt	(+)	(-)	(+)	(-)	(-)	(-)	(-)
6504-A	Morro del Robledal	Dike	0.20 m	228/75	Basalt	(+)	(+)	(+)	(+)	(-)	(-)	(-)
6504-B	Morro del Robledal	Dike	0.20 m	230/75	Basalt	(+)	(+)	(+)	(-)	(-)	(-)	(-)
6505	Morro del Robledal	Dike	1.00 m	233/75	Basalt	(+)	(-)	(+)	(-)	(-)	(-)	(-)
6506	Morro del Robledal	Dike	0.20 m	230/54	Basaltic Andesite	(+)	(-)	(+)	(-)	(-)	(-)	(-)
6507	Morro del Robledal	Dike	0.20 m	230/54	Basalt	(+)	(-)	(+)	(-)	(+)	(+)	(+)
6508	La Auyama	Dike	0.35 m	65/90	Basalt	(+)	(-)	(-)	(-)	(-)	(-)	(-)
6509	La Auyama	Dike	1.50 m	308/75	Basalt	(+)	(-)	(+)	(-)	(-)	(-)	(-)
6510	La Auyama	Dike	1.50 m	65/78	Basaltic Andesite	(+)	(-)	(+)	(+)	(-)	(-)	(-)

Table 12.2:

Electron microprobe analyses of chromites from Margarita magmas. Oxides as weight percent.
Structural formula on the basis of 4 (O).

Sample	6002	6002	6002	6003	6003	6003	6003	6003	6003	6056	6056	6056
MP	12	13	14	4	5	6	7	51	52	7	8	9
SiO2	0.16	0.12	0.13	7.95	3.43	0.13	0.19	0.13	1.19	3.13	0.23	0.15
TiO2	0.29	0.35	0.31	0.29	0.30	0.34	0.26	0.30	0.34	0.43	0.35	0.33
Al2O3	21.65	23.76	20.94	20.03	20.24	21.91	21.58	21.46	19.90	24.86	26.11	25.69
Cr2O3	45.19	43.02	45.97	36.19	39.93	44.97	43.98	45.49	42.89	35.73	38.26	38.45
Fe2O3	3.72	4.46	4.05	3.24	5.19	4.43	5.03	4.36	4.96	4.01	4.00	4.83
FeO	12.29	11.77	11.79	15.21	14.10	12.84	12.56	12.56	16.03	17.52	16.49	15.51
MnO	0.19	0.19	0.25	0.49	0.43	0.21	0.23	0.24	0.54	0.51	0.39	0.31
MgO	14.67	15.42	14.91	12.95	13.17	14.57	14.49	14.66	11.80	10.97	12.09	12.75
CaO	0.03	0.02	0.00	0.48	0.35	0.03	0.01	0.02	0.06	1.13	0.24	0.23
SUMK	99.94	100.78	99.93	98.63	98.81	100.85	99.90	100.87	99.11	99.69	99.53	99.66
Fe2+	0.3179	0.2982	0.3052	0.3860	0.3666	0.3286	0.3251	0.3226	0.4253	0.4490	0.4256	0.3992
Mn	0.0049	0.0048	0.0067	0.0126	0.0112	0.0055	0.0061	0.0063	0.0145	0.0131	0.0102	0.0081
Mg	0.6763	0.6964	0.6881	0.5859	0.6103	0.6650	0.6684	0.6706	0.5580	0.5009	0.5564	0.5850
Ca	0.0008	0.0006	0.0000	0.0155	0.0118	0.0009	0.0004	0.0005	0.0022	0.0370	0.0079	0.0076
SU1	1.0000	1.0000	1.0000	1.0000	1.0000	1.0000	1.0000	1.0000	1.0000	1.0000	1.0000	1.0000
Fe3+	0.0866	0.1017	0.0944	0.0741	0.1214	0.1020	0.1170	0.1007	0.1184	0.0925	0.0928	0.1118
Cr	1.1052	1.0306	1.1251	0.8685	0.9818	1.0886	1.0758	1.1040	1.0756	0.8657	0.9337	0.9355
Al	0.7893	0.8486	0.7641	0.7165	0.7419	0.7907	0.7871	0.7764	0.7442	0.8978	0.9498	0.9316
Ti	0.0068	0.0080	0.0072	0.0066	0.0071	0.0079	0.0061	0.0070	0.0081	0.0100	0.0081	0.0077
Si	0.0048	0.0037	0.0039	0.2414	0.1066	0.0038	0.0058	0.0040	0.0377	0.0959	0.0072	0.0045
SU2	1.9927	1.9925	1.9947	1.9070	1.9588	1.9930	1.9918	1.9920	1.9840	1.9619	1.9916	1.9912
O*	4.0000	4.0000	4.0000	4.0000	4.0000	4.0000	4.0000	4.0000	4.0000	4.0000	4.0000	4.0000

Table 12.2 (continued):

Sample	6056	6056	6056	6056	6056	6058	6058	6058	6058	6058	6108	6108	6108
MP	10	62	63	64	65	67	68	68	69	70	1	2	3
SiO2	1.85	0.32	0.20	0.12	1.37	0.12	0.03	0.03	0.16	0.12	0.14	0.08	0.11
TiO2	0.34	0.38	0.35	0.33	0.33	0.45	0.40	0.40	0.43	0.41	0.28	0.31	0.31
Al2O3	24.17	24.89	24.47	24.86	23.64	21.24	21.97	21.97	21.97	22.01	19.89	19.46	19.56
Cr2O3	35.55	40.23	42.13	42.09	38.85	39.29	39.79	39.79	39.08	39.64	45.42	45.78	46.00
Fe2O3	6.15	4.12	3.88	3.84	4.37	7.76	7.74	7.74	7.93	7.32	4.74	4.76	4.97
FeO	17.26	13.82	12.14	12.10	15.89	19.55	18.79	18.79	20.09	19.04	15.24	15.39	15.51
MnO	0.64	0.38	0.22	0.23	0.55	0.41	0.32	0.32	0.50	0.37	0.30	0.26	0.22
MgO	11.29	13.82	15.08	15.20	12.30	9.76	10.63	10.63	9.74	10.36	12.62	12.42	12.55
CaO	0.24	0.10	0.06	0.05	0.01	0.07	0.03	0.03	0.04	0.06	0.04	0.05	0.04
SUMK	98.78	99.42	100.12	100.32	98.68	99.85	100.99	100.99	101.40	100.72	101.09	100.38	101.43
Fe2+	0.4502	0.3547	0.3087	0.3062	0.4139	0.5220	0.4930	0.4930	0.5285	0.5018	0.4000	0.4064	0.4065
Mn	0.0168	0.0100	0.0056	0.0060	0.0145	0.0111	0.0085	0.0085	0.0133	0.0099	0.0078	0.0071	0.0058
Mg	0.5248	0.6321	0.6836	0.6860	0.5714	0.4645	0.4974	0.4974	0.4568	0.4863	0.5907	0.5849	0.5864
Ca	0.0081	0.0033	0.0020	0.0018	0.0002	0.0024	0.0012	0.0012	0.0014	0.0020	0.0015	0.0016	0.0013
SU1	1.0000	1.0000	1.0000	1.0000	1.0000	1.0000	1.0000	1.0000	1.0000	1.0000	1.0000	1.0000	1.0000
Fe3+	0.1444	0.0951	0.0889	0.0874	0.1024	0.1866	0.1828	0.1828	0.1877	0.1735	0.1119	0.1131	0.1171
Cr	0.8767	0.9757	1.0127	1.0073	0.9570	0.9920	0.9871	0.9871	0.9718	0.9874	1.1273	1.1430	1.1397
Al	0.8884	0.9000	0.8770	0.8871	0.8680	0.7996	0.8125	0.8125	0.8142	0.8173	0.7361	0.7243	0.7222
Ti	0.0081	0.0089	0.0081	0.0075	0.0078	0.0107	0.0094	0.0094	0.0101	0.0098	0.0066	0.0073	0.0074
Si	0.0577	0.0097	0.0060	0.0037	0.0427	0.0039	0.0010	0.0010	0.0050	0.0038	0.0043	0.0026	0.0035
SU2	1.9753	1.9894	1.9927	1.9930	1.9779	1.9928	1.9929	1.9929	1.9888	1.9917	1.9863	1.9903	1.9899
O*	4.0000	4.0000	4.0000	4.0000	4.0000	4.0000	4.0000	4.0000	4.0000	4.0000	4.0000	4.0000	4.0000

Table 12.3:

Selected electron microprobe analyses of clinopyroxenes from Margarita magmas. Oxides as weight percent. Structural formula on the basis of 6 (O).

Sample	6002	6002	6002	6002	6002	6003	6003	6003	6003	6003	6003	6003	6003
MP	20	21	23	25	26	23	24	25	26	27	28	29	30
SiO2	49.56	48.67	49.34	49.31	49.64	49.96	50.39	48.36	52.04	51.71	48.61	51.80	49.84
TiO2	0.59	0.83	0.53	0.66	0.74	0.65	0.41	0.88	0.32	0.39	0.85	0.36	0.53
Al2O3	5.29	6.23	5.10	5.69	5.39	5.46	3.60	6.44	2.37	2.64	5.90	2.52	4.92
Cr2O3	0.57	0.30	0.55	0.16	0.54	0.31	0.57	0.55	0.36	0.24	0.39	0.24	0.63
FeO*	4.80	5.35	4.48	5.47	4.80	5.17	4.73	5.23	4.85	5.18	5.58	5.21	4.82
MnO	0.10	0.13	0.10	0.14	0.07	0.15	0.12	0.09	0.11	0.07	0.12	0.14	0.13
MgO	14.65	14.21	14.88	14.70	14.60	14.76	16.69	14.29	17.05	16.61	14.49	16.46	14.94
CaO	22.32	22.61	22.82	22.39	22.70	23.22	21.23	22.49	21.93	21.70	22.68	21.96	22.86
Na2O	0.24	0.22	0.27	0.22	0.23	0.24	0.16	0.31	0.20	0.15	0.17	0.15	0.21
K2O	0.01	0.02	0.02	0.02	0.02	0.03	0.00	0.02	0.01	0.01	0.01	0.03	0.02
SUMK	98.14	98.68	98.16	98.99	99.02	100.11	98.20	98.66	99.25	98.86	99.04	98.97	99.10
Si	1.8575	1.8235	1.8517	1.8413	1.8508	1.844	1.8865	1.8112	1.9225	1.9205	1.8208	1.9232	1.857
Alt	0.1425	0.1765	0.1483	0.1587	0.1492	0.156	0.1135	0.1888	0.0775	0.0795	0.1792	0.0768	0.143
SU1	2.0000	2.0000	2.0000	2.0000	2.0000	2.0000	2.0000	2.0000	2.0000	2.0000	2.0000	2.0000	2.0000
Alo	0.0911	0.0987	0.0774	0.0917	0.0876	0.0814	0.0453	0.0956	0.0258	0.0361	0.0811	0.0336	0.0732
Ti	0.0166	0.0233	0.0149	0.0186	0.0207	0.0181	0.0116	0.0248	0.0089	0.0108	0.0238	0.0101	0.0148
Cr	0.0168	0.0089	0.0165	0.0047	0.0159	0.0091	0.0169	0.0163	0.0104	0.0071	0.0115	0.0070	0.0185
Fe	0.1505	0.1676	0.1405	0.1708	0.1495	0.1596	0.1481	0.1637	0.1499	0.1610	0.1749	0.1619	0.1503
Mn	0.0033	0.0040	0.0031	0.0044	0.0023	0.0046	0.0037	0.0029	0.0035	0.0023	0.0038	0.0044	0.0041
Mg	0.8182	0.7933	0.8322	0.8179	0.8110	0.8122	0.9313	0.7976	0.9390	0.9193	0.8089	0.9108	0.8295
Ca	0.8961	0.9074	0.9174	0.8956	0.9068	0.9183	0.8514	0.9023	0.8680	0.8636	0.9100	0.8736	0.9127
Na	0.0178	0.0163	0.0200	0.0156	0.0166	0.0169	0.0116	0.0223	0.0140	0.0109	0.0124	0.0111	0.0148
K	0.0006	0.0009	0.0011	0.0010	0.0011	0.0014	0.0000	0.0007	0.0007	0.0006	0.0006	0.0012	0.0008
SU2	2.0110	2.0204	2.0237	2.0209	2.0121	2.0237	2.0209	2.0263	2.0202	2.0137	2.0270	2.0143	2.0186
TiTs	0.0074	0.0104	0.0066	0.0083	0.0093	0.0082	0.0052	0.0110	0.0040	0.0049	0.0106	0.0045	0.0066
Jd	0.0082	0.0076	0.0094	0.0074	0.0079	0.0082	0.0051	0.0102	0.0066	0.0051	0.0057	0.0055	0.0070
CaTs	0.0404	0.0470	0.0388	0.0438	0.0397	0.0413	0.0276	0.0470	0.0159	0.0185	0.0444	0.0175	0.0382
Woll	0.1751	0.1729	0.1807	0.1735	0.1780	0.1824	0.1729	0.1715	0.1856	0.1818	0.1747	0.1848	0.1815
En	0.1817	0.1762	0.1846	0.1823	0.1811	0.1831	0.2070	0.1772	0.2115	0.2060	0.1797	0.2042	0.1853
Fs	0.0334	0.0372	0.0311	0.0381	0.0334	0.0360	0.0329	0.0364	0.0338	0.0361	0.0389	0.0363	0.0336
JADE	0.0183	0.0169	0.0208	0.0163	0.0177	0.0179	0.0114	0.0226	0.0145	0.0114	0.0127	0.0122	0.0155
AUGI	0.9817	0.9831	0.9792	0.9833	0.9823	0.9821	0.9886	0.9774	0.9855	0.9886	0.9873	0.9878	0.9845

Table 12.3:

Selected electron microprobe analyses of clinopyroxenes from Margarita magmas. Oxides as weight percent. Structural formula on the basis of 6 (O).

Sample MP	6002 20	6002 21	6002 23	6002 25	6002 26	6003 23	6003 24	6003 25	6003 26	6003 27	6003 28	6003 29	6003 30
SiO2	49.56	48.67	49.34	49.31	49.64	49.96	50.39	48.36	52.04	51.71	48.61	51.80	49.84
TiO2	0.59	0.83	0.53	0.66	0.74	0.65	0.41	0.88	0.32	0.39	0.85	0.36	0.53
Al2O3	5.29	6.23	5.10	5.69	5.39	5.46	3.60	6.44	2.37	2.64	5.90	2.52	4.92
Cr2O3	0.57	0.30	0.55	0.16	0.54	0.31	0.57	0.55	0.36	0.24	0.39	0.24	0.63
FeO*	4.80	5.35	4.48	5.47	4.80	5.17	4.73	5.23	4.85	5.18	5.58	5.21	4.82
MnO	0.10	0.13	0.10	0.14	0.07	0.15	0.12	0.09	0.11	0.07	0.12	0.14	0.13
MgO	14.65	14.21	14.88	14.70	14.60	14.76	16.69	14.29	17.05	16.61	14.49	16.46	14.94
CaO	22.32	22.61	22.82	22.39	22.70	23.22	21.23	22.49	21.93	21.70	22.68	21.96	22.86
Na2O	0.24	0.22	0.27	0.22	0.23	0.24	0.16	0.31	0.20	0.15	0.17	0.15	0.21
K2O	0.01	0.02	0.02	0.02	0.02	0.03	0.00	0.02	0.01	0.01	0.01	0.03	0.02
SUMK	98.14	98.68	98.16	98.99	99.02	100.11	98.20	98.66	99.25	98.86	99.04	98.97	99.10
Si	1.8575	1.8235	1.8517	1.8413	1.8508	1.844	1.8865	1.8112	1.9225	1.9205	1.8208	1.9232	1.857
Alt	0.1425	0.1765	0.1483	0.1587	0.1492	0.156	0.1135	0.1888	0.0775	0.0795	0.1792	0.0768	0.143
SU1	2.0000	2.0000	2.0000	2.0000	2.0000	2.0000	2.0000	2.0000	2.0000	2.0000	2.0000	2.0000	2.0000
Alo	0.0911	0.0987	0.0774	0.0917	0.0876	0.0814	0.0453	0.0956	0.0258	0.0361	0.0811	0.0336	0.0732
Ti	0.0166	0.0233	0.0149	0.0186	0.0207	0.0181	0.0116	0.0248	0.0089	0.0108	0.0238	0.0101	0.0148
Cr	0.0168	0.0089	0.0165	0.0047	0.0159	0.0091	0.0169	0.0163	0.0104	0.0071	0.0115	0.0070	0.0185
Fe	0.1505	0.1676	0.1405	0.1708	0.1495	0.1596	0.1481	0.1637	0.1499	0.1610	0.1749	0.1619	0.1503
Mn	0.0033	0.0040	0.0031	0.0044	0.0023	0.0046	0.0037	0.0029	0.0035	0.0023	0.0038	0.0044	0.0041
Mg	0.8182	0.7933	0.8322	0.8179	0.8110	0.8122	0.9313	0.7976	0.9390	0.9193	0.8089	0.9108	0.8295
Ca	0.8961	0.9074	0.9174	0.8956	0.9068	0.9183	0.8514	0.9023	0.8680	0.8636	0.9100	0.8736	0.9127
Na	0.0178	0.0163	0.0200	0.0156	0.0166	0.0169	0.0116	0.0223	0.0140	0.0109	0.0124	0.0111	0.0148
K	0.0006	0.0009	0.0011	0.0010	0.0011	0.0014	0.0000	0.0007	0.0007	0.0006	0.0006	0.0012	0.0008
SU2	2.0110	2.0204	2.0237	2.0209	2.0121	2.0237	2.0209	2.0263	2.0202	2.0137	2.0270	2.0143	2.0186
TiTs	0.0074	0.0104	0.0066	0.0083	0.0093	0.0082	0.0052	0.0110	0.0040	0.0049	0.0106	0.0045	0.0066
Jd	0.0082	0.0076	0.0094	0.0074	0.0079	0.0082	0.0051	0.0102	0.0066	0.0051	0.0057	0.0055	0.0070
CaTs	0.0404	0.0470	0.0388	0.0438	0.0397	0.0413	0.0276	0.0470	0.0159	0.0185	0.0444	0.0175	0.0382
Woll	0.1751	0.1729	0.1807	0.1735	0.1780	0.1824	0.1729	0.1715	0.1856	0.1818	0.1747	0.1848	0.1815
En	0.1817	0.1762	0.1846	0.1823	0.1811	0.1831	0.2070	0.1772	0.2115	0.2060	0.1797	0.2042	0.1853
Fs	0.0334	0.0372	0.0311	0.0381	0.0334	0.0360	0.0329	0.0364	0.0338	0.0361	0.0389	0.0363	0.0336
JADE	0.0183	0.0169	0.0208	0.0163	0.0177	0.0179	0.0114	0.0226	0.0145	0.0114	0.0127	0.0122	0.0155
AUGI	0.9817	0.9831	0.9792	0.9833	0.9823	0.9821	0.9886	0.9774	0.9855	0.9886	0.9873	0.9878	0.9845

Table 12.3 (continued):

Sample	6003	6003	6008	6008	6008	6008	6008	6008	6008	6008	6008	6056	6056
MP	31	32	2	3	4	5	6	7	8	9	10	53	56
SiO2	49.51	48.46	51.87	51.65	51.74	48.20	49.22	48.22	48.50	48.64	48.90	47.14	47.53
TiO2	0.67	0.73	0.45	0.41	0.45	0.94	0.59	0.80	1.01	0.75	0.64	1.59	1.21
Al2O3	5.19	5.75	2.51	2.52	2.63	6.37	5.51	6.02	6.54	5.82	5.17	6.17	6.39
Cr2O3	0.61	0.70	0.04	0.07	0.07	0.30	0.27	0.61	0.19	0.67	0.97	0.00	0.00
FeO*	4.91	5.37	6.47	6.49	6.66	6.13	5.80	5.62	5.87	5.30	4.87	10.01	7.87
MnO	0.14	0.11	0.20	0.22	0.16	0.15	0.14	0.09	0.16	0.06	0.11	0.20	0.26
MgO	14.94	14.93	16.56	16.76	16.27	14.18	14.88	14.78	14.06	14.58	15.00	12.33	12.96
CaO	22.48	22.38	21.00	20.99	20.85	22.29	21.95	22.20	22.41	22.47	22.66	21.19	21.94
Na2O	0.23	0.25	0.11	0.12	0.14	0.17	0.19	0.17	0.20	0.21	0.18	0.32	0.27
K2O	0.03	0.00	0.02	0.03	0.01	0.00	0.01	0.01	0.01	0.02	0.01	0.01	0.02
SUMK	98.72	99.10	99.22	99.42	99.22	98.78	98.62	98.58	98.98	98.57	98.89	99.04	98.61
Si	1.8483	1.8162	1.9241	1.9163	1.9242	1.8088	1.843	1.8107	1.813	1.8243	1.8331	1.7956	1.804
Alt	0.1517	0.1838	0.0759	0.0837	0.0758	0.1912	0.157	0.1893	0.187	0.1757	0.1669	0.2044	0.196
SU1	2.0000	2.0000	2.0000	2.0000	2.0000	2.0000	2.0000	2.0000	2.0000	2.0000	2.0000	2.0000	2.0000
Alo	0.0767	0.0701	0.0337	0.0265	0.0395	0.0907	0.0862	0.0772	0.1009	0.0814	0.0616	0.0725	0.0898
Ti	0.0189	0.0205	0.0127	0.0115	0.0126	0.0266	0.0167	0.0227	0.0284	0.0211	0.0181	0.0456	0.0345
Cr	0.0179	0.0207	0.0011	0.0019	0.0022	0.0090	0.0079	0.0180	0.0057	0.0199	0.0289	0.0000	0.0000
Fe	0.1533	0.1684	0.2006	0.2014	0.2070	0.1925	0.1816	0.1765	0.1834	0.1662	0.1528	0.3189	0.2498
Mn	0.0044	0.0036	0.0063	0.0070	0.0051	0.0048	0.0046	0.0029	0.0050	0.0018	0.0035	0.0065	0.0083
Mg	0.8312	0.8341	0.9156	0.9268	0.9018	0.7932	0.8304	0.8272	0.7836	0.8150	0.8382	0.7001	0.7333
Ca	0.8993	0.8986	0.8345	0.8345	0.8308	0.8962	0.8807	0.8931	0.8977	0.9030	0.9101	0.8649	0.8922
Na	0.0167	0.0181	0.0076	0.0086	0.0101	0.0127	0.0135	0.0126	0.0148	0.0150	0.0132	0.0233	0.0199
K	0.0013	0.0001	0.0010	0.0012	0.0006	0.0002	0.0005	0.0007	0.0007	0.0010	0.0007	0.0006	0.0009
SU2	2.0197	2.0343	2.0133	2.0222	2.0097	2.0267	2.0229	2.0320	2.0203	2.0244	2.0282	2.0323	2.0301
TiTs	0.0084	0.0091	0.0057	0.0052	0.0056	0.0118	0.0074	0.0101	0.0127	0.0094	0.0080	0.0199	0.0151
Jd	0.0080	0.0081	0.0039	0.0044	0.0048	0.0057	0.0062	0.0059	0.0069	0.0071	0.0062	0.0104	0.0091
CaTs	0.0385	0.0432	0.0170	0.0173	0.0178	0.0478	0.0435	0.0461	0.0480	0.0441	0.0396	0.0354	0.0430
Woll	0.1770	0.1734	0.1759	0.1759	0.1742	0.1689	0.1703	0.1699	0.1695	0.1736	0.1782	0.1613	0.1666
En	0.1853	0.1852	0.2054	0.2079	0.2018	0.1759	0.1846	0.1833	0.1745	0.1809	0.1861	0.1530	0.1608
Fs	0.0342	0.0374	0.0450	0.0452	0.0463	0.0427	0.0404	0.0391	0.0408	0.0369	0.0339	0.0697	0.0548
JADE	0.0177	0.0178	0.0086	0.0097	0.0106	0.0126	0.0138	0.0129	0.0152	0.0157	0.0137	0.0232	0.0203
AUGI	0.9823	0.9822	0.9914	0.9903	0.9894	0.9874	0.9862	0.9871	0.9848	0.9843	0.9863	0.9768	0.9797

Table 12.3 (continued):

Sample MP	6056 57	6056 58	6056 72	6056 73	6056 74	6056 77	6056 78	6056 79	6056 81	6058 6	6058 8	6109 12	6109 13
SiO2	48.07	48.30	51.70	51.14	51.68	48.14	47.42	48.06	48.03	48.60	49.53	50.30	49.97
TiO2	1.11	1.06	0.35	0.45	0.36	0.96	1.18	0.79	1.05	1.00	0.80	0.74	0.82
Al2O3	6.10	6.27	3.10	3.58	2.95	6.96	7.66	6.43	6.78	5.67	4.34	4.74	5.61
Cr2O3	0.00	0.10	0.38	0.58	0.63	0.76	0.43	1.06	0.13	0.36	0.12	0.01	0.92
FeO*	7.37	6.86	4.93	4.96	4.79	5.15	5.35	5.05	6.20	6.13	6.27	7.78	5.15
MnO	0.20	0.13	0.14	0.11	0.13	0.10	0.11	0.10	0.11	0.14	0.18	0.21	0.14
MgO	13.21	13.70	16.80	16.45	16.87	14.19	13.60	14.59	14.60	14.28	14.33	15.42	15.14
CaO	22.10	22.32	21.39	21.49	21.18	22.28	22.24	22.16	22.06	22.53	22.54	19.55	21.27
Na2O	0.32	0.23	0.10	0.18	0.15	0.22	0.25	0.19	0.19	0.31	0.25	0.15	0.20
K2O	0.05	0.01	0.02	0.02	0.03	0.01	0.01	0.01	0.03	0.04	0.01	0.06	0.05
SUMK	98.66	99.23	98.93	99.18	98.80	98.97	98.44	98.45	98.72	99.54	98.62	99.21	99.79
Si	1.8181	1.8132	1.9130	1.8941	1.9145	1.7988	1.7826	1.8033	1.8029	1.8203	1.8664	1.8742	1.8462
Alt	0.1819	0.1868	0.0870	0.1059	0.0855	0.2012	0.2174	0.1967	0.1971	0.1797	0.1336	0.1258	0.1538
SU1	2.0000	2.0000	2.0000	2.0000	2.0000	2.0000	2.0000	2.0000	2.0000	2.0000	2.0000	2.0000	2.0000
Alo	0.0898	0.0905	0.0483	0.0505	0.0433	0.1053	0.1220	0.0878	0.1029	0.0705	0.0591	0.0821	0.0904
Ti	0.0316	0.0300	0.0098	0.0124	0.0100	0.0271	0.0332	0.0224	0.0297	0.0283	0.0228	0.0208	0.0229
Cr	0.0000	0.0029	0.0112	0.0170	0.0185	0.0224	0.0128	0.0314	0.0039	0.0106	0.0036	0.0002	0.0268
Fe	0.2332	0.2154	0.1526	0.1537	0.1485	0.1609	0.1681	0.1586	0.1946	0.1921	0.1976	0.2424	0.1591
Mn	0.0064	0.0040	0.0043	0.0034	0.0041	0.0033	0.0035	0.0032	0.0033	0.0046	0.0056	0.0065	0.0044
Mg	0.7446	0.7664	0.9263	0.9080	0.9317	0.7901	0.7623	0.8162	0.7865	0.7970	0.8047	0.8561	0.8339
Ca	0.8955	0.8977	0.8480	0.8527	0.8408	0.8919	0.8957	0.8908	0.8872	0.9042	0.9099	0.7805	0.8419
Na	0.0235	0.0169	0.0069	0.0128	0.0110	0.0159	0.0182	0.0135	0.0136	0.0225	0.0183	0.0111	0.0144
K	0.0026	0.0005	0.0008	0.0007	0.0013	0.0006	0.0007	0.0007	0.0014	0.0019	0.0006	0.0027	0.0025
SU2	2.0273	2.0263	2.0089	2.0115	2.0091	2.0191	2.0163	2.0246	2.0237	2.0316	2.0223	2.0090	2.0050
TiTs	0.0139	0.0133	0.0044	0.0056	0.0045	0.0121	0.0147	0.0099	0.0132	0.0126	0.0101	0.0093	0.1030
Jd	0.0115	0.0077	0.0035	0.0061	0.0055	0.0074	0.0083	0.0063	0.0066	0.0108	0.0084	0.0062	0.0076
CaTs	0.0401	0.0443	0.0243	0.0265	0.0217	0.0525	0.0562	0.0500	0.0500	0.0376	0.0283	0.0341	0.0409
Woll	0.1700	0.1702	0.1764	0.1755	0.1758	0.1664	0.1628	0.1676	0.1651	0.1758	0.1818	0.1527	0.1640
En	0.1639	0.1699	0.2083	0.2040	0.2093	0.1760	0.1688	0.1810	0.1744	0.1771	0.1777	0.1912	0.1879
Fs	0.0513	0.0478	0.0343	0.0345	0.0334	0.0358	0.0372	0.0352	0.0431	0.0427	0.0437	0.0541	0.0358
JADE	0.0256	0.0171	0.0077	0.0135	0.0123	0.0164	0.0186	0.0140	0.0147	0.0237	0.0186	0.0164	0.0185
AUGI	0.9744	0.9829	0.9923	0.9865	0.9877	0.9836	0.9814	0.9860	0.9853	0.9763	0.9814	0.9836	0.9815

Table 12.3 (continued):

Sample MP	6109 14	6109 21	6109 22	6109 23	6109 24	6109 25	6109 26	6109 27	6109 28	6109 30	6109 31	6109 32	6109 33
SiO2	49.83	50.45	47.72	48.86	48.07	50.46	50.52	48.60	47.87	48.65	51.50	51.70	51.42
TiO2	0.74	0.61	1.44	1.08	1.15	0.54	0.64	0.69	1.32	1.07	0.33	0.33	0.31
Al2O3	5.72	4.32	6.58	6.83	7.41	5.07	5.04	6.75	7.23	6.85	3.31	3.30	3.47
Cr2O3	0.68	0.05	0.06	0.17	0.06	0.37	0.44	0.07	0.08	0.29	1.00	1.08	1.04
FeO*	5.43	8.05	8.40	5.97	6.69	5.07	5.24	6.73	6.26	6.36	4.07	4.18	4.21
MnO	0.09	0.22	0.24	0.10	0.13	0.14	0.11	0.17	0.14	0.16	0.07	0.10	0.14
MgO	15.37	16.03	12.53	14.07	13.62	15.29	15.22	14.22	13.51	14.29	16.26	16.06	16.33
CaO	21.10	19.02	21.59	21.99	21.69	21.96	21.78	21.38	22.36	20.86	22.40	22.30	22.34
Na2O	0.24	0.17	0.27	0.22	0.20	0.22	0.18	0.19	0.21	0.21	0.24	0.23	0.18
K2O	0.05	0.03	0.03	0.02	0.03	0.03	0.03	0.03	0.01	0.03	0.04	0.04	0.03
SUMK	99.54	99.51	99.26	99.69	99.40	99.41	99.38	99.18	99.22	99.20	99.93	99.88	99.83
Si	1.8425	1.8791	1.8027	1.8143	1.7950	1.8668	1.8685	1.8161	1.7914	1.8133	1.8992	1.9054	1.8928
Alt	0.1575	0.1209	0.1973	0.1857	0.2050	0.1332	0.1315	0.1839	0.2086	0.1867	0.1008	0.0946	0.1072
SU1	2.0000	2.0000	2.0000	2.0000	2.0000	2.0000	2.0000	2.0000	2.0000	2.0000	2.0000	2.0000	2.0000
Alo	0.0920	0.0686	0.0958	0.1131	0.1211	0.0881	0.0884	0.1134	0.1100	0.1140	0.0431	0.0489	0.0434
Ti	0.0206	0.0170	0.0410	0.0302	0.0324	0.0151	0.0178	0.0195	0.0371	0.0301	0.0091	0.0092	0.0086
Cr	0.0198	0.0015	0.0019	0.0051	0.0017	0.0110	0.0128	0.0020	0.0024	0.0086	0.0290	0.0316	0.0302
Fe	0.1679	0.2508	0.2654	0.1855	0.2087	0.1569	0.1622	0.2104	0.1958	0.1982	0.1255	0.1289	0.1295
Mn	0.0028	0.0069	0.0076	0.0030	0.0042	0.0042	0.0034	0.0053	0.0043	0.0049	0.0022	0.0033	0.0042
Mg	0.8471	0.8902	0.7057	0.7788	0.7578	0.8433	0.8394	0.7922	0.7532	0.7940	0.8936	0.8819	0.8959
Ca	0.8357	0.7591	0.8737	0.8748	0.8676	0.8705	0.8629	0.8561	0.8965	0.8330	0.8851	0.8807	0.8809
Na	0.0175	0.0125	0.0194	0.0159	0.0147	0.0155	0.0132	0.0140	0.0153	0.0154	0.0174	0.0167	0.0131
K	0.0024	0.0012	0.0013	0.0011	0.0014	0.0016	0.0012	0.0015	0.0004	0.0015	0.0020	0.0019	0.0015
SU2	2.0133	2.0156	2.0203	2.0132	2.0174	2.0104	2.0050	2.0236	2.0200	2.0115	2.0147	2.0083	2.0157
TiTs	0.0093	0.0076	0.0181	0.0135	0.0144	0.0068	0.0080	0.0087	0.0165	0.0134	0.0041	0.0041	0.0039
Jd	0.0090	0.0062	0.0091	0.0076	0.0072	0.0077	0.0065	0.0069	0.0070	0.0075	0.0088	0.0084	0.0066
CaTs	0.0424	0.0316	0.0419	0.0496	0.0546	0.0391	0.0382	0.0541	0.0509	0.0499	0.0240	0.0240	0.0268
Woll	0.1623	0.1500	0.1625	0.1645	0.1588	0.1729	0.1710	0.1593	0.1657	0.1543	0.1857	0.1848	0.1838
En	0.1907	0.1989	0.1555	0.1745	0.1689	0.1897	0.1889	0.1764	0.1675	0.1773	0.2017	0.1992	0.2025
Fs	0.0378	0.0560	0.0585	0.0416	0.0465	0.0353	0.0365	0.0469	0.0435	0.0443	0.0283	0.0291	0.0293
JADE	0.0176	0.0123	0.0135	0.0153	0.0157	0.0167	0.0132	0.0156	0.0135	0.0167	0.0166	0.0147	0.0125
AUGI	0.9824	0.9877	0.9865	0.9847	0.9843	0.9833	0.9853	0.9829	0.9867	0.9848	0.9823	0.9853	0.9875

Table 12.3 (continued):

Sample MP	6109 34	6109 43	6109 44	6109 45	6109 47	6109 48	6504 30	6504 31	6504 34	6504 35	6504 42	6504 43	6504 44
SiO2	48.81	49.15	46.20	49.11	49.73	51.41	50.15	50.48	50.33	50.61	50.43	50.35	50.45
TiO2	0.99	0.76	1.46	1.00	0.77	0.40	0.54	0.50	0.61	0.49	0.45	0.44	0.41
Al2O3	6.66	5.98	8.30	6.24	5.06	2.56	4.18	3.94	4.31	3.68	3.84	3.96	3.76
Cr2O3	0.14	0.10	0.10	0.22	0.18	0.08	1.00	1.15	0.98	1.00	1.05	1.14	1.15
FeO*	6.24	6.36	7.49	6.23	7.09	7.05	4.50	4.14	4.28	4.20	4.09	4.12	3.96
MnO	0.14	0.07	0.18	0.21	0.20	0.23	0.14	0.10	0.12	0.12	0.14	0.01	0.13
MgO	14.40	14.09	12.94	14.33	15.48	16.59	15.12	15.16	14.96	15.09	15.36	15.42	15.48
CaO	21.43	21.91	21.40	21.48	19.95	20.02	22.31	22.50	22.55	22.67	22.35	22.66	22.45
Na2O	0.21	0.24	0.33	0.21	0.20	0.13	0.25	0.24	0.21	0.17	0.20	0.21	0.21
K2O	0.03	0.02	0.02	0.03	0.00	0.01	0.04	0.00	0.03	0.02	0.02	0.06	0.01
SUMK	99.23	99.26	98.70	99.17	98.82	98.65	98.93	98.83	98.77	98.48	98.40	98.68	98.50
Si	1.8177	1.8388	1.7492	1.8298	1.8579	1.9216	1.8738	1.8857	1.8763	1.8942	1.8877	1.8785	1.8862
Alt	0.1823	0.1612	0.2508	0.1702	0.1421	0.0784	0.1262	0.1143	0.1237	0.1058	0.1123	0.1215	0.1138
SU1	2.0000	2.0000	2.0000	2.0000	2.0000	2.0000	2.0000	2.0000	2.0000	2.0000	2.0000	2.0000	2.0000
Alo	0.1098	0.1026	0.1193	0.1037	0.0806	0.0342	0.0581	0.0593	0.0657	0.0563	0.0570	0.0528	0.0521
Ti	0.0276	0.0214	0.0417	0.0280	0.0216	0.0112	0.0151	0.0139	0.0171	0.0139	0.0126	0.0125	0.0115
Cr	0.0041	0.0030	0.0029	0.0065	0.0052	0.0024	0.0295	0.0339	0.0289	0.0296	0.0311	0.0336	0.0340
Fe	0.1942	0.1990	0.2371	0.1940	0.2216	0.2203	0.1406	0.1294	0.1336	0.1314	0.1281	0.1284	0.1237
Mn	0.0043	0.0021	0.0057	0.0067	0.0062	0.0072	0.0044	0.0032	0.0038	0.0038	0.0045	0.0005	0.0041
Mg	0.7991	0.7858	0.7302	0.7956	0.8621	0.9242	0.8420	0.8442	0.8311	0.8415	0.8572	0.8575	0.8625
Ca	0.8549	0.8781	0.8678	0.8572	0.7986	0.8020	0.8929	0.9006	0.9008	0.9090	0.8965	0.9058	0.8993
Na	0.0152	0.0175	0.0239	0.0149	0.0147	0.0094	0.0178	0.0176	0.0154	0.0124	0.0143	0.0152	0.0152
K	0.0015	0.0008	0.0010	0.0015	0.0000	0.0003	0.0018	0.0000	0.0014	0.0009	0.0012	0.0031	0.0007
SU2	2.0161	2.0167	2.0362	2.0113	2.0150	2.0155	2.0021	2.0023	1.9978	1.9989	2.0025	2.0092	2.0030
TiTs	0.0123	0.0095	0.0183	0.0125	0.0096	0.0050	0.0067	0.0062	0.0076	0.0062	0.0056	0.0056	0.0051
Jd	0.0075	0.0082	0.0109	0.0073	0.0065	0.0043	0.0087	0.0079	0.0075	0.0060	0.0069	0.0069	0.0071
CaTs	0.0492	0.0451	0.0576	0.0450	0.0367	0.0179	0.0300	0.0285	0.0309	0.0269	0.0286	0.0286	0.0283
Woll	0.1603	0.1681	0.1528	0.1627	0.1547	0.1671	0.1805	0.1833	0.1818	0.1856	0.1822	0.1822	0.1835
En	0.1786	0.1748	0.1605	0.1777	0.1920	0.2058	0.1875	0.1881	0.1855	0.1871	0.1906	0.1906	0.1920
Fs	0.0434	0.0443	0.0521	0.0433	0.0494	0.0490	0.0313	0.0288	0.0298	0.0292	0.0285	0.0285	0.0275
JADE	0.0150	0.0166	0.0172	0.0152	0.0140	0.0133	0.0196	0.0179	0.0187	0.0135	0.0155	0.0155	0.0159
AUGI	0.9850	0.9834	0.9828	0.9848	0.9860	0.9867	0.9804	0.9821	0.9830	0.9865	0.9845	0.9845	0.9841

Table 12.4:

Selected electron microprobe anaylses of plagioclases from Margarita magmas. Oxides as weight percent. Structural formula on the basis of 8 (O).

Sample MP	6002 1	6002 2	6002 3	6003 17	6003 19	6008 61	6008 62	6008 67	6008 68	6008 69	6008 70	6008 71	6008 72
SiO2	67.61	67.05	66.39	60.99	58.12	57.68	61.70	52.59	55.39	51.98	48.51	53.86	57.95
Al2O3	21.98	22.44	22.49	19.77	23.47	22.72	23.15	29.16	27.50	29.33	31.37	28.24	26.08
Fe2O3*	0.18	0.18	0.04	1.93	0.84	5.13	0.39	0.44	0.41	0.48	0.75	0.57	0.24
BaO	0.00	0.00	0.00	0.00	0.01	0.13	0.04	0.07	0.00	0.00	0.00	0.00	0.03
CaO	1.13	1.34	2.70	4.98	5.28	2.71	4.73	12.46	10.23	12.74	15.47	11.00	8.34
Na2O	10.43	9.88	9.95	5.96	3.34	7.20	9.06	4.44	5.71	4.37	2.78	5.14	7.32
K2O	0.11	0.31	0.07	3.37	7.36	0.06	0.13	0.12	0.16	0.10	0.09	0.14	0.11
SUMK	101.66	101.61	101.70	99.66	99.00	99.56	99.37	99.40	99.55	99.16	99.18	99.03	100.17
Si	2.9442	2.9129	2.8674	2.7700	2.6880	2.6068	2.7591	2.4031	2.5100	2.3840	2.2452	2.4590	2.5980
Al	1.0801	1.1156	1.1447	1.0580	1.2813	1.2102	1.2203	1.5703	1.4687	1.5853	1.7110	1.5195	1.3779
Fe3+	0.0057	0.0056	0.0012	0.0661	0.0294	0.1744	0.0130	0.0151	0.0140	0.0164	0.0261	0.0196	0.0082
SU1	4.0299	4.0341	4.0135	3.8941	3.9987	3.9913	3.9925	3.9885	3.9927	3.9857	3.9824	3.9981	3.9841
Ba	0.0000	0.0000	0.0000	0.0000	0.0002	0.0023	0.0007	0.0012	0.0000	0.0000	0.0000	0.0000	0.0005
Ca	0.0506	0.0606	0.1249	0.2422	0.2617	0.1310	0.2268	0.6102	0.4968	0.6260	0.7673	0.5382	0.4004
Na	0.8435	0.8083	0.8330	0.5244	0.2999	0.6310	0.7858	0.3931	0.5019	0.3890	0.2499	0.4547	0.6360
K	0.0060	0.1680	0.0039	0.1952	0.4349	0.0033	0.0073	0.0070	0.0094	0.0059	0.0050	0.0082	0.0065
SU2	0.9001	0.8857	0.9619	0.9618	0.9967	0.7677	1.0206	1.0114	1.0081	1.0209	1.0222	1.0010	1.0434
An	0.0562	0.0684	0.1299	0.2518	0.2626	0.1711	0.2223	0.6040	0.4928	0.6132	0.7507	0.5376	0.3839
Ab	0.9372	0.9126	0.8660	0.5453	0.3010	0.8245	0.7705	0.3891	0.4979	0.3810	0.2444	0.4542	0.6098
Kf	0.0067	0.0190	0.0041	0.2030	0.4364	0.0044	0.0071	0.0069	0.0093	0.0058	0.0049	0.0082	0.0062

Table 12.4 (continued):

Sample	6009	6009	6009	6009	6009	6009	6009	6009	6009	6009	6009	6009	6009
MP	22	23	24	25	26	27	28	29	30	31	32	33	34
SiO2	48.86	48.68	49.44	49.85	49.06	49.40	49.98	49.89	49.97	49.56	49.98	50.57	51.19
Al2O3	31.42	31.35	31.17	31.08	31.72	31.19	31.03	30.54	30.96	31.14	31.30	31.58	30.47
Fe2O3*	0.67	0.54	0.63	0.45	0.54	0.49	0.50	0.55	0.61	0.70	0.62	0.73	0.64
BaO	0.00	0.04	0.00	0.00	0.20	0.06	0.00	0.00	0.00	0.15	0.00	0.08	0.02
CaO	15.81	16.12	14.59	15.00	15.34	15.99	15.89	15.69	15.82	14.59	14.04	13.42	14.52
Na2O	2.19	2.30	2.97	2.77	2.42	2.22	2.35	2.35	2.31	2.87	2.88	2.78	2.74
K2O	0.08	0.08	0.08	0.11	0.07	0.08	0.10	0.08	0.10	0.08	0.11	0.10	0.10
SUMK	99.03	99.48	99.25	99.26	99.35	99.43	99.85	99.10	99.77	99.09	98.93	99.26	99.68
Si	2.2317	2.2277	2.3027	2.2841	2.2594	2.2280	2.2432	2.2428	2.2454	2.3048	2.3082	2.3085	2.2928
Al	1.7316	1.7256	1.6559	1.6799	1.7019	1.7279	1.7099	1.7095	1.7078	1.6521	1.6687	1.6843	1.6738
Fe3+	0.0237	0.0191	0.0222	0.0157	0.0191	0.0172	0.0176	0.0197	0.0215	0.0246	0.0217	0.0257	0.0224
SU1	3.9870	3.9724	3.9809	3.9797	3.9804	3.9731	3.9707	3.9721	3.9747	3.9815	3.9986	4.0186	3.9890
Ba	0.0000	0.0008	0.0000	0.0000	0.0036	0.0011	0.0000	0.0000	0.0000	0.0027	0.0000	0.0014	0.0004
Ca	0.7921	0.8068	0.7281	0.7516	0.7726	0.8053	0.7957	0.7981	0.7934	0.7271	0.7027	0.6718	0.7251
Na	0.1985	0.2086	0.2682	0.2507	0.2209	0.2021	0.2128	0.2161	0.2097	0.2588	0.2611	0.2521	0.2475
K	0.0051	0.0050	0.0048	0.0066	0.0042	0.0051	0.0062	0.0051	0.0058	0.0048	0.0063	0.0058	0.0057
SU2	0.9957	1.0212	1.0011	1.0088	1.0014	1.0135	1.0147	1.0194	1.0089	0.9934	0.9701	0.9311	0.9788
An	0.7955	0.7907	0.7273	0.7450	0.7744	0.7954	0.7842	0.7830	0.7864	0.7339	0.7244	0.7226	0.7412
Ab	0.1994	0.2044	0.2679	0.2485	0.2214	0.1996	0.2097	0.2120	0.2079	0.2613	0.2691	0.2712	0.2530
Kf	0.0051	0.0049	0.0047	0.0065	0.0042	0.0050	0.0061	0.0050	0.0057	0.0049	0.0065	0.0062	0.0058

Table 12.4 (continued):

Sample	6009	6009	6009	6009	6009	6009	6009	6009	6009	6009	6009	6009	6013
MP	35	36	37	38	39	41	55	56	57	58	59	60	21
SiO2	50.80	50.58	51.16	50.84	50.12	67.67	50.02	49.57	49.35	50.39	51.32	51.75	50.63
Al2O3	30.21	30.43	30.15	29.94	30.33	18.50	30.96	30.95	30.97	30.67	30.34	29.57	30.22
Fe2O3*	0.50	0.55	0.54	0.58	0.65	0.79	0.52	0.56	0.57	0.51	0.61	0.68	0.72
BaO	0.03	0.03	0.04	0.08	0.01	0.01	0.00	0.01	0.08	0.01	0.02	0.02	0.00
CaO	14.91	15.22	15.00	15.28	15.52	5.88	15.86	16.21	15.70	15.66	15.00	13.68	13.92
Na2O	2.77	2.69	2.82	2.60	2.50	5.64	2.32	2.17	2.45	2.48	2.66	3.22	3.58
K2O	0.11	0.09	0.11	0.10	0.11	0.10	0.09	0.07	0.07	0.09	0.10	0.11	0.07
SUMK	99.33	99.59	99.82	99.42	99.24	98.59	99.77	99.54	99.19	99.81	100.05	99.03	99.33
Si	2.2894	2.2756	2.2960	2.2908	2.2635	2.9813	2.2463	2.2346	2.2524	2.2624	2.2928	2.3474	2.3243
Al	1.6701	1.6796	1.6598	1.6551	1.6811	0.9604	1.7072	1.7136	1.7002	1.6896	1.6622	1.6121	1.6349
Fe3+	0.0176	0.0193	0.0191	0.0205	0.0230	0.0263	0.0184	0.0197	0.0200	0.0180	0.0212	0.0237	0.2770
SU1	3.9771	3.9744	3.9750	3.9664	3.9676	3.9680	3.9719	3.9679	3.9727	3.9700	3.9762	3.9832	3.9869
Ba	0.0005	0.0006	0.0008	0.0015	0.0001	0.0001	0.0000	0.0003	0.0014	0.0002	0.0004	0.0003	0.0000
Ca	0.7493	0.7639	0.7504	0.7678	0.7821	0.2776	0.7947	0.8159	0.7836	0.7845	0.7473	0.6782	0.6845
Na	0.2517	0.2438	0.2553	0.2361	0.2284	0.4821	0.2100	0.1973	0.2217	0.2252	0.2402	0.2886	0.3198
K	0.0064	0.0055	0.0065	0.0061	0.0066	0.0056	0.0052	0.0043	0.0041	0.0051	0.0057	0.0067	0.0038
SU2	1.0078	1.0138	1.0129	1.0115	1.0173	0.7654	1.0099	1.0179	1.0109	1.0151	0.9935	0.9738	1.0072
An	0.7438	0.7539	0.7414	0.7602	0.7689	0.3627	0.7869	0.8018	0.7763	0.7731	0.7524	0.6966	0.6796
Ab	0.2499	0.2406	0.2522	0.2337	0.2246	0.6299	0.2079	0.1939	0.2196	0.2219	0.2419	0.2964	0.3166
Kf	0.0063	0.0055	0.0064	0.0061	0.0065	0.0073	0.0051	0.0043	0.0041	0.0051	0.0057	0.0069	0.0038

Table 12.4 (continued):

Sample	6013	6013	6013	6013	6037	6037	6037	6037	6037	6037	6050	6050	6050
MP	22	23	47	49	19	20	43	45	56	57	118	119	120
SiO2	51.05	50.23	62.38	62.61	52.89	51.73	53.61	52.80	53.67	56.34	51.78	53.67	61.84
Al2O3	29.83	30.35	22.99	24.16	28.79	28.72	27.51	28.99	28.23	26.90	30.18	28.97	23.79
Fe2O3*	0.66	0.62	1.13	0.01	0.33	1.15	1.14	0.54	1.09	0.49	0.35	0.37	0.10
BaO	0.00	0.00	0.17	0.00	0.00	0.00	0.00	0.00	0.00	0.00	0.00	0.07	0.00
CaO	13.55	14.01	4.24	5.44	11.71	11.91	10.92	11.94	10.59	9.16	13.28	11.72	5.28
Na2O	3.71	3.50	7.43	8.45	4.79	4.36	5.16	4.62	5.05	6.19	4.05	4.81	8.38
K2O	0.09	0.06	0.85	0.13	0.14	0.14	0.15	0.14	0.20	0.23	0.07	0.12	0.19
SUMK	99.12	99.04	99.66	101.02	98.69	98.15	98.85	99.17	99.33	99.40	99.93	99.87	99.58
Si	2.3454	2.3144	2.7787	2.7478	2.4274	2.3992	2.4626	2.4156	2.4494	2.5505	2.3587	2.4344	2.7526
Al	1.6148	1.6481	1.2096	1.2496	1.5578	1.5703	1.4898	1.5636	1.5189	1.4356	1.6202	1.5485	1.2483
Fe3+	0.0252	0.0237	0.0422	0.0059	0.0127	0.0446	0.0438	0.0207	0.0416	0.0186	0.0120	0.0125	0.0032
SU1	3.9855	3.9863	4.0278	4.0033	3.9979	4.0141	3.9962	3.9999	4.0099	4.0047	3.9909	3.9954	4.0041
Ba	0.0000	0.0000	0.0029	0.0000	0.0000	0.0000	0.0000	0.0000	0.0000	0.0000	0.0000	0.0012	0.0000
Ca	0.6668	0.6916	0.2023	0.2557	0.5759	0.5919	0.5375	0.5853	0.5179	0.4443	0.6479	0.5697	0.2520
Na	0.3306	0.3123	0.6421	0.7188	0.4263	0.3921	0.4596	0.4098	0.4469	0.5433	0.3579	0.4232	0.7228
K	0.0052	0.0034	0.0482	0.0072	0.0082	0.0083	0.0088	0.0082	0.0116	0.0133	0.0041	0.0067	0.0106
SU2	1.0025	1.0073	0.8955	0.9816	1.0104	0.9923	1.0059	1.0033	0.9764	1.0009	1.0099	1.0009	0.9854
An	0.6651	0.6866	0.2266	0.2605	0.5700	0.5965	0.5344	0.5834	0.5304	0.4439	0.6416	0.5699	0.2557
Ab	0.3297	0.3100	0.7193	0.7322	0.4219	0.3951	0.4569	0.4085	0.4577	0.5428	0.3544	0.4234	0.7335
Kf	0.0052	0.0033	0.0540	0.0073	0.0081	0.0083	0.0087	0.0081	0.0119	0.0133	0.0040	0.0067	0.0107

Table 12.4 (continued):

Sample	6050	6050	6050	6055	6055	6055	6055	6055	6055	6055	6055	6056	6056
MP	121	122	123	52	53	54	69	76	77	78	80	32	33
SiO2	58.27	61.06	64.90	53.21	53.67	54.04	57.81	48.46	46.79	46.77	46.78	49.62	49.38
Al2O3	25.75	23.90	21.65	29.42	29.05	29.45	27.31	33.29	33.85	34.07	33.36	31.28	31.05
Fe2O3*	0.29	0.14	0.08	0.42	0.39	0.24	0.30	0.61	0.46	0.57	0.54	0.67	0.62
BaO	0.05	0.00	0.00	0.00	0.08	0.01	0.00	0.00	0.00	0.06	0.07	0.03	0.02
CaO	7.58	5.36	2.61	12.13	11.76	11.43	9.35	15.60	17.71	17.46	16.43	14.82	14.48
Na2O	6.97	8.28	9.85	4.65	4.80	4.45	6.00	1.82	1.55	1.54	1.91	3.00	3.09
K2O	0.13	0.11	0.13	0.22	0.00	0.00	0.11	0.22	0.04	0.03	0.06	0.07	0.06
SUMK	99.10	98.92	99.33	100.17	99.96	100.04	100.95	100.48	100.60	100.61	99.26	99.62	98.95
Si	2.6282	2.7375	2.8741	2.4091	2.4319	2.4397	2.5667	2.2084	2.1445	2.1408	2.1662	2.2773	2.2820
Al	1.3690	1.2629	1.1299	1.5699	1.5513	1.5669	1.4292	1.7883	1.8286	1.8377	1.8204	1.6922	1.6909
Fe3+	0.0098	0.0046	0.0026	0.0143	0.0132	0.0082	0.0101	0.0208	0.0159	0.0198	0.0187	0.0230	0.0217
SU1	4.0071	4.0050	4.0066	3.9933	3.9965	4.0148	4.0060	4.0175	3.9890	3.9983	4.0053	3.9926	3.9946
Ba	0.0009	0.0000	0.0000	0.0000	0.0015	0.0001	0.0000	0.0000	0.0000	0.0010	0.0013	0.0005	0.0003
Ca	0.3664	0.2576	0.1238	0.5882	0.5710	0.5531	0.4447	0.7617	0.8697	0.8561	0.8153	0.7287	0.7167
Na	0.6092	0.7200	0.8459	0.4081	0.4219	0.3891	0.5161	0.1606	0.1381	0.1370	0.1716	0.2674	0.2771
K	0.0074	0.0062	0.0073	0.0128	0.0000	0.0000	0.0064	0.0126	0.0024	0.0018	0.0035	0.0039	0.0038
SU2	0.9840	0.9838	0.9769	1.0091	0.9944	0.9423	0.9672	0.9349	1.0102	0.9959	0.9917	1.0005	0.9979
An	0.3727	0.2619	0.1267	0.5829	0.5751	0.5870	0.4598	0.8148	0.8609	0.8605	0.8232	0.7287	0.7184
Ab	0.6198	0.7318	0.8659	0.4044	0.4249	0.4130	0.5336	0.1718	0.1367	0.1377	0.1733	0.2674	0.2778
Kf	0.0075	0.0063	0.0074	0.0127	0.0000	0.0000	0.0066	0.0135	0.0024	0.0018	0.0036	0.0039	0.0038

Table 12.4 (continued):

Sample	6056	6056	6056	6056	6056	6056	6056	6056	6056	6056	6056	6056	6056
MP	34	36	38	39	40	41	42	43	44	45	50	51	66
SiO2	49.18	53.98	48.85	54.87	49.19	52.63	53.72	52.68	50.79	50.95	51.37	48.89	51.84
Al2O3	31.22	27.88	31.40	26.71	30.57	29.47	28.69	28.76	28.54	30.43	28.37	31.62	29.24
Fe2O3*	0.81	0.45	0.83	1.53	0.86	0.52	0.66	0.65	2.56	0.72	1.43	0.61	0.86
BaO	0.00	0.00	0.09	0.04	0.02	0.00	0.07	0.08	0.00	0.00	0.02	0.00	0.00
CaO	14.52	10.34	14.60	8.10	14.36	12.43	11.62	12.00	12.19	13.87	11.07	14.05	10.45
Na2O	3.12	5.32	3.02	5.80	3.05	4.37	4.84	4.35	4.02	3.70	4.50	2.68	3.56
K2O	0.08	0.23	0.24	0.21	0.08	0.08	0.11	0.09	0.13	0.07	0.11	0.72	1.84
SUMK	99.27	98.47	99.39	98.58	98.54	99.59	99.85	98.87	98.57	99.96	98.59	98.84	98.45
Si	2.2673	2.4763	2.2554	2.5079	2.2838	2.3974	2.4374	2.4179	2.3565	2.3259	2.3738	2.2642	2.3960
Al	1.6965	1.5075	1.7085	1.4386	1.6726	1.5819	1.5340	1.5559	1.5605	1.6370	1.5451	1.7255	1.5930
Fe3+	0.0279	0.0157	0.0289	0.0526	0.0302	0.0179	0.0224	0.0225	0.0894	0.0249	0.0496	0.0211	0.0299
SU1	3.9917	3.9995	3.9928	3.9991	3.9866	3.9972	3.9938	3.9963	4.0064	3.9879	3.9685	4.0109	4.0189
Ba	0.0000	0.0000	0.0015	0.0007	0.0003	0.0000	0.0012	0.0014	0.0000	0.0000	0.0003	0.0000	0.0000
Ca	0.7174	0.5080	0.7221	0.3967	0.7144	0.6065	0.5648	0.5899	0.6059	0.6785	0.5479	0.6973	0.5173
Na	0.2786	0.4731	0.2707	0.5138	0.2750	0.3857	0.4259	0.3874	0.3613	0.3273	0.4035	0.2410	0.3191
K	0.0046	0.0136	0.0142	0.0125	0.0049	0.0047	0.0062	0.0050	0.0078	0.0038	0.0063	0.0423	0.1084
SU2	1.0006	0.9947	1.0085	0.9236	0.9946	0.9969	0.9981	0.9837	0.9750	1.0097	0.9580	0.9806	0.9448
An	0.7170	0.5107	0.7171	0.4298	0.7185	0.6083	0.5665	0.6005	0.6215	0.6720	0.5721	0.7111	0.5475
Ab	0.2785	0.4756	0.2688	0.5567	0.2766	0.3869	0.4272	0.3944	0.3705	0.3242	0.4213	0.2458	0.3377
Kf	0.0046	0.0137	0.0141	0.0135	0.0049	0.0048	0.0062	0.0051	0.0080	0.0038	0.0065	0.0432	0.1147

Table 12.4 (continued):

Sample	6056	6057	6057	6057	6057	6057	6057	6057	6057	6057	6058	6058	6058
MP	67	72	73	74	76	80	91	94	97	98	31	32	33
SiO2	51.39	62.65	60.04	57.67	64.12	62.63	63.63	62.65	61.63	62.13	45.71	46.57	49.03
Al2O3	29.20	23.17	24.32	26.03	22.25	23.20	22.42	23.64	23.83	23.45	33.92	33.27	30.50
Fe2O3*	0.76	0.54	1.14	0.42	0.29	0.14	0.33	0.04	0.15	0.12	0.46	0.49	0.81
BaO	0.01	0.00	0.00	0.10	0.00	0.04	0.00	0.00	0.05	0.01	0.06	0.03	0.00
CaO	13.10	4.52	6.01	8.10	3.30	4.36	3.36	4.53	5.33	4.80	17.89	17.24	13.96
Na2O	3.33	8.90	7.51	6.97	9.68	9.13	9.25	8.95	8.60	8.71	1.45	1.75	2.64
K2O	1.09	0.12	0.12	0.09	0.09	0.10	0.35	0.10	0.10	0.10	0.04	0.06	0.13
SUMK	99.34	99.99	99.41	99.45	99.88	99.66	99.57	99.97	99.71	99.41	99.86	99.53	98.10
Si	2.3648	2.7769	2.6912	2.6003	2.8355	2.7833	2.8227	2.7734	2.7439	2.7685	2.1184	2.1548	2.2852
Al	1.5840	1.2106	1.2850	1.3832	1.1597	1.2150	1.1721	1.2331	1.2505	1.2317	1.8525	1.8143	1.6755
Fe3+	0.0262	0.0181	0.0385	0.0143	0.0098	0.0048	0.0111	0.0013	0.0050	0.0039	0.0160	0.0169	0.0285
SU1	3.9750	4.0056	4.0147	3.9979	4.0050	4.0030	4.0059	4.0078	3.9994	4.0042	3.9869	3.9860	3.9893
Ba	0.0003	0.0000	0.0000	0.0018	0.0000	0.0006	0.0000	0.0000	0.0009	0.0002	0.0010	0.0006	0.0000
Ca	0.6458	0.2149	0.2887	0.3914	0.1564	0.2075	0.1598	0.2149	0.2545	0.2289	0.8882	0.8548	0.6970
Na	0.2971	0.7646	0.6528	0.6091	0.8297	0.7864	0.7955	0.7680	0.7421	0.7529	0.1305	0.1568	0.2386
K	0.0642	0.0069	0.0068	0.0053	0.0051	0.0055	0.0196	0.0054	0.0058	0.0055	0.0026	0.0033	0.0076
SU2	1.0074	0.9863	0.9483	1.0076	0.9912	1.0001	0.9748	0.9883	1.0032	0.9875	1.0223	1.0155	0.9431
An	0.6412	0.2178	0.3044	0.3891	0.1578	0.2076	0.1639	0.2174	0.2539	0.2319	0.8697	0.8422	0.7390
Ab	0.2950	0.7752	0.6884	0.6056	0.8370	0.7868	0.8161	0.7771	0.7403	0.7626	0.1278	0.1545	0.2530
Kf	0.0638	0.0070	0.0071	0.0053	0.0052	0.0055	0.0201	0.0055	0.0058	0.0055	0.0025	0.0032	0.0080

Table 12.4 (continued):

Sample MP	6058 34	6058 35	6058 37	6058 39	6058 40	6058 41	6058 42	6108 4	6108 6	6108 7	6108 8	6108 9	6108 10
SiO2	47.69	47.42	46.99	45.75	46.30	45.72	45.56	49.51	53.42	53.80	53.77	50.44	48.95
Al2O3	32.80	33.06	33.23	33.83	33.46	33.63	33.78	31.26	29.31	19.86	16.57	31.33	30.32
Fe2O3*	0.47	0.57	0.49	0.43	0.52	0.49	0.48	1.78	0.43	4.58	5.52	0.61	2.65
BaO	0.00	0.08	0.02	0.00	0.00	0.00	0.00	0.20	0.04	0.00	0.00	0.00	0.00
CaO	16.41	16.47	16.87	17.93	17.54	17.86	18.04	13.94	12.26	12.43	13.19	14.43	12.47
Na2O	2.26	2.08	1.82	1.48	1.69	1.51	1.37	2.60	4.66	2.76	2.49	3.15	2.25
K2O	0.06	0.05	0.04	0.02	0.04	0.03	0.05	0.28	0.16	0.30	0.23	0.14	0.46
SUMK	100.29	99.84	99.60	99.57	99.62	99.30	99.48	100.34	100.73	101.11	99.97	100.44	98.10
Si	2.1903	2.1827	2.1687	2.1212	2.1418	2.1243	2.1168	2.2658	2.4123	2.4629	2.5064	2.2944	2.2828
Al	1.7756	1.7931	1.8073	1.8483	1.8246	1.8413	1.8499	1.6863	1.5600	1.0713	0.9104	1.6796	1.6665
Fe3+	0.0161	0.0195	0.0171	0.0152	0.0181	0.0171	0.0166	0.0612	0.0147	0.1579	0.1938	0.2100	0.0931
SU1	3.9819	3.9953	3.9930	3.9847	3.9845	3.9827	3.9833	4.0134	3.9871	3.6921	3.6106	3.9950	4.0424
Ba	0.0000	0.0014	0.0003	0.0000	0.0000	0.0000	0.0000	0.0035	0.0007	0.0000	0.0000	0.0000	0.0000
Ca	0.8073	0.8119	0.8341	0.8907	0.8696	0.8893	0.8978	0.6835	0.5930	0.6098	0.6585	0.7034	0.6232
Na	0.2015	0.1858	0.1631	0.1329	0.1513	0.1361	0.1236	0.2305	0.4079	0.2447	0.2252	0.2775	0.2039
K	0.0035	0.0030	0.0025	0.0012	0.0023	0.0020	0.0027	0.0165	0.0092	0.0172	0.0139	0.0079	0.0274
SU2	1.0122	1.0020	1.0001	1.0248	1.0233	1.0273	1.0241	0.9340	1.0108	0.8718	0.8976	0.9888	0.8544
An	0.7975	0.8114	0.8343	0.8692	0.8498	0.8656	0.8767	0.7345	0.5871	0.6995	0.7336	0.7114	0.7294
Ab	0.1991	0.1856	0.1632	0.1297	0.1479	0.1325	0.1207	0.2477	0.4038	0.2807	0.2509	0.2807	0.2386
Kf	0.0034	0.0030	0.0025	0.0012	0.0023	0.0019	0.0027	0.0178	0.0091	0.0198	0.0155	0.0080	0.0320

Table 12.4 (continued):

Sample	6504	6504	6504	6504	6504	6504	6504	6504	6504
MP	11	12	13	14	15	16	17	80	83
SiO2	48.43	50.65	54.97	58.63	49.80	53.94	49.72	57.58	56.14
Al2O3	32.00	30.57	27.63	25.30	31.22	30.26	31.74	24.37	26.97
Fe2O3*	0.61	0.48	0.34	0.27	0.57	0.38	0.63	1.07	0.33
BaO	0.00	0.01	0.21	0.05	0.11	0.07	0.02	0.04	0.04
CaO	13.90	13.55	8.39	5.02	11.45	8.17	13.42	7.74	7.26
Na2O	2.61	3.17	2.77	3.01	2.38	3.59	2.08	4.78	2.96
K2O	0.91	0.58	4.76	7.21	1.91	2.81	1.15	2.35	5.35
SUMK	99.00	99.43	99.42	99.94	98.08	99.68	99.38	99.86	99.55
Si	2.2443	2.2858	2.5058	2.6396	2.2560	2.3921	2.2261	2.5581	2.5361
Al	1.7476	1.6926	1.5118	1.3898	1.7735	1.6744	1.7820	1.3463	1.4887
Fe3+	0.0212	0.0170	0.0120	0.0092	0.0204	0.0133	0.0227	0.0377	0.0116
SU1	4.0131	3.9954	4.0296	4.0386	4.0498	4.0798	4.0308	3.9421	4.0363
Ba	0.0000	0.0003	0.0038	0.0010	0.0021	0.0012	0.0004	0.0007	0.0008
Ca	0.6903	0.6820	0.4174	0.2508	0.5912	0.4108	0.6848	0.3888	0.3642
Na	0.2346	0.2890	0.2490	0.2720	0.2222	0.3264	0.1922	0.4347	0.2684
K	0.0541	0.0350	0.2819	0.4287	0.1176	0.1680	0.0699	0.1406	0.3198
SU2	0.9791	1.0063	0.9521	0.9525	0.9331	0.9064	0.9473	0.9647	0.9532
An	0.7051	0.6779	0.4401	0.2636	0.6350	0.4538	0.7231	0.4033	0.3824
Ab	0.2397	0.2873	0.2626	0.2858	0.2386	0.3606	0.2030	0.4509	0.2819
Kf	0.0552	0.0348	0.2973	0.4505	0.1263	0.1856	0.0739	0.1458	0.3357

Table 12.5:

Selected electron microprobe analyses of amphiboles from Margarita magmas. Oxides as weight percent. Structural formula on the basis of 22 (O).

Sample	6002	6002	6003	6003	6008	6008	6008	6008	6008	6008	6008	6008	6008
MP	4	5	49	50	11	12	17	19	27	28	30	31	43
SiO2	40.58	41.21	39.11	41.88	40.62	42.52	40.29	41.13	40.59	41.45	40.21	41.79	41.76
TiO2	3.08	2.73	3.35	2.43	2.96	2.18	2.86	2.69	2.15	2.09	3.31	3.35	1.78
Al2O3	11.93	11.51	12.48	10.40	10.67	8.75	11.08	10.15	10.39	9.93	11.30	10.19	9.85
FeO*	16.12	15.38	17.94	16.21	19.82	21.84	18.54	19.60	21.98	21.38	16.98	15.40	20.48
MnO	0.31	0.34	0.23	0.30	0.39	0.55	0.37	0.37	0.49	0.42	0.29	0.32	0.43
MgO	11.45	12.46	9.99	11.82	9.63	9.18	9.99	9.23	8.81	9.05	10.47	12.35	9.62
CaO	9.95	10.09	10.40	10.84	9.99	9.17	10.37	10.61	9.59	9.48	10.76	10.45	9.92
Na2O	2.57	2.48	2.21	2.10	2.14	1.99	2.29	2.09	2.16	2.11	2.33	2.24	2.08
K2O	0.25	0.24	0.29	0.24	0.34	0.29	0.38	0.45	0.32	0.30	0.37	0.27	0.32
F	0.00	0.00	0.11	0.19	0.24	0.38	0.17	0.21	0.21	0.43	0.21	0.17	0.12
SUM	96.43	96.91	96.16	96.46	96.96	97.07	96.51	96.66	96.91	96.89	96.34	96.78	96.55
H2O'	1.92	1.84	1.89	1.88	1.83	1.75	1.86	1.84	1.82	1.72	1.85	1.90	1.87
O#	0.06	0.13	0.05	0.09	0.13	0.21	0.09	0.11	0.13	0.22	0.10	0.09	0.09
SUMK	98.29	98.63	98.00	98.25	98.66	98.62	98.28	98.39	98.61	98.40	98.09	98.60	98.34
		98,28											
Si	6.1814	6.2353	6.0418	6.3748	6.2780	6.6024	6.2285	6.3757	6.3389	6.4514	6.1887	6.3322	6.4766
Alt	1.8186	1.7647	1.9582	1.6216	1.7220	1.3976	1.7715	1.6243	1.6611	1.5486	1.8113	1.6678	1.5234
SU1	8.0000	8.0000	8.0000	8.0000	8.0000	8.0000	8.0000	8.0000	8.0000	8.0000	8.0000	8.0000	8.0000
Alo	0.3237	0.2881	0.3146	0.2459	0.2223	0.2036	0.2470	0.2292	0.2516	0.2727	0.2386	0.1523	0.2778
Ti	0.3525	0.3103	0.3888	0.2783	0.3441	0.2545	0.3327	0.3138	0.2525	0.2442	0.3832	0.3814	0.2071
Fe	2.0536	1.9458	2.3177	2.0648	2.5618	2.8364	2.3972	2.5404	2.8696	2.7823	2.1852	1.9513	2.6561
Mn	0.0405	0.0441	0.0299	0.0386	0.0514	0.0726	0.0485	0.0482	0.0651	0.0554	0.0380	0.0405	0.0559
Mg	2.5998	2.8109	2.3009	2.6829	2.2189	2.1251	2.3011	2.1331	2.0495	2.0993	2.4019	2.7902	2.2238
SU2	5.3701	5.3992	5.3520	5.3104	5.3984	5.4923	5.3264	5.2647	5.4883	5.4539	5.2468	5.3155	5.4206
Na	0.7578	0.7279	0.6632	0.6200	0.6420	0.5985	0.6849	0.6277	0.6553	0.6374	0.6949	0.6573	0.6262
Ca	1.6247	1.6359	1.7220	1.7684	1.6538	1.5253	1.7178	1.7623	1.6038	1.5802	1.7744	1.6967	1.6491
K	0.0495	0.0454	0.0572	0.0468	0.0672	0.0568	0.0747	0.0887	0.0628	0.0604	0.0730	0.0518	0.0632
SU3	2.4321	2.4092	2.4424	2.4352	2.3630	2.1806	2.4775	2.4787	2.3219	2.2781	2.5423	2.4058	2.3385
F	0.0537	0.1426	0.0544	0.0933	0.1154	0.1854	0.0812	0.1006	0.1035	0.2103	0.1019	0.0811	0.0605
OH	1.9463	1.8574	1.9456	1.9067	1.8846	1.8146	1.9188	1.8994	1.8965	1.7897	1.8981	1.9189	1.9395

Table 12.5 (continued):

Sample	6008	6008	6050	6050	6050	6050	6050	6050	6050	6050	6050	6055	6055
MP	44	46	6	7	8	9	10	11	12	13	42	2	3
SiO2	40.43	49.58	41.99	42.36	41.90	42.75	42.58	42.94	40.75	41.29	41.21	42.15	41.45
TiO2	2.52	0.41	2.35	2.35	2.59	1.95	2.17	1.84	3.47	3.49	3.05	2.36	2.49
Al2O3	10.84	2.88	11.17	11.20	11.41	10.62	11.02	10.66	12.13	12.18	12.12	12.64	12.67
FeO*	19.37	21.97	16.40	15.99	15.67	13.85	13.92	13.94	12.08	12.19	13.24	12.69	11.95
MnO	0.43	0.82	0.26	0.29	0.34	0.19	0.19	0.22	0.10	0.14	0.13	0.13	0.13
MgO	10.16	10.21	11.61	11.55	11.51	12.99	12.82	12.63	13.11	13.03	12.61	13.74	13.52
CaO	9.70	10.45	10.61	10.57	10.84	10.92	11.05	10.93	11.39	11.38	11.20	11.48	11.02
Na2O	2.18	0.55	2.37	2.25	2.33	2.26	2.37	2.25	2.45	2.41	2.44	2.58	2.16
K2O	0.31	0.13	0.35	0.37	0.34	0.37	0.39	0.38	0.39	0.41	0.38	0.18	0.31
F	0.19	0.00	0.20	0.34	0.12	0.21	0.09	0.02	0.14	0.12	0.04	0.04	0.23
SUM	96.28	97.03	97.39	97.44	97.16	96.31	96.83	96.07	96.18	96.72	96.52	98.09	96.36
H2O'	1.84	1.97	1.89	1.83	1.93	1.89	1.96	1.98	1.93	1.95	1.97	2.02	1.89
O#	0.11	0.01	0.10	0.16	0.07	0.11	0.06	0.03	0.07	0.06	0.03	0.02	0.14
SUMK	98.01	98.99	99.18	99.11	99.02	98.09	98.72	98.02	98.04	98.61	98.47	100.09	98.12
Si	6.2735	7.5550	6.3386	6.3824	6.3185	6.4494	6.3911	6.4824	6.1335	6.1718	6.1934	6.2015	6.2092
Alt	1.7265	0.4450	1.6614	1.6176	1.6815	1.5506	1.6089	1.5176	1.8665	1.8282	1.8066	1.7985	1.7908
SU1	8.0000	8.0000	8.0000	8.0000	8.0000	8.0000	8.0000	8.0000	8.0000	8.0000	8.0000	8.0000	8.0000
Alo	0.2564	0.0730	0.3255	0.3704	0.3460	0.3373	0.3407	0.3795	0.2859	0.3169	0.3398	0.3929	0.4469
Ti	0.2942	0.0469	0.2663	0.2657	0.2939	0.2213	0.2448	0.2088	0.3928	0.3921	0.3451	0.2611	0.2805
Fe	2.5139	2.7992	2.0698	2.0151	1.9762	1.7473	1.7474	1.7597	1.5212	1.5238	1.6644	1.5608	1.4972
Mn	0.0570	0.1053	0.0335	0.0372	0.0430	0.0243	0.0245	0.0286	0.0123	0.0172	0.0171	0.0162	0.0166
Mg	2.3505	2.3193	2.6127	2.5948	2.5882	2.9203	2.8692	2.8423	2.9422	2.9033	2.8251	3.0123	3.0191
SU2	5.4719	5.3437	5.3077	5.2832	5.2473	5.2505	5.2266	5.2189	5.1544	5.1534	5.1914	5.2433	5.2603
Na	0.6553	0.1622	0.6923	0.6579	0.6802	0.6610	0.6884	0.6576	0.7141	0.6986	0.7113	0.7353	0.6277
Ca	1.6127	1.7055	1.7160	1.7062	1.7521	1.7644	1.7771	1.7673	1.8366	1.8218	1.8029	1.8103	1.7689
K	0.0615	0.0254	0.0670	0.0710	0.0664	0.0711	0.0755	0.0733	0.0742	0.0787	0.0724	0.0332	0.0601
SU3	2.3294	1.8932	2.4753	2.4350	2.4987	2.4965	2.5410	2.4983	2.6249	2.5991	2.5866	2.5788	2.4567
F	0.0954	0.0002	0.0957	0.1599	0.0575	0.0990	0.0405	0.0074	0.0644	0.0562	0.0212	0.0172	0.1087
OH	1.9046	1.9998	1.9043	1.8401	1.9425	1.9010	1.9595	1.9926	1.9356	1.9438	1.9788	1.9828	1.8913

Table 12.5 (continued):

Sample MP	6055 4	6055 5	6055 8	6055 10	6055 11	6055 12	6055 14	6055 15	6055 16	6055 17	6056 1	6056 2	6056 3
SiO2	41.42	41.38	44.09	41.35	41.32	42.55	42.43	43.30	42.36	41.60	40.58	40.58	39.87
TiO2	2.52	2.63	0.81	2.66	2.52	2.40	1.94	1.11	2.05	2.55	3.63	3.91	4.05
Al2O3	12.82	12.59	11.07	12.86	12.69	11.60	12.32	11.42	12.26	12.34	11.54	11.44	11.82
FeO*	12.05	12.09	13.16	11.53	11.78	12.00	12.55	13.55	12.60	11.91	17.62	16.62	16.54
MnO	0.18	0.16	0.35	0.16	0.22	0.14	0.26	0.18	0.19	0.12	0.31	0.29	0.28
MgO	13.41	13.44	14.15	13.73	13.79	13.69	13.63	13.58	13.46	13.62	10.01	10.50	10.94
CaO	11.71	11.64	10.83	11.38	11.58	11.46	11.38	11.05	11.36	11.63	10.72	10.61	10.64
Na2O	2.77	2.61	2.48	2.70	2.62	2.43	2.49	2.62	2.58	2.67	2.49	2.55	2.56
K2O	0.25	0.29	0.22	0.24	0.26	0.24	0.23	0.22	0.25	0.25	0.26	0.25	0.25
F	0.00	0.25	0.12	0.21	0.18	0.22	0.17	0.00	0.00	0.00	0.25	0.08	0.04
SUM	97.37	97.15	97.36	96.85	97.09	96.81	97.62	97.16	97.23	96.73	97.58	96.99	97.05
H2O'	2.02	1.89	1.97	1.91	1.93	1.91	1.95	2.02	2.02	2.01	1.85	1.93	1.95
O#	0.01	0.11	0.06	0.09	0.09	0.10	0.07	0.01	0.01	0.01	0.12	0.04	0.02
SUMK	99.38	98.93	99.26	98.67	98.94	98.61	99.49	99.17	99.25	98.73	99.31	98.88	98.98
Si	6.1475	6.1629	6.5216	6.1507	6.1460	6.3313	6.2747	6.4361	6.2797	6.1973	6.1797	6.1773	6.0669
Alt	1.8525	1.8371	1.4784	1.8493	1.8540	1.6687	1.7253	1.5639	1.7203	1.8027	1.8203	1.8227	1.9331
SU1	8.0000	8.0000	8.0000	8.0000	8.0000	8.0000	8.0000	8.0000	8.0000	8.0000	8.0000	8.0000	8.0000
Alo	0.3906	0.3721	0.4512	0.4048	0.3706	0.3659	0.4225	0.4361	0.4223	0.3641	0.2512	0.2306	0.1861
Ti	0.2807	0.2943	0.0902	0.2979	0.2819	0.2686	0.2160	0.1244	0.2284	0.2851	0.4162	0.4472	0.4632
Fe	1.4953	1.5059	1.6280	1.4337	1.4654	1.4930	1.5526	1.6843	1.5624	1.4837	2.2445	2.1159	2.1044
Mn	0.0227	0.0200	0.0439	0.0196	0.0274	0.0171	0.0332	0.0222	0.0242	0.0151	0.0395	0.0379	0.0360
Mg	2.9673	2.9826	3.1195	3.0438	3.0582	3.0372	3.0047	3.0079	2.9737	3.0245	2.2723	2.3825	2.4818
SU2	5.1567	5.1750	5.3328	5.1999	5.2035	5.1819	5.2289	5.2750	5.2109	5.1725	5.2237	5.2140	5.2715
Na	0.7972	0.7544	0.7119	0.7775	0.7569	0.6997	0.7153	0.7547	0.7419	0.7725	0.7361	0.7537	0.7544
Ca	1.8622	1.8565	1.7158	1.8128	1.8456	1.8278	1.8028	1.7597	1.8040	1.8559	1.7492	1.7311	1.7352
K	0.0464	0.0543	0.0417	0.0454	0.0495	0.0450	0.0441	0.0411	0.0467	0.0466	0.0499	0.0487	0.0478
SU3	2.7057	2.6652	2.4695	2.6357	2.6519	2.5725	2.5623	2.5555	2.5926	2.6750	2.5352	2.5334	2.5374
F	0.0002	0.1196	0.0554	0.1003	0.0824	0.1041	0.0811	0.0002	0.0002	0.0002	0.1205	0.0365	0.0170
OH	1.9998	1.8804	1.9446	1.8997	1.9176	1.8959	1.9189	1.9998	1.9998	1.9998	1.8795	1.9635	1.9830

Table 12.5 (continued):

Sample MP	6056 4	6056 5	6056 6	6056 11	6056 12	6058 50	6058 51	6058 52	6058 53	6058 54	6058 55	6058 56	6058 57
SiO2	41.20	40.76	44.75	40.51	39.81	46.09	45.88	46.49	45.53	47.21	48.05	47.53	45.16
TiO2	3.74	3.74	2.71	3.92	3.98	0.48	0.55	0.53	0.57	0.48	0.62	0.47	0.42
Al2O3	10.99	10.89	8.41	11.89	11.92	9.75	9.97	9.49	9.83	9.53	6.63	8.68	10.19
FeO*	16.53	15.99	15.18	17.70	16.44	9.97	10.29	10.23	10.63	10.28	11.75	10.37	10.28
MnO	0.31	0.32	0.28	0.30	0.29	0.09	0.16	0.14	0.17	0.19	0.22	0.20	0.19
MgO	11.22	10.91	11.87	10.25	10.79	15.94	15.69	15.65	15.85	15.47	15.76	15.50	15.73
CaO	10.27	10.37	11.01	10.52	10.49	10.95	10.91	11.01	10.82	11.62	11.15	11.33	11.28
Na2O	2.38	2.33	1.65	2.60	2.54	2.32	2.23	2.18	2.31	1.87	1.71	1.86	2.54
K2O	0.21	0.25	0.20	0.23	0.21	0.25	0.25	0.25	0.25	0.27	0.26	0.17	0.26
F	0.36	0.00	0.06	0.20	0.03	0.20	0.00	0.12	0.17	0.00	0.13	0.00	0.17
SUM	97.26	95.73	96.19	98.43	96.59	96.22	96.02	96.24	96.31	97.02	96.51	96.13	96.37
H2O'	1.81	1.95	1.96	1.89	1.95	1.95	2.04	1.99	1.95	2.06	1.97	2.05	1.95
O#	0.16	0.02	0.03	0.09	0.02	0.10	0.02	0.07	0.08	0.02	0.08	0.01	0.09
SUMK	98.91	97.67	98.12	100.23	98.52	98.06	98.04	98.21	98.26	99.07	98.47	98.17	98.32
Si	6.2467	6.2563	6.7448	6.1183	6.0799	6.7737	6.7496	6.8241	6.7134	6.8623	7.0801	6.9602	6.6626
Alt	1.7533	1.7437	1.2552	1.8817	1.9201	1.2263	1.2504	1.1759	1.2866	1.1377	0.9199	1.0398	1.3374
SU1	8.0000	8.0000	8.0000	8.0000	8.0000	8.0000	8.0000	8.0000	8.0000	8.0000	8.0000	8.0000	8.0000
Alo	0.2114	0.2255	0.2386	0.2350	0.2259	0.4623	0.4789	0.4663	0.4209	0.4949	0.2316	0.4574	0.4349
Ti	0.4266	0.4318	0.3073	0.4456	0.4566	0.0525	0.0606	0.0590	0.0634	0.0528	0.0687	0.0514	0.0464
Fe	2.0954	2.0519	1.9135	2.2356	2.0994	1.2258	1.2659	1.2557	1.3106	1.2499	1.4478	1.2703	1.2676
Mn	0.0400	0.0420	0.0362	0.0385	0.0376	0.0110	0.0202	0.0169	0.0218	0.0240	0.0269	0.0243	0.0239
Mg	2.5365	2.4967	2.6675	2.3064	2.4560	3.4914	3.4408	3.4251	3.4842	3.3510	3.4601	3.3834	3.4578
SU2	5.3099	5.2479	5.1631	5.2612	5.2755	5.2431	5.2665	5.2231	5.3009	5.1726	5.2353	5.1868	5.2306
Na	0.7005	0.6932	0.4815	0.7624	0.7519	0.6606	0.6347	0.6213	0.6604	0.5274	0.4893	0.5276	0.7263
Ca	1.6681	1.7049	1.7772	1.7025	1.7165	1.7244	1.7201	1.7317	1.7095	1.8103	1.7601	1.7771	1.7823
K	0.0406	0.0490	0.0385	0.0450	0.0411	0.0471	0.0466	0.0467	0.0470	0.0505	0.0492	0.0327	0.0489
SU3	2.4092	2.4471	2.2972	2.5099	2.5095	2.4322	2.4014	2.3997	2.4168	2.3882	2.2987	2.3374	2.5575
F	0.1712	0.0002	0.0294	0.0934	0.0147	0.0930	0.0002	0.0561	0.0776	0.0002	0.0622	0.0002	0.0778
OH	1.8288	1.9998	1.9706	1.9066	1.9853	1.9070	1.9998	1.9439	1.9224	1.9998	1.9378	1.9998	1.9222

Table 12.5 (continued):

Sample	6058	6058	6108	6109	6109	6109	6109	6504	6504	6504	6504	6504	6504
MP	60	61	50	129	139	141	146	2	47	48	50	53	54
SiO2	52.12	53.44	43.86	60.61	46.85	68.65	49.17	50.91	48.10	52.21	51.51	45.86	47.57
TiO2	0.34	0.25	2.27	0.04	0.56	0.02	0.10	0.30	1.12	0.50	0.60	1.40	1.08
Al2O3	3.71	2.81	14.47	18.49	13.18	14.65	24.94	4.05	15.66	21.04	18.86	11.67	15.95
FeO*	10.06	9.60	14.59	2.63	5.18	2.12	2.54	14.55	8.58	4.66	5.53	11.48	8.60
MnO	0.22	0.24	0.23	0.05	0.11	0.02	0.02	0.40	0.14	0.11	0.09	0.20	0.15
MgO	17.98	18.18	8.79	2.65	10.00	2.20	2.63	13.57	9.29	5.26	6.73	11.89	9.45
CaO	10.77	10.96	9.49	4.95	17.10	5.50	10.49	11.64	8.98	9.56	9.29	10.71	10.28
Na2O	0.85	0.60	3.02	3.76	1.13	2.13	3.12	0.53	3.47	4.49	4.30	2.13	2.40
K2O	0.18	0.11	0.33	0.68	0.16	0.14	1.39	0.17	0.30	0.23	0.19	0.31	0.85
F	0.00	0.12	0.25	0.19	0.09	0.09	0.19	0.00	0.12	0.04	0.00	0.01	0.00
SUM	96.41	96.37	97.61	94.18	94.56	95.66	94.81	96.40	96.10	98.47	97.37	96.03	96.67
H2O'	2.08	2.03	1.91	2.12	2.00	2.26	2.50	2.03	2.03	2.19	2.17	2.03	2.09
O#	0.02	0.05	0.11	0.08	0.04	0.04	0.08	0.00	0.06	0.02	0.00	0.01	0.01
SUMK	98.47	98.40	99.40	96.22	96.53	97.88	96.78	98.43	98.07	100.64	99.54	98.05	98.75
Si	7.5290	7.6840	6.4799	8.2193	6.8703	8.9497	6.8997	7.5336	6.9102	7.0992	7.1195	6.7674	6.8172
Alt	0.4710	0.3160	1.5201	0.0000	1.1297	0.0000	1.1003	0.4664	1.0898	0.9008	0.8805	1.2326	1.1828
SU1	8.0000	8.0000	8.0000	8.2193	8.0000	8.9497	8.0000	8.0000	8.0000	8.0000	8.0000	8.0000	8.0000
Alo	0.1604	0.1594	1.0001	2.9559	1.1487	2.2506	3.0241	0.2392	1.5619	2.4705	2.1909	0.7969	1.5119
Ti	0.0368	0.0274	0.2524	0.0043	0.0622	0.0022	0.0101	0.0329	0.1209	0.0508	0.0624	0.1553	0.1167
Fe	1.2152	1.1540	1.8022	0.2980	0.6357	0.2309	0.2984	1.8003	1.0310	0.5301	0.6391	1.4163	1.0311
Mn	0.0273	0.0290	0.0286	0.0057	0.0139	0.0023	0.0029	0.0499	0.0171	0.0121	0.0109	0.0249	0.0186
Mg	3.8706	3.8954	1.9360	0.5357	2.1848	0.4276	0.5497	2.9932	1.9890	1.0663	1.3868	2.6159	2.0191
SU2	5.3102	5.2653	5.0193	3.7995	4.0453	2.9135	3.8853	5.1154	4.7199	4.1298	4.2901	5.0092	4.6974
Na	0.2391	0.1681	0.8657	0.9895	0.3223	0.5374	0.8477	0.1526	0.9655	1.1842	1.1517	0.6083	0.6674
Ca	1.6662	1.6882	1.5028	0.7194	2.6719	0.7682	1.5764	1.8462	1.3821	1.3932	1.3760	1.6936	1.5782
K	0.0328	0.0195	0.0621	0.1182	0.0307	0.0230	0.2485	0.0324	0.0550	0.0392	0.0337	0.0587	0.1560
SU3	1.9381	1.8758	2.4306	1.8271	3.0249	1.3287	2.6726	2.0311	2.4026	2.6165	2.5613	2.3606	2.4017
F	0.0002	0.0557	0.1189	0.0829	0.0420	0.0373	0.0838	0.0002	0.0536	0.0176	0.0002	0.0037	0.0002
OH	1.9998	1.9443	1.8811	1.9171	1.9580	1.9627	1.9162	1.9998	1.9464	1.9824	1.9998	1.9963	1.9998

Table 12.6:

Electron microprobe analyses of sphenes from Margarita magmas. Oxides as weight percent.

Sample	6009	6009	6009	6009	6043	6043	6055	6055	6055	6055	6055	6055
MP	125	126	127	130	2	10	29	30	44	45	46	47
SiO2	31.86	31.67	30.39	30.65	29.71	30.11	30.79	30.19	30.69	30.88	30.43	30.50
TiO2	32.31	32.70	34.90	34.49	37.81	36.99	36.52	38.40	35.74	33.62	36.83	36.27
Al2O3	2.25	2.17	1.80	1.80	1.46	1.56	2.38	1.28	2.44	4.04	1.88	1.75
Cr2O3	0.13	0.16	0.22	0.09	0.00	0.10	0.03	0.00	0.00	0.00	0.03	0.05
FeO*	1.79	1.67	1.02	1.20	1.23	0.17	0.56	0.43	0.42	0.41	0.49	0.40
MnO	0.04	0.03	0.00	0.03	0.10	0.00	0.02	0.00	0.05	0.00	0.00	0.00
MgO	1.14	0.95	0.35	0.63	0.00	0.10	0.04	0.02	0.00	0.00	0.01	0.00
CaO	27.27	27.62	28.37	27.78	28.31	28.16	28.43	28.91	28.99	29.17	29.03	29.19
Na2O	0.01	0.01	0.00	0.02	0.00	0.00	0.00	0.00	0.00	0.01	0.00	0.00
K2O	0.04	0.04	0.04	0.03	0.04	0.03	0.08	0.10	0.00	0.01	0.02	0.04
F	0.00	0.00	0.00	0.00	0.00	0.39	0.00	0.25	0.00	0.00	0.11	0.25
Cl	0.00	0.00	0.00	0.00	0.01	0.00	0.00	0.00	0.02	0.00	0.04	0.00
SUM	97.53	97.70	97.65	97.64	99.28	97.88	99.12	99.95	98.36	98.29	99.22	98.78
H2O'	0.62	0.59	0.44	0.47	0.41	0.30	0.49	0.16	0.48	0.77	0.33	0.24
O#	0.13	0.04	0.11	0.18	0.00	0.16	0.00	0.10	0.00	0.00	0.05	0.11
SUMK	98.22	98.44	98.10	98.06	99.83	98.03	99.68	100.05	98.88	99.10	99.55	98.96
Si	1.0457	1.0394	1.0048	1.0152	0.9763	1.0021	1.0021	0.9840	1.0019	1.0013	0.9931	0.9996
Ti	0.7976	0.8069	0.8677	0.8593	0.9334	0.9257	0.8937	0.9411	0.8774	0.8196	0.9041	0.8938
Cr	0.0033	0.0042	0.0059	0.0023	0.0000	0.0004	0.0008	0.0000	0.0001	0.0000	0.0008	0.0014
Al	0.0870	0.0839	0.0700	0.0704	0.0564	0.0613	0.0911	0.0490	0.0939	0.1543	0.0722	0.0677
Fe	0.0492	0.0457	0.0281	0.0333	0.0337	0.0048	0.0153	0.0116	0.0115	0.0112	0.0135	0.0110
Mg	0.0556	0.0464	0.0173	0.0312	0.0000	0.0004	0.0017	0.0008	0.0000	0.0000	0.0003	0.0000
SU1	0.9926	0.9872	0.9889	0.9964	1.0234	0.9927	1.0026	1.0025	0.9829	0.9852	0.9908	0.9740
Ca	0.9591	0.9710	1.0047	0.9860	0.9956	1.0041	0.9914	1.0096	1.0138	1.0133	1.0153	1.0247
Na	0.0004	0.0009	0.0001	0.0016	0.0000	0.0000	0.0000	0.0002	0.0000	0.0006	0.0000	0.0000
K	0.0016	0.0016	0.0015	0.0014	0.0018	0.0011	0.0033	0.0040	0.0000	0.0003	0.0007	0.0017
Mn	0.0011	0.0009	0.0000	0.0010	0.0028	0.0000	0.0006	0.0000	0.0014	0.0000	0.0000	0.0000
SU2	0.9621	0.9744	1.0063	0.9900	1.0003	1.0053	0.9953	1.0138	1.0152	1.0141	1.0161	1.0264
F	0.0314	0.0089	0.0277	0.0443	0.0004	0.0409	0.0001	0.0255	0.0001	0.0001	0.0113	0.0262
Cl	0.0000	0.0000	0.0000	0.0000	0.0004	0.0000	0.0000	0.0000	0.0009	0.0000	0.0021	0.0000
OH	0.1362	0.1296	0.0981	0.1037	0.0900	0.0662	0.1063	0.0351	0.1044	0.1655	0.0724	0.0526
O*	4.8433	4.8468	4.8739	4.8743	4.9079	4.9269	4.8930	4.9211	4.8794	4.8206	4.8969	4.8925
SU3	4.9795	4.9764	4.9720	4.9778	4.9979	4.5531	4.9993	4.9817	4.9847	4.9862	4.9826	4.9712

Table 12.6 (continued):

Sample MP	6055 48	6055 49	6055 50	6108 30	6108 32	6108 33	6108 35	6504 21	6504 22	6504 23
SiO2	30.54	30.86	30.65	30.80	31.14	30.99	30.68	34.18	38.59	42.26
TiO2	35.50	33.25	34.14	32.77	31.99	32.25	32.52	29.63	26.17	23.39
Al2O3	2.63	4.13	3.13	3.20	3.54	3.43	3.62	4.05	5.50	6.76
Cr2O3	0.00	0.04	0.06	0.02	0.00	0.00	0.00	0.04	0.00	0.00
FeO*	0.52	0.63	1.64	1.94	2.01	1.86	1.88	1.25	1.43	1.26
MnO	0.03	0.03	0.08	0.02	0.03	0.06	0.04	0.00	0.01	0.00
MgO	0.00	0.07	0.53	0.67	0.31	0.26	0.03	2.36	2.18	2.06
CaO	28.99	29.28	28.15	27.57	27.95	28.10	28.24	24.62	22.15	22.12
Na2O	0.00	0.03	0.33	0.02	0.03	0.02	0.00	0.64	1.09	1.70
K2O	0.00	0.03	0.05	0.12	0.16	0.21	0.09	0.10	0.10	0.10
F	0.00	0.00	0.19	0.00	0.00	0.00	0.00	0.19	0.13	0.23
Cl	0.03	0.00	0.04	0.00	0.00	0.00	0.00	0.00	0.02	0.02
SUM	98.50	98.57	99.01	97.15	97.18	97.18	97.10	97.65	97.78	98.34
H2O'	0.52	0.81	0.66	0.81	0.88	0.84	0.87	0.78	1.08	1.24
O#	0.01	0.00	0.09	0.03	0.06	0.04	0.07	0.08	0.06	0.10
SUMK	99.07	99.45	99.76	97.99	98.12	98.06	98.04	98.48	98.96	99.61
Si	0.9974	0.9974	0.9939	1.0092	1.0188	1.0143	1.0069	1.1105	1.2439	1.3540
Ti	0.8720	0.8081	0.8326	0.8074	0.7871	0.7940	0.8026	0.7241	0.6342	0.5636
Cr	0.0000	0.0011	0.0015	0.0006	0.0000	0.0000	0.0000	0.0010	0.0000	0.0000
Al	0.1011	0.1572	0.1197	0.1234	0.1364	0.1324	0.1398	0.1550	0.2089	0.2554
Fe	0.0142	0.0171	0.0445	0.0531	0.0550	0.0509	0.0516	0.0339	0.0387	0.0339
Mg	0.0000	0.0032	0.0254	0.0328	0.0152	0.0127	0.0013	0.1142	0.1049	0.0983
SU1	0.9873	0.9867	1.0238	1.0173	0.9937	0.9900	0.9953	1.0281	0.9867	0.9512
Ca	1.0144	1.0138	0.9782	0.9678	0.9799	0.9853	0.9928	0.8571	0.7651	0.6906
Na	0.0000	0.0016	0.0206	0.0014	0.0020	0.0015	0.0000	0.0402	0.0683	0.1057
K	0.0000	0.0012	0.0019	0.0051	0.0069	0.0087	0.0037	0.0042	0.0040	0.0042
Mn	0.0009	0.0009	0.0022	0.0006	0.0008	0.0017	0.0012	0.0001	0.0002	0.0000
SU2	1.0154	1.0175	1.0030	0.9749	0.9896	0.9972	0.9978	0.9016	0.8377	0.8005
F	0.0001	0.0001	0.0191	0.0001	0.0002	0.0001	0.0001	0.0198	0.0130	0.0237
Cl	0.0019	0.0000	0.0021	0.0000	0.0001	0.0001	0.0000	0.0001	0.0013	0.0012
OH	0.1133	0.1743	0.1430	0.1766	0.1913	0.1833	0.1914	0.1690	0.2332	0.2643
O*	4.8694	4.8049	4.8254	4.8118	4.7990	4.7996	4.0858	4.8308	4.8741	4.9135
SU3	4.9846	4.9792	4.9896	4.9884	4.9904	4.9829	4.9972	5.0197	5.1217	5.2027

Table 12.7:

Electron microprobe analyses of ilmenites from Margarita magmas. Oxides as weight percent. Structural formula on the basis of 6(O).

Sample	6037	6037	6037	6037	6037
MP	1	23	24	25	26
SiO2	0.45	0.07	1.65	0.85	0.01
TiO2	50.47	50.27	50.37	50.41	50.72
Al2O3	0.13	0.01	0.56	0.18	0.05
Cr2O3	0.07	0.13	0.02	0.08	0.10
FeO*	43.51	45.62	44.07	44.43	45.38
MnO	2.20	2.15	2.14	2.20	2.22
MgO	0.17	0.10	0.09	0.12	0.16
CaO	0.19	0.14	0.43	0.45	0.12
SUMK	97.21	98.53	99.60	98.85	98.75
Fe	0.9424	0.9846	0.9245	0.9467	0.9758
Mn	0.0484	0.0471	0.0455	0.0475	0.0483
Mg	0.0067	0.0038	0.0032	0.0047	0.0059
Ca	0.0054	0.0038	0.0117	0.0123	0.0032
Ba	0.0000	0.0000	0.0000	0.0000	0.0000
SU1	1.0028	1.0392	0.9849	1.0112	1.0332
Ti	0.9830	0.9757	0.9501	0.9659	0.9808
Cr	0.0013	0.0026	0.0004	0.0016	0.0021
Al	0.0040	0.0004	0.0166	0.0054	0.0015
Si	0.0117	0.0019	0.0413	0.0216	0.0003
SU2	1.0000	0.9806	1.0084	0.9945	0.9846

Table 12.8

Electron microprobe analyses of muscovites from Margarita magmas. Oxides as weight percent.
Structural formula on the basis of 22 (O).

Sample	6009	6009	6009	6009	6009	6009	6009	6050	6050	6050	6050	6050	6050
MP	63	67	68	70	72	79	84	33	34	35	36	37	38
SiO2	46.37	46.10	46.23	49.93	48.60	49.67	49.99	45.26	46.05	48.09	48.18	49.22	46.84
TiO2	0.04	0.02	0.02	0.04	0.00	0.02	0.06	0.02	0.02	0.04	0.02	0.05	0.04
Al2O3	33.32	33.33	32.64	30.03	31.99	31.25	30.72	33.64	37.06	32.29	32.11	32.34	33.14
Cr2O3	0.02	0.01	0.00	0.02	0.01	0.04	0.01	0.02	0.00	0.00	0.00	0.03	0.02
FeO*	1.16	1.50	1.71	1.10	1.10	1.14	0.96	1.85	0.71	1.13	1.40	1.33	1.66
MnO	0.01	0.00	0.00	0.03	0.03	0.00	0.00	0.03	0.04	0.02	0.01	0.01	0.00
MgO	0.85	0.82	0.63	0.88	0.45	0.59	0.61	2.49	0.31	1.60	1.77	1.93	1.52
CaO	0.05	0.05	0.24	0.74	0.42	0.57	0.79	0.03	0.01	0.00	0.39	0.41	0.00
BaO	0.59	0.39	0.75	0.06	0.30	0.34	0.31	0.00	0.00	0.06	0.00	0.14	0.01
Na2O	0.32	0.31	0.96	1.87	1.47	2.47	2.23	0.15	0.14	0.17	0.57	0.55	0.14
K2O	10.65	10.74	10.13	8.53	9.08	8.49	8.41	10.24	10.96	11.28	10.39	9.33	10.86
Cl	0.00	0.00	0.00	0.00	0.03	0.00	0.00	0.00	0.00	0.01	0.00	0.01	0.00
F	0.09	0.17	0.00	0.00	0.00	0.03	0.00	0.00	0.15	0.00	0.12	0.00	0.00
SUM	93.84	93.80	93.80	93.56	93.72	94.92	94.33	93.76	95.47	94.72	94.96	95.35	94.23
H2O'	4.36	4.32	4.38	4.46	4.44	4.49	4.49	4.42	4.45	4.47	4.43	4.54	4.44
O#	0.04	0.07	0.00	0.00	0.01	0.01	0.00	0.00	0.06	0.00	0.05	0.00	0.00
SUMK	98.17	98.05	98.18	98.02	98.15	99.39	98.82	98.18	99.86	99.19	99.33	99.89	98.67
Si	6.3128	6.2906	6.3231	6.7153	6.5470	6.6128	6.6756	6.1455	6.1077	6.4489	6.4421	6.4970	6.3204
Alt	1.6872	1.7094	1.6769	1.2847	1.4530	1.3872	1.3244	1.8545	1.8923	1.5511	1.5579	1.5030	1.6796
SUt	8.0000	8.0000	8.0000	8.0000	8.0000	8.0000	8.0000	8.0000	8.0000	8.0000	8.0000	8.0000	8.0000
Alo	3.6589	3.6498	3.5856	3.4756	3.6259	3.5161	3.5115	3.5284	3.9016	3.5523	3.5018	3.5278	3.5906
Cr	0.0016	0.0006	0.0000	0.0021	0.0011	0.0041	0.0010	0.0019	0.0000	0.0005	0.0000	0.0035	0.0019
Ti	0.0038	0.0021	0.0017	0.0036	0.0000	0.0023	0.0057	0.0017	0.0023	0.0037	0.0017	0.0051	0.0039
Fe	0.1316	0.1710	0.1956	0.1236	0.1241	0.1272	0.1071	0.2098	0.0790	0.1269	0.1566	0.1473	0.1875
Mn	0.0007	0.0003	0.0000	0.0039	0.0031	0.0002	0.0000	0.0040	0.0049	0.0017	0.0017	0.0016	0.0000
Mg	0.1716	0.1662	0.1277	0.1769	0.0907	0.1178	0.1215	0.5046	0.0618	0.3205	0.3526	0.3787	0.3059
SUo	3.9683	3.9900	3.9107	3.7857	3.8449	3.7676	3.7469	4.2503	4.0497	4.0056	4.0145	4.0639	4.0897
Ca	0.0055	0.0075	0.0355	0.1063	0.0602	0.0816	0.1130	0.0042	0.0009	0.0000	0.0560	0.0577	0.0000
Ba	0.0314	0.0209	0.0399	0.0030	0.0157	0.0178	0.0164	0.0000	0.0000	0.0034	0.0000	0.0072	0.0004
Na	0.0847	0.0809	0.2542	0.4876	0.3841	0.6375	0.5766	0.0391	0.0352	0.0451	0.1475	0.1417	0.0371
K	1.8495	1.8695	1.7677	1.4642	1.5605	1.4414	1.4331	1.7738	1.8540	1.9304	1.7721	1.5705	1.8702
SUz	1.9711	1.9787	2.0973	2.0612	2.0205	2.1786	2.1392	1.8172	1.8901	1.9789	1.9757	1.7771	1.9077
Cl	0.0000	0.0000	0.0000	0.0002	0.0118	0.0000	0.0000	0.0000	0.0000	0.0018	0.0000	0.0017	0.0008
F	0.0379	0.0716	0.0002	0.0000	0.0000	0.0137	0.0000	0.0002	0.0623	0.0002	0.0518	0.0002	0.0002
OH	3.9621	3.9284	3.9998	3.9998	3.9882	3.9863	3.9998	3.9998	3.9377	3.9980	3.9481	3.9981	3.9991

Table 12.8 (continued):

Sample MP	6050 39	6050 40	6050 41	6050 58	6050 59	6050 62	6050 63	6050 64	6057 37	6057 38	6057 39	6057 40	6057 41
SiO2	46.15	45.48	45.28	47.24	51.24	47.49	52.91	48.21	47.12	57.01	47.99	47.30	47.36
TiO2	0.03	0.04	0.03	0.05	0.01	0.00	0.02	0.04	0.01	0.01	0.09	0.02	0.03
Al2O3	35.73	37.75	37.18	32.52	30.18	33.51	29.83	31.93	31.09	26.47	30.40	30.88	31.15
Cr2O3	0.00	0.00	0.00	0.06	0.01	0.00	0.00	0.00	0.01	0.00	0.05	0.02	0.00
FeO*	1.10	0.57	0.68	1.44	0.89	1.16	0.97	1.26	2.77	0.77	2.31	2.72	2.79
MnO	0.02	0.00	0.00	0.05	0.00	0.00	0.02	0.01	0.00	0.03	0.04	0.00	0.00
MgO	0.60	0.16	0.24	2.13	1.12	1.37	0.78	1.46	1.94	0.72	1.82	2.05	2.15
CaO	0.00	0.02	0.00	0.02	3.30	0.78	3.66	0.03	0.00	2.62	0.46	0.00	0.00
BaO	0.00	0.00	0.00	0.13	0.03	0.00	0.02	0.13	0.15	0.02	0.02	0.00	0.07
Na2O	0.23	0.23	0.21	0.25	2.57	0.43	3.39	0.36	0.12	5.80	0.78	0.23	0.22
K2O	10.45	10.79	10.93	10.56	6.96	10.14	5.26	10.51	10.98	3.62	9.89	10.83	10.25
Cl	0.03	0.01	0.01	0.03	0.02	0.01	0.04	0.03	0.02	0.01	0.08	0.00	0.01
F	0.22	0.14	0.00	0.00	0.20	0.00	0.00	0.00	0.00	0.00	0.17	0.00	0.00
SUM	94.58	95.19	94.57	94.47	96.53	94.89	96.93	93.97	94.19	97.11	94.10	94.13	94.04
H2O'	4.36	4.44	4.48	4.45	4.50	4.49	4.66	4.44	4.40	4.72	4.26	4.35	4.36
O#	0.10	0.06	0.00	0.01	0.09	0.00	0.01	0.01	0.00	0.00	0.09	0.00	0.00
SUMK	98.84	99.57	99.05	98.91	100.94	99.38	101.58	98.41	98.59	101.83	98.27	98.48	98.40
Si	6.1835	6.0434	6.0588	6.3549	6.6811	6.3356	6.8019	6.4958	6.4161	7.2364	6.4557	6.3767	6.3693
Alt	1.8165	1.9566	1.9412	1.6451	1.3189	1.6644	1.1981	1.5042	1.5839	0.7636	1.5443	1.6233	1.6307
SUt	8.0000	8.0000	8.0000	8.0000	8.0000	8.0000	8.0000	8.0000	8.0000	8.0000	8.0000	8.0000	8.0000
Alo	3.8245	3.9554	3.9225	3.5102	3.3186	3.6036	3.3213	3.5662	3.4046	3.1964	3.3787	3.3893	3.4136
Cr	0.0000	0.0000	0.0000	0.0059	0.0009	0.0000	0.0000	0.0000	0.0007	0.0000	0.0050	0.0020	0.0000
Ti	0.0032	0.0042	0.0030	0.0051	0.0013	0.0000	0.0016	0.0044	0.0006	0.0013	0.0091	0.0024	0.0032
Fe	0.1238	0.0632	0.0760	0.1625	0.0970	0.1293	0.1040	0.1425	0.3150	0.0822	0.2656	0.3137	0.3209
Mn	0.0027	0.0003	0.0000	0.0054	0.0000	0.0000	0.0020	0.0016	0.0000	0.0036	0.0049	0.0000	0.0006
Mg	0.1201	0.0312	0.0483	0.4263	0.2178	0.2721	0.1498	0.2933	0.3941	0.1362	0.3735	0.4199	0.4400
SUo	4.0743	4.0542	4.0498	4.1153	3.6355	4.0051	3.5786	4.0080	4.1151	3.4196	4.0368	4.1273	4.1783
Ca	0.0000	0.0028	0.0000	0.0029	0.4610	0.1108	0.5044	0.0041	0.0000	0.3559	0.0677	0.0000	0.0000
Ba	0.0000	0.0000	0.0000	0.0066	0.0015	0.0000	0.0012	0.0069	0.0079	0.0011	0.0009	0.0000	0.0040
Na	0.0585	0.0587	0.0557	0.0650	0.6507	0.1114	0.8441	0.0932	0.0322	1.4286	0.2069	0.0626	0.0581
K	1.7867	1.8282	1.8656	1.8122	1.1582	1.7259	0.8630	1.8062	1.9067	0.5863	1.7330	1.9031	1.7961
SUz	1.8452	1.8898	1.9213	1.8868	2.2714	1.9481	2.2128	1.9104	1.9468	2.3720	2.0085	1.9657	1.8583
Cl	0.0071	0.0029	0.0025	0.0062	0.0052	0.0031	0.0083	0.0058	0.0038	0.0017	0.0193	0.0005	0.0023
F	0.0945	0.0601	0.0002	0.0002	0.0807	0.0002	0.0002	0.0002	0.0002	0.0002	0.0729	0.0002	0.0002
OH	3.8984	3.9369	3.9973	3.9936	3.9142	3.9967	3.9916	3.9941	3.9960	3.9981	3.9078	3.9993	3.9975

Table 12.9:

Electron microprobe analyses of chlorites from Margarita magmas. Oxides as weight percent.
Structural formula on the basis of 28 (O).

Sample	6003	6003	6008	6008	6013	6013	6013	6013	6013	6050	6050	6050
MP	43	44	66	82	18	25	26	28	29	18	19	20
SiO2	29.75	29.70	31.69	29.99	36.16	32.24	33.58	34.07	32.26	27.88	27.97	27.86
Al2O3	17.54	16.98	17.33	18.40	17.57	19.80	20.61	20.94	19.08	20.28	20.23	20.38
MgO	24.43	23.59	22.29	21.51	19.63	22.73	22.09	21.11	23.11	23.07	23.26	23.18
FeO*	13.68	13.73	14.5	15.19	11.96	12.03	11.94	11.55	12.44	13.28	13.69	14.18
MnO	0.20	0.24	0.24	0.18	0.21	0.15	0.14	0.18	0.21	0.20	0.18	0.21
TiO2	0.00	0.00	0.02	0.01	0.07	0.02	0.05	0.02	0.05	0.02	0.01	0.00
CaO	0.15	0.13	0.15	0.10	2.07	0.08	0.15	0.22	0.24	0.04	0.02	0.03
Na2O	0.10	0.14	0.01	0.08	0.30	0.04	0.08	0.07	0.05	0.01	0.02	0.03
K2O	0.02	0.04	0.03	0.01	0.04	0.03	0.03	0.05	0.04	0.03	0.06	0.01
F	0.00	0.10	0.09	0.23	0.15	0.00	0.21	0.00	0.00	0.09	0.03	0.00
Cl	0.02	0.00	0.00	0.01	0.02	0.00	0.04	0.01	0.00	0.01	0.00	0.02
SUM	86.74	85.59	86.54	86.30	88.28	87.16	89.00	88.29	87.77	85.44	85.78	86.41
H2O'	11.97	11.74	11.96	11.72	12.39	12.31	12.48	12.58	12.32	11.77	11.84	11.89
O#	0.00	0.04	0.04	0.10	0.07	0.00	0.10	0.00	0.00	0.04	0.01	0.00
SUMK	98.70	97.29	98.47	97.93	100.60	99.47	101.38	100.86	100.09	97.17	97.61	98.30
Si	5.9619	6.0439	6.3317	6.0780	6.9587	6.2804	6.3982	6.4971	6.2778	5.6607	5.6612	5.6169
Alt	2.0381	1.9561	1.6683	1.9220	1.0413	1.7196	1.6018	1.5029	1.7222	2.3393	2.3388	2.3831
SUt	8.0000	8.0000	8.0000	8.0000	8.0000	8.0000	8.0000	8.0000	8.0000	8.0000	8.0000	8.0000
Alo	2.1034	2.1156	2.4133	2.4732	2.9427	2.8269	3.0269	3.2034	2.6556	2.5139	2.4858	2.4609
Ti	0.0000	0.0000	0.0036	0.0011	0.0102	0.0023	0.0073	0.0035	0.0074	0.0027	0.0015	0.0000
Fe	2.2930	2.3355	2.3475	2.5752	1.9249	1.9589	1.9028	1.8425	2.0244	2.2539	2.3162	2.3916
Mn	0.0332	0.0410	0.0398	0.0315	0.0341	0.0255	0.0222	0.0283	0.0350	0.0352	0.0301	0.0361
Mg	7.2977	7.1555	6.6395	6.4969	5.6293	6.5985	6.2717	6.0000	6.7032	6.9813	7.0161	6.9665
Ca	0.0324	0.0283	0.0321	0.0225	0.4276	0.0169	0.0297	0.0456	0.0493	0.0078	0.0036	0.0063
K	0.0052	0.0101	0.0077	0.0035	0.0104	0.0065	0.0076	0.0112	0.0105	0.0073	0.0156	0.0021
Na	0.0404	0.0541	0.0058	0.0312	0.1125	0.0138	0.0277	0.0248	0.0194	0.0027	0.0059	0.0101
SUo	11.8054	11.7402	11.4893	11.6352	11.9170	11.4493	11.2959	11.1592	11.5048	11.8048	11.8749	11.8737
F	0.0003	0.0628	0.0583	0.1456	0.0918	0.0002	0.1283	0.0002	0.0002	0.0579	0.0196	0.0003
Cl	0.0058	0.0010	0.0000	0.0038	0.0068	0.0005	0.0128	0.0037	0.0000	0.0020	0.0007	0.0052
OH	15.9940	15.9362	15.9417	15.8507	15.9015	15.9992	15.8589	15.9960	15.9997	15.9401	15.9796	15.9945
O*	28.0000	28.0000	28.0000	28.0000	28.0000	28.0000	28.0000	28.0000	28.0000	28.0000	28.0000	28.0000

Table 12.9 (continued):

Sample	6050	6055	6055	6057	6057	6057	6057	6057	6057	6057	6057
MP	21	73	75	14	16	18	19	22	23	89	90
SiO2	27.84	29.45	30.03	27.03	28.55	35.06	50.06	53.34	49.85	26.10	27.33
Al2O3	20.24	19.02	19.40	20.68	21.08	26.87	23.87	24.85	29.33	21.78	21.01
MgO	22.98	23.39	22.93	18.75	17.54	11.21	1.28	0.42	2.38	18.00	17.58
FeO*	13.27	13.32	13.62	18.86	18.72	10.91	2.04	1.20	2.56	20.29	19.24
MnO	0.28	0.26	0.16	0.24	0.23	0.11	0.03	0.04	0.00	0.30	0.22
TiO2	0.02	0.00	0.00	0.00	0.03	0.01	0.09	0.04	0.06	0.01	0.01
CaO	0.04	0.07	0.01	0.04	0.28	0.06	2.15	3.14	0.22	0.06	0.11
Na2O	0.00	0.13	0.11	0.07	0.42	0.29	3.90	5.42	0.60	0.01	0.14
K2O	0.03	0.04	0.08	0.03	0.05	0.14	0.35	0.18	0.23	0.02	0.32
F	0.02	0.19	0.08	0.00	0.00	0.01	0.00	0.09	0.00	0.00	0.00
Cl	0.02	0.02	0.04	0.02	0.05	0.06	0.27	0.09	0.18	0.01	0.02
SUM	85.31	85.91	86.69	85.84	86.95	84.74	84.11	88.88	85.53	86.60	86.00
H2O'	11.79	11.81	11.99	11.54	11.73	12.31	12.99	13.74	13.52	11.55	11.54
O#	0.01	0.08	0.04	0.00	0.01	0.02	0.06	0.06	0.04	0.00	0.00
SUMK	97.09	97.64	98.64	97.37	98.67	97.04	97.04	102.55	99.01	98.15	97.54
Si	5.6595	5.9341	5.9867	5.6165	5.8304	6.8175	9.1962	9.2707	8.8138	5.4195	5.6786
Alt	2.3405	2.0659	2.0133	2.3835	2.1696	1.1825	0.0000	0.0000	0.0000	2.5805	2.3214
SUt	8.0000	8.0000	8.0000	8.0000	8.0000	8.0000	9.1962	9.2707	8.8138	8.0000	8.0000
Alo	2.5087	2.4506	2.5435	2.6813	2.9046	4.9773	5.1682	5.0896	6.1123	2.7496	2.8251
Ti	0.0024	0.0000	0.0000	0.0000	0.0040	0.0008	0.0118	0.0049	0.0083	0.0017	0.0019
Fe	2.2564	2.2434	2.2696	3.2766	3.1969	1.7749	0.3130	0.1746	0.3789	3.5227	3.3426
Mn	0.0481	0.0443	0.0264	0.0421	0.0401	0.0189	0.0051	0.0065	0.0000	0.0525	0.0391
Mg	6.9622	7.0228	6.8142	5.8072	5.3377	3.2501	0.3497	0.1093	0.6280	5.5692	5.4451
Ca	0.0084	0.0157	0.0027	0.0087	0.0613	0.0124	0.4241	0.5853	0.0420	0.0131	0.0249
K	0.0078	0.0103	0.0211	0.0083	0.0129	0.0346	0.0813	0.0400	0.0510	0.0057	0.0846
Na	0.0002	0.0503	0.0412	0.0266	0.1653	0.1106	1.3886	1.8268	0.2058	0.0053	0.0579
SUo	11.7942	11.8375	11.7187	11.8508	11.7227	10.1795	7.7417	7.8371	7.4263	11.9198	11.8214
F	0.0116	0.1198	0.0487	0.0003	0.0003	0.0050	0.0003	0.0495	0.0003	0.0003	0.0003
Cl	0.0060	0.0072	0.0120	0.0075	0.0172	0.0211	0.0837	0.0279	0.0551	0.0036	0.0053
OH	15.9824	15.8731	15.9394	15.9922	15.9825	15.9739	15.9160	15.9226	15.9446	15.9961	15.9945
O*	28.0000	28.0000	28.0000	28.0000	28.0000	28.0000	28.0000	28.0000	28.0000	28.0000	28.0000

Table 12.10:

Electron microprobe analyses of epidotes from Margarita magmas. Oxides as weight percent. Structural formula on the basis of 12.5 (O).

Sample	6003	6009	6009	6009	6009	6009	6057	6057	6057	6057	6057	6057	6057
MP	11	6	7	116	117	118	8	9	10	57	58	60	61
SiO2	36.67	37.00	37.42	37.87	37.62	37.78	37.98	38.12	37.56	36.46	36.62	36.60	36.66
TiO2	0.14	0.33	0.10	0.14	0.12	0.08	0.04	0.03	0.00	0.10	0.08	0.10	0.12
Al2O3	21.34	22.53	23.76	26.85	26.66	27.24	25.09	24.41	25.39	23.67	24.06	23.72	23.47
Fe2O3*	14.63	13.20	11.93	6.76	6.55	6.32	9.57	11.04	10.64	12.07	12.09	12.66	13.54
MnO	0.10	0.46	0.04	0.09	0.08	0.09	0.06	0.01	0.06	0.07	0.12	0.13	0.18
MgO	0.47	0.30	0.11	0.05	0.29	0.11	0.07	0.06	0.02	0.09	0.06	0.07	0.08
CaO	22.34	22.24	23.52	23.70	23.34	23.95	22.89	23.09	23.96	22.84	22.95	23.21	23.17
H2O'	3.67	3.70	3.74	3.79	3.75	3.79	3.74	3.76	3.78	3.68	3.70	3.71	3.73
SUMK	99.67	100.11	100.94	100.60	99.41	100.48	99.67	100.67	101.51	99.06	99.74	100.45	100.97
Si	2.9996	3.0012	2.9982	2.9969	3.0041	2.9905	3.0439	3.0391	2.9759	2.9738	2.9662	2.9559	2.9500
Alt	0.0004	0.0000	0.0018	0.0031	0.0000	0.0095	0.0000	0.0000	0.0241	0.0262	0.0338	0.0441	0.0500
SU1	3.0000	3.0012	3.0000	3.0000	3.0041	3.0000	3.0439	3.0391	3.0000	3.0000	3.0000	3.0000	3.0000
Alo	2.0568	2.1537	2.2414	2.5012	2.5097	2.5317	2.3700	2.2933	2.3465	2.2490	2.2627	2.2139	2.1754
Fe3+	0.9004	0.8057	0.7194	0.4024	0.3937	0.3766	0.5774	0.6620	0.6341	0.7411	0.7371	0.7693	0.8200
SU2	2.9572	2.9593	2.9607	2.9035	2.9034	2.9083	2.9473	2.9554	2.9806	2.9901	2.9998	2.9832	2.9954
Ti	0.0084	0.0203	0.0057	0.0084	0.0073	0.0049	0.0022	0.0020	0.0000	0.0058	0.0052	0.0063	0.0072
Mn	0.0071	0.0313	0.0028	0.0058	0.0054	0.0061	0.0041	0.0007	0.0042	0.0051	0.0083	0.0090	0.0119
Mg	0.0576	0.0364	0.0126	0.0055	0.0345	0.0133	0.0089	0.0071	0.0020	0.0103	0.0075	0.0085	0.0095
Ca	1.9576	1.9326	2.0188	2.0097	1.9969	2.0306	1.9657	1.9716	2.0335	1.9963	1.9912	2.0081	1.9974
SU3	2.0307	2.0206	2.0400	2.0294	2.0441	2.0549	1.9808	1.9815	2.0396	2.0175	2.0121	2.0319	2.0259
OH	2.0000	2.0000	2.0000	2.0000	2.0000	2.0000	2.0000	2.0000	2.0000	2.0000	2.0000	2.0000	2.0000
O*	12.5000	12.5000	12.5000	12.5000	12.5000	12.5000	12.5000	12.5000	12.5000	12.5000	12.5000	12.5000	12.5000

Table 12.10 (continued):

Sample MP	6057 62	6057 63	6057 64	6057 65	6057 66	6057 67	6057 68	6057 69	6057 70	6057 71	6057 109	6057 113	6057 116
SiO2	37.23	37.16	37.04	36.92	38.40	36.37	36.24	36.63	36.86	36.96	37.27	38.04	38.71
TiO2	0.10	0.13	0.11	0.07	0.15	0.12	0.08	0.13	0.10	0.12	0.05	0.09	0.03
Al2O3	23.69	23.39	23.35	22.91	20.26	22.69	22.99	23.02	23.34	23.48	27.47	28.61	31.67
Fe2O3*	13.33	13.39	13.26	13.49	14.07	13.75	13.76	13.54	13.25	12.84	8.23	5.76	2.32
MnO	0.16	0.18	0.07	0.16	0.19	0.14	0.17	0.13	0.20	0.01	0.31	0.09	0.06
MgO	0.09	1.22	0.10	0.35	1.64	0.06	1.95	0.05	0.12	0.04	0.05	0.03	0.04
CaO	22.96	21.19	23.27	21.89	20.71	22.52	20.79	22.89	22.80	23.31	23.28	23.85	24.61
H2O'	3.75	3.74	3.73	3.69	3.68	3.67	3.70	3.70	3.71	3.72	3.78	3.81	3.90
SUMK	101.46	100.63	100.98	99.73	99.28	99.46	99.77	100.42	100.49	100.68	100.45	100.34	101.46
Si	2.9754	2.9819	2.9755	2.9993	3.1258	2.9726	2.9392	2.9681	2.9748	2.9772	2.9538	2.9918	2.9753
Alt	0.0246	0.0181	0.0245	0.0007	0.0000	0.0274	0.0608	0.0319	0.0252	0.0228	0.0462	0.0082	0.0247
SU1	3.0000	3.0000	3.0000	3.0000	3.1258	3.0000	3.0000	3.0000	3.0000	3.0000	3.0000	3.0000	3.0000
Alo	2.2068	2.1942	2.1863	2.1927	1.9438	2.1582	2.1364	2.1663	2.1948	2.2065	2.5197	2.6432	2.8447
Fe3+	0.8020	0.8085	0.8014	0.8246	0.8617	0.8453	0.8394	0.8254	0.8050	0.7781	0.4905	0.3411	0.1341
SU2	3.0089	3.0026	2.9877	3.0173	2.8055	3.0035	2.9758	2.9916	2.9997	2.9846	3.0102	2.9843	2.9788
Ti	0.0058	0.0078	0.0065	0.0044	0.0093	0.0072	0.0048	0.0077	0.0062	0.0075	0.0031	0.0052	0.0016
Mn	0.0112	0.0120	0.0051	0.0110	0.0133	0.0100	0.0114	0.0092	0.0134	0.0010	0.0210	0.0060	0.0040
Mg	0.0102	0.1459	0.0118	0.0420	0.1990	0.0075	0.2362	0.0061	0.0140	0.0043	0.0057	0.0031	0.0047
Ca	1.9664	1.8218	2.0024	1.9054	1.8056	1.9715	1.8059	1.9874	1.9720	2.0117	1.9768	2.0093	2.0270
SU3	1.9935	1.9875	2.0258	1.9628	2.0271	1.9962	2.0581	2.0105	2.0056	2.0245	2.0066	2.0236	2.0373
OH	2.0000	2.0000	2.0000	2.0000	2.0000	2.0000	2.0000	2.0000	2.0000	2.0000	2.0000	2.0000	2.0000
O*	12.5000	12.5000	12.5000	12.5000	12.5000	12.5000	12.5000	12.5000	12.5000	12.5000	12.5000	12.5000	12.5000

Table 12.11:

Electron microprobe analyses of hematites from Margarita magmas. Oxides as weight percent.

Sample	6003	6003	6037	6037	6057	6057	6057	6057	6109	6109	6109
MP	33	34	2	12	128	129	132	133	45	46	47
SiO2	4.61	4.57	4.14	4.37	5.78	21.20	16.00	3.89	7.85	5.30	5.81
TiO2	0.00	0.02	0.35	0.20	0.02	0.18	0.33	0.03	0.00	0.00	0.00
Al2O3	0.03	0.00	1.00	0.01	0.04	8.45	4.64	0.00	1.72	0.24	0.14
Cr2O3	0.00	0.02	0.00	0.03	0.00	0.01	0.00	0.00	0.12	0.02	0.03
FeO*	79.68	78.36	84.10	82.54	82.30	57.97	65.92	81.24	75.37	84.19	81.14
MnO	0.01	0.00	0.01	0.06	0.04	0.00	0.04	0.04	0.08	0.01	0.07
NiO	0.07	0.08	n.d.	n.d.	0.38	0.00	0.00	0.00	n.d.	n.d.	n.d.
MgO	0.45	0.37	0.46	0.66	0.00	1.31	0.77	0.87	3.37	0.80	1.04
CaO	0.18	0.19	0.35	0.34	0.31	0.78	0.64	0.15	0.13	0.11	0.12
Fe2O3	88.52	87.06	93.42	91.07	92.21	66.84	74.49	92.03	83.74	93.54	90.15
SUM	90.93	89.35	89.90	88.47	89.50	91.45	89.77	86.39	89.79	91.49	89.16
SUMK	99.77	98.05	99.23	97.64	99.41	100.32	98.33	97.19	98.16	100.83	98.16
Fe	1.9792	1.9832	1.9704	1.9661	1.9813	1.6026	1.7777	1.9609	1.7973	1.9587	1.9490
Ti	0.0000	0.0005	0.0073	0.0043	0.0005	0.0045	0.0081	0.0007	0.0000	0.0000	0.0001
Al	0.0010	0.0000	0.0032	0.0004	0.0013	0.3289	0.1766	0.0001	0.0579	0.0077	0.0046
Mn	0.0001	0.0000	0.0002	0.0012	0.0010	0.0000	0.0011	0.0010	0.0019	0.0003	0.0018
Mg	0.0200	0.0165	0.0192	0.0281	0.0161	0.0642	0.0367	0.0376	0.1431	0.0335	0.0447
SU	2.0000	2.0000	2.0000	2.0000	2.0000	2.0000	2.0000	2.0000	2.0000	2.0000	2.0000

Table 12.12:

CIPW normative mineralogy and Differentiation Index (D.I.) of whole rocks from Isla Margarita.

Sample	qz	or	ab	an	c	di	hy	ol	mt	il	ap	cc	D.I.
6001	0.00	8.39	18.19	29.16	0.00	12.31	20.05	8.66	1.88	1.42	0.19	0.07	26.58
6002	0.00	0.41	25.29	36.92	0.00	26.39	0.00	7.68	1.09	1.67	0.16	0.09	25.70
6003	0.20	9.22	15.32	29.80	0.03	0.00	40.85	0.00	3.99	1.44	0.19	0.32	24.74
6004	0.22	0.71	11.93	33.78	0.00	31.06	17.73	0.00	3.32	1.31	0.19	0.45	12.86
6005	0.00	0.71	10.41	39.50	0.19	0.00	42.82	2.99	2.81	1.56	0.16	0.71	11.12
6006	2.70	0.47	20.14	31.92	0.00	5.50	33.52	0.00	3.42	1.44	0.23	0.05	23.31
6007	1.03	1.12	18.19	34.10	0.00	4.77	34.91	0.00	1.86	1.37	0.21	2.91	20.34
6008	11.20	1.83	20.90	24.57	4.69	0.00	31.80	0.00	3.89	1.48	0.23	0.05	33.93
6009	15.88	0.83	22.51	28.41	0.00	6.52	19.60	0.00	4.54	0.78	0.14	0.09	39.22
6010	4.63	1.95	28.94	28.89	0.00	13.42	17.47	0.00	3.28	1.42	0.14	0.07	35.52
6011	3.75	1.18	15.32	36.94	0.00	1.17	34.75	0.00	4.34	1.41	0.19	0.11	20.25
6012	2.41	3.07	21.58	30.49	0.85	0.00	36.20	0.00	3.00	1.67	0.30	0.02	27.06
6013	3.03	2.54	18.11	34.51	1.40	0.00	33.65	0.00	4.54	1.58	0.21	0.05	23.68
6014	1.20	2.72	21.32	30.33	1.47	0.00	38.61	0.00	1.78	1.42	0.19	0.18	25.24
6037	0.00	1.30	23.44	26.62	0.00	16.92	24.49	1.81	0.35	3.29	0.35	0.57	24.74
6038	11.49	2.13	40.79	23.49	1.77	0.00	13.56	0.00	4.42	2.11	0.49	0.07	54.41
6039	0.00	0.95	29.36	29.49	0.00	3.10	31.24	1.39	2.25	1.46	0.25	0.02	30.31
6040	0.16	1.24	14.81	34.99	0.00	4.30	39.72	0.00	2.29	1.42	0.23	0.02	16.21
6041	2.24	1.77	22.42	30.58	0.00	4.06	35.21	0.00	2.84	1.22	0.14	0.05	26.43
6042	0.00	2.87	16.67	31.87	0.00	8.55	29.79	4.32	1.75	1.31	0.16	2.07	19.54
6043	0.52	2.54	25.47	23.64	0.00	10.16	25.68	0.00	2.62	3.10	0.42	6.32	28.53
6044	6.15	1.36	21.07	28.82	0.43	0.00	33.95	0.00	3.13	3.84	0.49	0.71	28.58
6045	0.00	0.65	18.87	31.52	0.00	1.88	37.35	2.53	3.13	1.42	0.19	4.41	19.52
6046	0.00	5.26	18.02	30.84	0.00	3.65	33.06	5.55	1.64	1.46	0.25	0.05	23.28
6047	1.06	2.95	23.69	31.36	0.00	5.84	32.23	0.00	1.41	1.50	0.32	0.05	27.70
6048	0.00	8.45	28.09	28.52	0.00	3.11	24.09	2.25	2.91	1.58	0.32	0.05	36.54
6049	11.63	4.37	12.44	23.25	6.03	0.00	37.84	0.00	2.07	1.52	0.23	0.09	28.44
6050	0.00	7.62	31.05	27.88	0.00	2.80	24.18	2.75	1.49	1.80	0.32	0.48	38.67
6051	0.00	6.74	21.15	26.01	0.00	6.14	21.01	16.38	1.15	1.33	0.19	0.07	27.89
6052	0.70	4.31	23.86	31.79	0.00	2.13	32.76	0.00	2.55	1.54	0.25	0.02	28.87
6053	0.00	7.74	13.62	25.83	2.18	0.00	40.99	1.72	1.03	1.50	0.21	6.09	21.36
6054	0.00	3.96	19.55	33.58	0.00	3.61	33.06	2.21	1.91	1.52	0.25	0.09	23.51
6055	0.00	1.48	21.49	27.07	0.00	12.27	26.05	7.79	2.65	1.65	0.25	0.11	22.97
6056	0.00	3.31	8.55	36.76	0.00	2.66	32.29	12.13	0.51	1.35	0.12	2.05	11.86
6057	0.90	3.96	36.89	27.15	1.14	0.00	22.89	0.00	3.74	1.99	0.30	0.05	41.75
6058	0.00	0.77	8.21	40.18	0.00	18.44	15.09	15.63	1.01	0.78	0.09	0.05	8.98

Table 12.12 (continued):

Sample	qz	or	ab	an	c	di	hy	ol	mt	il	ap	cc	D.I.
6060	0.00	6.97	20.82	29.90	0.00	6.91	30.44	1.35	1.93	1.48	0.28	0.32	27.79
6061	0.00	4.67	15.65	31.88	0.00	3.44	36.00	0.75	2.09	1.54	0.28	3.43	20.32
6062	0.00	5.67	20.14	32.35	0.00	0.84	28.48	6.16	2.23	1.73	0.30	2.96	25.81
6063	0.00	13.00	12.02	29.59	0.00	2.91	34.02	3.79	3.28	1.25	0.19	0.05	25.02
6064	0.00	6.68	6.77	34.14	0.00	7.73	40.61	1.05	2.23	1.23	0.16	0.02	13.45
6065	4.41	5.08	11.68	33.64	0.00	5.84	35.37	0.00	3.58	1.27	0.14	0.02	21.17
6066	0.55	3.85	16.33	36.13	0.00	6.06	30.47	0.00	3.65	1.63	0.25	0.07	20.73
6068	4.01	4.96	21.24	29.69	0.84	0.00	33.49	0.00	3.86	1.44	0.19	0.09	30.21
6069	16.88	6.86	11.25	13.71	9.43	0.00	34.98	0.00	3.97	1.56	0.25	1.00	34.99
6070	0.42	4.55	34.61	24.75	0.00	2.18	28.72	0.00	2.17	1.44	0.19	1.59	39.58
6101	6.39	0.35	12.52	36.45	0.89	0.00	35.95	0.00	4.18	1.46	0.19	1.80	19.26
6102	4.57	0.18	10.07	34.35	1.67	0.00	43.64	0.00	2.60	1.39	0.16	2.43	14.82
6103	5.66	0.18	10.75	38.17	0.10	0.00	37.62	0.00	2.94	1.37	0.19	2.25	16.59
6104	6.78	0.24	11.76	36.11	0.37	0.00	37.86	0.00	2.16	1.39	0.19	2.46	18.78
6105	8.29	0.24	12.95	28.30	3.51	0.00	39.42	0.00	2.75	1.39	0.19	2.16	21.48
6106	7.44	0.30	11.17	37.10	0.65	0.00	38.33	0.00	1.33	1.44	0.21	1.02	18.91
6107	5.34	0.18	8.12	30.96	3.22	0.00	45.76	0.00	2.32	1.41	0.21	1.91	13.64
6108	1.28	4.85	14.05	33.05	0.00	14.04	27.13	0.00	4.13	1.41	0.19	0.18	20.18
6109	0.08	5.73	13.79	31.68	0.00	13.34	29.74	0.00	3.28	1.37	0.19	0.36	19.60
6201	0.43	0.59	22.09	30.58	0.00	21.76	16.41	0.00	3.70	1.60	0.07	1.41	23.11
6202	0.00	0.59	14.89	43.00	0.00	29.97	1.41	4.13	3.67	1.67	0.19	0.16	15.48
6203	0.00	1.36	7.28	22.15	0.00	30.03	31.71	0.60	3.65	1.82	0.16	0.02	8.64
6204	1.61	1.24	15.57	35.44	0.00	27.85	12.02	0.00	3.67	0.85	0.12	0.16	18.42
6205	0.00	0.65	19.80	31.79	0.00	30.11	8.39	3.97	3.68	1.41	0.09	0.09	20.45
6206	0.00	0.41	26.15	36.49	0.00	24.98	2.51	3.06	3.65	1.65	0.14	0.09	26.56
6207	14.97	0.71	12.19	32.91	0.00	22.01	9.30	0.00	3.67	2.24	0.39	0.09	27.87
6208	0.44	0.71	11.42	33.21	0.00	31.05	16.18	0.00	3.67	1.29	0.16	0.07	12.57
6501	0.00	5.44	19.46	27.26	0.00	10.30	16.45	16.05	2.15	1.44	0.23	0.68	24.90
6502	0.00	3.49	22.09	29.08	0.00	10.88	23.16	7.50	2.19	1.25	0.19	0.09	25.58
6503	0.00	4.43	20.05	28.62	0.00	6.71	29.50	4.40	2.70	1.58	0.28	1.52	24.48
6504-A	0.00	4.61	15.65	30.68	0.00	7.92	32.98	2.24	2.03	1.33	0.19	1.48	20.26
6504-B	0.00	1.60	14.89	29.12	0.00	15.45	24.36	9.66	2.38	1.58	0.23	0.16	16.49
6505	0.00	6.03	18.53	26.59	0.00	9.01	21.72	13.41	1.38	1.33	0.21	0.59	24.56
6506	0.00	8.16	22.09	24.16	0.00	10.08	24.64	6.95	2.10	1.31	0.19	0.05	30.25
6507	0.00	6.86	24.96	25.38	0.00	9.20	12.52	16.76	1.96	1.35	0.21	0.23	31.82
6509	2.46	2.07	15.99	33.54	0.00	12.51	26.95	0.00	4.45	1.33	0.19	0.07	20.52
6510	4.46	2.60	20.22	32.70	0.00	9.56	25.10	0.00	3.62	1.41	0.21	0.05	27.28

Table 12.13-a:

X-Ray Fluorescence analyses of whole rocks from Isla Margarita. Analyses are normalized to 100 weight% (volatile free). Oxides as weight%, trace elements as ppm.

Sample	SiO2	TiO2	Al2O3	FeO	Fe2O3	MnO	MgO	CaO	Na2O	K2O	P2O5	CO2	H2O	Sum
6001	51.75	0.75	15.76	6.65	1.30	0.17	11.15	9.11	2.15	1.42	0.08	0.03	3.76	100.32
6002	50.87	0.88	18.82	5.63	0.75	0.12	5.99	14.13	3.17	0.07	0.07	0.04	3.62	100.55
6003	52.85	0.76	15.62	6.00	2.75	0.34	13.14	6.29	1.81	1.56	0.08	0.14	4.70	101.34
6004	50.28	0.69	14.83	5.60	2.29	0.14	10.06	15.00	1.41	0.12	0.08	0.20	4.01	100.70
6005	49.89	0.82	16.82	8.04	1.94	0.18	13.99	8.45	1.23	0.12	0.07	0.31	5.81	101.85
6006	52.61	0.76	15.70	5.95	2.36	0.15	11.30	7.98	2.38	0.08	0.10	0.02	4.22	99.40
6007	51.05	0.72	16.24	6.73	1.28	0.16	10.76	9.82	2.15	0.19	0.09	1.28	3.55	100.45
6008	55.31	0.78	18.09	4.91	3.78	0.16	9.70	5.12	2.47	0.31	0.10	0.02	6.79	100.75
6009	58.93	0.41	14.94	3.87	3.13	0.13	7.47	7.51	2.66	0.14	0.06	0.04	3.18	99.30
6010	55.44	0.75	16.57	4.37	2.26	0.15	7.50	9.33	3.42	0.33	0.06	0.03	1.21	100.22
6011	51.45	0.74	16.73	5.63	2.99	0.17	11.68	7.91	1.81	0.20	0.08	0.05	4.83	99.43
6012	52.82	0.88	16.78	6.34	2.07	0.15	11.02	6.33	2.55	0.52	0.13	0.01	4.59	99.62
6013	51.24	0.83	18.03	5.55	3.13	0.16	10.89	7.10	2.14	0.43	0.09	0.02	5.20	99.62
6014	52.25	0.75	17.23	7.05	1.23	0.16	11.09	6.32	2.52	0.46	0.08	0.08	3.65	99.22
6037	50.98	1.73	14.55	10.54	0.24	0.19	7.49	10.02	2.77	0.22	0.15	0.25	1.86	99.15
6038	58.43	1.11	18.70	5.03	3.05	0.14	3.38	5.05	4.82	0.36	0.21	0.03	2.66	100.32
6039	53.22	0.77	16.69	6.38	1.55	0.16	10.12	6.88	3.47	0.16	0.11	0.01	3.68	99.51
6040	50.92	0.75	15.93	6.94	1.58	0.15	12.57	8.28	1.75	0.21	0.10	0.01	5.05	99.19
6041	54.08	0.64	15.89	6.08	1.96	0.16	11.39	7.29	2.65	0.30	0.06	0.02	4.42	100.51
6042	49.93	0.69	15.34	7.01	1.21	0.21	11.55	9.82	1.97	0.47	0.07	0.91	3.29	99.17
6043	49.28	1.63	14.08	8.32	1.81	0.18	7.71	11.06	3.01	0.43	0.18	2.78	2.90	100.46
6044	52.64	2.02	15.34	8.80	2.16	0.24	9.02	6.48	2.49	0.23	0.21	0.31	3.09	99.93
6045	49.59	0.75	15.92	7.33	0.90	0.17	11.31	9.40	2.23	0.11	0.08	1.94	4.22	99.73
6046	51.65	0.77	15.77	7.62	1.13	0.19	12.19	7.30	2.13	0.89	0.11	0.02	4.22	99.77
6047	53.79	0.79	16.64	6.92	0.97	0.16	9.70	7.99	2.80	0.50	0.14	0.02	4.70	100.42
6048	53.17	0.83	17.46	5.62	2.01	0.14	8.50	6.74	3.42	1.43	0.14	0.02	3.41	99.48
6049	54.18	0.80	17.77	6.98	1.43	0.18	10.92	4.87	1.47	0.74	0.10	0.04	5.92	99.48
6050	54.21	0.95	17.65	6.42	1.03	0.13	7.92	6.77	3.67	1.29	0.14	0.21	2.68	100.39
6051	51.66	0.70	14.88	7.30	0.79	0.16	13.99	6.93	2.50	1.14	0.08	0.03	4.19	100.16
6052	53.09	0.81	17.08	6.39	1.76	0.18	9.84	7.10	2.82	0.73	0.11	0.01	4.03	99.91
6053	49.02	0.79	15.71	7.73	0.71	0.18	12.34	8.74	1.61	1.31	0.09	2.68	4.67	100.91
6054	51.79	0.80	16.83	6.83	1.32	0.16	11.02	7.87	2.31	0.67	0.11	0.04	3.62	99.75
6055	51.58	0.87	14.37	7.92	1.83	0.19	12.37	8.74	2.54	0.25	0.11	0.05	2.83	100.81
6056	48.02	0.71	15.74	8.47	0.35	0.17	14.45	9.29	1.01	0.56	0.05	0.90	4.60	99.70
6057	53.28	1.05	18.99	5.67	2.58	0.14	6.46	5.67	4.36	0.67	0.13	0.02	4.42	99.02

Table 12.13-a (continued):

Sample	SiO2	TiO2	Al2O3	FeO	Fe2O3	MnO	MgO	CaO	Na2O	K2O	P2O5	CO2	H2O	Sum
6058	48.09	0.41	16.46	6.59	0.70	0.12	13.90	12.82	0.97	0.13	0.04	0.02	3.24	100.28
6060	52.90	0.78	16.28	6.83	1.33	0.18	10.10	8.09	2.46	1.18	0.12	0.14	3.76	100.38
6061	49.87	0.81	15.58	6.81	1.44	0.16	11.41	9.37	1.85	0.79	0.12	1.51	3.71	99.71
6062	50.21	0.91	16.81	7.14	1.54	0.17	10.75	8.56	2.38	0.96	0.13	1.30	3.97	100.85
6063	51.85	0.66	15.56	6.22	2.26	0.15	12.83	6.83	1.42	2.20	0.08	0.02	5.96	100.08
6064	51.17	0.65	15.05	7.28	1.54	0.15	13.84	8.93	0.80	1.13	0.07	0.01	5.49	100.60
6065	53.55	0.67	15.53	5.85	2.47	0.16	12.15	8.35	1.38	0.86	0.06	0.01	5.41	101.04
6066	50.25	0.86	17.12	6.43	2.52	0.17	9.94	8.99	1.93	0.65	0.11	0.03	4.52	99.01
6068	53.18	0.76	16.77	5.03	5.26	0.27	9.20	6.14	2.51	0.84	0.08	0.04	5.75	100.09
6069	54.50	0.82	17.90	4.07	6.16	0.26	10.05	3.47	1.33	1.17	0.11	0.44	9.01	100.29
6070	54.94	0.76	16.63	6.18	1.50	0.16	8.28	6.53	4.09	0.77	0.08	0.70	3.46	100.63
6101	51.14	0.77	16.75	6.94	2.88	0.18	10.65	8.46	1.48	0.06	0.08	0.79	3.84	100.18
6102	50.64	0.73	16.25	8.59	1.79	0.20	12.12	8.38	1.19	0.03	0.07	1.07	3.74	101.07
6103	50.57	0.72	16.21	7.43	2.03	0.17	10.65	9.06	1.27	0.03	0.08	0.99	3.10	99.21
6104	51.59	0.73	15.93	7.50	1.49	0.23	10.48	8.76	1.39	0.04	0.08	1.08	2.92	99.30
6105	51.38	0.73	16.44	8.11	1.90	0.18	10.83	7.02	1.53	0.04	0.08	0.95	3.63	99.18
6106	52.45	0.76	16.47	7.88	0.92	0.16	10.27	8.17	1.32	0.05	0.09	0.45	2.96	99.00
6107	49.76	0.74	16.18	8.97	1.60	0.19	12.64	7.43	0.96	0.03	0.09	0.84	3.86	99.42
6108	51.30	0.74	15.73	5.94	2.85	0.16	10.52	10.41	1.66	0.82	0.08	0.08	2.91	100.30
6109	50.89	0.72	15.34	6.39	2.26	0.15	10.91	10.05	1.63	0.97	0.08	0.16	2.80	99.55
6201	50.59	0.84	15.61	2.68	5.09	0.15	8.49	12.63	2.61	0.10	0.03	0.62	1.59	99.45
6202	47.88	0.88	18.76	2.74	4.03	0.17	6.85	16.44	1.76	0.10	0.08	0.07	1.34	99.78
6203	50.13	0.96	9.78	5.93	3.60	0.24	15.06	12.21	0.86	0.23	0.07	0.01	1.02	99.07
6204	50.56	0.45	16.24	1.91	4.20	0.15	8.62	14.39	1.84	0.21	0.05	0.07	1.17	98.70
6205	50.53	0.74	15.62	3.31	3.77	0.16	9.30	14.15	2.34	0.11	0.04	0.04	1.87	100.14
6206	50.18	0.87	18.53	1.47	5.22	0.12	5.95	13.80	3.09	0.07	0.06	0.04	0.76	99.41
6207	54.17	1.18	14.56	3.26	8.34	0.17	3.40	12.21	1.44	0.12	0.17	0.04	0.95	99.07
6208	49.11	0.68	14.52	3.61	4.26	0.13	9.82	14.67	1.35	0.12	0.07	0.03	1.08	98.38
6501	49.76	0.76	14.77	7.17	1.48	0.16	13.14	8.60	2.30	0.92	0.10	0.30	2.60	99.48
6502	51.77	0.66	15.59	6.66	1.51	0.16	11.49	8.75	2.61	0.59	0.08	0.04	1.90	99.91
6503	50.97	0.83	15.20	6.68	1.86	0.16	11.72	8.47	2.37	0.75	0.12	0.67	2.62	99.80
6504-A	50.70	0.70	15.13	6.56	1.40	0.15	12.00	9.11	1.85	0.78	0.08	0.65	2.77	99.11
6504-B	49.71	0.83	13.86	7.28	1.64	0.17	13.75	9.98	1.76	0.27	0.10	0.07	2.48	99.43
6505	50.34	0.70	14.45	7.48	0.95	0.16	13.08	8.07	2.19	1.02	0.09	0.26	2.44	98.79
6506	52.83	0.69	14.64	6.81	1.45	0.15	11.52	7.53	2.61	1.38	0.08	0.02	2.66	99.72
6507	51.04	0.71	15.41	6.98	1.35	0.15	11.81	7.67	2.95	1.16	0.09	0.10	3.04	99.43
6509	51.41	0.70	15.78	5.47	3.07	0.18	10.53	10.07	1.89	0.35	0.08	0.03	3.03	99.56
6510	53.44	0.74	16.39	5.68	2.50	0.16	8.93	9.14	2.39	0.44	0.09	0.02	2.98	99.93

Table 12.13-a (continued):

Sample	Ba	Co	Cr	S	V	Cl	Cu	Nb	Ni	Rb	Sr	Y	Zn	Zr
6001	49	49	429	12	231	67	13	4	260	46	362	5	56	67
6002	55	41	262	22	221	58	64	5	215	21	289	25	59	75
6003	44	48	28	1	377	56	68	12	332	57	145	13	63	68
6004	77	54	204	1	265	64	34	7	297	21	192	18	80	86
6005	214	57	830	29	203	107	43	8	342	25	81	24	88	77
6006	112	60	712	43	179	93	71	8	298	16	149	19	64	76
6007	175	54	535	2	204	3	56	7	226	23	162	18	71	71
6008	212	54	499	17	172	26	67	8	221	17	143	20	71	73
6009	257	50	265	1	178	92	99	6	79	16	392	15	53	74
6010	221	48	270	22	207	67	37	8	96	20	294	20	46	67
6011	170	58	709	11	191	79	32	5	298	22	112	29	71	63
6012	228	56	600	12	196	122	67	9	275	30	196	17	69	94
6013	269	55	654	2	207	194	74	7	244	29	149	19	65	72
6014	205	57	633	7	199	147	11	9	252	16	185	28	66	74
6037	286	53	157	24	376	152	41	10	72	6	171	41	90	115
6038	196	40	18	19	231	159	24	11	12	19	247	29	79	128
6039	130	53	438	11	180	333	29	5	200	18	201	19	75	70
6040	85	58	852	7	190	480	64	7	324	20	125	18	68	65
6041	187	53	953	18	189	89	63	8	319	29	138	17	70	62
6042	410	53	727	32	209	53	13	7	276	23	153	18	103	59
6043	317	46	180	72	334	166	86	12	74	30	230	33	83	106
6044	112	46	187	43	368	266	216	13	69	24	160	40	158	129
6045	105	54	688	109	195	257	66	7	251	17	155	18	74	64
6046	327	53	835	16	192	8	41	11	349	28	173	18	108	80
6047	211	44	549	28	176	219	43	8	218	14	227	22	83	96
6048	571	49	481	38	196	92	47	10	170	32	269	23	78	101
6049	178	49	533	48	174	465	46	9	219	28	176	19	78	77
6050	277	48	281	6	219	139	36	10	133	40	263	22	63	98
6051	264	57	929	5	174	144	34	8	388	23	198	19	74	67
6052	133	52	554	13	183	178	60	10	196	30	212	19	77	80
6053	142	56	740	37	190	118	50	7	301	44	172	17	80	69
6054	230	49	624	30	168	115	24	9	279	36	236	18	80	91
6055	108	58	681	12	226	272	30	8	206	22	166	20	75	72
6056	83	63	793	48	194	189	46	6	359	27	109	15	70	61
6057	238	51	72	133	224	424	60	10	43	19	363	24	43	89

Table 12.13-a (continued):

Sample	Ba	Co	Cr	S	V	Cl	Cu	Nb	Ni	Rb	Sr	Y	Zn	Zr
6058	58	63	608	23	154	233	70	6	263	17	158	10	44	33
6060	472	49	607	62	195	304	39	7	208	46	235	19	76	90
6061	126	52	685	35	206	149	61	9	235	33	172	19	61	79
6062	157	47	536	17	203	106	36	10	222	46	196	21	69	82
6063	221	57	908	23	167	300	38	8	355	58	94	16	62	64
6064	214	51	931	3	175	86	34	8	361	36	92	15	70	57
6065	182	52	843	29	176	87	58	6	310	26	122	17	63	60
6066	204	47	472	56	196	45	38	9	183	34	166	20	104	74
6068	362	63	571	11	209	154	67	9	292	36	159	30	251	64
6069	691	58	661	33	132	122	74	11	396	37	146	29	238	82
6070	421	43	396	17	169	178	31	8	172	26	264	19	75	68
6101	85	96	549	170	201	220	41	8	249	21	114	23	153	74
6102	52	78	668	263	198	80	32	9	319	29	99	20	135	69
6103	53	65	534	436	193	148	45	8	224	15	114	20	86	71
6104	73	64	558	56	190	80	43	8	324	22	133	20	204	72
6105	57	50	574	591	198	160	26	9	250	15	113	23	173	76
6106	51	64	578	757	201	188	20	8	373	6	118	34	263	75
6107	45	61	762	217	197	168	36	9	342	17	94	30	127	71
6108	179	52	578	122	233	171	58	7	219	43	131	20	96	66
6109	205	60	623	240	226	180	90	8	252	47	132	19	119	65
6201	111	50	217	74	233	135	34	7	73	19	239	9	73	27
6202	85	40	336	51	217	149	13	8	69	21	345	16	94	46
6203	214	76	424	53	279	105	13	8	126	23	80	15	112	48
6204	230	48	225	77	165	80	50	6	84	38	269	7	67	28
6205	55	47	427	40	234	168	14	7	65	18	244	14	151	42
6206	69	41	263	31	223	175	17	7	37	17	285	18	38	56
6207	51	51	27	17	390	170	48	9	16	27	505	24	76	84
6208	69	54	204	39	267	170	60	6	76	16	231	13	36	38
6501	201	64	833	47	209	171	17	8	342	43	185	18	72	74
6502	184	52	645	136	201	305	16	8	277	33	206	18	64	64
6503	228	54	645	89	215	258	20	8	273	37	207	20	75	81
6504-A	264	55	678	59	221	254	13	8	295	35	194	18	68	66
6504-B	96	64	933	5	218	389	20	9	336	26	153	18	81	78
6505	276	58	809	11	200	273	7	8	352	19	161	21	72	67
6506	283	52	680	53	202	244	6	8	297	49	180	17	69	69
6507	245	56	669	38	200	205	9	9	286	40	244	18	72	71
6509	260	56	630	27	215	91	35	9	225	29	184	18	78	62
6510	298	42	505	20	203	109	33	8	171	31	234	19	67	68

Table 12.13-b:

Mg-numbers and characteristic elemental ratios of whole rocks from Isla Margarita.

Sample	Fe2O3/FeO	FeO*/MgO	Mg#	Zr/Nb	Zr/Rb	Zr/Y	Zr/Ti	Rb/Sr	Rb/K	Rb/Zr	Sr/Zr
6001	0.19	0.70	56.44	16.75	1.46	13.40	66.88	0.13	3.89	0.69	5.40
6002	0.13	1.05	45.09	15.00	3.57	3.00	70.42	0.07	34.84	0.28	3.85
6003	0.46	0.64	62.87	5.67	1.19	5.23	66.51	0.39	4.39	0.84	2.13
6004	0.41	0.76	58.12	12.29	4.10	4.78	47.88	0.11	20.24	0.24	2.23
6005	0.24	0.70	57.35	9.63	3.08	3.21	63.52	0.31	25.82	0.32	1.05
6006	0.40	0.72	59.47	9.50	4.75	4.00	60.09	0.11	23.07	0.21	1.96
6007	0.19	0.73	55.28	10.14	3.09	3.94	60.35	0.14	14.85	0.32	2.28
6008	0.77	0.86	60.44	9.13	4.29	3.65	64.23	0.12	6.59	0.23	1.96
6009	0.81	0.90	59.84	12.33	4.63	4.93	33.45	0.04	13.33	0.22	5.30
6010	0.52	0.85	57.00	8.38	3.35	3.35	66.97	0.07	7.21	0.30	4.39
6011	0.53	0.71	61.57	12.60	2.86	2.17	69.95	0.20	13.27	0.35	1.78
6012	0.33	0.74	57.31	10.44	3.13	5.53	56.11	0.15	6.89	0.32	2.09
6013	0.56	0.77	60.26	10.29	2.48	3.79	69.34	0.19	8.08	0.40	2.07
6014	0.17	0.74	54.87	8.22	4.63	2.64	60.51	0.09	4.22	0.22	2.50
6037	0.02	1.44	35.46	11.50	19.17	2.80	90.24	0.04	3.22	0.05	1.49
6038	0.61	2.30	34.16	11.64	6.74	4.41	51.92	0.08	6.37	0.15	1.93
6039	0.24	0.77	55.10	14.00	3.89	3.68	65.75	0.09	13.92	0.26	2.87
6040	0.23	0.67	58.32	9.29	3.25	3.61	68.94	0.16	11.43	0.31	1.92
6041	0.32	0.69	59.16	7.75	2.14	3.65	61.64	0.21	11.52	0.47	2.23
6042	0.17	0.70	56.01	8.43	2.57	3.28	70.36	0.15	5.95	0.39	2.59
6043	0.22	1.29	41.74	8.83	3.53	3.21	91.94	0.13	8.36	0.28	2.17
6044	0.24	1.19	44.19	9.92	5.38	3.23	93.91	0.15	12.74	0.19	1.24
6045	0.12	0.72	54.39	9.14	3.76	3.56	70.36	0.11	17.83	0.27	2.42
6046	0.15	0.71	55.27	7.27	2.86	4.44	57.85	0.16	3.80	0.35	2.16
6047	0.14	0.80	52.00	12.00	6.86	4.36	49.09	0.06	3.35	0.15	2.36
6048	0.36	0.87	53.89	10.10	3.16	4.39	49.13	0.12	2.70	0.32	2.66
6049	0.21	0.76	54.75	8.56	2.75	4.05	62.04	0.16	4.53	0.36	2.29
6050	0.16	0.93	48.81	9.80	2.45	4.45	57.78	0.15	3.72	0.41	2.68
6051	0.11	0.57	59.70	8.38	2.91	3.53	62.52	0.12	2.44	0.34	2.96
6052	0.28	0.81	54.34	8.00	2.67	4.21	60.86	0.14	4.95	0.38	2.65
6053	0.09	0.68	55.24	9.86	1.57	4.06	68.27	0.26	4.04	0.64	2.49
6054	0.19	0.73	55.50	10.11	2.53	5.06	52.59	0.15	6.43	0.40	2.59
6055	0.23	0.77	54.68	9.00	3.27	3.60	72.76	0.13	10.73	0.31	2.31
6056	0.04	0.61	56.86	10.17	2.26	4.07	70.00	0.25	5.85	0.44	1.79
6057	0.45	1.24	46.80	8.90	4.68	3.71	70.45	0.05	3.42	0.21	4.08

Table 12.13-b (continued):

Sample	Fe2O3/FeO	FeO*/MgO	Mg#	Zr/Nb	Zr/Rb	Zr/Y	Zr/Ti	Rb/Sr	Rb/K	Rb/Zr	Sr/Zr
6058	0.11	0.52	61.97	5.50	1.94	3.30	75.03	0.11	15.24	0.52	4.79
6060	0.19	0.79	53.35	12.86	1.96	4.74	51.86	0.20	4.68	0.51	2.61
6061	0.21	0.71	56.42	8.78	2.39	4.16	61.43	0.19	5.04	0.42	2.18
6062	0.22	0.79	53.79	8.20	1.78	3.90	66.16	0.23	5.79	0.56	2.39
6063	0.36	0.64	61.46	8.00	1.10	4.00	61.70	0.62	3.17	0.91	1.47
6064	0.21	0.63	59.50	7.13	1.58	3.80	67.80	0.39	3.83	0.63	1.61
6065	0.42	0.67	61.60	10.00	2.31	3.53	66.45	0.21	3.66	0.43	2.03
6066	0.39	0.88	54.43	8.22	2.18	3.70	69.55	0.20	6.30	0.46	2.24
6068	1.05	1.06	58.57	7.11	1.78	2.13	71.51	0.23	5.17	0.56	2.48
6069	1.51	0.96	65.61	7.45	2.22	2.83	60.21	0.25	3.83	0.45	1.78
6070	0.24	0.91	50.88	8.50	2.62	3.58	66.59	0.10	4.09	0.38	3.88
6101	0.41	0.89	54.27	9.25	3.52	3.22	62.29	0.18	40.55	0.28	1.54
6102	0.21	0.84	52.17	7.67	2.38	3.45	63.10	0.29	112.14	0.42	1.43
6103	0.27	0.87	52.56	8.88	4.73	3.55	60.96	0.13	58.35	0.21	1.61
6104	0.20	0.84	51.92	9.00	3.27	3.60	60.86	0.17	64.31	0.31	1.85
6105	0.23	0.91	50.79	8.44	5.07	3.30	57.27	0.13	43.52	0.20	1.49
6106	0.12	0.85	50.19	9.38	12.50	2.21	60.92	0.05	14.02	0.08	1.57
6107	0.18	0.82	52.14	7.89	4.18	2.37	62.32	0.18	65.61	0.24	1.32
6108	0.48	0.81	57.76	9.43	1.53	3.30	67.30	0.33	6.29	0.65	1.98
6109	0.35	0.77	56.88	8.13	1.38	3.42	66.37	0.36	5.85	0.72	2.03
6201	1.90	0.86	70.99	3.86	1.42	3.00	187.14	0.08	22.52	0.70	8.85
6202	1.47	0.93	65.90	5.75	2.19	2.88	114.83	0.06	24.96	0.46	7.50
6203	0.61	0.61	66.24	6.00	2.09	3.20	119.79	0.29	11.92	0.48	1.67
6204	2.20	0.66	77.72	4.67	0.74	4.00	95.26	0.14	21.54	1.36	9.61
6205	1.14	0.72	68.48	6.00	2.33	3.00	106.10	0.07	19.34	0.43	5.81
6206	3.55	1.04	75.76	8.00	3.29	3.11	92.70	0.06	29.03	0.30	5.09
6207	2.56	3.16	44.65	9.33	3.11	3.50	84.24	0.05	26.84	0.32	6.01
6208	1.18	0.76	67.76	6.33	2.38	2.92	106.79	0.07	15.89	0.42	6.08
6501	0.21	0.65	58.63	9.25	1.72	4.11	61.51	0.23	5.61	0.58	2.50
6502	0.23	0.70	57.15	8.00	1.94	3.56	62.02	0.16	6.72	0.52	3.22
6503	0.28	0.71	57.57	10.13	2.19	4.05	61.51	0.18	5.95	0.46	2.56
6504-A	0.21	0.65	58.55	8.25	1.89	3.67	63.49	0.18	5.39	0.53	2.94
6504-B	0.23	0.64	59.35	8.67	3.00	4.33	63.80	0.17	11.75	0.33	1.96
6505	0.13	0.64	57.46	8.38	3.53	3.19	62.33	0.12	2.25	0.28	2.40
6506	0.21	0.70	56.65	8.63	1.41	4.06	59.76	0.27	4.29	0.71	2.61
6507	0.19	0.69	56.66	7.89	1.78	3.94	60.05	0.16	4.17	0.56	3.44
6509	0.56	0.78	59.82	6.89	2.14	3.44	67.76	0.16	9.96	0.47	2.97
6510	0.44	0.89	54.85	8.50	2.19	3.58	65.37	0.13	8.43	0.46	3.44

Table 12.14:

ICP-AES analyses of rare earth element concentrations of whole rocks from Isla Margarita.

Sample	La	Ce	Nd	Sm	Eu	Gd	Dy	Ho	Er	Yb	Lu	Sum REE
6002	5.20	12.00	8.00	2.40	0.93	3.10	3.70	0.77	2.40	2.20	0.34	41.04
6003	3.00	8.30	5.50	1.70	0.68	2.30	2.90	0.58	1.80	1.70	0.26	28.72
6005	3.50	10.00	6.20	1.90	0.73	2.60	3.20	0.64	2.00	1.90	0.29	32.96
6006	7.80	17.00	11.00	2.80	0.89	2.80	3.00	0.59	1.90	1.80	0.28	49.86
6010	2.50	8.40	6.30	1.90	0.77	2.70	3.30	0.64	2.10	2.10	0.32	31.03
6037	5.10	16.00	11.00	3.50	1.43	4.80	6.00	1.22	3.80	3.50	0.52	56.87
6038	12.00	26.00	14.00	3.40	1.29	4.20	4.70	0.97	3.00	2.90	0.46	72.92
6043	4.20	14.00	10.00	3.30	1.53	4.50	5.70	1.15	3.60	3.20	0.49	51.67
6044	5.40	18.00	13.00	4.20	1.51	5.70	7.00	1.43	4.40	4.00	0.61	65.25
6050	9.30	21.00	11.00	2.90	0.96	3.30	3.70	0.73	2.30	2.20	0.33	57.72
6055	3.80	11.00	7.40	2.40	0.89	2.90	3.50	0.73	2.10	2.10	0.30	37.12
6056	2.00	6.30	4.60	1.40	0.60	2.20	2.80	0.57	1.80	1.70	0.27	24.24
6057	7.70	19.00	10.00	3.10	1.18	3.30	4.00	0.82	2.50	2.30	0.37	54.27
6058	1.70	4.00	3.00	1.00	0.48	1.40	1.70	0.33	1.00	0.90	0.14	15.65
6106	5.50	13.00	9.80	3.10	1.03	4.30	4.90	1.02	3.00	2.60	0.39	48.64
6107	5.60	15.00	9.50	2.90	0.91	4.10	4.80	0.98	2.90	2.60	0.39	49.68
6201	0.90	2.30	2.50	0.90	0.59	1.40	1.80	0.34	1.00	0.90	0.13	12.76
6207	7.50	18.00	12.00	3.70	1.30	4.20	4.80	0.96	2.90	2.90	0.45	58.71
6504-A	4.00	10.00	6.20	2.00	0.75	2.60	3.00	0.61	1.90	1.80	0.28	33.14
6510	5.70	13.00	7.30	2.10	0.78	2.50	3.20	0.65	2.00	2.00	0.31	39.54

Table 12.14 (continued):

Normalized rare earth element concentrations of whole rocks from Isla Margarita; normalizing values from Sun & McDonough (1989).

Sample	La/N	Ce/N	Nd/N	Sm/N	Eu/N	Gd/N	Dy/N	Er/N	Yb/N	Lu/N
6002	21.94	19.61	17.13	15.69	16.03	15.09	14.57	14.50	12.94	13.39
6003	12.66	13.56	11.78	11.11	11.72	11.19	11.42	10.88	10.00	10.24
6005	14.77	16.34	13.28	12.42	12.59	12.65	12.60	12.08	11.18	11.42
6006	32.91	27.78	23.55	18.30	15.34	13.63	11.81	11.48	10.59	11.02
6010	10.55	13.73	13.49	12.42	13.28	13.14	12.99	12.69	12.35	12.60
6037	21.52	26.14	23.55	22.88	24.66	23.36	23.62	22.96	20.59	20.47
6038	50.63	42.48	29.98	22.22	22.24	20.44	18.50	18.13	17.06	18.11
6043	17.72	22.88	21.41	21.57	26.38	21.90	22.44	21.75	18.82	19.29
6044	22.78	29.41	27.84	27.45	26.03	27.74	27.56	26.59	23.53	24.02
6050	39.24	34.31	23.55	18.95	16.55	16.06	14.57	13.90	12.94	12.99
6055	16.03	17.97	15.85	15.69	15.34	14.11	13.78	12.69	12.35	11.81
6056	8.44	10.29	9.85	9.15	10.34	10.71	11.02	10.88	10.00	10.63
6057	32.49	31.05	21.41	20.26	20.34	16.06	15.75	15.11	13.53	14.57
6058	7.17	6.54	6.42	6.54	8.28	6.81	6.69	6.04	5.29	5.51
6106	23.21	21.24	20.99	20.26	17.76	20.92	19.29	18.13	15.29	15.35
6107	23.63	24.51	20.34	18.95	15.69	19.95	18.90	17.52	15.29	15.35
6201	3.80	3.76	5.35	5.88	10.17	6.81	7.09	6.04	5.29	5.12
6207	31.65	29.41	25.70	24.18	22.41	20.44	18.90	17.52	17.06	17.72
6504-A	16.88	16.34	13.28	13.07	12.93	12.65	11.81	11.48	10.59	11.02
6510	24.05	21.24	15.63	13.73	13.45	12.17	12.60	12.08	11.76	12.20

Table 12.15:

Mass-spectrometer analyses of strontium and rubidium isotopic ratios and concentrations in plagioclase mineral separates from Isla Margarita.

Sample	Sr 84/86 meas	Sr 84/86 corr	Sr 87/86 meas	Sr 87/86 corr	Sr 87/86 initial	Rb 85/87 meas	Rb87/Sr86 meas	ppm Sr	ppm Rb
6012	0.0753080	0.0753102	0.7043270	0.7043314	0.7040993	2.1366150	0.3353608	25.000	2.156
6042	0.0764680	0.7647040	0.7044870	0.7044916	0.7043881	1.7055740	0.1457468	145.995	0.883
6050	0.0754460	0.0754482	0.7050980	0.7051024	0.7048327	2.1968829	0.4003631	369.343	2.555
6055	0.0791390	0.0791418	0.7051380	0.7051433	0.7047222	2.1648890	0.4362298	618.022	2.329
6056	0.0826030	0.0826064	0.7043540	0.7043600	0.7041519	1.8804472	0.2620518	138.395	1.213
6061	0.0810470	0.0815013	0.7042500	0.7042557	0.7040137	2.0348118	0.3407253	142.326	1.678
6501	0.6907200	0.0690734	0.7054970	0.7054999	0.7052663	2.3275388	0.4200742	605.526	4.044
6507	0.1013340	0.1013412	0.7064760	0.7064864	0.7061544	1.9421174	0.5093943	109.509	1.373
6058					0.7043150				
6103					0.7049830				
country rock					0.7139100				

Table 12.16:

Mass-spectrometer analyses of lead, uranium and thorium isotopic ratios and concentrations in plagioclase mineral separates from Isla Margarita.

Sample	Pb 208/206 meas	Pb 207/206 meas	Pb 205/206 meas	Pb 204/206 meas	Pb 206/204 corr	Pb 207/204 corr	Pb 208/204 corr
6012	1.9702280	0.7919457	0.0001911	0.0503382	19.9163200	15.7926800	39.3393100
6042	2.0121913	0.8130246	0.0348789	0.0520428	19.2724600	15.6803900	38.8660800
6050	2.0214400	0.8173370	0.0235207	0.0522669	19.1861700	15.6966500	38.8757500
6055	2.0189241	0.8153406	0.0277083	0.0521837	19.2180500	15.6830000	38.8902200
6056	2.0282262	0.8212963	0.0221202	0.0520000	19.0714500	15.6794000	38.7746600
6061	2.0306029	0.8228712	0.0223315	0.0526788	19.0344600	15.6792500	38.7451800
6501	2.0411490	0.8293899	0.0139223	0.0532063	18.8434400	15.6469700	38.5584000
6507	2.0521246	0.8325943	0.0255061	0.0534482	18.7579800	15.6356000	38.5909400

Table 12.16 (continued):

Sample	Pb 206/204 initial	Pb207/204 initial	Pb 208/204 initial	Th 232/Pb204 meas	Th 230/232 meas	U234/238 meas
6012	19.9132047	15.7924855	39.3374061	0.7227451	0.012387	0.6943065
6042	19.1224116	15.6733502	38.8023410	28.5972060	0.056101	2.3370305
6050	18.8168691	15.6793059	38.6129217	111.8725350	0.009582	0.6742365
6055	18.6931203	15.6581317	38.5350317	112.7579450	0.011237	0.7513071
6056	19.0127214	15.6766320	38.7538788	7.5036511	0.133448	4.6241768
6061	18.8397143	15.6701131	38.7292787	7.1342846	0.141434	1.1366810
6501	18.7621782	15.6431563	38.4764942	36.1764870	0.017156	1.6980020
6507	18.7298393	15.6342328	38.5754133	7.2505538	0.156848	8.3856310

Table 12.16 (continued):

Sample	Kappa	MU	ppm Pb	ppm U	ppm Th
6012	1.7825426	0.4054574	153.270	0.945	1.630
6042	1.3350677	21.4200427	0.506	0.168	0.217
6050	2.2370552	50.0088394	1.817	1.406	3.043
6055	2.1278950	52.9903722	3.080	2.520	5.190
6056	1.1127583	6.7432896	1.001	0.105	0.113
6061	0.2566218	27.8007742	0.960	0.415	0.103
6501	3.1679164	11.4196472	3.379	0.603	1.848
6507	1.7195925	4.2164373	4.460	0.078	0.131

Table 12.17:

Mass-spectrometer analyses of argon isotopic ratios and inferred ages from incremental heating steps.

Sample 6012

T(°C)	40Ar(mol)	40/39	37/39	36/39	K/Ca	39Ar	40Ar	Age	±
800	2.4087	15.0505	4.6531	0.2026	0.110	0.445	0.201	48.71	2.90
950	0.6448	12.8655	14.5987	0.0725	0.033	0.713	0.386	41.72	2.30
1050	0.6185	20.1018	19.4763	0.0851	0.025	0.909	0.456	64.77	3.49
1120	0.3367	24.3952	18.7975	0.1451	0.026	0.980	0.368	78.31	10.36
1300	5.5636	8.2331	17.3663	12.6898	0.028	1.000	0.002	26.81	

TFA = 51.66±19.60 (Total Fusion age)

WMPA = 49.39±1.58 (Weighted mean plateau age)

IIA = 45.35±12.74 (Inverse Isochrone age)

Sample 6050

T(°C)	40Ar(mol)	40/39	37/39	36/39	K/Ca	39Ar	40Ar	Age	±
700	3.8023	13.7426	1.6098	0.0140	0.300	0.081	0.774	44.45	0.31
900	4.3362	14.6762	10.3595	0.0177	0.047	0.167	0.767	47.43	0.31
950	2.0481	14.0052	11.3361	0.0165	0.043	0.211	0.777	45.29	0.49
1000	3.8367	15.0629	13.2421	0.0141	0.037	0.291	0.826	48.66	0.32
1030	6.0818	14.4808	13.7408	0.0107	0.035	0.431	0.872	46.80	0.19
1050	4.3674	16.6382	14.3552	0.0123	0.034	0.518	0.868	53.67	0.30
1070	7.9227	17.5470	14.5794	0.0116	0.033	0.670	0.884	56.56	0.20
1090	11.1308	16.7757	14.3679	0.0106	0.034	0.896	0.892	54.11	0.15
1130	4.7675	16.4578	14.3404	0.0096	0.034	0.996	0.905	53.11	0.26
1300	0.2938	17.0951	15.4421	0.0406	0.031	1.000	0.611	55.13	3.87

TFA = 51.15±0.10

WMPA = 51.54±0.09

IIA = 94.69±90.41

Table 12.17 (continued):

Sample 6055

T (°C)	40Ar(mol)	40/39	37/39	36/39	K/Ca	39Ar	40Ar	Age	±
700	3.5484	23.0611	2.7547	0.0459	0.180	0.066	0.663	73.84	0.72
850	2.4991	18.8357	9.4702	0.0282	0.051	0.131	0.712	60.53	0.65
930	2.9452	18.8582	19.1768	0.0332	0.025	0.205	0.691	60.60	0.57
990	4.8428	19.7871	20.9802	0.0286	0.023	0.331	0.741	63.54	0.41
1070	11.2383	21.1853	18.6058	0.0196	0.026	0.663	0.828	67.94	0.23
1120	12.5147	20.6392	20.8493	0.0190	0.023	0.983	0.836	66.22	0.23
1300	0.5054	19.9291	24.1007	0.0073	0.020	1.000	0.986	63.99	1.71

TFA = 66.09±0.15 WMPA = 66.26±0.15 IIA = 64.29±3.29

Sample 6056

T(°C)	40Ar(mol)	40/39	37/39	36/39	K/Ca	39Ar	40Ar	Age	±
700	6.4472	17.4048	10.2080	0.0778	0.048	0.133	0.438	55.90	0.64
900	14.4034	30.2810	25.6492	0.0751	0.019	0.367	0.596	96.17	0.50
970	3.3882	20.5916	21.3982	0.0336	0.023	0.463	0.711	65.95	0.60
1030	5.5953	19.0475	19.1322	0.0245	0.025	0.648	0.766	61.09	0.35
1070	10.4921	22.7732	19.2774	0.0251	0.025	0.949	0.792	72.80	0.31
1100	1.6749	30.0665	27.9219	0.0467	0.017	0.982	0.717	95.51	1.51
1300	2.3722	44.8700	44.0995	0.2202	0.011	1.000	0.414	140.74	3.98

TFA = 75.28±0.22 WMPA = 71.04±0.20 IIA = 55.83±8.48

Table 12.17 (continued):

Sample 6501

T(°C)	40Ar(mol)	40/39	37/39	36/39	K/Ca	39Ar	40Ar	Age	±
600	3.4863	16.0205	2.0224	0.0635	0.240	0.038	0.462	51.33	0.67
700	2.7444	13.2445	1.1162	0.0482	0.440	0.075	0.483	42.54	0.71
800	2.5837	12.1817	2.2754	0.0253	0.220	0.125	0.625	39.16	0.43
900	5.0068	13.9739	13.6570	0.0314	0.036	0.210	0.628	44.85	0.39
930	2.1953	15.7000	19.5852	0.0325	0.025	0.245	0.657	50.32	0.67
960	2.9276	14.1074	17.1754	0.0242	0.028	0.300	0.706	45.27	0.66
990	2.9686	14.0006	16.4867	0.0208	0.029	0.360	0.740	44.94	0.58
1020	3.3066	14.2435	15.4949	0.0238	0.031	0.422	0.708	45.71	0.51
1040	2.0959	14.6334	15.5244	0.0226	0.031	0.461	0.725	46.94	0.59
1070	7.6744	16.1561	15.2670	0.0275	0.032	0.587	0.698	51.76	0.25
1100	17.0915	16.1909	14.9634	0.0251	0.032	0.874	0.720	51.87	0.18
1150	6.4566	16.3176	16.0750	0.0267	0.030	0.980	0.708	52.27	0.31
1300	1.9460	17.5035	25.6909	0.0748	0.019	1.000	0.461	56.01	1.47

TFA = 48.97±0.12 WMPA = 49.56±0.11 IIA = 45.86±3.34

Sample 6507

T(°C)	40Ar(mol)	40/39	37/39	36/39	K/Ca	39Ar	40Ar	Age	±
700	4.1720	15.9987	2.4496	0.0624	0.200	0.038	0.467	51.35	0.68
850	3.1964	12.4638	7.7714	0.0285	0.063	0.087	0.613	40.13	0.40
920	5.6088	14.2744	22.1006	0.0340	0.022	0.164	0.628	45.89	0.38
960	4.5577	13.3095	18.2502	0.0233	0.027	0.240	0.706	42.82	0.34
990	3.8003	13.2777	17.6468	0.0196	0.027	0.307	0.748	42.72	0.35
1010	2.6243	13.0887	17.2842	0.0181	0.028	0.355	0.763	42.12	0.44
1030	3.5967	12.9734	16.5885	0.0172	0.029	0.422	0.772	41.75	0.32
1050	4.2872	14.0393	16.7694	0.0190	0.029	0.495	0.763	45.14	0.30
1065	6.5704	14.8023	16.8877	0.0208	0.029	0.599	0.752	47.56	0.28
1080	9.8848	14.6255	16.5510	0.0194	0.029	0.761	0.766	47.00	0.19
1100	11.6343	14.2466	16.4943	0.0173	0.029	0.962	0.787	45.80	0.18
113	1.3591	14.7602	20.6361	0.0190	0.023	0.985	0.784	47.43	0.75
1300	2.9543	16.5381	31.0156	0.1556	0.015	1.000	0.271	53.06	2.13

TFA = 45.34±0.10 WMPA = 45.22±0.10 IIA = 43.41±1.41